Alma Mater Studiorum – Università di Bologna

DOTTORATO DI RICERCA IN

CHIMICA

Ciclo XXIX

Settore Concorsuale di afferenza: 03/C1

Settore Scientifico disciplinare: CHIM/06

SPIN-LABELLING OF MECHANICALLY INTERLOCKED MOLECULES WITH NITROXIDE RADICALS

Presentata da: Valentina Bleve

Coordinatore Dottorato

Prof. Aldo Roda

Relatore

Prof. Marco Lucarini

Correlatore

Prof. ssa Elisabetta Mezzina

Esame finale anno 2017

Contents

Abstract

Molecular machines, namely assemblies of a distinct number of molecular components that are designed to perform machine like movements (output) as a result of an appropriate external stimulation (input) in order to accomplish a specific function, have been described in the recent years, with possible utility in the field of information and communication technology (ICT), materials science, catalysis, and medicine. The first step towards the design of artificial molecular machines is represented by [2]rotaxanes, based on a ring threaded over an axle with stoppers at each end, because the movement of the ring component can be easily obtained by application of external stimuli and controlled as well. The characterization of these systems, depending on the nature and chemical properties of their molecular components, is typically carried out by high-resolution X ray crystallography, nuclear magnetic resonance (NMR) spectroscopy, electrochemical and photophysical techniques. As an alternative, electron paramagnetic resonance (EPR) spectroscopy can be useful to investigate these systems because offers different advantages. However, in order to use EPR spectroscopy, organic radicals, such as nitroxides, must be introduced in the system. The aim of my project was devoted to prepare and investigate bistable [2]rotaxanes, containing nitroxide units to exploit EPR spectroscopy for their characterization. In Chapter 1 a brief overview of the principal concepts of rotaxane, the spin labelling approach and the employment of ESR and PELDOR methods applied to paramagnetic systems are described. Chapter 2 is focused on the synthesis and characterization of a series of rotaxanes comprising a dibenzo[24]-crown-8-ether (DB24C8) interlocked with a dumbbell component that possesses two different recognition sites, namely, a dialkylammonium (NH^{2+}) and a 4,4'-bipyridinium (BPY^{2+}) units. The introduction of nitroxide units in these systems allows both to monitorate the macrocycle movement driven by chemical stimulus by using EPR spectroscopy and to understand in detail the structural and conformational changes occurring after the movement of their molecular components by performing PELDOR (Double Electron Electron Resonance) technique. Chapter 3 is devoted to the synthesis and EPR characterization of a novel spin labelled macrocycle in which the nitroxide unit is part of its structure, playing a key role in the interaction with suitably chosen recognition sites when this novel spin-labelled macrocycle is employed as wheel in bistable [2]rotaxanes, and acting as EPR probe. In Chapter 4 a series of spin-labelled rotaxanes driven by electrochemical stimuli, containing in the dumbbell either redox active tetrathiafulvalene (TTF) station or the 1,5-dioxynaphthalene (DNP) unit or both and cyclobis-(paraquat-*p*-phenylene) ($CBPQT^{4+}$) as macrocycle, are reported.

Abbreviations, Acronyms, and Symbols

°C degrees Celsius

Å angstroms

ATP adenosine triphosphate

ACN acetonitrile

$BIPY^{2+}$ 4,4´-bipyridinium

Bu_4NI tetra-n-butylammonium iodide

$CBPQT^{4+}$ cyclobis(paraquat-*p*-phenylene); blue box

CD cyclodextrin

cm centimeters

COSY NMR correlation spectroscopy

CuAAC copper(I)-catalyzed azide-alkyne cycloaddition

CV cyclic voltammetry

Cy cyclohexyl

DB24C8 dibenzo[24]crown-8

DBV dibenzylviologen

DCC dicyclohexylcarbodiimide

DCM dichloromethane

DIPEA diisopropylethylamine

DMAP *N*,*N*-dimethyl-4-aminopyridine

DMF *N*,*N*-dimethylformamide

DNP 1,5-dioxynaphthalene

Dtbp3,5-di-*tert*-butylphenyl

EPR electron paramagnetic resonance

Et ethyl

EtOAc ethyl acetate

Et_2O diethyl ether

g grams

GSCC ground state co-conformation

Hz Hertz (cycles per second)

i or *i- isoi-*

*i*PrOH 2-propanol

DB24C8 *iso*-dibenzo[24]crown-8

J Joules

K degrees Kelvin

K equilibrium constant

k rate constant
kbar kilobar
kcal kilocalories
kDa kilodaltons
kg kilograms
kHz kilohertz
M molar
m- meta-
MD molecular dynamics
Me methyl
MeOH methanol
Me_2CO acetone
MIM mechanically interlocked molecule
min minutes
mM millimolar
mol moles
MS mass spectrometry/mass spectrum
ms milliseconds
MSCC metastable state co-conformation
MTO methyltrioxorhenium
mV millivolts
*M*w weight average molecular weight
N number of molecules
n number
nm nanometers
NMR nuclear magnetic resonance
nN nanonewtons
NOE nuclear Overhauser effect
NOESY nuclear Overhauser effect NMRspectroscopy
NP naphthalene
o- ortho-
OMe methoxyl
p- para-
PEG poly(ethylene glycol)
PELDOR pulsed electron double resonance
Ph phenyl
ppm parts per million

ps picoseconds

PY^+ pyridinium

ref. reference

r.t. room temperature

s seconds

SN_1 unimolecular nucleophilic substitution

SN_2 bimolecular nucleophilic substitution

STTFS tetrathiafulvalene dithioether

T temperature

t time

t or *t-* *tert-*

TBTA tris(benzyltriazolylmethyl)amine

TCM chloroform

TEA triethylamine

TEMPO (2,2,6,6-tetramethylpiperidin-1-yl)oxidanyl

TFA trifluoroacetic acid

THF tetrahydrofuran

TLC thin layer chromatography

Ts tosyl

TTF tetrathiafulvalene

UHP urea hydrogen peroxide

UV ultraviolet

V volts

v/v; v/v volume ratio

w/w; w/w weight ratio

wt. % weight percent

α-CD α-cyclodextrin

β-CD β-cyclodextrin

Δ thermal energy

ΔG change in Gibbs free energy

ΔH change in enthalpy

ΔS change in entropy

δ chemical shift

λ wavelength; persistence length

μ micro

μM micromolar

μm micrometers

$\pi\pi$ bond

ν frequency

$\tau_{1/2}$ half-life

Chapter 1

Introduction

1 Mechanical interlocked molecules

1.1 Catenane, Rotaxane and Knot

<*There is a chemical bound between two atoms or group of atoms in case that the forces acting between them are such as to lead to the formation of an aggregate with sufficient stability to make it convenient for the chemist to consider it as an independent molecular species*>[1].

In this definition Linus Pauling had anticipated the concept of mechanical bonding in his monograph, “The Nature of the Chemical bond” (1931).

Two decades later the mechanical bond became a more concrete concept. In the chemistry field the mechanical bond is a kind of link which is obtained when groups of atoms are sufficiently large to allow the formation of entanglements in space. This kind of bond differs from the chemical bond because is not established between atoms but groups of atoms or molecular entities. Following, the mechanical bond determines the formation of aggregate in space between two or more entities such that they cannot be separated without breaking or distorting covalent bonds between atoms. A molecule with one or more mechanical bonds is considered a mechanical interlocked molecule (MIM).

The main classes of mechanomolecule are represented catenates, rotaxanes and knot[2] (figure 1).

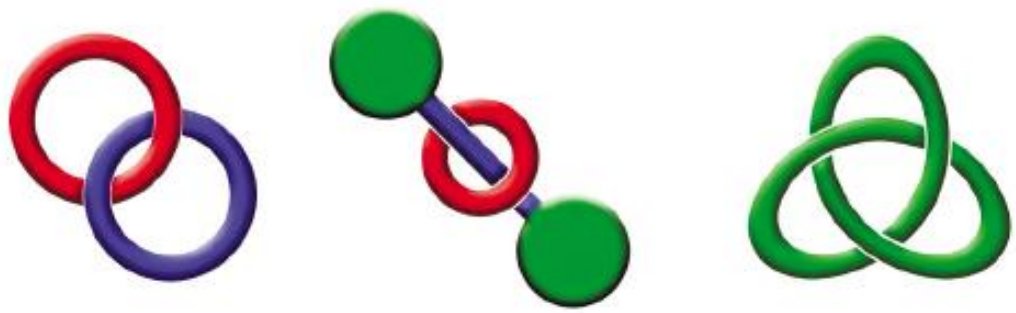

Figure 1. *Graphical representations of catenane (left), rotaxane (middle) and knot (right).*

A catenane,[3] whose name derives from the Latin word *catena* (chain), is composed by two or more interlocked chains. The word rotaxane[3] is derived from the Latin *rota* meaning wheel and *axis* meaning axle. Consequently a [n]rotaxanes based on a macrocycle threaded by a linear component having two end groups, called stoppers bulky enough to prevent the unthreading of the macrocycle and the disassociation of these molecular components. The prefix, n, indicates the number of interlocked components; rotaxanes containing three components of which two macrocycles and one thread are called [3]rotaxanes. This prefix can be used for

catenanes to indicate the number of interlocked chains as well. Architectures similar to rotaxanes, in which the stoppers on the ends of the thread are so small so that the macrocycle can slip off, are known as pseudo-rotaxane.

Not all MIMs own mechanical bond; the classic example is represented by knots, in which is possible to obtain entanglements without distinguishing different component parts.

1.2 Brief History of Synthetic method

Two first examples of successful synthesis approaches of MIMs, in particular of catenane and rotaxane are reported by Wasserman[4] and Harrison,[5] respectively. This synthetic method, known as the statistical synthesis, was based only on statistical probability that two components dissolved in solution were able to interact each other to form the desired complex. In detail Wasserman's approach[4] (1960) was made up of the cyclization of polymethylene chain, possessing two ester groups at both ends, in the presence of a large cycloalkane, to give a catenane in very low yield (Scheme 1). Using the same method, in the 1967, Harrison[5] performed the synthesis of the rotaxane reported in Scheme 1 in 6 % yield. To overcome the problem of the low yield this synthetic method was repeated 70 times.

In the course of time, this poor statistical approach has undergone some changes without increasing significantly the yield because the main limitation of this synthesis is represented by the absence of any stabilizing noncovalent bonding interaction among the different components of the intermediate disfavouring entropically its formation, which is depending simply on statistical probability.

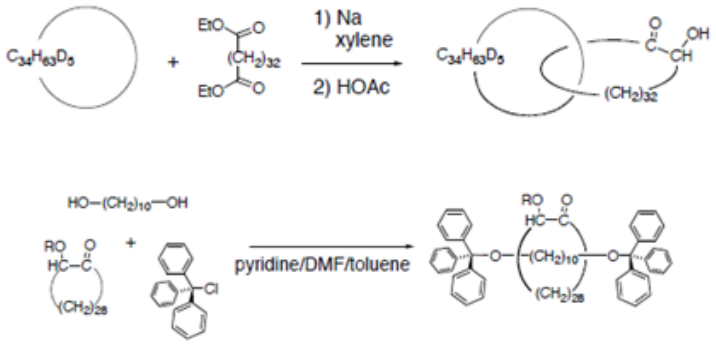

Scheme 1. *Early synthetic procedures to obtain catenane (top) and rotaxane (bottom).*

Another interesting approach is the directed synthesis, supported by Schill.[6] This method consisted in a multistep process which required the formation of precatenane composed of macrocyclic and linear components linked by covalent bonds. Subsequently covalent bonds

determining the association between two components are broken, affording the corresponding catenane. However, this multistep approach, using to synthesize [3]catenane and [2]rotaxane as well, is laborious, time-consuming, and low yielding overall.

These strategies are far from being efficient and too difficult for chemists, having a limited experience in organic chemistry; therefore, this field has been neglect for about 20 years.

The most important turning point came during the 1980s with Jean-Pierre Sauvage,[7] who suggested the development of an efficient metal-ion templating approach to obtain catenanes and, later on, rotaxanes, marking the beginning of the modern era for obtaining the MIMs. The structure of Sauvage catenane's is reported in Scheme 2. Two diphenolphenantroline derivates fit in together in a deep red complex, using of $Cu(ACN)_4^{+}\cdot BF_4^{-}$ form. The metallocatenane intermediate was obtained reacting this stable complex and diiodotetraoxatetradecan in the presence of Cs_2CO_3, under high dilution conditions. The subsequent demetallation afforded the cuprocatenane in 27% yield (Scheme 2). A modification of this synthesis[8] is carried out by mixing the macrocycle, previously synthesized, with a phenanthroline derivative and Cu(I). Complexation of two components to Cu(I) resulted in quantitative formation of the pseudorotaxane as intermediate. Adding glycol chain the macrocyclization and the consequent formation of the catenane was obtained in 42 % yield. The high dilution conditions are necessary to reduce any intermolecular reactions, and consequently to maximize intramolecular cyclization, increasing considerably the yield. Sauvage used copper-phenantroline template strategy to prepare other systems, including rotaxanes.[9]

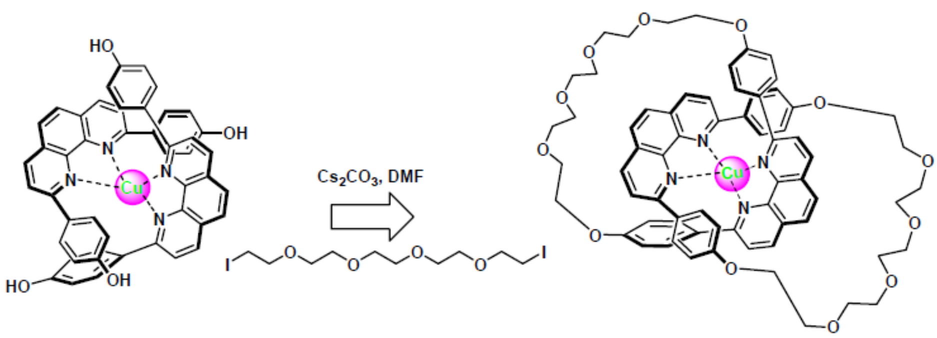

Scheme 2. *Synthesis of [2]catenane using metal coordination.*

Following on from the pioneering work of Sauvage, a number of different systems based on the template effect have been developed. Therefore, this approach became the reference point for the preparation of many rotaxane and catenane architectures.

The field took a giant leap forward when Fraser Stoddart and his co-workers proposed a template synthesis based on three distinct routes: Threading, Capping, Clipping.[10]

"Threading"[11] involves the initial interaction of a preformed macrocycle with one or more complementary recognition sites of an acyclic guest, obtaining a self-assemble complex called [2] pseudorotaxane. During the "Capping"[12] this pseudorotaxane is converted to the corresponding rotaxane by reacting the ends of the threaded guest with two bulky stoppers. Alternatively, the covalent attachment of one stopper, yields a stable [2]pseudorotaxane after the threading of the preformed macrocyclic component. Introduction of a second stopper to the other end of the acyclic component of the [2]pseudorotaxane affords a [2]rotaxane. If the end groups of the dumbbell have an appropriate size compared to the cavity of the macrocycle, thermal energy can be employed to obtain the slipping of the macrocycle over one of the stoppers, while the dynamic complex, becomes kinetically trapped as a rotaxane by cooling. "Clipping"[13] is instead obtained when the macrocycle is assembled in the presence of the complete dumbbell shaped molecule. Analogously, the synthesis of catenanes is called "clipping procedure":[14] 'switching on' the recognition sites of linear component in the presence of a preformed complementary macrocycle, affords a precatenane (also called a [2]pseudorotaxane) which, after macrocyclization, evolves into a [2]catenane, consisting of two different macrocycle components. An alternative method consists of the simultaneous formation of both rings. These approaches for the synthesis of rotaxanes and catenanes are reported in Figure 2.

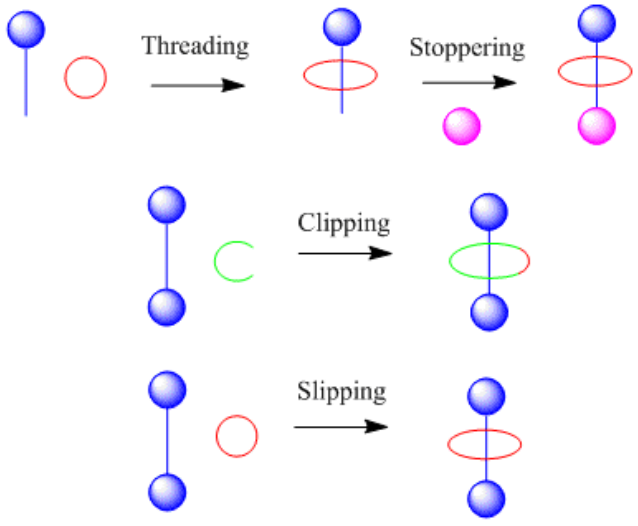

Figure 2. *The routes for rotaxane and catenane synthesis: Threading, Capping or Stoppering , Clipping, Slippage.*

Both [2]pseudorotaxane and precatenane are formed as the result of the establishment of stabilizing noncovalent bonding interactions between specific recognition sites incorporated both into the thread and macrocycle. The different types of interaction, which allow designing various MIM structures with specific properties, can be classified into $\pi - \pi$ stacking donor-

acceptor,[14] hydrogen bonding,[15] hydrophilic interactions[16] and transition metal coordination.[7] In detail hydrophilic interactions are typical of catenanes and rotaxanes having cyclodextrins (CDs) as cyclic component, while transition metal coordination has been previously explained, citing the metal-ion templating approach of Sauvage. In this thesis I will focus the attention especially on the formation of rotaxane structures due to the formation of $\pi - \pi$ stacking donor-acceptor and hydrogen bonding interactions between component parts. The most important examples of MIMs, in which the above mentioned interactions play a role, will be analysed in the following paragraphs. Generally, a combination of these interactions can be identified within MIMs; however, the classification is based on the predominant interaction.

1.3 MIMs based on donor–acceptor interactions

The template strategy introduced by Stoddart[17] during the 1980s was based on the interactions between π-electron acceptors and π-electron donors providing the inspiration for the synthesis of a wide range of mechanically interlocked structures, such as catenanes and rotaxanes.

The cyclobis(paraquat-*p*-phenylene) ($CBPQT^{4+}$),[18] is an interesting member of the cyclophanes's family, class of synthetic macrocycles largely used in supramolecular chemistry for its versatile host-guest properties. In details, $CBPQT^{4+}$ is a tetracationic receptor composed by two 4,4'-bipyridinium units connected thought p-xylylene groups. This macrocycle is considered an electron-accepting moiety due to the presence of positive charges within its structure and consequently exhibits exciting binding abilities with electron-donating aromatic guests such as tetrathiafulvalene (TTF) and 1,5-dioxynaphtalene (DNP) units.[19]

In Figure 3 are reported a redox bistable [2]rotaxane[20] and [2]catenane[21] consisting of $CBPQT^{4+}$, as electron-accepting moiety, interlocked with a dumbbell (for rotaxanes) or ring (for catenanes) incorporating two different electron-donating stations, TTF and DNP, linked together by di(ethylene glycol) chains. The unthreading does not take place because the diisopropylphenol units at the both ends of the dumbbell are bulky enough to behave as efficient stoppers. As previously mentioned, both TTF unit and DNP moiety are suitable recognition sites for this macrocycle, because they are able to establish [π… π], [C-H…O], and [C-H…π] interactions with $CBPQT^{4+}$, thereby they allow introducing bistability into the [2]rotaxane or [2]catenane.

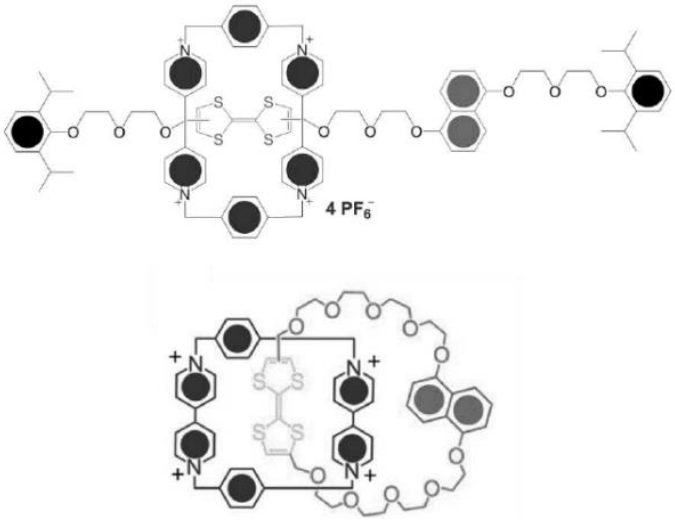

Figure 3. *Example of [2]rotaxane (top) and [2]catenane (bottom) consisting CBPQT^{4+} interlocked with a linear component incorporating two different electron-donating moieties, TTF and DNP.*

Consequently, two translational isomerase considered the ground state co-conformation (GSCC) in which the TTF unit is included inside the CBPQT^{4+} ring, and the metastable state co-conformation (MSCC) where the CBPQT^{4+} ring is located on DNP.[22]

The free energy of binding (ΔG^{o}) of the groundstate co-conformation is 1.6 kcal mol^{-1} lower than of the metastable state co-conformation, causing the bistable [2]catenane[23]/[2]rotaxane[24] exists preferentially (>9:1) as the groundstate co-conformation (Figure 4a and 4b). This preferred conformation is due to the much stronger binding of TTF to the macrocycle compared with DNP. According to thermodynamic data, ^{1}H NMR and absorption spectroscopies, together with electrochemical investigations, reveal the preferential position of the macrocycle.

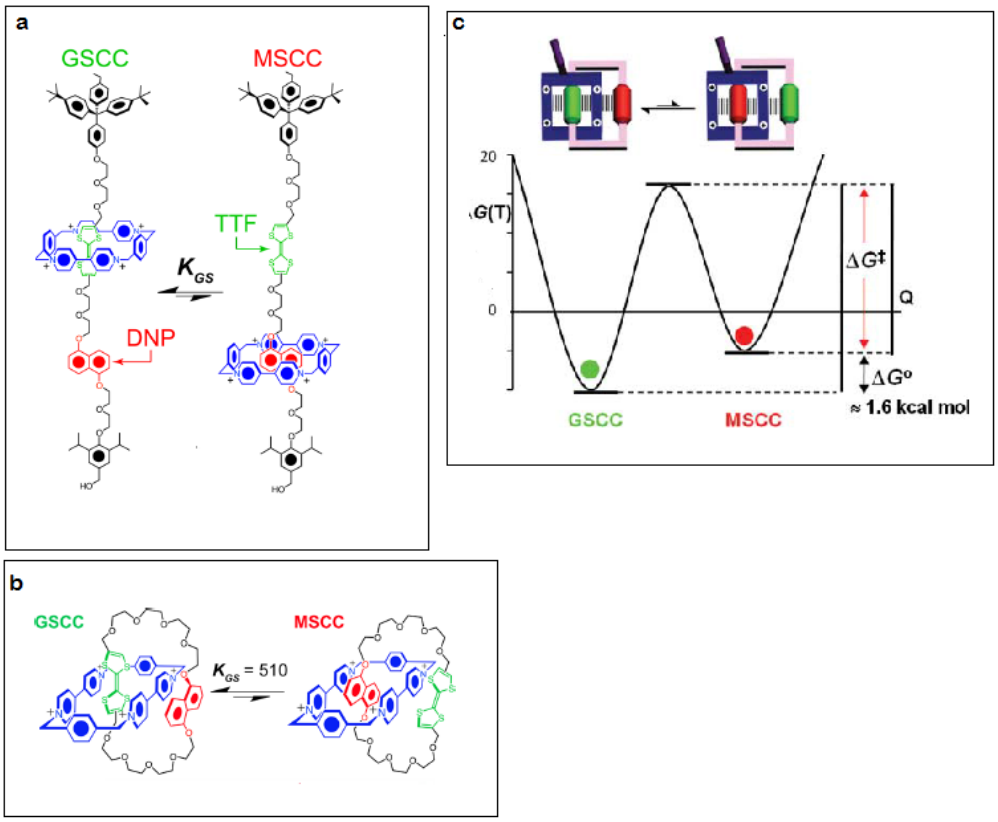

Figure 4. *The graphical representations of the GSCC and MSCC of a rotaxane (a) and catenane (b), illustrating the fact that the GSCC is preferred to MSCC. (c) A comparison of the potential-energy surfaces illustrating the ΔG^{o} for GSCC and MSCC in the bistable [2]catenane and is defined against a normal coordinate Q, representing circumrotation from the GSCC to the MSCC.*

The movement of the macrocycle between the two different stations can be controlled by means of redox stimuli, which can be provided both by the addition of oxidants/reductants and electrochemical method. Indeed, TTF has an extensive redox chemistry, in particular the first two oxidation processes determine the removal of one or two electrons from the redox-active TTF system, resulting in the sequential formation of the TTF radical cation ($TTF^{\bullet+}$) and dication ($TTF^{\cdot 2+}$) respectively. Electrochemical or chemical oxidation of TTF unit to $TTF^{\bullet+}$ induces electrostatic charge repulsion between TTF station and $CBPQT^{4+}$ ring, which drives the $CBPQT^{4+}$ toward the neutral DNP station, altering the GSCC:MSCC exclusively in favour of the second one. The Columbic repulsion of the $TTF^{\bullet+}$ unit, coupled with the π-donor ability of the DNP station, provides a powerful “push-pull” mechanism for the translocation of the $CBPQT^{4+}$ ring along the rotaxane dumbbell component.

Reduction of TTF unit back to its neutral state moves $CBPQT^{4+}$ to its original thermodynamically favored location. Chemical oxidation of TTF to its radical cation is

performed by adding one equivalent of $Fe(ClO_4)_3$. This oxidized form of TTF unit is stable and can be reduced back to its neutral form by adding a stoichiometric amount of ascorbic acid.

1.4 MIMs based on hydrogen-bonding-interactions

Pedersen had discovered the ability of some crown ethers,[25] containing five to ten oxygen atoms, to form complexes with organic and metal cations. These salt-polyether complexes are formed by ion-dipole interaction between the cation and the negatively charged oxygen atoms symmetrically placed in the polyether ring.

As a result of this discovery numerous investigations of the binding of NH_4^+ and RNH_3^+ ammonium ions with crown ethers have been reported. Stoddart and co-workers have designed [2]rotaxanes based on the inclusion complexes between dibenzylammonium ions and crown ethers.[26]

This kind of bistable [2]rotaxane (Figure 5) comprises a dibenzo[24]crown-8 ring (DB24C8) interlocked with a dumbbell component that possesses a dialkylammonium (NH_2^+) and a 4,4'-bipyridinium (BPY^{2+}) recognition sites. Anthracene moiety is used both as stopper unit and probe because its absorption, luminescence, and redox properties are useful to monitor the state of the system. The [2]rotaxane, was self-assembled by using the template-directed threading approach. In detail a pseudorotaxane was made initially by threading the half thread which already contains the ammonium centre and the anthracene as stopper, with the DB24C8. Subsequently a single stoppering reaction with 3,5-di-*tert*-butylbenzyl bromide led to the formation of the bipyridinium dicationic unit and the corresponding rotaxane.

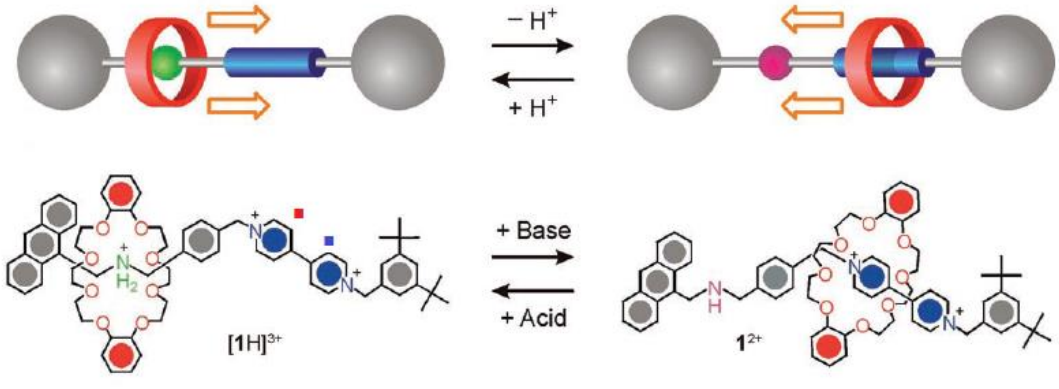

Figure 5. *Chemical controllable molecular shuttle.*

X-ray crystallography[27] has revealed that the macrocycle shows complete selectivity for the ammonium recognition site, which results in the establishment of the non-covalent bonding interactions, in particular [$^{+}$N-H….O] and [C-H….O] hydrogen bonds between the hydrogen atoms of the $^{+}NH_2$ and $^{+}NCH_2$ groups of the thread and the polyether oxygen atoms of the macrocycle, amplified by some stabilizing [$\pi - \pi$] stacking forces between the components. The main consequence is that the reported [2]rotaxane exists as only one of two possible translational isomers. This preferential position of the macrocycle for the dialkyl ammonium units was confirmed by performing NOE spectroscopy of the rotaxane in $(CD_3)_2CO$ at 298 K. Indeed, irradiation of the peak of methylene protons close to the ammonium site reveals significant host–guest enhancement of signals corresponding to the OCH_2 protons of the ring, indicating that the NH_2^+ station is encircled by the crown ether.

Deprotonation of the dibenzylammonium center by using an excess of base induces a quantitative displacement of the macrocyclic ring to the bipyridinium station,[28] because of the lack of hydrogen bonds between the neutral amino group and the macrocycle. However, the original state is restored after the addition of CF_3COOH, which determines the re-establishment of the NH_2^+ recognition site and the shuttling of the macrocycle back on NH_2^+ center.

The shuttling can be followed by ^{1}H NMR spectroscopy by employing the bipyridinium protons $H_\beta{}^1$ and $H_\beta{}^2$ as probes. In the normal state the ^{1}H NMR of the rotaxane shows a single resonance for these protons while after deprotonating followed by the displacement of the macrocycle two distinct resonances can be identified for the protons $H_\beta{}^1$ (red label in Figure 5) and $H_\beta{}^2$ (blue label). The original signal for the protons $H_\beta{}^1$ and $H_\beta{}^2$ is restored when the macrocycle moves back to the initial recognition site, highlighting the reversibility of the molecular shuttling.

This switching process has been investigated in solution by^{1}H NMR spectroscopy as well as by electrochemical and photophysical techniques.

1.5 Motions in Catenanes and Rotaxanes

A fascinating aim is represented by the possibility to control the relative intramolecular movements of components in MIMs. Having control over the motions is a crucial point to provide guidance in developing new and more sophisticated mechanical interlocked structures and in the employment of these movements to perform a practically useful function.

Low energy dynamic processes are specific to most interlocked molecules and include different kinds of translation (linear) and circumrotation (rotary) motion.[29] Pirouetting consists in the rotation of a ring around a fixed axis. This is illustrated for a catenane in Figure 6 and for

a rotaxane in Figure 7. The movement of one ring along the other in a catenane is called spinning. The corresponding linear motion in a rotaxane is named shuttling of a macrocycle along a thread (Figure 7).

Such motions can be referred to as circumrotational (or circumvolutional) when they involve a complete rotation of a macrocycle around the other interlocked unit. In a homocircuitcatenane, i.e., where the two component macrocycles are identical, shuttling and pirouetting are the same process, and therefore, either can describe a circumrotational action. This claim is not valid for heterocatenanes.

These motions can, in principle, be controlled by external stimuli, such as chemical, electrical, or photochemical and consequently have been most extensively studied for their applications in molecular devices.

Another dynamic process less studied is represented by rocking (pendular motion, see Figure 6), which involves changes in the orientation of the planes of the interlocked macrocycles.[30]

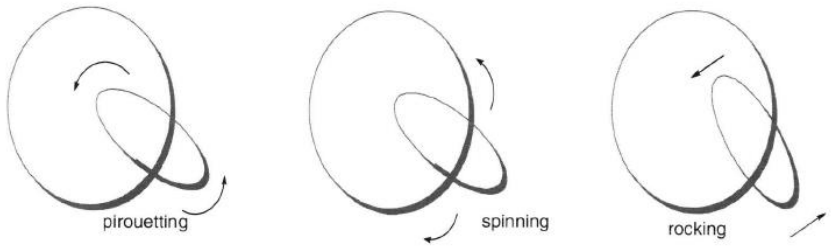

Figure 6. *The three possible macrocyclic ring rotations that can occur in a [2]catenane architecture.*

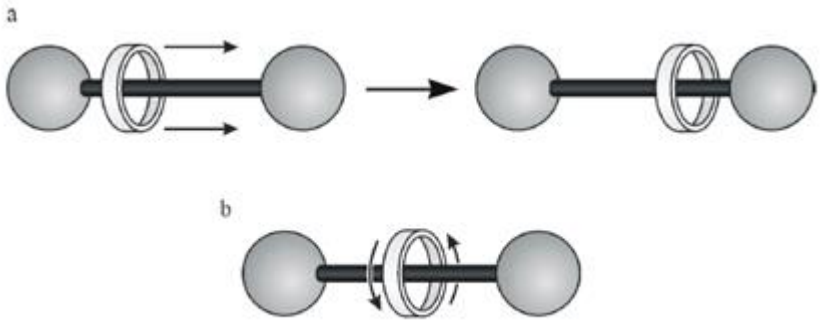

Figure 7. *Schematic representation of some of the intercomponent motions that can be obtained in rotaxanes: shuttling (a) and pirouetting (b).*

The control of the molecular component motions in a MIM is an essential point to design artificial molecular machine. Most of artificial [2]rotaxanes are founded on a macrocycle

shuttling along a linear component. In the next few paragraphs [2]rotaxanes whose operation is based on linear movements will be examined in depth.

2 Molecular Machines

The top-down approach, namely the miniaturization of components employed in the construction of working devices, requires to use progressively smaller and smaller pieces of matter, having intrinsic limitations. A different approach is the bottom-up one,[31] based on the opposite concept to the top-down method; smallest composition of matter characterised by distinct shapes and specific properties, known as molecules, can be assembled in more complicated systems such as molecular machine. This strategy has been developed because of a better knowledge of self-assembly and self-organization processes.

Working in that way, the concept of a macroscopic machine can be extended to the molecular level.

How artificial molecular machines and molecular motors can be defined? They are assemblies of two or more molecular components which after application of appropriate external stimuli (input) can perform mechanical like movements (output). The words motor and machine are often used interchangeably. It should be recalled, however, that a motor converts energy into mechanical work, while a machine is a device, usually containing a motor component, designed to accomplish a function.

Molecular machines and motors have the same features of macroscopic machine:[32]

1) the kind of external stimulus (input) applied to allow its work. In principle, the best energy inputs which drive the movements are represented by photons[33] and electrons[34] because they do not contaminate and compromise the functioning of the system. Consequently, the use of photochemically or electrochemically driven reactions allows to obtain interesting molecular machines.[35] On the contrary, the acid/base reactions, involving the successive addition of acid or base, determine the formation of by-products which can affect the system unless they are removed. The removal process from these systems is not always accessible.

2) The nature of the movements of its components. As mentioned above the mechanical movements taking place at molecular-level machines can be various and are a consequence of formation and cleavage of noncovalent bonds linking the molecular components.

3) The manner in which the movement can be monitored. In this regard, the reciprocal position of the component parts has to associate with significant changes in chemical or physical proprieties of the system, which can be detected by photochemical, electrochemical and spectroscopic techniques.

4) The opportunity to repeat its operation in order to obtain a cyclic process. For this purpose the reversibility of any chemical change or reaction taking place in the system becomes a fundamental requirement. Any kind of chemical process that determines motion of the component parts- isomerization, acid/base reactions, oxidation/reduction processes- can be employed as long as the requirement of reversibility is satisfied.

5) The timescale has to allow the completeness of a cycle. The time necessary to the operation of the molecular machine is strictly dependent on the nature of the components and type of movements and transform nanoseconds to seconds.

6) The function performed. According to the view described above this characteristic is exclusively peculiar to molecular machine.

The first time these molecular machines were mentioned was in 1959 by Richard Feynman (Nobel laureate in physics), who affirmed:[36]

What would be the utility of such machines? Who knows? I cannot see exactly what would happen, but I can hardly doubt that when we have some control of the arrangements of things on a molecular scale we will get an enormously greater range of possible properties that substances can have, and of the different things we can do.

Feynman had already recognized the potential of these molecular machines without having a full understanding of the mechanisms responsible for their operation. Forty years since Feynman the knowledge concerning the molecular machines has made great strides in terms of synthetic methods and characterization of these systems. However, the functions that can be performed by exploiting the movements of the components remain a weak point because most of these systems carried out in solution where incoherence remains a major impediment. In fact, this represented a limit when these systems are designed to obtain molecular-level devices with machine-like characteristics that performed useful functions. Despite laboratory demonstration of the potential utility of molecular machines in information and communication technology (ICT),[37] materials science,[38] catalysis,[39] and medicine[40] has been recently reported, much progress remains to be made at a fundamental level before to allow the use of these molecular machines.

Before examining artificial molecular machine, I will analyse a few examples of natural molecular machines. In effect the greatest source of inspiration toward the design of artificial molecular machines is represented by molecular machines existing in nature. Almost all processes in a living cell are performed by molecular machines.[41] Most of these are made of proteins (with the notable exception of the ribosome, which is mostly made of RNA). One class of molecular machines that is particularly well suited to a physical description is represented by molecular motors which can be defined as devices consuming energy in one form and converting it into motion or mechanical work.

An example of a fascinating rotary motor is the enzyme ATP-synthase[42] which is able to assemble adenosine triphosphate (ATP) from adenosine diphosphate (ADP) and inorganic phosphate exploiting the free energy stored in transmembrane ion gradients. This complex enzyme consists of two regions, the F_0 portion (embedded within the membrane) containing a proton channel and the F_1 portion (outside the membrane) containing three catalytic sites. The schematic structure of this enzyme is illustrated in Figure 8.

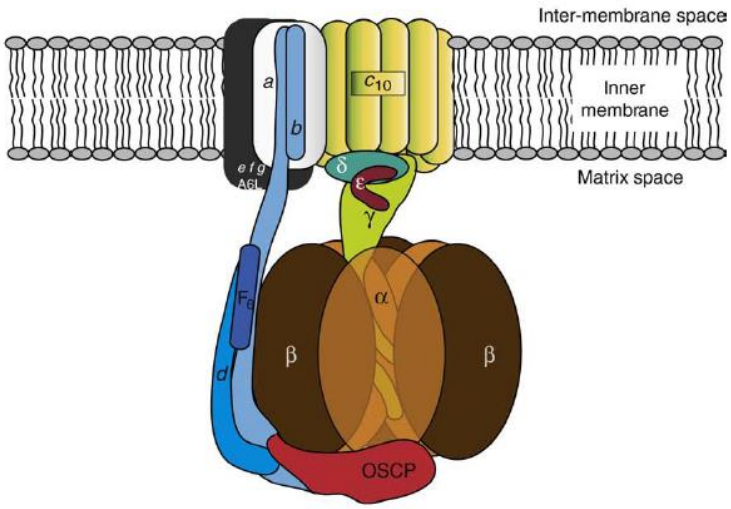

Figure 8. *Schematic structure of F_1F_0-ATP synthase composed of F_1 and F_0 regions.This enzyme is organized in four subdomains: the catalytic headpiece ($\alpha_3\beta_3$), the central rotor stalk ($\gamma\delta\varepsilon$), the stator stalk (b d F_6 f OSCP), and the proton channel (ac_{10}).*

The flow of the protons through the channel of F_0 (input) generates the movement of enzyme components, in detail a torque of F_0 which is transmitted to F_1. The spinning within F_1 determines the release of ATP molecules from the three active sites. The ATP synthase is a combination of two motors working together, an electric motor (F_0) and a chemical motor (F_1). The F_0-F_1-ATP synthase is reversible because can catalyse both the synthesis and hydrolysis of ATP to ADP and Pi. All things considered ATP-synthase satisfies the requirements above mentioned for the molecular machines, representing a natural molecular machine based on a rotary motion.

Differently, natural molecular machines using a linear motion to perform their operate are represented by motor proteins, such as myosin, kinesin, dynein.[41] These essential proteins are enzymatic molecules that convert chemical energy, typically obtained from the hydrolysis of ATP, into mechanical work associated with linear movements of some components. Molecular motors that move unidirectionally along protein polymers (actin or microtubules) drive the motions of muscles, as well as much smaller intracellular cargoes. Particularly, myosin which

is one of the major components of muscle, plays an essential role in the contraction of voluntary muscles (running, walking, etc.) as well as involuntary muscles (beating heart). Myosin is composed by two end heads connected to a long filament. The myosin molecules are interdigitated with thinner actin filaments in the sarcomere, forming the basic contractile unit of muscle. Each myosin head has two binding sites: one selective for ATP where the hydrolysis of ATP occurs and another for actin. Initially myosin through its specific binding site binds the ATP, hydrolysing it in ADP and P and forming the complex myosin–ADP-P that is however not able to attach to its corresponding site in the actin because this site is blocked by troponin linked to the tropomyosin.

The entry of Ca^{2+} into the cell, a necessary input for the contraction, induces the formation of troponin-Ca^{2+} complex causing radical conformational changes which determine tropomyosin to slide over and unblock the remainder of the actin binding site. Unblocking allows the two myosin heads approach and the bond with actin forming actomyosin system. Upon binding with actin, the myosin head releases the inorganic phosphate, determining the formation of a power stroke. This stroke moves the actin filament inwards, shortening the sarcomere and affording the muscle contraction, which is the most obvious macroscopic manifestation. At the end, ADP is released from the myosin head, leaving myosin attached to actin in a rigor state until another ATP binds to myosin. The myosin motor dissociates from the actinfilament, and a new cycle starts. The complete molecular mechanism is reported in Figure 9.

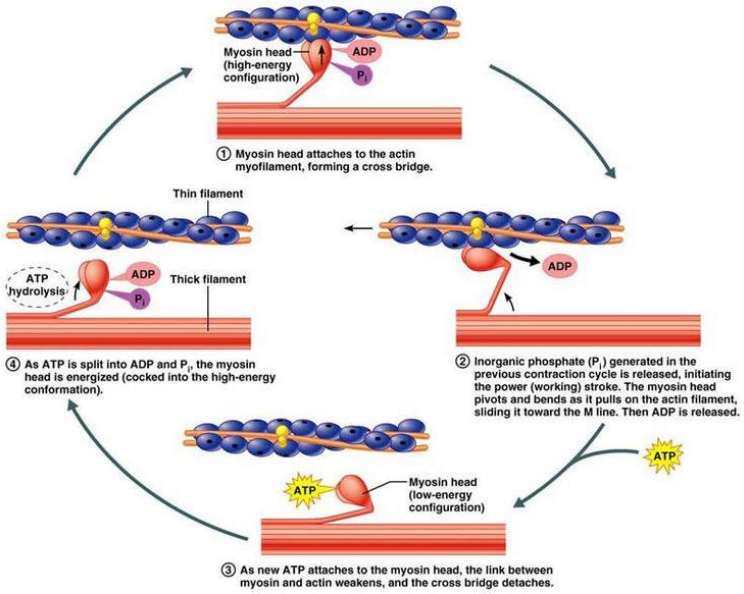

Figure 9. *Schematic representation of the molecular mechanisms involved in the muscle contraction.*

2.1 Toward artificial molecular machine

Countless such machines exist in nature and it is possible to build artificial ones by mimicking the nature. In this direction, the most serious limit of natural molecular machines lies in their complexity related both to the structure and mechanism which is at the base of their operation, not allowing their artificial reproduction. In effect the bottom-up construction of machines as complex as those present in nature is an impossible aim. Therefore, chemists have tried to construct much simpler systems, without recurring the complexity of the biological structures but respecting the molecular machine definition, namely an assembly of a discrete number of molecular components in which the component parts can display changes in their relative positions as a result of some external stimulus. In this context, rotaxanes and catenanes are appealing systems for the construction of molecular machines because motions of their molecular components can be easily obtained and controlled.

Molecular shuttles in which thermal energy fuels the relative motion of their component parts represent the first step toward molecular machines. The rotaxane reported in Figure 10 is an example of molecular shuttle studied by Stoddart in 1991.[43]

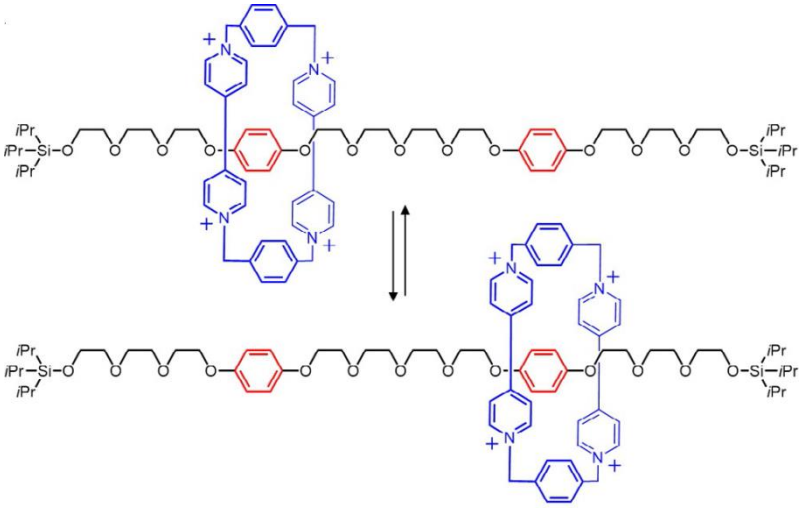

Figure 10. *Example of prototype molecular machine powered by thermal energy.*

This [2] rotaxane is composed by a dumbbell containing two equivalent electron-rich recognition sites and an electron-poor ring. The ring is not located on one of two recognition sites but the result is a degenerate co-conformation equilibrium state in which the macrocyclic component darts back and forth around 2000 times a second at room temperature between the two stations. This structure is known as molecular shuttle. This system can be energetically represented as a double-minimum potential in which it is possible to identify two equivalent minima corresponding to the two stations and an energy barrier deriving from ethylene glycol

bridge (Figure 11).[44] The height of the energy barrier is closely related to the nature of the rotaxane and for the cyclophane–polyether systems is 13 kcal.mol^{-1}.

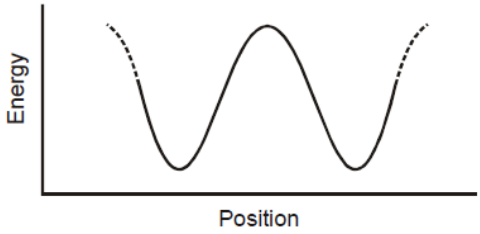

Figure 11. *Potential energy curve for a cyclophane on a polyether thread, bearing two electron-rich hydroquinone groups.*

At room temperature, in solution the cyclophane's kinetic energy is high enough to overcome the energy barrier and the shuttling takes place. If the solution is cooled down to –50 °C, the shuttling motion ceases. Summarizing, a [2]rotaxane containing two equivalent stations can be considered a molecular shuttle because the ring, having a kinetic energy higher than the energy barrier, moves randomly between two recognition sites.

In order to gone step further and turn a molecular shuttle into a molecular switch, bistability has to be introduced into the system. The most intuitive way to generate bistability is to design a [2]rotaxane possessing two chemically different recognition sites[45] in the dumbbell, exhibiting different degree of affinity for the macrocycle. In this case, the two stations are characterised by different values of energy minima causing the macrocycle becomes preferentially localised in the station with the lowest energy, i.e. in station 1 reported in Figure 12.

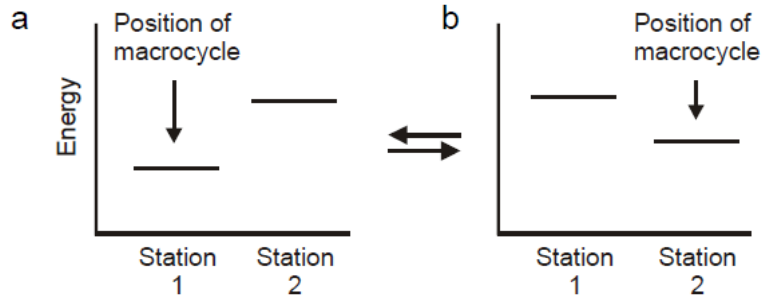

Figura 12. *Potential energy diagrams for a molecular switch.*

The application of external stimulus affecting on chemical properties of one of two recognition sites, switches off the stronger station and inverts the relative energy levels of two stations, thus determining a change in the macrocycle location, which shifts from station 1 to station 2.

A system in whichthe ring position between different stations can be controlled reversibility by external stimuli is called molecular switch and it represents a key step towards the development of molecular machines (Figure 13).

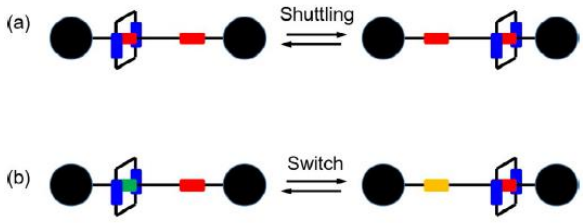

Figure 13. *a) Graphical illustration of a molecular shuttle in which the ring moves randomly between two identical recognition sites. b) A molecular switch in which the ring is located on a favorite station and its movement is obtained modifying the proprieties of the system.*

The outside stimulus used to obtain such molecular switches must be able to break and create the non-covalent bonds that occur between the macrocycle and the recognition sites of the dumbbell. Therefore, the suitable stimulus depends on the nature of these bonds and chemical properties of molecular components involved in the switching.
Our research work is focused on two types of molecular switch: *chemically driven molecular switches* and *electrochemically driven molecular switches*.

Chemically driven molecular switches[26]

As regards to chemically driven switch the stimulus that determines the movement of the macrocycle into a bistable [2]rotaxane is generally represented by the addition of an acid or base.
A system which behaves as a chemically controllable molecular switch is [2]rotaxane shown in Figure 5 and analysed in detail in Paragraph 1.4. It is made of a dibenzo[24]crown-8 (DB24C8) macrocycle and a dumbbell-shaped component containing a dialkylammonium center and a 4,4'-bipyridinium unit. This system can be considered as a molecular switch due to the presence of two different recognition sites in the dumbbell component. The macrocycle is located on NH_2^+ station because the hydrogen bonding interactions between the DB24C8 macrocycle and the ammonium centre are much stronger than the electron donor-acceptor interactions of the macrocycle with the bipyridinium unit. Deprotonation of the ammonium center with a base effects the displacement of the macrocycle to the bipyridinium unit; reprotonation directs the macrocycle back on to the ammonium center.

It is worth to note that switching cycle requires successive additions of acid and base causing the formation of side products, which might affect the system. For this reason, the focus has been shifted to electrochemically driven molecular switches lacking this drawback.

Electrochemically driven molecular switches

An example of molecular switch[20] activated by electrochemical stimulus is described in section 1.3 and consists of a bistable [2]rotaxane having $CBPQT^{4+}$, as electron-accepting moiety, interlocked with a dumbbell possessing tetrathiafulvalene and 1,5-dioxynaphthaleneunits, as strong and weak recognition sites, respectively. In keeping with detailed definition of molecular switch this system possessing different recognition sites, represents an interesting member of molecular switches. This switching has the great advantage of being controlled by an electrochemical stimulus, which prevents the contamination and the resulting turning off the system.
These molecular switches are a further step towards the molecular machines but they are not defined as such because lacking the ability to deliver useful work.
In the next paragraph, molecular machines consisting of bistable [2]rotaxanes will be analysed.

2.2 Application of MIMs

MIMs have been studied in depth by chemists in the last 50 years, paying specific attention to rotaxanes and catenanes. The design, synthesis and investigation of chemical systems able to function as molecular machines and motors is of interest not only for basic research, but also for the growth of nanoscience and the subsequent development of nanotechnology. As mentioned above the field of applications represents a weakness because the molecular-level machines described in this thesis operate in solution, that is, in an incoherent fashion.
The solution studies of these complicated systems are a fundamental point but, in order to employ them as molecular machine, they should be organized at interfaces,[46] deposited onsurfaces,[47] or immobilized into membranes,[48] or porous materials.[49] In this way they can behave coherently.
The most important systems interfaced with the macroscopic world and related with the previously described structures are presented below.

2.2.1 Artificial muscles

In the previous section, the mechanism at the base of the muscle contraction was examined in detail, namely the unidirectional movement of a thick myosin filament along a thin actin filament. Appropriately designed rotaxanes can emulate the behaviour of artificial muscles.
An interesting example is reported by the groups of Ho and Stoddart[50] and consists of a rotaxane muscle that contracts and expands in response to electrochemical oxidation or reduction. This model differs from the daisy chain approach described by Sauvage[51] who was amongst the first to recognise the ability of a double rotaxane to imitate the action of biological muscles.
This system reported in Figure 14, is made by a [3]rotaxane containing a single palindromic axle and two rings. The rings are based on $CBPQT^{4+}$ and the axle incorporates two pairs of complementary TTF (green) and DNP (red) recognition stations arranged symmetrically along the axle component. DNP stations are positioned at the centre while TTF moieties are located at the outsides of the axle. The rigid moiety between the two DNP stations, spaced of about 1.4 nm, assures the rigidity of the backbone balancing the flexibility due to the glycol chains, which are important to maintain enhanced yields for the template-directed synthesis of the rotaxane. Considering that the molecule is fully stretched, the distance between the $CBPQT^{4+}$ rings can be varied from between ca. 4.2 to ca. 1.4 nm apart.
The $CBPQT^{4+}$ ring possesses a dramatically greater affinity for the TTF unit than for the competing naphthalene ring system.

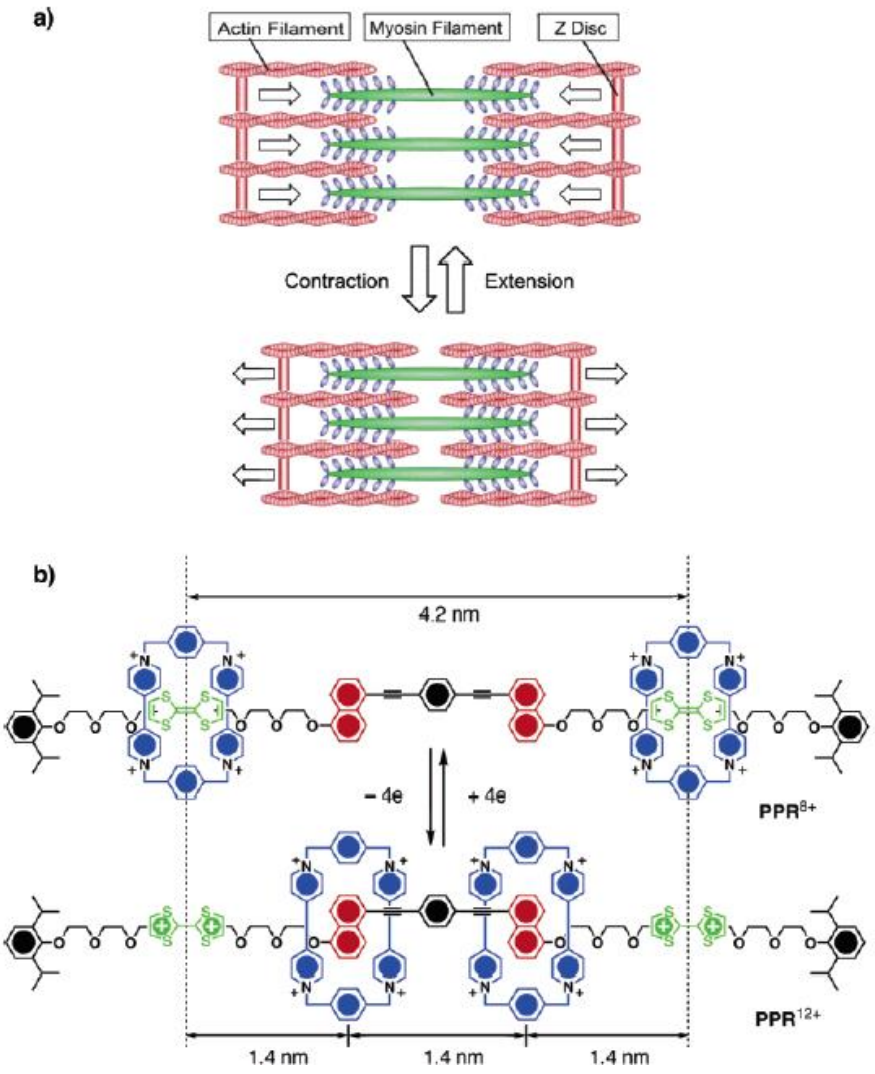

Figure 14. *(a) Graphical representations of the constitution and cycle of contraction and extension of the sarcomeres. (b) Molecular structures of the [3]rotaxane in its extended (top) and contracted (bottom) state.*

The chemical oxidation of TTF units to their dication radical form determines a electrostatically repulsion between the macrocycles and TTF recognition sites and drives them towards the now favourable DNP stations, obtaining the contracted state. A subsequent reduction of TTF^{2+} dication to their neutral form induces the displacement of the macrocycles to their original thermodynamically favored positions, carrying out the extended state. The initial state could be restored after passive diffusion due to the electrostatic repulsion between two rings. This system is not yet able to mimic the skeletal muscle contraction.

In order to explain this function the rings were functionalised with a disulphide tether to allow their immobilisation on a gold-coated silicon cantilever array (Figure 15a).[50] When this array, housed within a solution cell, was treated with chemical oxidants ($Fe(ClO_4)_3$) the cantilevers were able to bend upwards by ca. 35 nm to an apparent saturation point in 1 min. The

subsequent addition of ascorbic acid as reductant brought the cantilevers back to their original positions. The movement of the cantilever beams is directly correlated with the cycling of the oxidant and reductant solutions.The cantilevers were shown optically to bend back and forth over at least 25 cycles[52] (Figure 15b). After 25 cycles, a slight attenuation ascribing to chemical and/or physical degradation of the applied monolayer of rotaxane molecules was observed.

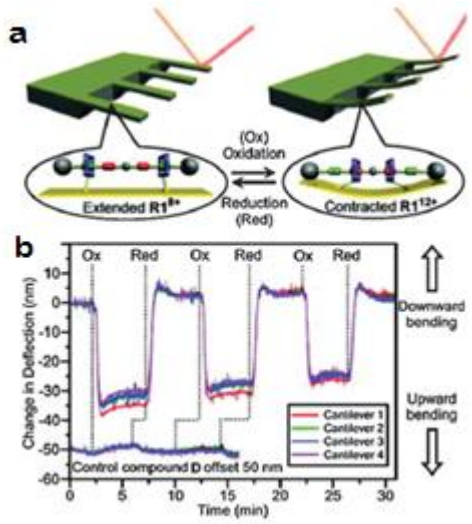

Figure 15. *(a) By attaching the macrocycles to a gold coated silicon cantilever array, the cantilever could be bent. (b) Repeating bending of the cantilever.*

These redox bistable [3]rotaxanes aligned randomly on an unordered surface can perform a macroscopic effect due to their ability to work together, representing interesting examples of molecular machines.

2.2.2 Molecular Elevator

Another molecular machine based on linear movement is the molecular elevator developed by the groups of Stoddart, Balzani and Credi.[53]

The molecular elevator reported in Figure 16, comprises a trifurcated rig-like component (compound **2**) bearing three of the dumbbell-like components of the [2]rotaxane, which are linked at one of their ends *via* aromatic central core. These dumbbells bear competitive recognition sites positioned at two different levels, namely a dialkylammonium (NH_2^+) station anda 4,4'-bipyridinium (BPY^{2+}) moiety.

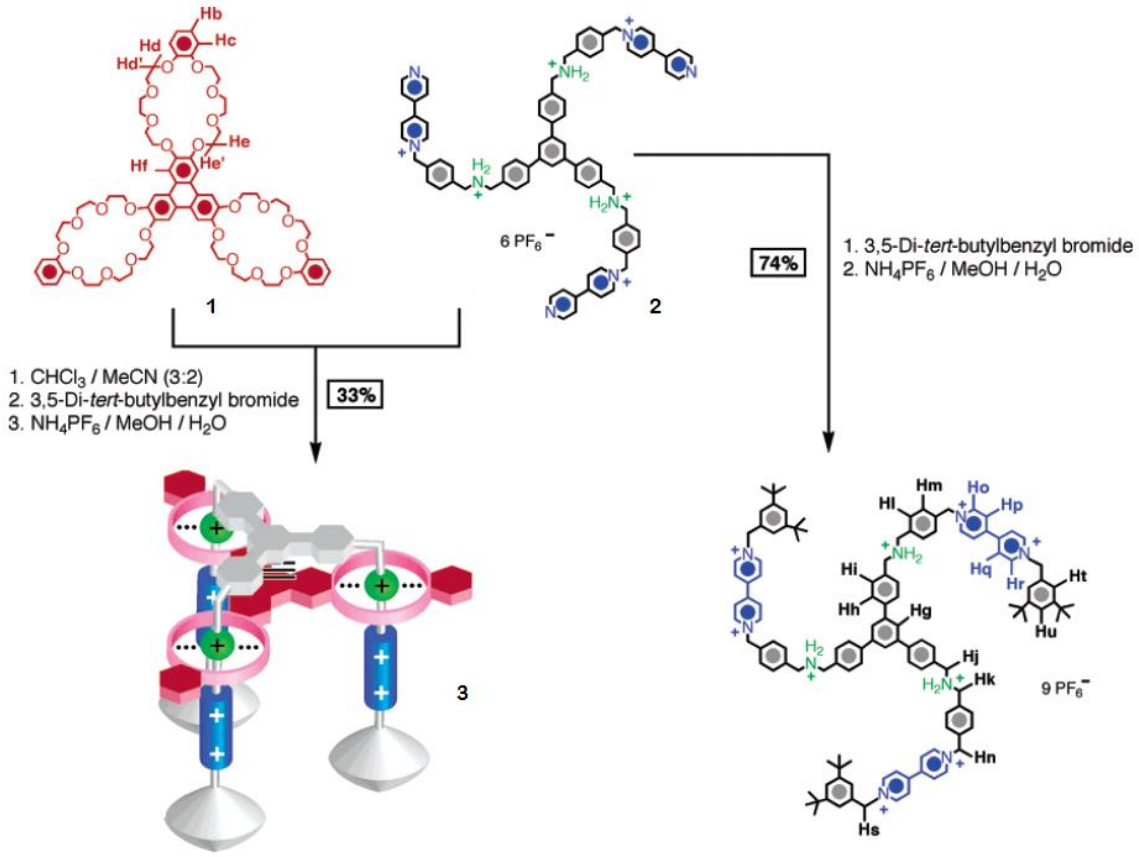

Figure 16. *Schematic representation of the first generation of the molecular elevators. The trifurcated guest salt **1** and the tritopic host **2** in a TCM/ACN solution form a 1:1 adduct, was converted to the molecular elevator.*

Three macrocyclic rings, represented by dibenzo[24]crown-8 (DB24C8), are fused onto a triphenylene core to form a tritopic platform (compound **1**). The bistable tripod-shaped component is triply interlocked with the tritopic platform forming the first generation of molecular elevators. The tris-crown ether platform is located on ammonia stations, which allowed for the formation of hydrogen bonds interactions with the rings. Deprotonation of the ammonium center by using phosphazene as base induces a quantitative displacement of the tritopic platform to the bipyridinium stations. Reacidification drives the platform back up to the ammonia stations suggesting the reversibility of this process.

The tritopic platform was successively modified by introducing dioxynaphthalene π-electron-rich to obtain the second generation of the molecular machines that acts like nanometer scale elevators (Figure 17). This structural modification confers stronger electron donating proprieties compared with the simple benzo units directing and enhancing the formation of $[\pi - \pi]$ stacking and charge-transfer (CT) interactions with the electron-acceptor bipyridinium (BPY^{2+}) units.[54]

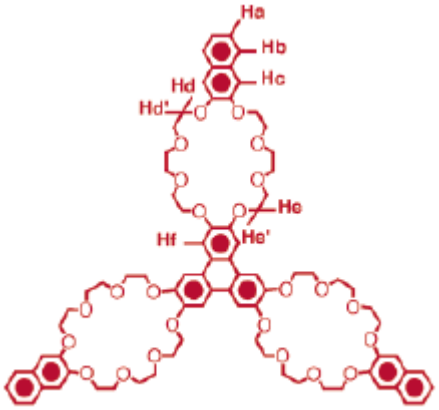

Figure 17. *Tritopic platform modified by introducing dioxynaphthalene π-electron-rich units onto the termini to obtain the second generation of molecular elevators.*

Both the first and the second generation of molecular elevators were obtained using a template directed approach in 33 and 23% yield, respectively. The trifurcated guest salt and the tritopic host in a TCM/ACN solution form a 1:1 adduct (super bundle) which was converted to the corresponding molecular elevator reacting with 3,5-di-tert-butylbenzyl bromide, followed by counterion exchange (NH_4PF_6/MeOH/H_2O).

Both systems and their component parts were all characterized by ^{1}H NMR spectroscopy, including ^{1}H-COSY and TROESY two-dimensional experiments to achieve full assignments in the cases of the molecular elevator systems.

This molecular elevator does not work exactly like a macroscopic lift. Indeed, a more detailed investigation on the mechanism of the elevator motions obtained by observing the changes in the voltammetric and spectroscopic properties of the compounds upon titration with the base, reveals the presence of three quite distinct steps indicating that the three deprotonation processes are not equivalent. This is confirmed by molecular modeling that suggests the possibility to obtain species in which two (or one) ring(s) surround NH_2^+center(s) and one (or two) rings surround(s) BPY^{2+} unit(s). Hence, the platform, being associated with the three-deprotonation processes, descends one ring at a time. The authors described this one-at-a-time mechanism using this metaphor: “the molecular elevator is more reminiscent of a legged animal than it is of the passenger elevator”.

From the redox potential and thermodynamic constant values, it could be estimated that the energy available for the upwards and downwards movements is >4 kcal mol^{-1} and 21 kcal mol^{-1}, respectively. In response to the chemical stimuli, the platform component travels a distance of 0.7 nm from the upper to the lower level of the rig, generating a force up to 200 pN, a number which is one order of magnitude higher than that exerted by the natural motors, like myosin and kinesin.

2.2.3 Valves

A macroscopic valve is a device that regulates, directs and controls the flow of a fluid (gases and liquids) by opening, closing or partially obstructing various passageways, exploiting the movement of its component parts. Basing on this definition, a nanoscale valve has to supply suitable requirements: (i) movable control elements, (ii) a method for operating, and (iii) appropriately sized passageways. Molecular machines represent interesting systems in the development of nanovalves, holding all of these requirements. The first example of nanovalve is reported by the group of Stoddart and Zink.[55] This system employed [2]bistable rotaxane having a $CBPQT^{4+}$ macrocycle and an axle incorporating a TTF and a DNP station. This [2]bistable rotaxane shown in figure 18a and structurally similar to the previously mentioned rotaxanes, is settled on the surface of mesoporous silica particles through the formation of carbamate linkage between the hydroxyl group on one of the two different stoppers and the isocyanate group of the silicate surface.[56]

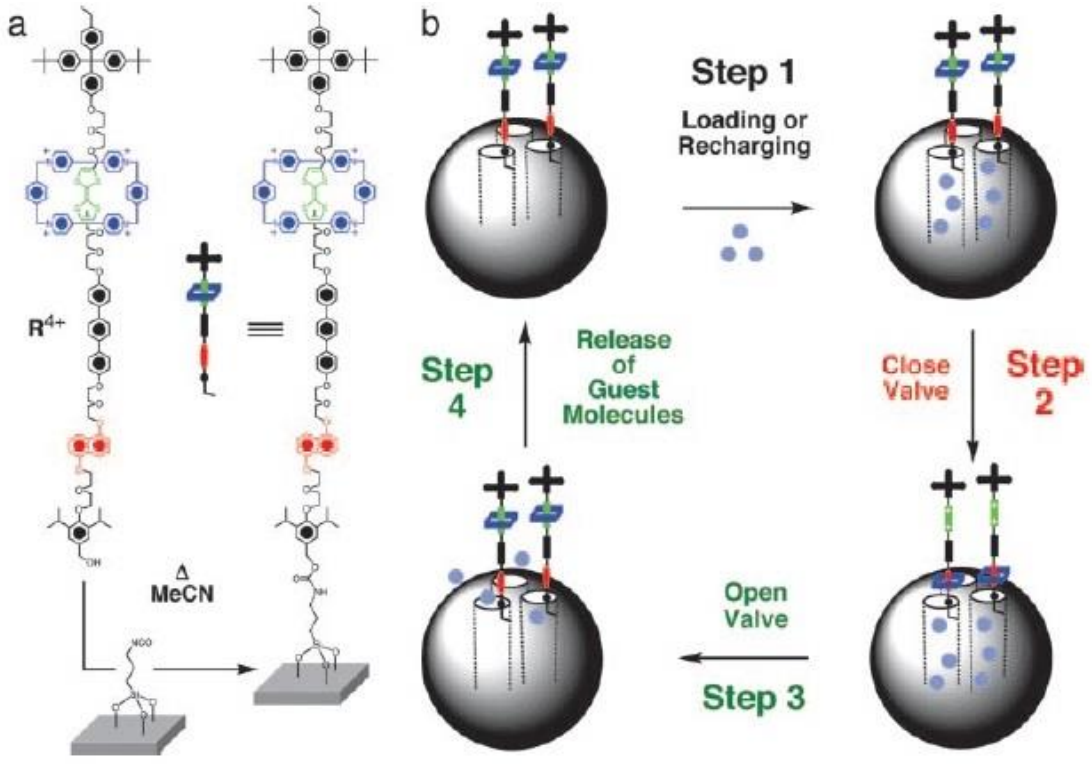

Figure 18. *(a)The structural formula of a nanovalve based on a redox responsive bistable [2]rotaxane. (b) The proposed mechanism for the operation of the nanovalve.*

The proposed mechanism for the operation of the nanovalve is illustrated in figure 18b. When the $CBPQT^{4+}$ ring is located on the TTF station the valve can be defined “open”, allowing the

loading of the guest molecules (turquoise spheres) by diffusion into the open pores (step 1). Oxidation of the TTF unit to its radical dication determines the movement of $CBPQT^{4+}$ ring to the DNP station, which is closer to the openings of the pores. In this state, the valve is close and prevents the release of the guest molecule because the openings of the cylindrical pores on the silica are blocked by the presence of $CBPQT^{4+}$ ring (step 2). The addition of ascorbic acid (step 3) reduces the TTF radical dication back to its neutral state, determining the relocation of $CBPQT^{4+}$ ring around TTF station and the reopening of the valve. The opened state after releasing of the guest molecules is ready for recharging (i.e., returning to step 1).Thus, the valve can be closed and opened reversibly by the movement of $CBPQT^{4+}$ ring (blue), which shuttles between a TTF station (green) and a DNP station (red) under redox control. Luminescent guest molecules such as fluorescent iridium complex ($Ir(ppy)_3$) that do not react with the redox reagents are loaded into the pores, in order to measure the confinement and release of these luminescent molecules by monitoring their luminescence in solution at 506 nm, which is the maximum emission band. In the 'open' state, a fluorescent iridium complex diffuse into the pores of the particle. Addition of $Fe(ClO_4)_3$ determined the closing of the valve and the trapping of the fluorescent iridium complex inside the valve. When the valve is closed the fluorescence spectroscopy did not reveal the leakage of the guest molecules through the pores, as a consequence a flat baseline was obtained. Addition of ascorbic acid determines the opening of the valve and a consequent and fast increase in emission intensity is observed, suggesting that trapped molecules are released from the pores. In Figure 19 the release of $Ir(ppy)_3$ over time is reported.

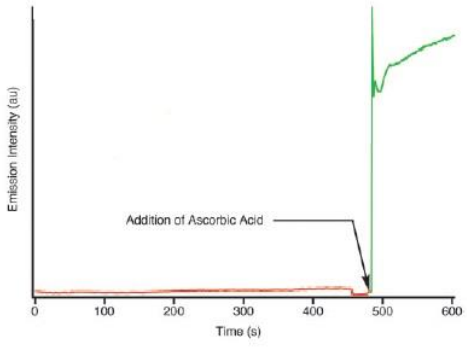

Figure 19. *Release of the $Ir(ppy)_3$ molecules from the pores can be monitored by luminescence spectroscopy.*

The same fluorescence studied have been conducted using cationic compounds as guest molecules such as rhodamine B, to exclude that electrostatic interactions between the guest molecules and the functional material affect the operation of the valve.

Furthermore, it has been shown that the release process was not a result of an artifact of the conditions but occurred in concert with the shuttling of tetracationic cyclophane between the DNP and the TTF station, by following the luminescence of the DNP station. When the valve is close, the $CBPQT^{4+}$ ring quenched the luminescence of DNP station, while when the valve is open the naphthalene intensity increases 4-fold, lacking the quenching effect of the macrocycle.

These studies have been made to establish proof of principle and establish the nanovalve action. This operational valve is a true molecular machine consisting of a solid framework, which is able to perform a specific task by means of the movement of its component parts. Systems of this kind are especially interesting because they could be used to obtain the controlled release of drugs.

3 Spin Labelling

3.1 Introduction of Nitroxides

The host-guest complexes have been studied by a variety of spectroscopic methods and important information about the structure and operation of these systems are reported in the scientific literature. However, NMR spectroscopy, which is one of the most important method for obtaining structural elucidation, does not allow achieving a complete and accurate characterization of these systems, especially as regards the kinetic of the association and dissociation processes, which occur in the microsecond and submicrosecond time range.[57] This limitation is due to the nature of these processes taking place at higher frequencies which are not accessible (or accessible only in very peculiar situations) to NMR. Thus, in most cases, the peaks in the NMR spectra are obtained as the weighted averages between the signals of free and complexed molecules since the exchange between free and complexed species is usually too fast (the time range is between 10^{-5} and 10^{-9} seconds) and this technique operates at a time scale relatively slow.[58] On the contrary the electron spin resonance (ESR) spectroscopy is characterized by a faster time scale compared to NMR allowing to detect different signals for the complexed and uncomplexed forms.[57b] Thus, ESR represents an appealing technique which has been exploited to investigate the kinetics of association and dissociation in supramolecular chemistry and to valuable mechanistic information on the dynamics of these processes. ESR is responsive to transitions involving unpaired electrons and therefore can be used for studying paramagnetic species containing one or more unpaired electrons.

Unfortunately, rotaxanes and catenanes do not generally contain paramagnetic units and in order to employ ESR spectroscopy for their characterization free radicals are introduced ad hoc either covalently (spin labels) or non-covalently (spin probes). Any free radical or paramagnetic metal ion or even a group with an accessible triplet state,[59] could be used but the most widely used class of stable spin probes and labels is represented by nitroxide compounds[60] containing the paramagnetic N–O unit.

The most representative member of this class is 2,2,6,6-tetramethylpiperidine-N-oxyl (TEMPO), which is shown in Figure 20 together with other nitroxide derivatives.

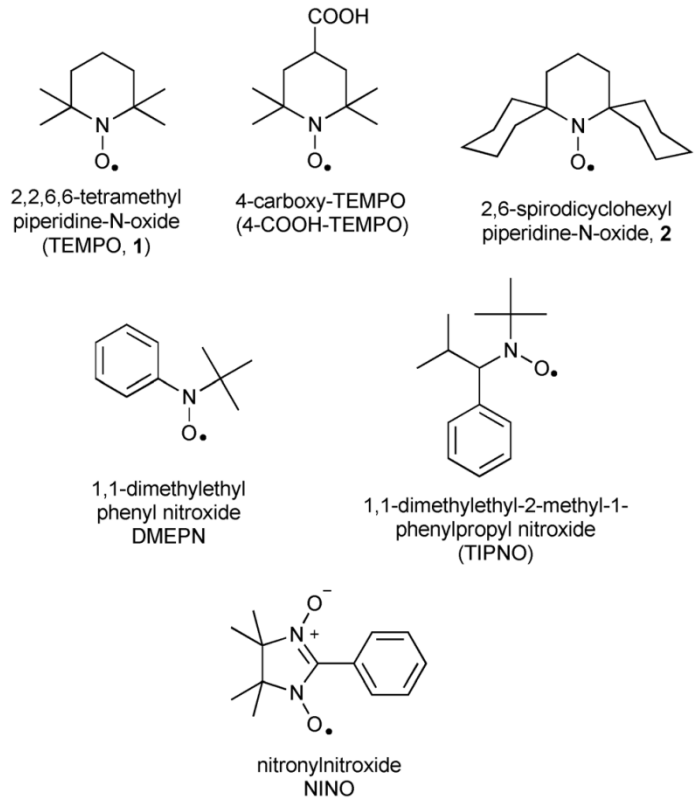

Figure 20. *Some representative nitroxide radicals.*

Their resonance structure (Figure 21) shows the existence of a stabilizing $\pi_{N\text{-}O}$ three-electron bond with an unpaired electron in a π^* orbital and large spin density on both N and O (aminoxyl group). As consequence of this stable electronic arrangement these radical do not undergo dimerization at the oxygen atom, because the gain in energy from dimerization is lower than the loss of resonance energy of two aminoxyl groups.

Figure 21. *The resonance structures of nitroxide radicals.*

Their lifetime instead is mainly determined by the tendency to react with themselves via disproportionation obtaining the corresponding hydroxylamine and nitrone compounds. The possibility of disproportionation is related to the presence of hydrogen atoms in the β position. Thus, dialkylnitroxides like TEMPO, lacking hydrogen atoms in the beta position, are very persistent molecules.

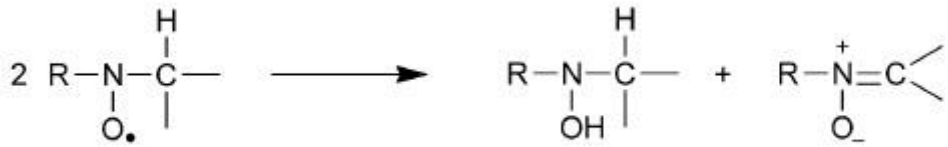

Figure 22. *Disproportionation process for a dialkyl nitroxide containing a hydrogen atom at the β position.*

Their stability and persistence allow the safely employment of these radicals in common organic reactions without modifying their paramagnetic proprieties, making them the best candidates as paramagnetic probes. The aim of this thesis was to use the spin-labelling approach, namely the introduction of specific nitroxide labels into a [2]rotaxane by formation of covalent bonds, in order to increase the information on these systems by using ESR spectroscopy.

In the field of [2]rotaxanes three main different situation can be investigated: i) the spin label is covalently bound to the macrocycle; ii) the spin label is bound to the dumbbell component of the rotaxane; iii) both macrocycle and dumbbell are spin-labelled.

This spin-labelling approach was reported for the first time by the group of Lucarini, who was the first to functionalized rotaxanes with nitroxides moieties, detecting and identifying the rotaxane formation and clarifying their structure and properties by using this technique. In particular, they reported in 2006[61] the first example of a spin-labelled rotaxane, having a dumbbell functionalized at the both ends with TEMPO moieties and α-CD as the wheel component. Other examples of spin-labelled rotaxanes will be discussed in detail in following chapters.

3.2 Electron Spin Resonance (ESR)

I have already mentioned how ESR spectroscopy, also known as EPR (Electron Paramagnetic Resonance), is able to extend the time range into the microsecond region, obtaining kinetic information on the formation of host-guest complex.[62] This technique offers other interesting advantages: 1) the high sensitivity, which makes possible to detect free radicals at concentrations of the order of 10^{-6} M; 2) the ability to measure distances between spin labels in the nanometer range,[63] than Angstrom scale as usually observed in NMR measurements; 3) only unpaired electrons are responsible for the ESR signals. Thus, even complicated systems frequently result in very simple ESR spectra.

3.2.1 Principle of spectroscopy

The electron with its spin has an associated magnetic moment just as does the proton. The spin of an electron is characterized by the *s* quantum number. Quantum mechanics shows that the electron has two spin states corresponding to the two orientations in space. In the absence of an external magnetic field, the electron spin is oriented randomly in space. If a magnetic field, B_0, is applied, the energetic level of the free electron is split in two because of the Zeeman effect. The two levels are separated by ΔE:

$$\Delta E = g \cdot \mu_B \cdot B_0$$

Where *g* is a dimension less proportionality constant (generally referred to as the *g*-factor) and μ_B is the Bohr magneton. If an electromagnetic radiation is applied one induces a transition between the two spin states, called electron spin (or paramagnetic resonance). For the study of organic radicals, a frequency of about 9000 MHz, provided by a microwave source, is generally employed. Because of Boltzmann factor (as found with NMR), the use of higher frequency should increase the sensitivity, but in practice this is about compensated by the smaller size of the cavity resonator, and hence the need for small samples.

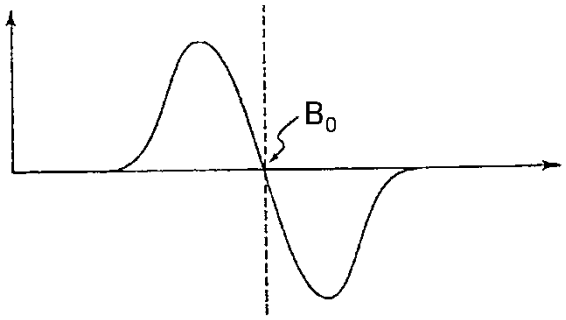

Figure 23. *Curve used in the presentation of ESR spectra: first derivative of absorption curve.*

In contrast to NMR spectrometers, ESR spectrometers are arranged to record the first derivative of the absorption curve rather than the absorption curve itself (Figure 23). This gives somewhat greater sensitivity and better resolution. In order to obtain information about the number of spins in the sample, which is proportional to the integral of the absorption signal, now the double integral of the ESR spectrum has to be evaluated. Since the probability of absorption and induced emission are the same, the populations in each level tend to became equivalent. However, an excess population of about 10^{-3} in the lower level is maintained by relaxation phenomena. For the nuclear spin of the proton this excess population is only about 10^{-5} at room temperature, with ΔE of about 6×10^{-3} cal/mol; in principle, therefore, it is easier to observe a signal in ESR than in NMR. Actually, ESR is very sensitive, making possible the detection of free radicals at concentrations of the order of 10^{-7} M.

3.2.2 Characterization of ESR spectrum

ESR spectra are characterized by three parameters: *g-factors*, *hyperfine splitting constants*, and *line width*. A careful study of these parameters enables much detailed structural information about the particular radical to be deduced.

g-factor

When placed in a magnetic field, an unpaired electron has, in addition to its spin angular momentum, a small amount of extra orbital angular momentum. The interaction between these, called spin-orbit coupling, results in the electron having a slightly different effective magnetic moment from that of the free electron and consequently the condition for resonance is altered ($h\nu = g\mu_B \cdot B_0$ where g depends on the nature of the radical).

Consequently, for a given frequency, radicals with different *g*-factors resonate at different field values. The difference between the *g*-factor of a radical and that for the free electron is analogous to the chemical shift in NMR. These differences in organic radicals are very small, being placed within the rather narrow range of 2.00 to 2.01 (the value for free electron is 2.0023). Nevertheless, it can give important information about the radical structure. The spin-orbit coupling is particularly effective in heavy atoms. Thus, significant deviations from 2.0023 occur when the radical contains heteroatoms, and these deviations are the largest for heavier heteroatoms like P and S. The *g*-factors of various classes of organic radicals are reported in Scheme 3. For alkyl radicals like methyl the *g*-factor is very close to that of free electron (2.0026). As stated before, introduction of heteroatoms into a radical generally increases the *g*-factor. This is particularly true with radical having high probability of finding the unpaired electron at these atoms (Scheme 3). For sigma radicals the *g*-factors are usually lower than for their π counterparts. As an example, it is 2.0006 for acyl radicals like acetyl.

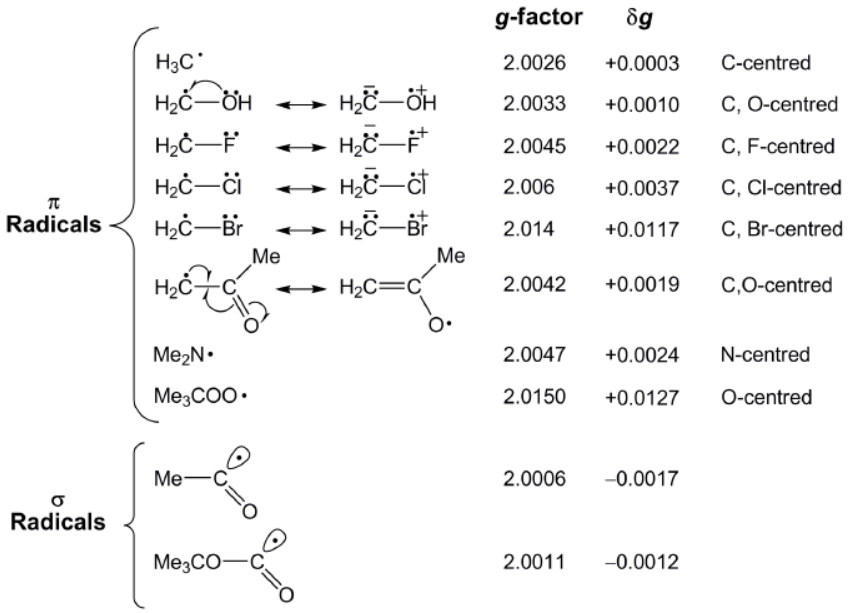

Scheme 3

Hyperfine coupling

This is undoubtedly the most useful characteristic of ESR spectra both for elucidating the structure and the shape of the radical under study. It derives from interaction between the unpaired electron and adjacent magnetic nuclei (^{1}H, ^{13}C, ^{14}N, ^{31}P, etc.). For those familiar with

NMR spectroscopy it may be useful to realize that electron-nuclear hyperfine coupling is comparable with nuclear-nuclear spin-spin coupling.

This is related to the degree of *s*-character of the orbital containing the single unpaired electron (SOMO). In figure 2 is reported the orbital diagram for the formyl radical, a s-radical, in which the unpaired electron is in an orbital possessing a substantial s-character and the coupling between the unpaired electron and α-H nucleus is quite strong (a splitting of 132 G is measured). Because of the direct interaction of the unpaired electron with the magnetic nucleus, the hyperfine splitting constant is designated positive.

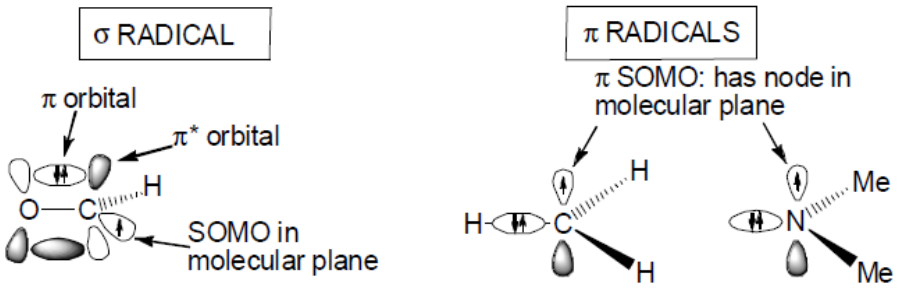

Figure 24. *Orbital diagrams for σ- and π-type radicals.*

On the contrary, if the unpaired electron is in a *p*-orbital (as in the case of methyl radical, see Fig. 24), which has a node at the nucleus, there would be no mechanism for it to interact with protons attached to the trigonal carbon.

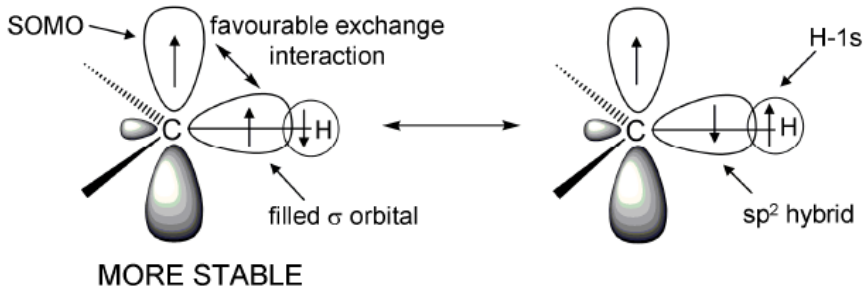

Figure 25. *Orbital diagrams showing the two-possible spin polarization in the C-H bond.*

However, the ESR spectrum of methyl radical, consisting of 1:3:3:1 quartet, clearly suggests that the unpaired electron does interact with the three protons. This is due to spin polarization. There are two possible arrangements of electron spin about the trigonal carbon atom (see Fig. 25): that one in which the spin of the electron associated with the proton has the opposite sign to that of the unpaired electron is more stable. Because of spin orientations, there is a net unpaired negative spin density in the *s* orbital of the proton, which gives rise to hyperfine

splitting constant with a negative sign. Couplings between the unpaired electron and protons attached to β-carbon atoms are also observed. This interaction is due to the $2p_z$ orbital containing the single electron and the orbital associated to the beta C-H bond. This gives a spin population in the 1*s* orbital of hydrogen atom. Invalence-bond terms there is a contribution to the resonance hybrid of the canonical structure II (Fig. 26).

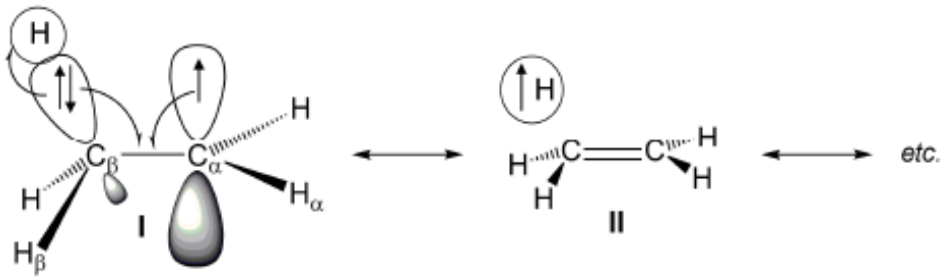

Figure 26. *Orbital diagrams showing the coupling with β-protons.*

The value of the hyperfine splitting constant is given by the Heller-McConnel equation (Fig. 26), which is analogous to that of Karplus in NMR. Thus, the value of β-proton coupling can give information about preferred conformations of radicals and of the barriers to rotation about Cα-Cβ bond.

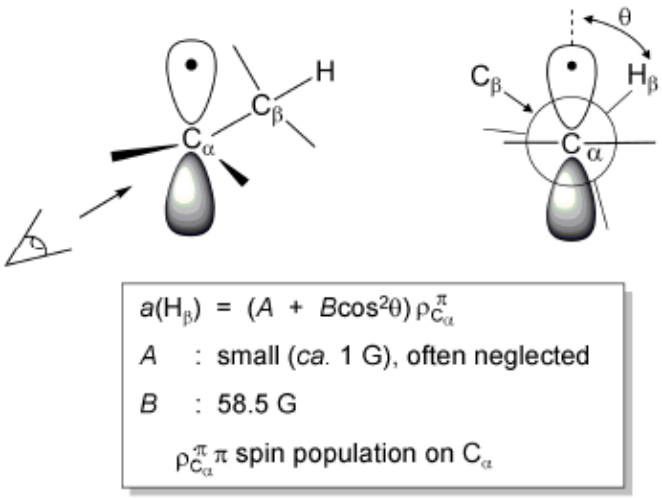

Figure 26. *Dependence of β-coupling on the conformation adopted by radicals.*

Many nuclei have net magnetic moment (which in diamagnetic compounds give rise to NMR spectra). Those with nuclear spin (*I*) of 1/2 taken up to (± 1/2) orientations in the resultant magnetic field, those with *I*=1 have three choices (+1, 0, -1), etc. Consider a radical containing

a single nucleus with I=1/2. Half of these radicals will have nuclei with m_I=+1/2 and the other half will have m_I=-1/2 (see Fig. 27).

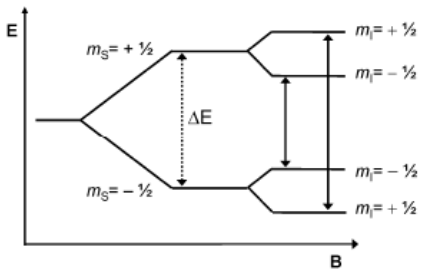

Figure 27. *Splitting of electron levels in a magnetic field B_0. Allowed transitions are indicated by arrows.*

Consequently, two resolved lines are expected in the ESR spectrum, the separation giving the *hyperfine coupling constant (a).* If I=1 there are three possible orientations (+1, 0, -1) giving three ESR transitions, the separation again giving the hyperfine coupling.
Several coupled nuclei will make the pattern more complicated. Thus, the coupling between the unpaired electron and one I=1/2 nucleus and one I=1 nucleus (e.g. ^{1}H and ^{14}N) will give six lines from which both coupling constants can be derived. The spectrum “shape” depends on the relative value of hyperfine splitting (see figure28).

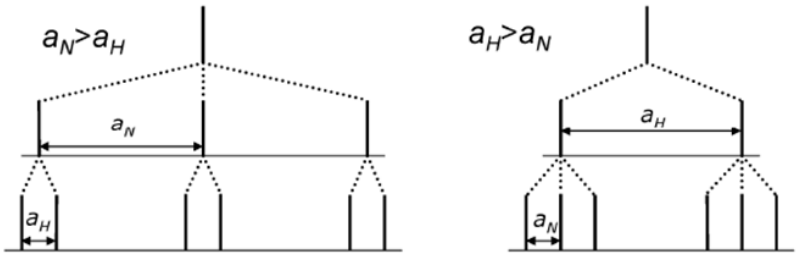

Figure 28. *Stick diagram for the coupling of the unpaired electron with one ^{1}H nucleus and one ^{14}N nucleus.*

When the unpaired electron interacts with 1, 2, 3….k groups of equivalent nuclei, the number of spectra lines, is given by

$$(2I_{tot},1 + 1)(2I_{tot,\,2} + 1)(2I_{tot,\,3} + 1)\ldots\ldots\ldots (2I_{tot,\,k} + 1)$$

Where I_{tot} for a group of n equivalent nuclei is

$$I_{tot} = \sum_{i=1}^{n} I_i$$

For each multiplet the hyperfine splitting exhibits a characteristic distribution of intensities which is binomial for *I*=1/2.

Line width

Line-widths in ESR are mainly affected by electron relaxation times. The unpaired electronspin has a magnetic moment that is roughly a 1000-fold greater than the nuclear spin moments of protons. Relaxation times scale roughly are the square of the magnetic moment, so that electrons relax ca. 10^6 times faster than nuclei. The fast relaxation time of the electron had an important consequence for the development of pulsed ESR instrumentation that lagged about a decade behind that of pulsed NMR instrumentation because of the nature of the spins involved. The faster relaxation time of the electron requires pulse width, pulse delays, and repetition times that are 10^6 times shorter for pulsed ESR than for pulsed NMR and very sophisticated digital integrated circuits are required for signal detection. Nowadays, pulsed ESR represents an important area of modern ESR (see paragraph on PELDOR). Line broadening by relaxation time is described as homogenous, while it is called inhomogeneous when originated by other factors. Many reasons can be responsible of inhomogeneous broadening of spectral lines. From the organic chemist point of view, the most interesting are dynamic (or time dependent) phenomena which can be either intramolecular or intermolecular. Some such processes are: hindered rotation, tumbling of the molecule in a viscous liquid, interaction with other paramagnetic species, chemical equilibria or reactions. In such cases, the broadening occurs from dynamic fluctuations in the local field experienced by the unpaired electron(s).

3.2.3 ESR spectrum of Mononitroxide

Basing on the previously consideration, the ESR spectrum of a dialkyl nitroxide such as TEMPO moiety is typically characterized by three lines (Figure 29a), because it is possible to observe just the coupling between the unpaired electron and ^{14}N nucleus (*I*=1). The separation between these lines is proportional to the corresponding isotropic nitrogen *hyperfine splitting constant*, a_N. In this specific example the couplings between the unpaired electron and protons attached to β-carbon atoms are not observed because of the lack of these protons.

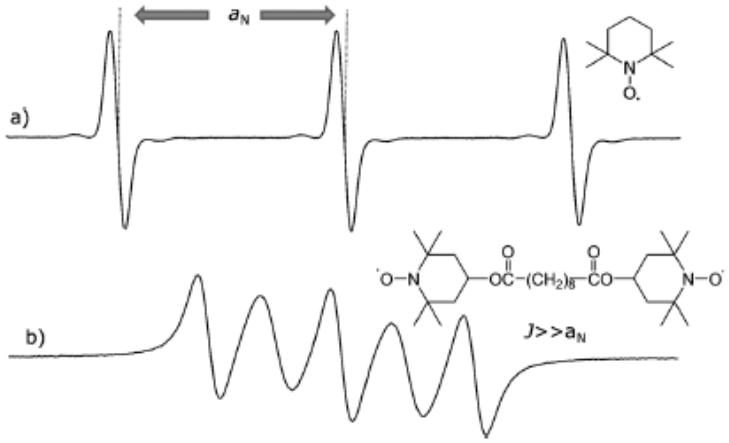

Figure 29. *ESR spectra of a) TEMPO and b) a bis(nitroxide) showing an exchange interaction (J).*

For these kind of radicals, the value of a_N ranges from 13.5 to 18 G and is strictly related to the nature of the environment. In detail the polarity and/or the hydrogen-bonding capability of the medium surrounding the radical center are the most important factors having an influence both on spin density on the nitrogen and value of the nitrogen hyperfine coupling as well. The value of a_N increases if the radical center is in a polar medium[64] while decreases in a hydrophobic environment. As a consequence, nitroxide radicals can be used as probes in order to detect changes in the surrounding environment which are connected to different value of a_N. During the complexation process, the distribution of the nitroxide probe from the solvent into the hydrophobic environment of the host occurs inducing a considerable modification in the hyperfine coupling constant. As mentioned before, ESR spectroscopy is usually characterized by a shorter time scale compared with that of host-guest complex formation. Consequently when the a_N values forth nitroxide used as a probe are different for the free and complexed species thespectra are characterized by separate signals for the two species,[62] making possible to obtain kinetic information on different host–guest complexationevents.[65]

The line shapes of the ESR spectra reflect the probe's motional dynamics which are affected by the local viscosity, the tumbling of the macromolecule and the flexibility of the backbone to which it is bound. The mobility in ESR studies is represented by the correlation time, τ_c, corresponding to the characteristic time during which a molecule turns over ca. 1 radian. The inclusion of the nitroxide probe into the host compound is associated with a decrease in its tumbling rate and mobility compared to the free nitroxide. Consequently, the formation of a spin-labelled complex can be detected by the analysis of the ESR line shapes and by determining τ_c.

3.2.4 Distances between radical centres

Spatial information about distance between radical center can be achieved by using ESR spectroscopy. The continuous wave (CW)-ESR spectrum of a system containing two relatively close radicals, can give interesting information on the degree of through-space spin exchange coupling (J) between the two nitroxides.[66] If two radicals are too far to undergo exchange interaction the EPR spectrum is characterized by a three-line spectrum. On the contrary if the radical units are sufficiently close to interact ($J>a_N$), a five-line signal will appear in the ESR spectrum (see figure 29b), owing the spin exchange coupling is large enough. In particular, the spectra can show a simple three-line spectrum (1:1:1 intensities) or a five-line spectrum (1:2:3:2:1 intensities) when the spin system is completely delocalized.[67-69] Changes in the distance between the spin centers after a binding event can be used to monitor the binding process of a guest.

3.3 Double Electron Electron Resonance (DEER)

PELDOR, also known as DEER (Double Electron Electron Resonance), has been demonstrated as a powerful tool for measuring of distances and distance distribution between spin labels by analyzing their dipole-dipole interactions.[70-74]

PELDOR is sensitive to spin-spin distance between 2 and 8 nm,[75] which is suitable range to study biological molecules such as protein complexes containing paramagnetic species. The determination of distances has been performed using a variety of methods X-ray crystallography, fluorescence quenching, electron or X-ray scattering, and a number of magnetic resonance techniques (ESR, NMR, ENDOR). However, the distances that can be measured by dipolar NMR methods are limited by the size of the magnetic moments of nuclear spins. The introduction into the coupled spin system of an electron spin with a magnetic moment several orders of magnitude larger than nuclear moments makes possible the measurement of a broader range of distancespossible.[76]

Generally, when the interparticle magnetic interactions in disordered systems are weak compared to the anisotropic hyperfine and spin-orbital (*g*-tensor) interactions, the CW ESR method may be useless. The weak magnetic interactions are not detected because of ESR lines broadening due to stronger interactions in disordered systems.

Such difficulties have been overcome through PELDOR, which prevents the broadening of lines and reveals weak interactions. The two-pulse echo is one of the first protocols of the ESE experiment reported by Milov, Ponomarev, and Tsvetkov[77,78] in 1984 and is able to generate an echo using a two-pulse electron spin echo sequence with fixed separation τ between

pulses. The three-pulse echo reported by Laser and Singer[76] in 1993 used an additional pulse maintaining τ constant.

The ‘‘2 + 1’’ pulse train electron spin resonance method suggested by Kurshev et al. was a variation of the three-pulse echo with the only difference that the three pulses are characterized by the same frequency. Another protocol is represented by four-pulse DEER sequence, which is able to eliminate the dead time, and makes it possible to obtain a distances distribution.[79]

The group of prof. Lucarini in collaboration with the group of Marina Bennati was the first to determine the distances between two TEMPO moieties at the both ends of the cucurbit[6]uril-based [3]rotaxane by using PELDOR technique.[80] The structure of the rotaxane and the corresponding dumbbell are reported in figure 30.

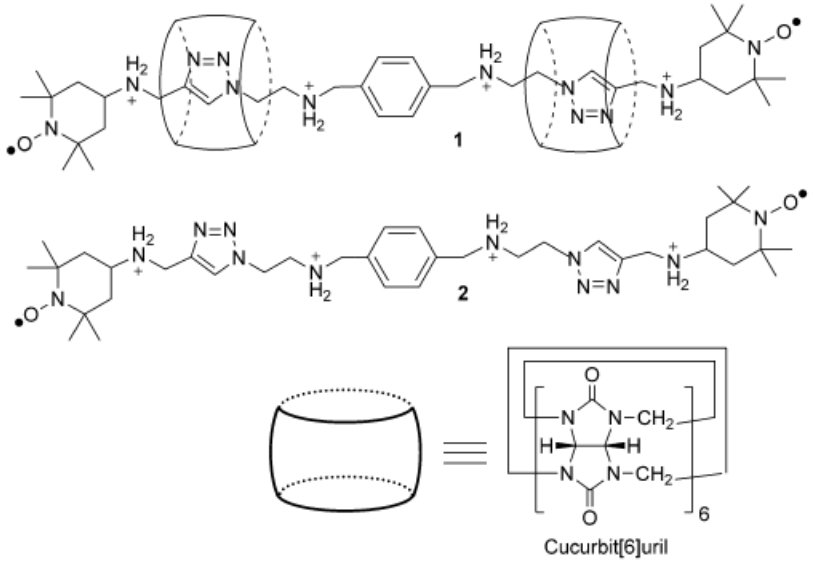

Figure 30. *Structure of the [3]rotaxane and the corresponding dumbbell.*

PELDOR measurements were performed at 40 K using the four-pulse, dead time free, PELDOR sequence given by: $\pi/2(\upsilon_{obs})–\tau_1–\pi(\upsilon_{obs})–\tau–\pi(\upsilon_{pump})–(\tau_1+\tau_2–\tau)–\pi(\upsilon_{obs})–\tau_2$–echo.[81] The ELDOR pulse (υ_{pump}, 40 ns) was positioned at the maxima of the echo-detected nitroxide spectrum, whereas the $\pi/2$ and π observe pulses (υ_{obs}, 16 and 32 ns) were positioned at the low field side of the spectrum ($\upsilon_{obs}–\upsilon_{pump}\approx$72 MHz). Distance distribution *p(r)* of the [3]rotaxane, obtained by the model-free Tikhonov regularizationmethod,[82] was centered at 30.7 ($\pm$ 0.7) Å (figure 31, solid red line). Stochastic dynamic (SD) calculations were performed to support the PELDOR results. Concerning these studies the N-O bond was modelled by the C=O bond, owing to their similar geometries and the higher reliability of the parameters of the latter group in the AMBER* force field.[83] The estimate of *p(r)* obtained by performing MD calculations was in agreement with the experimental data.

On the contrary the PELDOR time-trace of the dumbbell **2**, did not display any pronounced dipolar modulation, suggesting the possibility of the free thread to assume several different conformations and leading to a very broad distance distribution, not detectable by PELDOR. In fact molecular dynamics (MD) simulations on the dumbbell showed a very broad distance distribution with a mean value of <18.5>Å (figure 31, dotted black line).

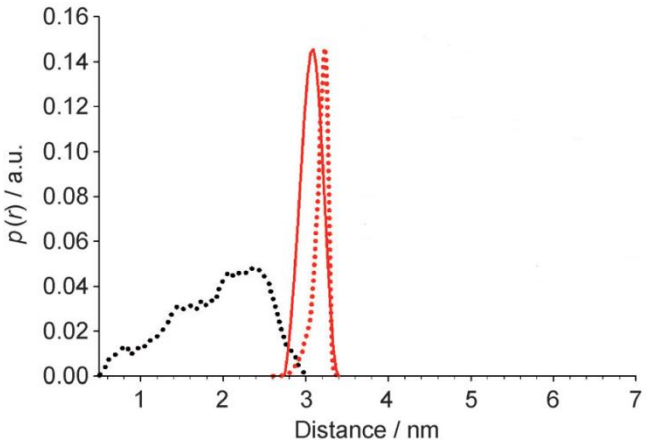

Figure 31. *Normalized distance distributions derived by Tikhonov regularization for rotaxane **1** (red solid line). The dotted lines show the molecular dynamically determined distance distributions calculated for **1** (red) and **2** (black).*

The application of PELDOR has allowed not only to obtain the measurement of a distance distribution between two radicals but also to extract of interesting information on intrinsic flexibility of the mechanically interlocked assembly. In fact, these results proved that the rotaxanation process gave a more rigid system allowing the determination of the distance distribution by PELDOR technique. While the impossibility to achieve a distance distribution in the dumbbell confirmed the more flexibility of the free thread compared to the rotaxane.

4 Aim of the thesis

Molecular machines have been described in the recent years because they appear to have large possible application in the field of information and communication technology (ICT), materials science, catalysis, and medicine. The first step towards the design of artificial molecular machines is represented [2]rotaxanes because the motions of their molecular components can be easily obtained by application of external stimuli and controlled as well. The characterization of these systems, depending on the nature and chemical properties of their molecular components, is typically carried out by high-resolution X-ray crystallography, nuclear magnetic resonance (NMR) spectroscopy, electrochemical and photophysical

techniques. As an alternative, electron paramagnetic resonance (EPR) spectroscopy can be useful to investigate these systems because offers several advantages that were previously discussed.

However, in order to use EPR spectroscopy, organic radicals characterized by high stability and persistence (spin labels) such as nitroxides, must be introduced in the system. The aim of my project was devoted to prepare and investigate bistable [2]rotaxanes, containing nitroxide units in both the ring and dumbbell components to exploit EPR spectroscopy for monitoring the molecular motion, measuring intercomponent distances on the nanometer scale and understanding in detail the structural and conformational changes occurring after the movement of their molecular components.

In this contest my research activity was focused on the synthesis and characterization of rotaxanes driven by chemical and electrochemical stimuli.

In chapter 2, molecular shuttles working by means of the application of chemical stimuli are described in detail. In Figure 32a series of [2]rotaxanes comprising a dibenzo[24]-crown-8-ether (DB24C8) interlocked with a dumbbell component that possesses two different recognition sites, namely, a dialkylammonium (NH_2^+) and a 4,4'-bipyridinium (BPY^{2+}) units, are reported (**R-1**, **R-2**, **R-3**). A pair of stable TEMPO radicals were covalently attached both to the ring and to one extremity of the dumbbell in rotaxanes **R-1** and **R-3** while in rotaxane **R-2** the TEMPO unit is solely present in the dumbbell. The macrocycle shuttling between two different stations, arising from subsequent additions of base and acid, was confirmed for the first time by performing EPR spectroscopy. The [2]rotaxane **R-3** is characterised by a more rigid connection of the spin label to the molecular ring allowing the use of pulsed electron–electron double resonance (PELDOR). The combination of (PELDOR) and molecular dynamic calculations has provided important information on the geometry adopted by the macrocycle during the shuttling process.

Chapter 2 is focused on the synthesis and characterization of a novel spin label crown ether having the nitroxide unit as part of its ring structure. This macrocycle allowed to obtain a new class of bistable [2]rotaxanes **R-4** and **R-5** reported in figure 33 and driven by chemical stimulus. I have also synthesised and characterized spin-labelled rotaxanes driven by electrochemical stimuli. Actually, in chapter 4 single and bistable [2]rotaxanes consisting of an electron accepting ring (cyclobis(paraquat)-p-phenylene, $CBPQT^{4+}$) interlocked with a dumbbell component containing bisthiotetrathiafulvalene (STTFS) or/and 1,5-dioxynaphthalene (DNP) as electron-donating units are outlined (Figure 34). In addition, in this case nitroxides were covalently attached both to the ring and to one extremity of the dumbbell in order to investigate the magnetic proprieties of these rotaxanes by using EPR spectroscopy.

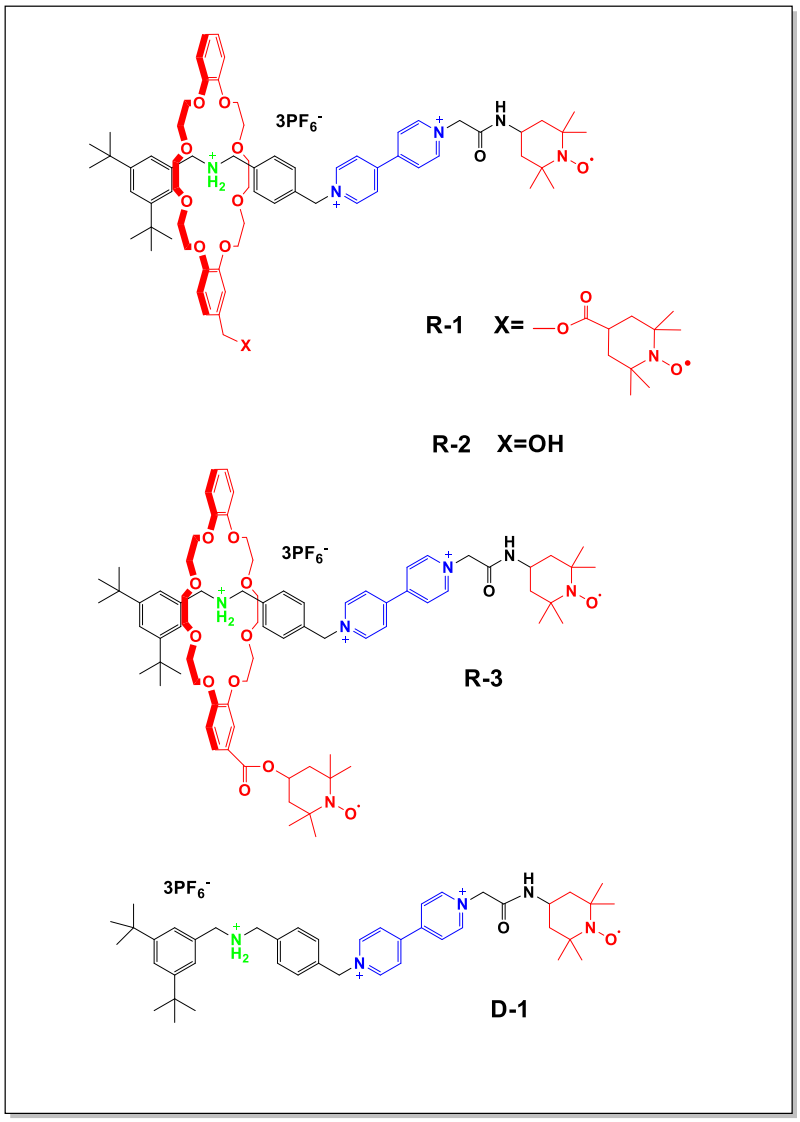

Figure 32. *Spin-labelled dumbbell (**D-2**) and a series of spin-labelled [2]rotaxanes comprising a dibenzo[24]-crown-8-ether (DB24C8) interlocked with a dumbbell incorporating a dialkylammonium (NH^{2+}) and a 4,4'-bipyridinium (BPY^{2+}) units, which are described in chapter 2.*

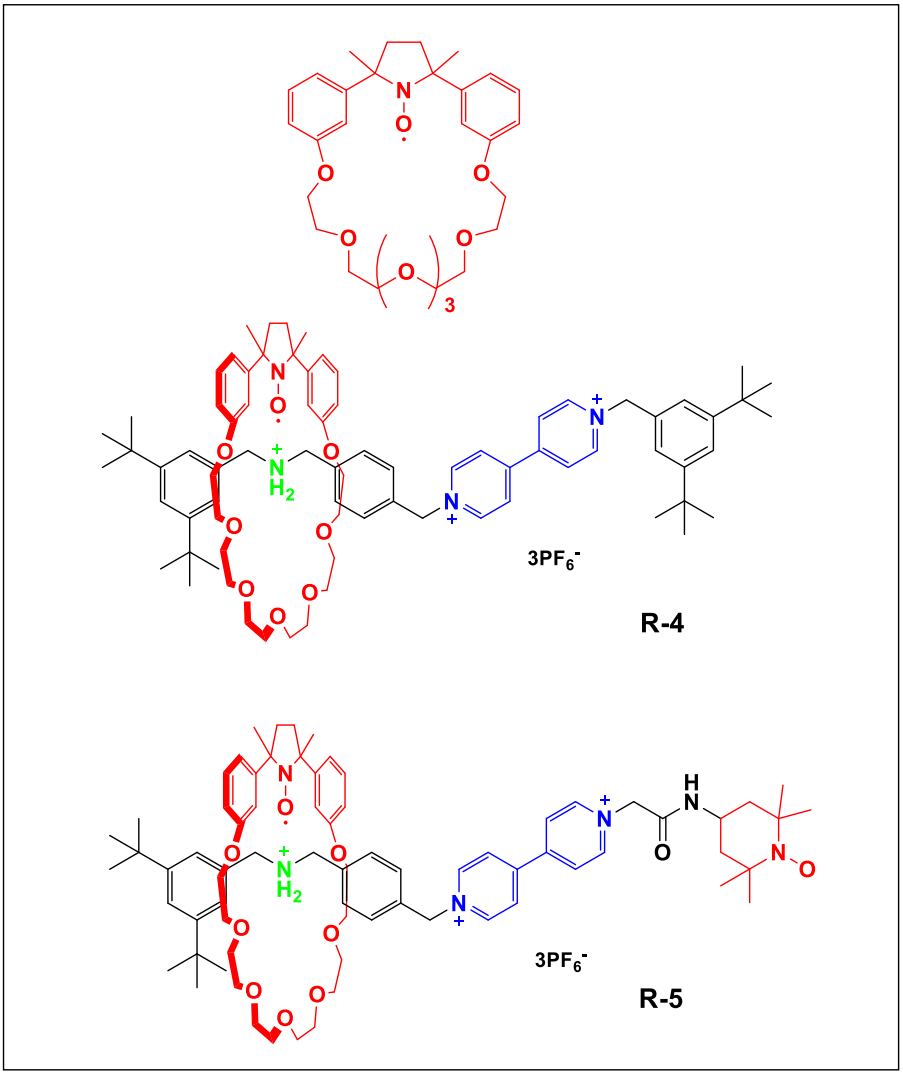

Figure 33. *A new class of spin-labelled [2]rotaxanes comprising a novel spin label crown ether.*

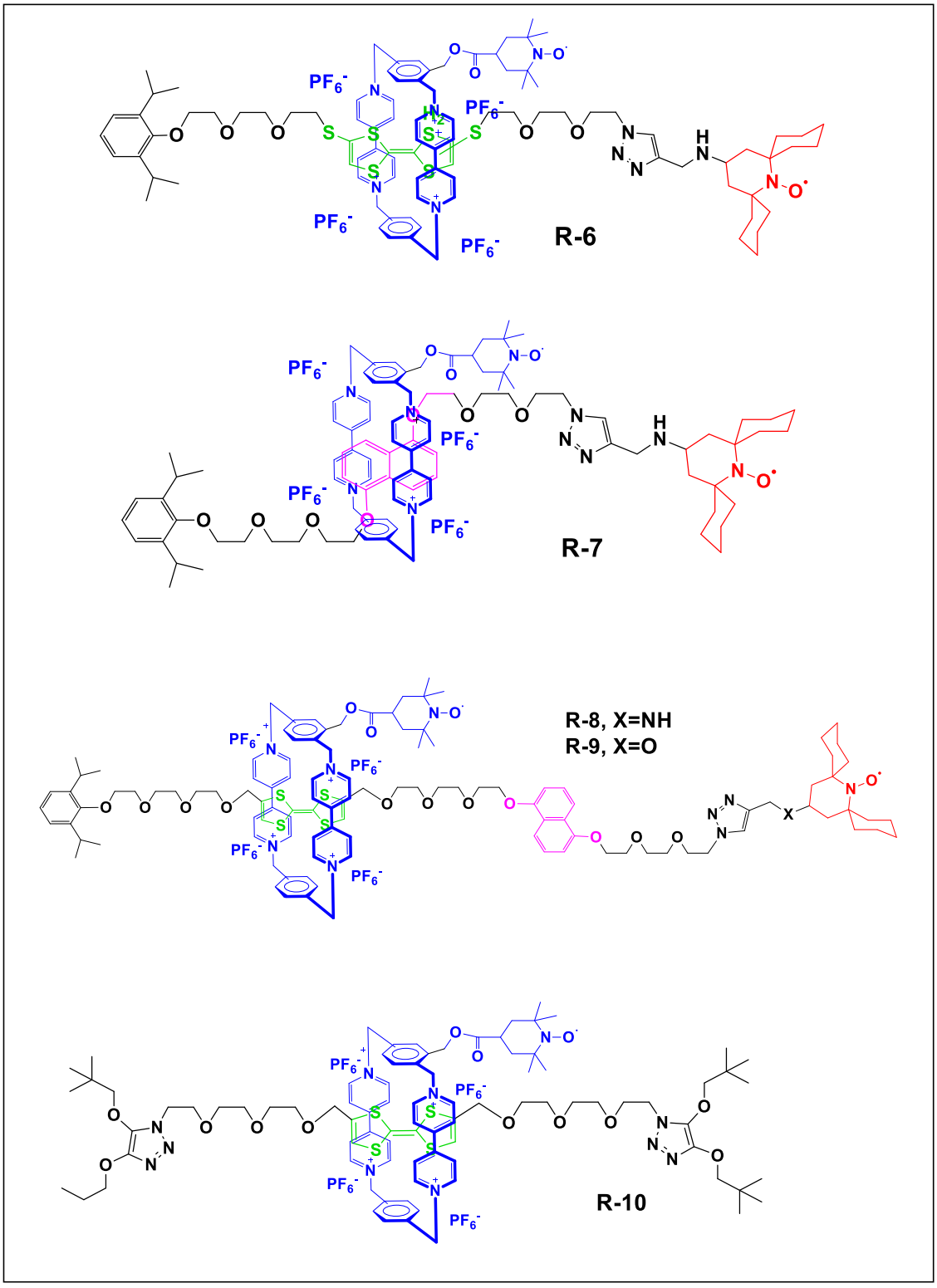

Figure 34. *Single [2]rotaxanes based on spin-labelled cyclobis(paraquat-p-phenylene) ($CBPQT^{4+}$) interlocked with a dumbbell containing bisthiotetrathiafulvalene (STTFS, **R-6**) or 1, 5-dioxynaphthalene (DNP, **R-7**). Bistable [2]rotaxanes having both TTF and DNP in the thread (**R-8** and **R-9**) and the single station rotaxane possessing a diamagnetic dumbbell and a paramagnetic macrocycle (**R-10**).*

References

[1] Pauling, L. *The nature of the Chemical Bond: An Introduction to Modern Structural Chemistry*; Cornell University Press: Ithaca, **1939**.

[2] a) Anelli, P. L.; Ashton, P. R.; Ballardini, R.; Balzani, V.; Delgrado, M.; Gandolfi, M.T.; Goodnow, T. T.; Kaifer, A. E.; Philp, D.; Pietraszkiewicz, M.; Prodi. L.; Reddington, M. V.; Slawin, A. M. Z.; Spencer, N.; Stoddart, J.F.; Vincent, C.; Williams, D. J. Molecular Meccano 1. [2]Rotaxanes and a [2]Catenane Made to Order. *J. Am. Chem. Soc*. **1992**, *114*, 193-218; b) Amabilio, D. B.; Stoddart, J. F. Interlocked and Interwined Structures and Superstructures. *Chem. Rev*. **1995**, *95*, 2725-2828; c) Stoddart, J. F. The Chemistry of the Mechanical Bond. *Chem. Soc. Rev*. **2009**, *38*, 1802-1820; d) Olson, M. A.; Botros, Y. Y.; Stoddart, J. F. Mechanostereochemistry. *Pure Appl. Chem*. **2010**, *82*, 1569-1574; e) Barin, G. Forgan, R. S.; Stoddart, J. F.;Mechanostereochemistry and the Mechanical Bond. *Proc. R. Soc*. *A.* **2012**, *468*, 2849-2880.

[3] Schill, G. Catenaries, *Rotaxanes and Knots*: New York and London, **1971**.

[4] Wasserman, E. et al.,*J. Am. Chem. Soc*. **1960**, *82* , 4433.

[5] Harrison, T., Harrison, S.,*J. Am. Chem. Soc*. **1967**, *89*, 5723.

[6] Schill, G., Luttringhaus, *A. Angew. Chem*. **1964**, *76*,567.

[7] Dietrich-Buchecker, C., Sauvage, J. P.,*J. Am. Chem. Soc*. **1984**, *106*, 3043.

[8] Dietrich-Buchecker, C. O., Sauvage, J. P., Kintzinger, J. P. Une nouvelle famille de molécules: Les métallo-caténanes. *Tetrahedron Lett*. **1983**, *24* (46), 5095–5098.

[9] Armaroli, N.; Balzani, V., Sauvage, J. P., Collin, J. P., Gavina, P.,Sauvage, J. P., Ventura, B. *J. Am. Chem. Chem. Soc*. **1999**, *727*,4397.

[10] Structures formed by ‘slippage’ are formally not rotaxanes, rather they are pseudorotaxanes that are kinetically stable under some conditions. Rotaxanes are ‘molecules in which a ring encloses another, rod-like molecule having end-groups too large to pass through the ring opening and thus holds the rod-like molecule in position without covalent bonding’. [A. D. McNaught and A. Wilkinson, The IUPAC Compendium of Chemical Terminology, Blackwell Science, Oxford, 2nd edn, 1997]. A structure obviously cannot be said to have ‘end-groups too large to pass through the ring opening’ if they have passed through in order to form it.

[11] Liittringhaus, A., Cramer. F., Prinzbach. H., Henglein. F. M., Liebigs, *Ann. Chem*. **1958**, *613*. 185-198.

[12] Ashton, P. R., Chrystal, E. J. T., Glink, p. T., Menzer, S., Schiavo, C., Spencer, N., Stoddart, J. F., Tasker, P. A., White, A. J. P., Williams, D. J.,*Chem.–Eur. J.* **1996**, *2,* 709–728.

[13] Ashton, P. R., Chrystal, E. J. T., Glink, p. T., Menzer, S., Schiavo, C., Spencer, N., Stoddart, J.

F., Tasker, P. A., White, A. J. P., Williams, D. J.,*Chem. Eur. J*. **1996**, *2*, 709–728.

[14] Ashton, P. R., Ballardini, R., Balzani, V., Credi, A., Gandolfi, M. T., Menzer. S., Perez, L. Prodi, J. F. Stoddart, Venturi, M., White, A. J. P., Williams, D.,*J. Am. Chem. Soc*. **1995**,*117*, 11171- 11197.

[15] a) Desiraju, G. R.,*Acc. Chem. Res*. **1996**, *29*, 441-449; b) Steiner T.,*Chem. Commun*. **1997**, 727-734; c) Steiner T., *Chem. Commun*. **1999**, 313-314.

[16] Liittringhaus A., Cramer F., Prinzbach H., Henglein F., M. Liebigs,*Ann. Chem*. **1958**, *613*. 185- 198.

[17] Anelli, P. L., Spencer, N., Stoddart, J. F., *J. Am. Chem. Soc*. **1991**, *113* (13), 5131–5133.

[18] Odell, B., Reddington, M. V., Slawin, A. M. Z., Spencer, N., Stoddart, J. F., Williams, D. J., *Angew. Chem. Int. Ed*. **1988**, *27* (11), 1547–1550.

[19] a) B. Odell, M. V. Reddington, A. M. Z. Slawin, N. Spencer, J. F. Stoddart, D. J. Williams, *Angew. Chem, Int. Ed. Engl.*, **1988**, *27*, 1547-1553; b) P. L. Anelli, N. Spencer, J. F. Stoddart, *J. Am. Chem. Soc*. **1991**, *113*, 5131-5133; c) T. Goodnow, M. V. Reddington, J. F. Stoddart, *J. Am. Chem. Soc.***1991**, *113*, 4335-4337; d) M. C. T. Fyfe, J. F. Stoddart, *Acc. Chem. Res*. **1997**, *30*, 393-401.

[20] J. F. Stoddart, et al. *Acc. Chem. Res*. **2012**, *45*, 1581-1592.

[21] C. Wang, M. A. Alson, L. Fang, D. Benitez, E. Tkatchouk, S. Basu, A. N. Basuray, D. Zhang, D. Zhu, W. A. Goddard, J. F. Stoddart, *PNAS* **2010**, *107*, 13991-13996.

[22] M. A. Olson, A. B. Braunschweig, T. I Lei Fang, A. Trabolsi, A. M. Z. Slawin, S. I. Khand, J. F. Stoddart, *Org. Biomol. Chem*. **2009**, *7*, 4391–4405.

[23] C. Wang, M. A. Olson, L. Fang, D. Benítez, E. Tkatchouk, S. Basu, A. N. Basuray, D. Zhang, D. Zhu, W. A. Goddard, J. F. Stoddart, *PNAS***2010**, *32*, 13991–13996.

[24] A. C. Fahrenbach, C. J. Bruns, D. Cao, J. F. Stoddart, *Accounts of Chemical Research* **2012**, *45*, 1581-1592.

[25] C. J. Pedersen, *Journal of the American Chemical Society* **1967**, 7017-7036.

[26] a) M. V. Martinez-Diaz, N. Spencer, J. F. Stoddart, *Angew. Chem*. **1997**, *109*, 1991-1994; *Angew. Chem. Int. Ed. Engl*. **1997**, *36*, 1904-1907; b) P. R. Ashton, R. Ballardini, V. Balzani, I. Baxter, A. Credi, M. C. T. Fyfe, M. T. Gandolfi, M. Go´mez-Lo´pez, M.V. Martı´nez-Dı´az, A. Piersanti, N. Spencer, J. F. Stoddart, M. Venturi, A. J. P. White, and D. J. Williams, *J. Am. Chem. Soc.* **1998**, *120*, 11932-11942.

[27] Cantrill, S. J., Pease, A. R., Stoddart, J. F*. J., Chem. Soc*., *Dalton Trans*. **2000**, 3715-3734.

[28] Astumian, R. D*. Proc. Natl. Acad. Sci. U.S.A*. **2005**, *102*, 1843-1847.

[29] a) Leigh, D. A., Murphy, A., Smart, J. P., Deleuze, M. S., Zerbetto, F.,*J. Am. Chem. Soc*. **1998**, *120*, 6458-6467; b) Deleuze, M. S., Leigh, D. A., Zerbetto, F.,*J. Am. Chem. Soc*. **1999**, *121*, 2364-2379.

[30] a) *Molecular Electronic Devices* (Ed.: F.L. Carter), Dekker, New York, 1982; b) *Handboock of Nanostructured Materials and Nanotecnology*, Academic Press, New York, **2000**.

[31] K. Hirose, K. Ishibashi, Y. Shiba, Y. Doi, Y. Tobe, *Chem. Eur. J.* **2008**, *14*, 5803 – 5811.

[32] J.M. Hawkins*, The Oxford Paperback Dictionary*, Oxford University Press, Oxford, **1979**.

[33] (a) Ballardini, R., Balzani, V., Credi, A., Gandolfi, M.T., Venturi, M. *Acc. Chem. Res.* **2001**, *34*, 445. (b) Ballardini, R., Balzani, V., Credi, A., Gandolfi, M.T., Venturi, M., *Int. J. Photoenergy* **2001**, 63.

[34] Kaifer, A.E., Gómez-Kaifer, M., Supramolecular Electrochemistry, Wiley-VCH, Weinheim (**1999**).

[35] Balzani, V., Credi, A., Venturi, *A Journey into the Nano World*, Wiley-VCH, Weinheim (**2003**).

[36] a) R. P. Feynman, *Eng. Sci*. **1960**, *23*, 22-36; b) R. P. Feynman, *Saturday Rev*. **1960**, *4*3, 45-47.

[37] A. Coskun, J. M. Spruell, G. Barin, W. R. Dichtel, A. H. Flood, Y. Y. Botros, J. F. Stoddart, *Chem. Soc*. *Rev*. **2012**, *41*, 4827 –4859.

[38] a) V. N. Vukotic, K. J. Harris, K. Zhu, R. W. Schurko, S. J. Loeb, *Nat. Chem*. **2012**, *4*, 456 –460.

[39] a) J. Bern, M. Alajarin, R. A. Orenes*, J. Am. Chem. Soc*. **2010**, *132*, 10741 –10747; b) J. Wang, B. L. Feringa, *Science* **2011**, *331*, 1429 –1432; c) S. F. M. Van Dongen, J. Clerx, K. Nørgaard, T. G. Bloemberg, J. J. L. M. Cornelissen, M. A. Trakselis, S. W. Nelson, S. J. Benkovic, A. E. Rowan, R. J. M. Nolte, *Nat. Chem*. **2013**, *5*, 945– 951; d) V. Blanco, D. A. Leigh, V. Marcos, J. A. Morales-Serna, A. L. Nussbaumer, *J. Am. Chem. Soc.* **2014**, *136*, 4905– 4908.

[40] a) Z. Li, J. C. Barnes, A. Bosoy, J. F. Stoddart, J. I. Zink, *Chem. Soc. Rev*. **2012**, *41*, 2590 –2605; b) Z. Zhang, D. Balogh, F. A. Wang, S. Y. Sung, R. Nechushtai, I. Willner, *ACS Nano* **2013**, *7*, 8455 –8468.

[41] a) D. S. Goodsell, *Our Molecular Nature*: *The Body' s Motors, Machines, and Messages*, Copernicus, New York, **1996**; b) R. D. Vall, R. A. Milligan, *Science* **2000**, *288*, 88-95.

[42] a) R. Cross, T. Ducan, *J. Bioenerg. Biomen*. **1996**, *28*, 403-408; b) P. Boyer, *Biochim. Biophys. Acta*, **1993**, *1140*, 215-250; c) S. M. Block, *Nature* **1997**, *386*, 317-319.

[43] P.-L. Anelli, N. Spencer, J. F. Stoddart, *J. Am. Chem. Soc*. **1991**, *113*, 5131–5133.

[44] D. A. Leigh, A. Troisi, F. Zerbetto, *Angew. Chem. Int. Ed*. **2000**, *39*, 350.

[45] A. C. Fahrenbach, J. C. Barnes, D. A. Lanfranchi, H. Li, A. Coskun, J. J. Gassensmith, Z. C. Liu, D. Bentez, A. Trabolsi, W. A. Goddard III, M. Elhabiri, J. F. Stoddart, *J. Am. Chem. Soc*. **2012**, *134*, 3061–3072.

[46] (a) Lynch, D.E., Hamilton, D.G., Calos, N.J., Wood, B., Sanders, J.K.M., *Langmuir* 15 (**1999**) 5600. (b) Brown, C.L., Jonas, U., Preece, J.A., Ringsdorf, H., Seitz, M., SToddart, J.F.,

Langmuir 16 (**2000**) 1924. (c) Asakawa, M., Higuchi, M., Mattersteig, G., Nakamura, T., Pease, A.R., Raymo, F.M., Shimizu, T., Stoddart, J.F., *Adv. Mater*. 12 (**2000**) 1099. (d) Gonzalez-gaitano, G., Guerrero-martinez, A., Ortega, F., Tardajos, G., *Langmuir* 17 (**2001**) 1392.

[47] (a) Buey, J., Swager, T.M. *Angew. Chem. Int. Ed*. 39 (**2000**) 608. (b) Kleverlaan, C.J., Indelli, M.T., Bignozzi, C.A., Pavanin, L., Scandola, F., Hasselman, G.M., Meyer, G.J. *J. Am. Chem. Soc*. 122 (**2000**) 2840. (c) Shipway, A. N., Willner, I. *Acc. Chem. Res*. **2001**, *34*, 421. (d) Cavallini, M., Lazzaroni, R., Zamboni, R., Biscarini, F., Timpel, D., Zerbetto, F., Clarkson, G.J., Leigh, D.A., J. *Phys. Chem*. B 105 (**2001**) 10826. (e) Samorì, P., Jackel, F., Unsal, O., Godt, A., Rabe, J.P. *Chemphyschem* **2001**, *2*, 461. (f) Auletta, T., Van Veggel, F.C.J.M., Reinhoudt, D.N., *Langmuir* 18 (**2002**) 1288. (g) Cavallini, M., Biscarini, F., Leon, S., Zerbetto, F., Bottari, G., Leigh, D.A. *Science* 299 (**2003**) 531. (h) Long, B., Nikitin, K., Fitzmaurice, D. *J. Am. Chem. Soc.* 125 (**2003**) 5152.

[48] (a) Steinberg Yfrach, G., Rigaud, J.L., Durantini, E.N., Moore, A.L., Gust, D., Moore, T.A. *Nature* 392 (**1998**) 479. Steinberg Yfrach, G., Liddell, P.A., Hung, S.C., Moore, A.L., Gust, D., Moore, T.A. *Nature* 385 (**1997**) 239. (b) Gust, D., Moore, T.A., Moore, A.L*. Acc. Chem. Res*. *34* (**2001**) 40. (c) Bennett, I.M., Farfano, H.M.V., Bogani, F., Primak, A., Liddell, P.A., Otero, L., Sereno, L., Silber, J.J., Moore, A.L., Moore T.A., Gust, D. *Nature 420* (**2002**) 398.

[49] (a) Chia, S., Cao, J., Stoddart, J.F., Zink, J.I*., Angew. Chem. Int. Ed. 40* (**200**1) 2447. (b) Álvaro, M., Ferrer, B., García, H., Palomares, E.J., Balzani, V., Credi, A., Venturi, M., Stoddart, J. F., Wenger, S., J. *Phys. Chem. B 107* (**2003**) 14319.

[50] T. J. Huang, B. Brough, C.M. Ho, Y. Liu, A. H. Flood, P. A. Bonvallet, H.R. Tseng, J. F. Stoddart, M. Baller, S. Magonov, *Appl. Phys. Lett*. **2004**, *85*, 5391–5393.

[51] M. C. Jime´nez, C. Dietrich-Buchecker and J. P. Sauvage, *Angew. Chem., Int. Ed.* **2000**, *39*, 3284–3287.

[52] Y. Liu, A. H. Flood, P. A. Bonvallet, S. A. Vignon, B. H. Northrop, H. R. Tseng, J. O. Jeppesen, T. J. Huang, B. Brough and M. Baller, *J. Am. Chem. Soc*. **2005**, *127*, 9745–9759.

[53] J. D. Badjic, C. M. Ronconi, J. F. Stoddart, V. Balzani, S. Silvi, A. Credi, *J. Am. Chem. Soc*. **2006**, *128*, 1489–1499.

[54] (a) Ballardini, R., Balzani, V., Credi, A., Gandolfi, M. T., Langford, S. J., Menzer, S., Prodi, L., Stoddart, J. F., Venturi, M., Willians, D. J., *Angew. Chem., Int. Ed. Engl*. **1996**, *35*, 978-981. (b) Stoddart, J. F., et al., *Chem. Eur. J*. **1998**, *12*, 2413-2422. (c) D'Acerno, C., Doddi, G., Ercolani, G., Mencarelli, P*., Chem. Eur. J.* **2000**, *6*, 3540-3546. (d) Ballardini R., Balzani, V., Leon, M. C., Credi, A., Gandolfi, M. T., Ishow, E., Perkins, J., Stoddart, J. F., Tseng, H.-R., Wenger, S. *J. Am. Chem. Soc*. **2002**, *124*, 12786-12795.

[55] T. D. Nguyen, H. R. Tseng, P. C. Celestre, A. H. Flood, Y. Liu, J. F. Stoddart, J. I., Zink *PNAS*, **2005**, *102*, 10029–10034.

[56] Entelis, S. G.; Nesterov, O. V., (**1966**) *Russ. Chem. Rev*. *35*, 917–929.

[57] a) M. Eigen, *Pure Appl. Chem*. **1963**, *6*, 97-115; b) W. M. Nau, X. Wang, *ChemPhysChem*. **2002**, *3*, 393-398.

[58] H. J. Schneider, F. Hacket, V. Rüdiger, *Chem. Rev*. **1998**, *98*, 1755-1786.

[59] M. Di Valentin, M. Albertini, E. Zurlo, M. Gobbo, D. Carbonera, *J. Am. Chem. Soc.* **2014**, *136*, 6582–6585.

[60] G. I. Likhtenshtein, J. Yamauchi, S. Nakatsuji, A. I. Smirnov, R. Tamura, *Nitroxides: Applications in Chemistry, Biomedicine and Materials Science*, Wiley-VCH, Weinheim, **2008**.

[61] E. Mezzina, M. Fan , F. Ferroni, P. Franchi, M. Menna, M. Lucarini, *J. Org. Chem*. **2006**, *71*, 3773–3777.

[62] P. Franchi, M. Lucarini, G. F. Pedulli, *Curr. Org. Chem*. **2004**, *8*, 1831 –1849.

[63] A. D. Milov, A. B. Ponomarev, Y. D. Tsvetkov, *Chem. Phys. Lett*. **1984**, *110*, 67–72.

[64] P. Franchi, M. Lucarini, P. Pedrielli, G. F. Pedulli, *ChemPhysChem*., **2002**, *3*, 789-793.

[65] M. Lucarini, L. Pasquato, *Nanoscale* **2010**, *2*, 668–676.

[66] M. Abe, *Chem. Rev*. **2013**, *113*, 7011–7088.

[67] J. A. Weil, J. R. Bolton, J. E. Wertz, Electron *Paramagnetic Resonance: Elementary Theory and Practical Applications*, Wiley, New York, **1994**.

[68] N. M. Atherton, *Principles of Electron Spin Resonance*, Ellis Horwood and Prentice Hall, Chichester, **1993**.

[69] Electron Paramagnetic Resonance: *A Practitioner's Toolkit* (Eds.: M. Brustolon, E. Giamello), Wiley, Hoboken, New Jersey, **2009**.

[70] A. D. Milov, A. B. Ponomarev, Y. D. Tsvetkov, *Chem. Phys. Lett*. **1984**, *110*, 67–72.

[71] R. E. Martin, M. Pannier, F. Diederich, V. Gramlich, M. Hubrich, H. W.Spiess, *Angew. Chem.* **1998**, *110*, 2993 –2998; *Angew. Chem. Int. Ed.* **1998**, *37*, 2833 –2837.

[72] G. Jeschke, A. Koch, U. Jonas, A. Godt, *J. Magn. Reson*. **2002**, *155*, 72–82.

[73] M. Bennati, A. Weber, J. Antonic, D. L. Perlstein, J. Robblee, J. A. Stubbe, *J. Am. Chem. Soc.* **2003**, *125*, 14988– 14989.

[74]S. S. Eaton, G. R. Eaton, *Specialist Periodical Reports on Electron Spin Resonance* **2004**, *19*, 318 –337.

[75] R. Ward, A. Bowman, H. El-Mkami, T. Owen-Hughes, D. G. Norman, *J. Am. Chem. Soc*. **2009**, *131*, 1348 –1349.

[76] R. G.Larsen, D.J. Singel, *Journal of Chemical Physics* **1993**, *98*, 5134-5146.

[77] A. D. Milov, K. M. Salikhov, M. D. Shirov, *Fizi. Tv. Tela*. **1981**, *23*, 975 (Russian); SOY. *Phys. Solid State* **1981**, *23*, 565.

[78] A. D. Milov, A. B. Ponomarev, Yu. D. Tsvetkov, *Chern. Phys. Lett*. **1984**, *110*, 67-72.

[79] M. Pannier, S. Veit, A. Godt, G. Jeschke, and H. W. Spiess, *Journal of Magnetic Resonance* **2000**, *142***,** 331–340.

[80] R. Pievo, C. Casati, P. Franchi, E. Mezzina, M. Bennati, M.Lucarini, *ChemPhysChem* **2012**, *13*, 2659 – 2661.

[81] R. E. Martin, M. Pannier, F. Diederich, V. Gramlich, M. Hubrich, H. W.Spiess, *Angew. Chem*. **1998**, *110*, 2993 –2998; *Angew. Chem. Int. Ed.* **1998**, *37*, 2833 –2837.

[82] Y. W. Chiang, P. P. Borbat, J. H. Freed, *J. Magn. Reson*. **2005**, *172*, 279 –295.

[83] F. Perez, C. Jaime, X. Sánchez-Ruiz, *J. Org. Chem*. **1995**, *60*, 3840 –3845.

Chapter 2

Spin labelled [2]rotaxane driven by chemical stimulus

1 Reversible Mechanical Switching of Magnetic Interactions in a Molecular Shuttle

1.1 Introduction

In this chapter It is reported the first example of an acid–base-controllable molecular shuttle, in which through-space magnetic interactions between two mechanically interlocked nitroxide units connected to the ring and dumbbell components could be switched on and off reversibly by chemical stimulation. This molecular switch (Figure 1) is based on a well-known [2]rotaxane architecture[1] comprising a dibenzo[24]crown-8(DB24C8) ring interlocked with a dumbbell component that possesses two different recognition sites, namely, a dialkylammonium (NH_2^+) and a 4,4'-bipyridinium (BPY^{2+}) unit. A pair of stable 2,2,6,6-tetramethylpiperidine-1-oxyl (TEMPO) radicals are covalently attached to the ring and to one extremity of the dumbbell, obtaining a bis-labelled [2]rotaxane.[2]

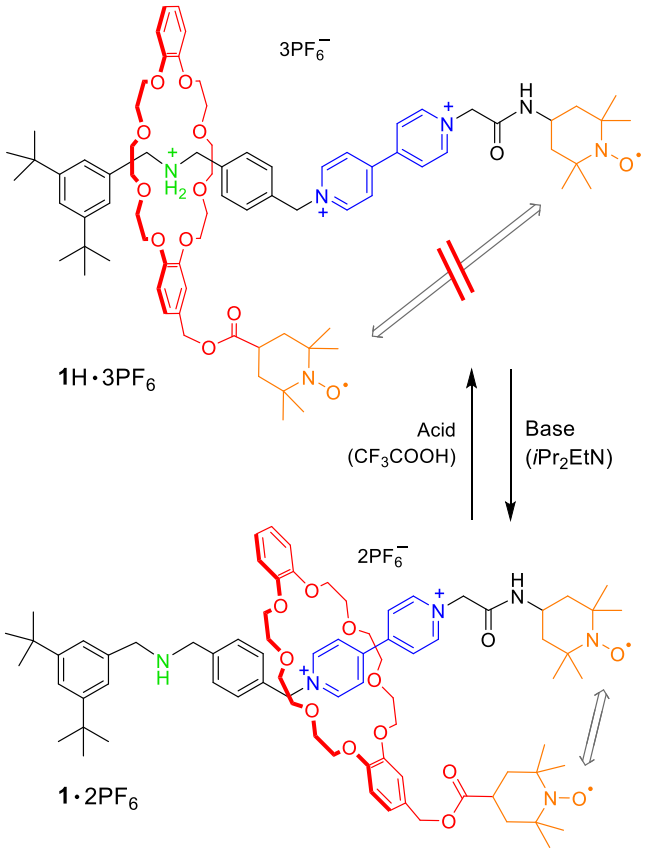

Figure 1. *Acid–base controlled shuttling based on a [2]rotaxane and schematic representation of the variation of distance between the two TEMPO radicals after the macrocycle displacement.*

The spin-labelled DB24C8 macroring displacement is obtained by means of the application of chemical stimulus; the addition of *i*Pr_2EtN determines the deprotonation of the rotaxane NH_2^+ centre and the consequently displacement of the DB24C8 macroring from NH_2^+ station toward BPY^{2+} unit, a process that can be reversed by acid treatment. This acid–base-driven displacement of the macrocycle affects the distance between the two TEMPO radicals, which are close together or far apart before and after deprotonation of NH_2^+ station respectively, thus influencing their through-space magnetic interaction (Figure 1).

1.2 Synthesis and ^{1}H NMR characterization

The synthetic procedure followed to obtain the rotaxane **1**H•3PF_6, its spin-labelled macrocycle **2** and spin-labelled dumbbell **3**H•3PF_6 is outlined in Scheme 1.

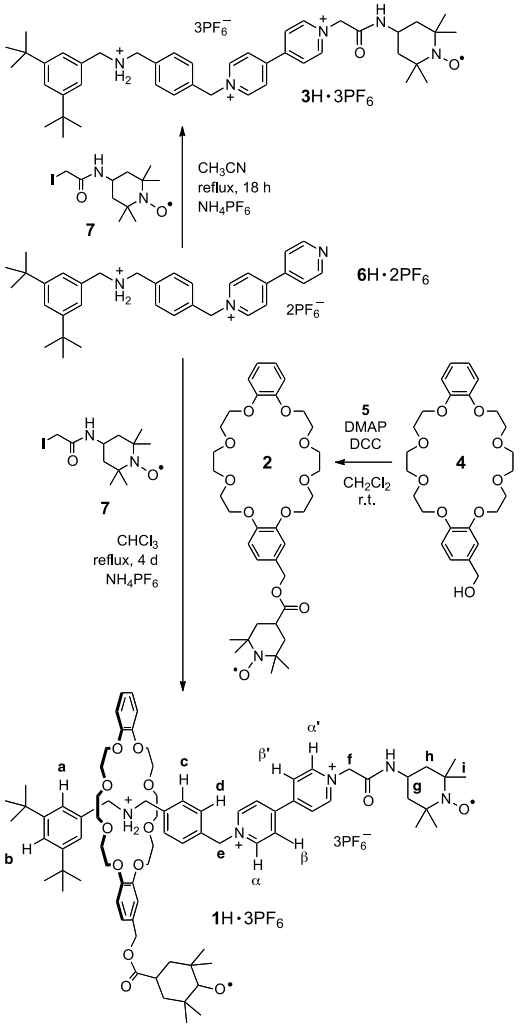

Scheme 1. *Synthesis of the rotaxane **1**H•3PF_6* and *of its components **2** and **3**H•3PF_6.*

The condensation of the macrocyclic alcohol **4** with 4-carboxy-TEMPO **5** using N,N'-dicyclohexyl-carbodiimide (DCC) and 4-dimethylaminopyridine (DMAP) as the condensing reagents afforded paramagnetic DB24C8 derivative **2** in 70% yield. The paramagnetic dumbbell **3**H•3PF_6 was obtained in 50% yield by adding the commercially available 4-(2-iodoacetamido)-TEMPO (**7**) to the half-thread **6**H•2PF_6 in ACN under reflux for 18h followed by anion exchange.

The next step was to investigate whether the size of TEMPO moiety was suitable to be used as the end-cap group in paramagnetic rotaxanes based on DB24C8 derivatives by performing studies of interlocking between the diamagnetic host **4** and the half-dumbbell **6**H•2PF_6.

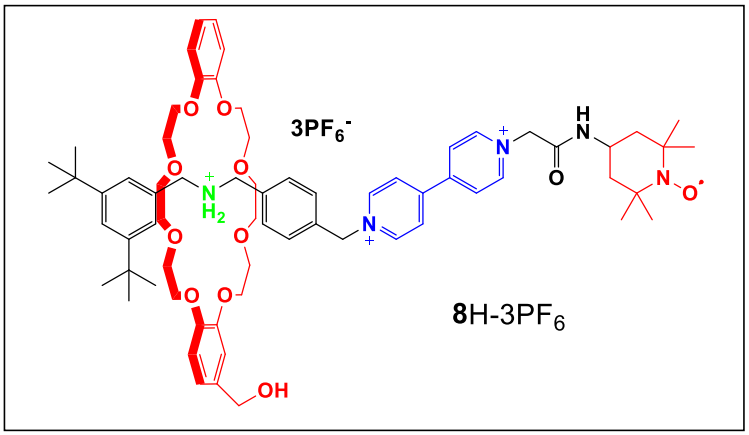

Figure 2. *Structure of [2]rotaxane **8**H•3PF_6 containing a diamagnetic macrocycle interlocked with a paramagnetic axle.*

Thus, we undertook the synthesis of **8**H•3PF_6 by following the synthetic strategy reported by Stoddart and coworkers, that exploits "threading and stoppering approach". In detail the diamagnetic macrocycle **4** was stirred with the half-thread **6**H•2PF_6 in chloroform to favour the formation of the pseudorotaxane, arising from the establishment of the hydrogen-bond interactions between the diamagnetic macrocycle and NH_2^+ recognition site.[1a,b] The mixture was then held at reflux for four days in the presence of the paramagnetic stopper **7** to give the corresponding [2]rotaxane in 30% yield. The diamagnetic macrocycle allowed to improve the spectral resolution of the NMR spectrum and consequently to check the robustness of the mechanical link by measuring a 1D Rotating-Frame Nuclear Overhauser Effect Spectroscopy (ROESY) spectrum of the sample in ACN (see Figure 3) following selective irradiation of the peak of methylene protons close to the ammonium site. The formation of host-guest complex was highlighted by the Nuclear Overhauser Effect (NOE) spectrum, which showed a significant enhancement of signals corresponding to the OCH_2

protons of the ring. This behaviour, typical of the complexation process, suggested that the macrocycle was located on NH_2^+ station and the dissociation of the component parts did not occur. Moreover the formation of a threaded complex was not detected heating a mixture of the crown ether **4** and the dumbbell **3**H•3PF6, further confirming that the TEMPO moiety was a suitable stopper .

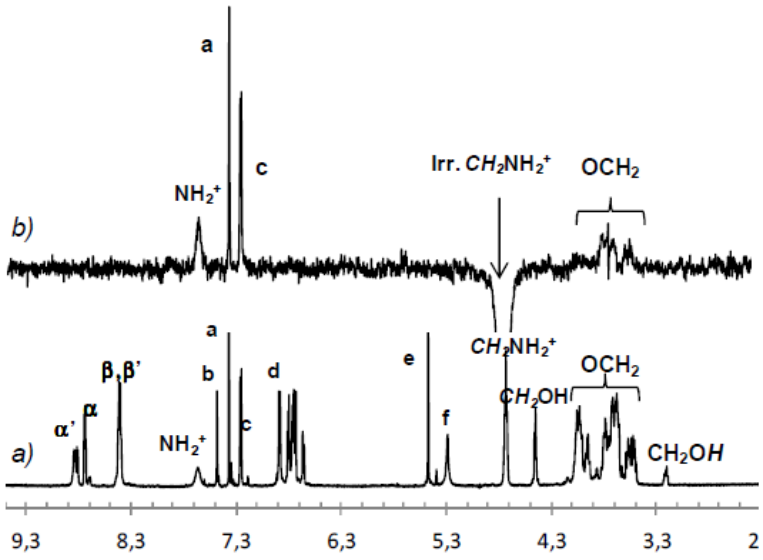

Figure 3. *a) ^{1}H NMR spectrum (600 MHz, CD_3CN, 298 K) of [2]rotaxane **8**H•3PF$_6$; b) 1D Roesy spectrum obtained by selective irradiation of the protons **CH$_2$**NH$_2^+$.*

Based on these successful synthetic results, the preparation of the target biradical rotaxane **1**H•3PF$_6$ was similarly obtained by threading **6**H•2PF$_6$ with the radical-armed DB24C8 **2** and using the TEMPO derivative **7** to introduce the second stopper (Scheme 1). The reaction progress was monitored by thin-layer chromatography and purification by silica gel column allowed to isolate **1**H•3PF$_6$ in 30% yield after anion exchange.

The rotaxane formation was confirmed by ^{1}H NMR spectroscopy comparing the spectra of the rotaxane, dumbbell and macrocycle. Partial spectra of the dumbbell **3**H•3PF$_6$ and the rotaxane **1**H•3PF$_6$ before and after addition of *i*Pr$_2$EtN in ACN are reported in Figure 4.

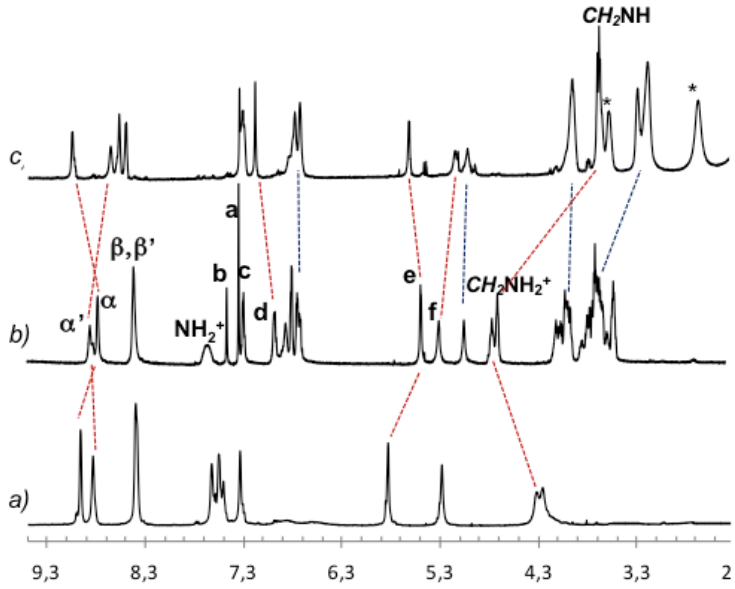

Figure 4. *Partial ^{1}H NMR spectra (600 MHz, CD_3CN, 298 K) of the dumbbell **3H**•3PF$_6$ (a), the rotaxane **1H**•3PF$_6$ (b), and the rotaxane **1**•2PF$_6$ obtained from **1H**•3PF$_6$ sample after addition of iPr_2EtN (c).*

Generally, the ^{1}H NMR of a paramagnetic specie is characterised by broadened peaks and the signals of the heterocycle radical are not detected because of the radical presence having a quenching effect on the nearby protons. In order to improve the spectral resolution and to confirm the nitroxide presence, the ^{1}H NMR spectra of the rotaxanes **1**H•3PF$_6$ and **8**H•3PF$_6$ and their dumbbell **3**H•3PF$_6$ were recorded also after *in situ* reduction by using phenylhydrazine to reduce the nitroxide unit into the corresponding hydroxylamine. ESI-MS analysis was used to provide evidence of the formation of the interlocked structure as well. The shuttling of the macrocycle towards the secondary BPY^{2+} station (Figure 1) was obtained by treating the **1**H•3PF$_6$ rotaxane in ACN with diisopropylethylamine (iPr$_2$EtN), which is strong enough to deprotonate the NH_2^+ center.[1a] Replacement of the ring onto the ammonium station was triggered by addition of trifluoroacetic acid. ^{1}H NMR spectrum of the spin labelled [2]rotaxane recorded after addition of the base afforded a clear evidence of the macrocycle displacement. In particular the peaks corresponding to the methylene protons close to ammonium station undergone large upfield shifts at 3.7 ppm (Figure 4C). Bipyridinium H$_{\alpha'}$ and H$_\alpha$ showed shifts of $\Delta\delta$=-0.19 and +0.27 ppm respectively, and H$_{\beta'}$ and H$_\beta$ showed downfield shifts of $\Delta\delta$=+0.09 and +0.19 ppm. A similar trend to bipyridinium protons was also detected for the methylene protons (protons f and e) adjacent to viologen, which undergo shifts of $\Delta\delta$=-0.15 and +0.13 ppm, respectively. In Figure 4 red dashed lines evidence the shift of guest protons caused by the movement of the paramagnetic crown

ether while blue dashed lines evidence the macrocycle signal changes. The signals marked with a star are relative to the protons of the amine.

The successive addition of CF_3COOH restored the original ^1H NMR spectrum (see Figure 4b), indicating the reversibility of the switching process.[1] Considering these experiments it is worth to note that the presence of the radical centers had not an influence on the macrocycle movement, allowing the use of nitroxide units as probes to investigate the systems.

1.3 ESR characterization

The magnetic interaction between the two TEMPO moieties of **1**H•3PF_6 rotaxane, which is influenced by the shutting motion of the macrocyclic ring, was monitored by ESR spectroscopy.

The ESR spectrum of the **1**H•3PF_6 rotaxane before addition of *i*Pr_2EtN and recorded in ACN at 298 K is reported in Figure 5a. The spectrum is characterized by three lines (g=2.0060, a_N=15.75 G) which is the typical spectrum of an isolated TEMPO, deriving from the coupling between the unpaired electron and the nitrogen atom. This observation indicated the absence of significant spin coupling between the two radicals when the macrocycle is located on the NH_2^+ station, suggesting that they are too far apart to interact. Upon addition of *i*Pr_2EtN, the EPR spectrum showed a noticeable change from a three- to a five-line spectrum, retaining the same a_N value (15.75 G) (Figure 5b). The appearance of extra lines in the ESR spectrum is due to the exchange interaction between the nitroxide units, which are sufficiently close to undergo exchange coupling. In fact, the exchange coupling constant between unpaired electron, *J*, is greater than the hyperfine splitting, a_N. Conversely, the same addition performed on a 1:1 mixture of the non-interlocked rotaxane components (**2** and **3**H•3PF_6) did not cause variations in the EPR signals. Such a control experiment confirmed that the observed EPR changes derived from through-space radical–radical interactions, which became possible because of ring shuttling in the deprotonated rotaxane.

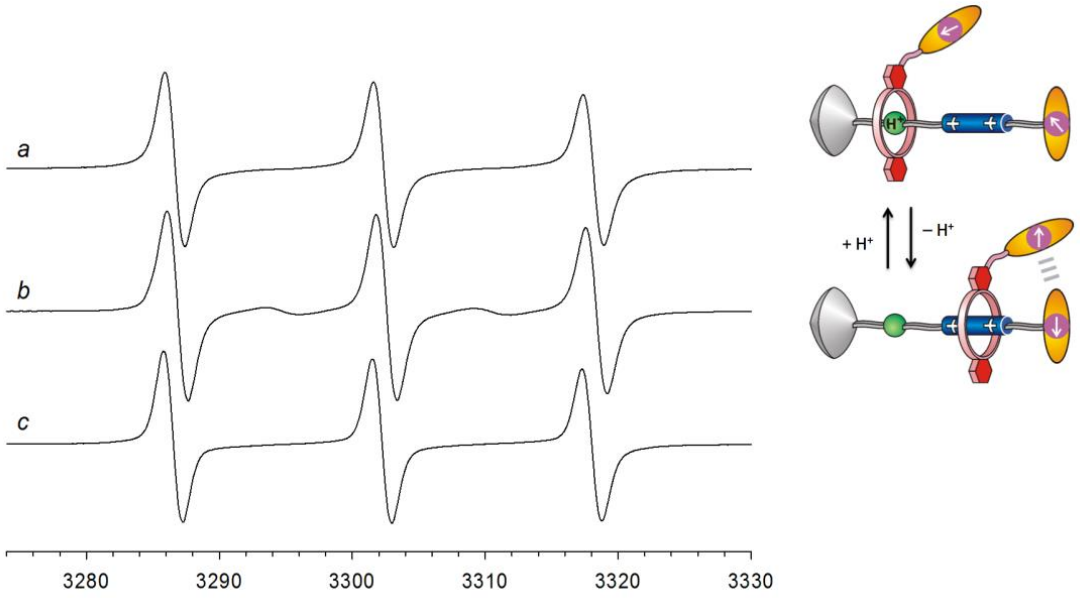

Figure 5. *Room temperature EPR spectra of rotaxane **1H•3PF$_6$** (0.15 mM) before (a) and after sequential addition of 2 equivalents of iPr$_2$EtN (b) and CF$_3$COOH (c).*

The ratio of line intensities, however, differed substantially from the 1:2:3:2:1 pattern expected in case all the conformations of the [2]rotaxane were characterized by strong spin exchange between the nitroxide units. Thus, the spectrum of the [2]rotaxane observed after addition of *i*Pr$_2$EtN was the superposition of the ESR signals due to the biradical where the two spin labels are too far apart to interact (three-line spectrum), and to biradical in with the TEMPO moieties are sufficiently close to undergo exchange coupling (five-line spectrum). By measuring the relative EPR line intensities,[3] it was possible to estimate that, in ACN at 298 K, about 15% of the deprotonated rotaxane molecules assume (co-)conformations in which the two nitroxide units are sufficiently close to one another to allow a strong electron exchange ($J>a_N$).

Such a behaviour is a consequence of the relatively large flexibility of the connectors that link the TEMPO centers to the rotaxane components and of the conformational degrees of freedom of the ring and dumbbell relative to each another. The addition of a stoichiometric amount of trifluoroacetic acid after the addition of the base caused the quantitative recovery of the initial three-line EPR spectrum (Figure 5c) as a consequence of the replacement of the macrocyclic ring to the ammonium station. The complete base- and acid-induced switching cycle of the EPR pattern was repeated for six times without an appreciable loss of signal, highlighting the reversibility of the process (see Figure 6).

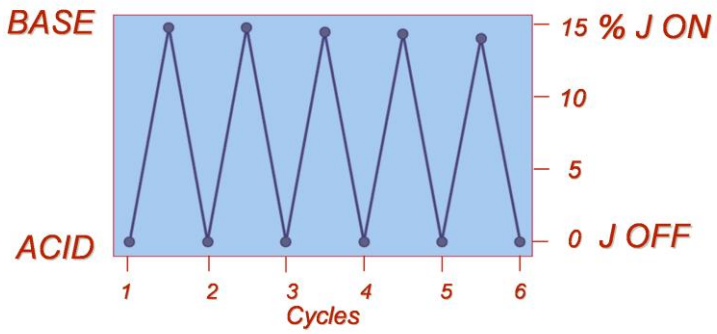

Figure 6. *Co-conformations (%) showing spin-exchange as function of sequential acid–base additions.*

The same experiments was carried out at a higher temperature (328 K) with similar results, confirming that this switching is not affected by the temperature.
In summary, we have developed a molecular machine, based on a spin labelled [2]rotaxane which is capable of switching on/off magnetic interactions by chemically driven reversible mechanical effects. The flexibility of this biradical molecular machine prevents to measure distances between two spin labels. To this aim is required a more rigid system which will be discussed in the following session.

2 Structural Changes of a Doubly Spin-Labelled Chemically Driven Molecular Shuttle Probed by PELDOR Spectroscopy

2.1 Introduction

An important key point to develop new synthetic molecular machines is represented by gaining accurate structural information about the accessible conformations, which are at the basis of the molecular machines operation. As previously mentioned, the most important members of synthetic molecular machines are bistable [2]rotaxane, in which it is possible to control the movement of the macrocycle between two different stations by application of appropriate stimuli.[4] Generally both the ring and the axle components are characterised by high degrees of freedom and as a consequence their relative displacement causes conformational changes[5] which can interfere with the primary motion (the ring shuttling).[6] To overcome this disadvantage, the design of bistable [2]rotaxanes having more rigid components could represented an interesting alternative.[7,8]

Information about conformations taking place in the molecular machines, are typically obtained by using high-resolution X-ray crystallography, which requires a crystalline sample, and nuclear magnetic resonance (NMR) spectroscopy, which provides structural information in the Angstrom scale using a solution of the sample. Thus, these techniques are useful but have some intrinsic limits, which can be bypass by performing electron-electron double resonance (PELDOR) spectroscopy. As mentioned in the introduction, PELDOR is a powerful pulsed electron paramagnetic resonance (EPR) which can measure the distance and distance distribution between a pair of spin labels[10] spaced by distances as large as 106 Å by measuring their dipolar coupling. This technique does not require a crystalline sample but simply a frozen solution and is able to afford structural information in the nanometer scale, typical range of the molecular machines operation.[9]

In this context we was able to observe for the first time the structural changes of molecular components of a spin-labelled rotaxane during a chemically induced shutting process by performing PELDOR supported by molecular dynamics (MD) calculations, thus obtaining interesting information on its functioning in solution. In the previous paragraph I have described a bistable [2]rotaxane composed of dibenzo[24]-crown-8 (DB24C8) ring and an axle component having dialkylammonium (NH_2^+) and 4,4'-bipyridinium (BPY^{2+}) recognition sites.[1] In this kind of rotaxane the macrocycle shutting between the different stations is fuelled by chemical stimulus. In particular, the addition of the base determined deprotonation of NH_2^+ and as a consequence the macrocycle movement towards BPY^{2+} site. Conversely, the addition of acid moved back the ring. The presence of paramagnetic moieties in both the ring and dumbbell components allowed to monitored the macrocycle displacement by ESR spectroscopy.[2] In fact interactions between these radicals could be switched between non coupled (three-line spectrum) and coupled (five-line spectrum) upon base-acid-induced displacement of the macrocycle. However analysing in detail the EPR lines intensity, it was resulted that about 15% of the rotaxane molecules have the two spin labels sufficiently close to another to show a strong interaction in consequence of ring shutting.[2] This result is strictly related to the high degree of freedom of the link between TEMPO moiety and the macrocycle and of the whole rotaxane structure. It is well know that a high flexibility in a spin-labelled system is responsible for a broadening of the distance distribution making impossible to achieve the determination of an exact distance.[11] In order to circumvent this inconvenient without affecting significant structural variations of the system, I modified the structure of the previously reported spin-labelled rotaxane[2] by removing a methylene spacer between the TEMPO moiety and the aromatic component of macrocycle, thus obtaining a more rigid connection of the spin label to the ring (rotaxane **10**H•3PF_6 in Scheme 2). This slight modification allowed on the one hand to ensure an accurate measure of the distance distribution avoiding the distance distribution broadening

and on the other hand to reduce structural changes maintaining most of the rotaxane architecture and as a consequence its operation.

2.2 Synthesis and ^{1}H NMR characterization

The synthesis of the rotaxane **10**H•3PF_6 and its more rigid macrocycle **9** is outlined in Scheme 2. The functionalization of the macrocycle with the spin label was achieved in 57% yield by condensation of the macrocyclic carboxylic acid with 4-hydroxy-TEMPO using N,N'-dicyclohexylcarbodiimide (DCC) and 4-dimethylaminopyridine (DMAP) as the condensing reagents. Using the same procedure previously mentioned, the target biradical rotaxane **10**H•3PF_6 was made by threading **6**H•2PF_6 with the paramagnetic DB24C8 **9** and using the 4-(2-iodoacetamido)-TEMPO to introduce the second stopper (Scheme 2). The rotaxane reaction was performed in chloroform to promote the pseudorotaxane formation due to the establishment of hydrogen bonding interactions between the crown ether and ammonium center. The paramagnetic rotaxane **10**H•3PF_6 was obtained in 36% yield following the same procedure employed for the rotaxane **1**H•3PF_6.

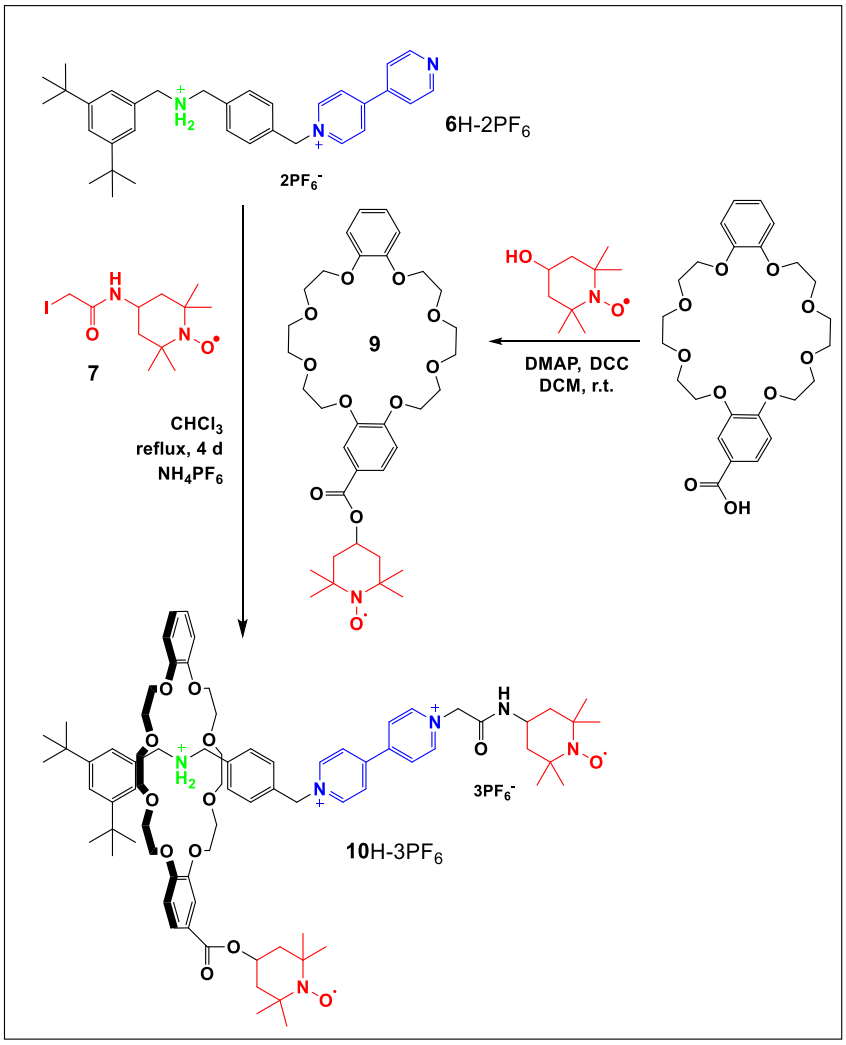

Scheme 2. *Synthesis of rotaxane **10**H•3PF$_6$.*

The ^{1}H NMR spectrum of **10**H•3PF$_6$ proved its interlocked nature. Also in this case the spectrum of **10**H•3PF$_6$ was recorded after the addition *in situ* of phenylhydrazine to improve the spectral resolution and to detect the proton signals close to the radical units.

The partial ^{1}H NMR spectra of the rotaxane **10**H•3PF$_6$, dumbbell **3**H•3PF$_6$ and macrocycle **7** are outlined in Figure 7. The direct comparison between the ^{1}H NMR spectra of the rotaxane and its non-interlocked components indicates the threading of the macrocycle and its preferred localization around the ammonium moiety. The red dashed lines in Figure 7 evidence the shielding of some guest protons caused by the presence of the paramagnetic crown ether.

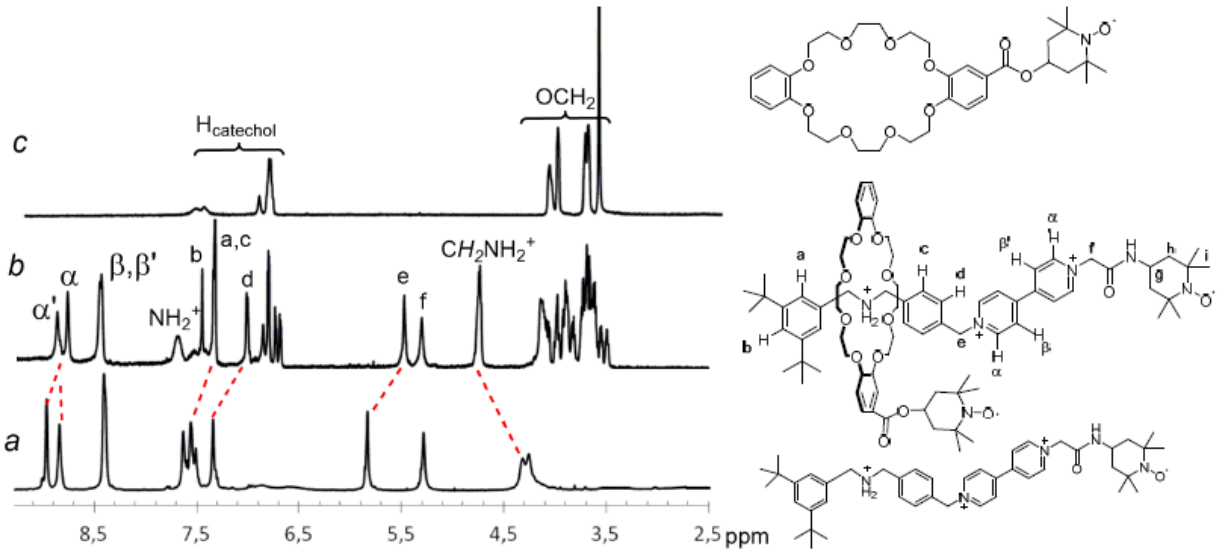

Figure 7. *Partial ^{1}H NMR spectra (600 MHz, CD_3CN, 298 K) of a) dumbbell **3H•3PF$_6$**; b) rotaxane **10H•3PF$_6$**; c) spin-labelled ring **9**.*

The acid/base reversible switch of the macrocycle from NH_2^+ to BPY^{2+} recognition site upon sequential treatment of DIPEA and CF_3COOH (Figure 8) was monitored by ^{1}H NMR spectroscopy and is reported in Figure 9.

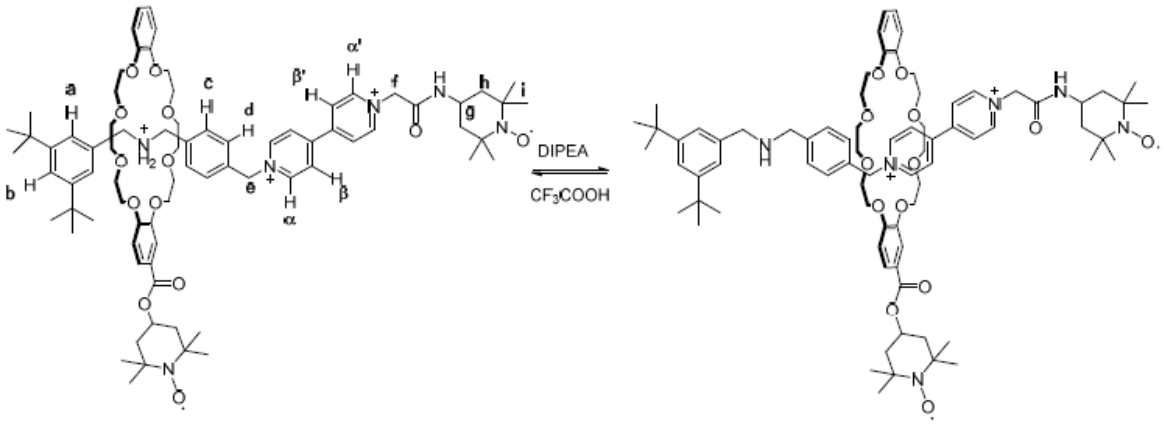

Figure 8. *Acid-base molecular shuttle.*

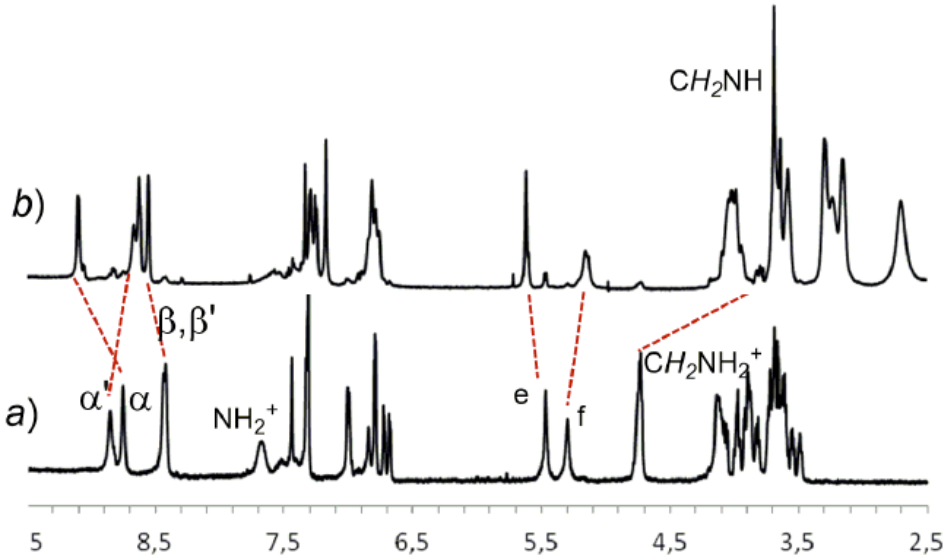

Figure 9. *Partial ^{1}H NMR spectra (600 MHz, CD_3CN, 298 K) of rotaxane a) in the absence, and b) in the presence of DIPEA.*

The addition of *i*Pr$_2$EtN caused shifts comparable to those observed for the rotaxane **1**H•3PF$_6$ upon deprotonation of ammonium center. The red dashed lines evidence the shift of guest protons caused by the movement of the paramagnetic crown ether. In more detail these shifts concern the protons close to ammonium station (C*H*$_2$NH^{2+}), the protons of bipyridinium system (H$_{\alpha'}$, H$_\alpha$, H$_{\beta'}$, H$_\beta$) and the protons adjacent to viologen (e, f) while the macrocycle signals are not affected by its displacement. The addition of trifluoroacetic acid triggered the return of the ring onto the ammonium station and reverted the ^{1}H NMR spectrum to the original one, verifying the reversibility of the shuttling process.

2.3 ESR characterization

The paramagnetic properties of the rotaxane were investigated by continuous-wave EPR spectroscopy at room temperature in methanol. A three-line spectrum (g=2.0060, a_N=15.75 G) typical of isolated TEMPO radicals was observed when the macrocycle is located on the NH$_2^+$ station, suggesting the absence of strong through-space spin coupling between the two radical units which are too far apart to interact.[12]

Against all our expectations, upon the addition of DIPEA to the rotaxane the EPR did not change from three to five lines, but its shape remained quite similar (Figure 9).[13]

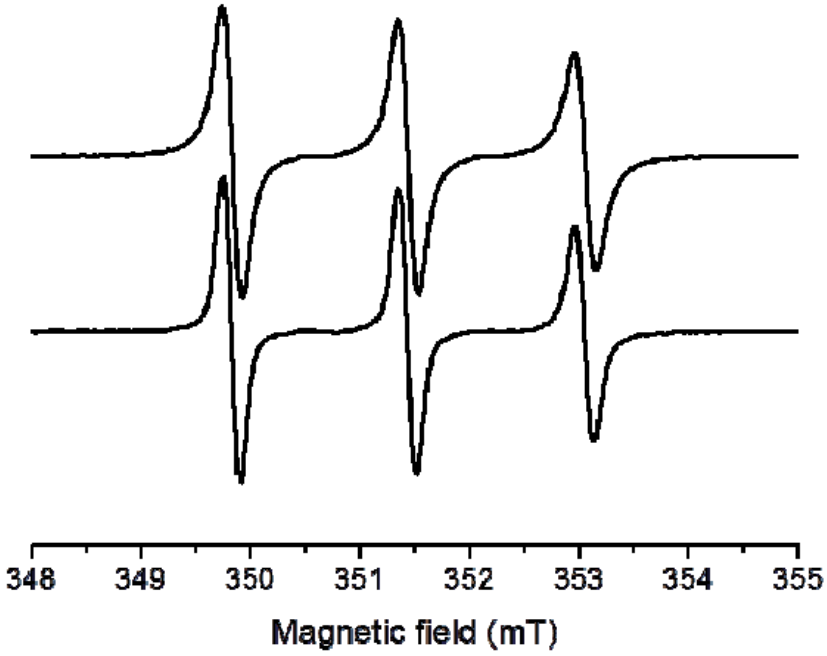

Figure 9. *EPR spectrum of **10**H•3PF$_6$ before (up) and after (bottom) addition of DIPEA.*

This behaviour, which is different from the rotaxane reported in paragraph 1.2, could be ascribed to a large spatial separation between the nitroxide units also after the ring displacement to the BPY^{2+} site. This counterintuitive feature suggested that the macrocycle displacement was associated with a structural rearrangement, which did not influence the distance between the spin labels. In order to determine the correct geometry of the paramagnetic rotaxane, the nitroxide distance distributions were investigated by PELDOR spectroscopy.

2.4 PELDOR experiments

PELDOR experiments were carried out at 50 K on a Q-band spectrometer operated at 33.85 GHz on a glassy frozen solution of the rotaxane dissolved in a mixture of perdeuterated methanol and water (98:2) at a concentration of about 80 µM both in the absence and in the presence of 1 M DIPEA. A standard four-pulse dead-time free sequence was used with the pump pulse (56 ns) set in correspondence of the maximum of the absorption EPR spectrum of the compound while the observer sequence (28/56/56 ns) was set to -80 MHz. The PELDOR traces (Figure 10) were processed and analysed by using the DeerAnalyis2013 software package.[14]

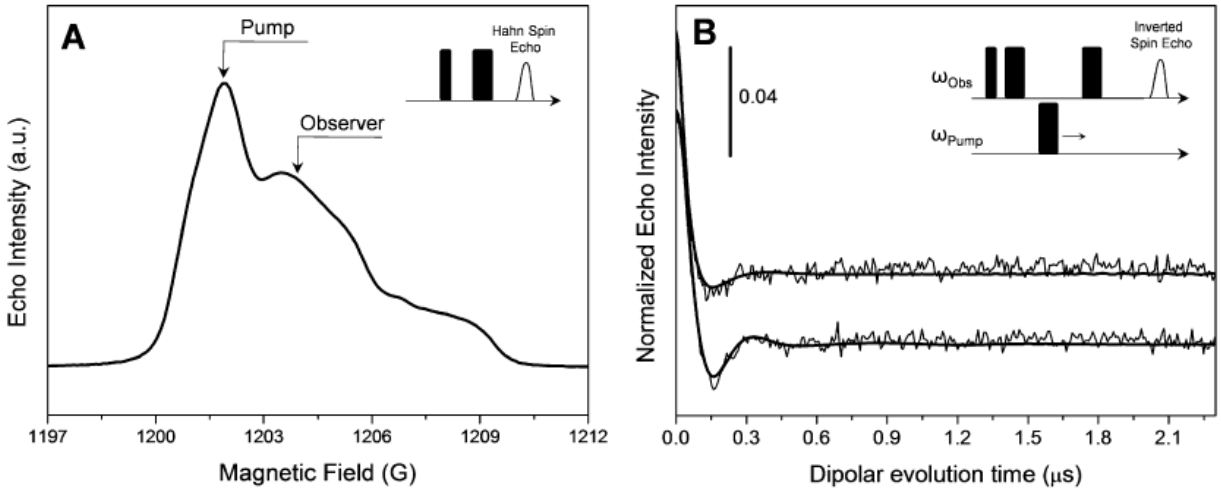

Figure 10. *Q-Band pulsed EPR experiments at 50 K. A) Field-swept electron spin-echo experiment on the **10**H•3PF$_6$ sample. B) PELDOR time traces after background correction and corresponding simulations obtained from DeerAnalysis before (upper traces, **10**H•3PF$_6$) and after (lower traces, **10**•2PF$_6$) the addition of the DIPEA base.*

Distance distributions *p(r)*, obtained by the model-free Tikhonov regularization method, were centered at 22.6 Å (width at half-height of about 11 Å) for **10**H•3PF$_6$ (Figure 11a, grey line) and at 24.2 Å (width at half-height of about 5 Å) for **10**•2PF$_6$ (Figure 11b, greyline).[15]
A careful analysis of these PELDOR traces showed interesting considerations: 1) the shuttling process had not an influence on the distance distributions between spin labels, according to the evidences obtained by EPR spectroscopy (see session 2.3); 2) when the macrocycle resided on the ammonium site a broad distance profile (half-height width of 11 Å) was observed, suggesting a large degree of conformational freedom of the rotaxane in this state; and 3) when the macrocycle encircled the bipyridinium station a significant narrowing of distance profile corresponding to a reduction of the conformational freedom of the rotaxane was detected.
The large conformational degree of freedom characterising the rotaxane is mainly due to the mechanical linkage between the molecular components. Thus, in order to sample the conformational space available to the spin label probes and to deduce the geometry in agreement with the PELDOR distance distributions, stochastic dynamic (SD) calculation were performed. The simulations were performed in gas phase at 298 K both on the rotaxane with the macrocycle encircling the ammonium and on the rotaxane having the macrocycle on the bipyridinium site, by using the AMBER* force field. The N-O bond was modeled by the C=O bond. This is made possible by the similar geometries of these groups and the higher reliability of the carbonilic group in AMBER* force field.[16] This computational approach consisted in the arrangement of the thread inside the macrocycle cavity, energy-

minimizing the mechanical complex, and carrying out standard equilibrations and production runs to derive distance distributions, *p(r)*, between the midpoint of N-O·bonds.

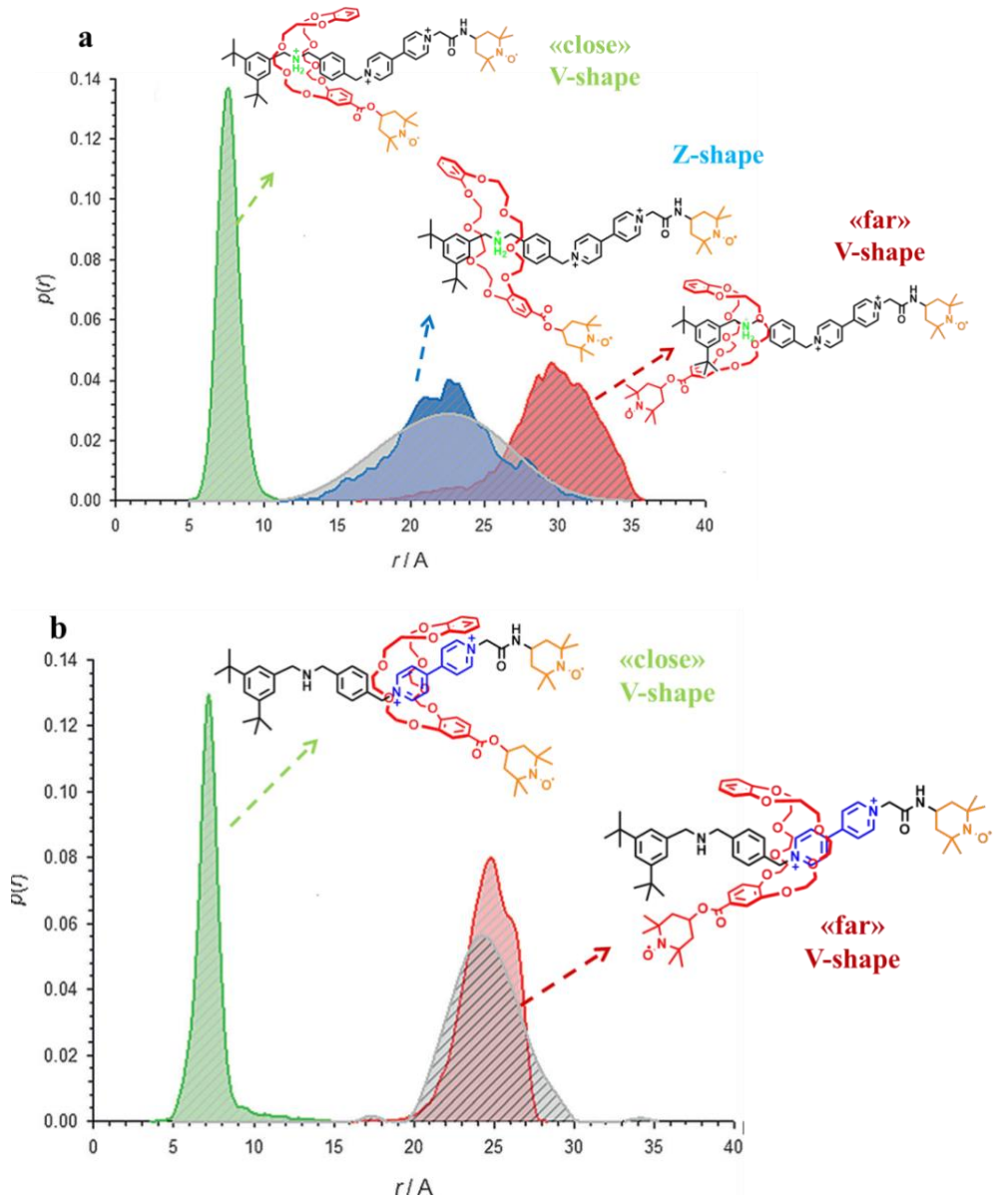

Figure 11. *Experimental (determined by PELDOR, grey) and theoretical (SD calculations) label-to-label distance distributions of the [2]rotaxane when the ring is on NH_2^+ station (a) and BPY^{2+} unit (b) in frozen ACN solution.*

It should be noted that long SD simulations might be required to adequately sample all the accessible (co-)conformations of the spin-labeled rotaxane in the two states. To overcome this drawback, SD calculations were performed considering the following starting geometrical constraints, derived from X-rayinvestigations[1b,17]: 1) the geometry of the (tBu)$_2$Ph-CH$_2$NH$_2^+$CH$_2$-p-Xy portion of the thread was set *all*-anti with the phenyl units oriented approximately orthogonal; 2) the *p*-Xy and nearby Py$^+$ rings were put in an “open-

book" conformation; and 3) the mean torsional twist around the bond linking the two Py^+ rings was 40°. The ring component was forced to adopt an extended *all*-gauche conformation for the O-C-C-O units in its ethylene glycol chains.

According to published crystallographic data,[1b,17] the macrocycle can adopt two main conformations: a V-shape geometry, in which the two catechol rings form an angle of 80°,and a Z-shaped form, in which the two catechol rings are parallel to each other (Figure 12).

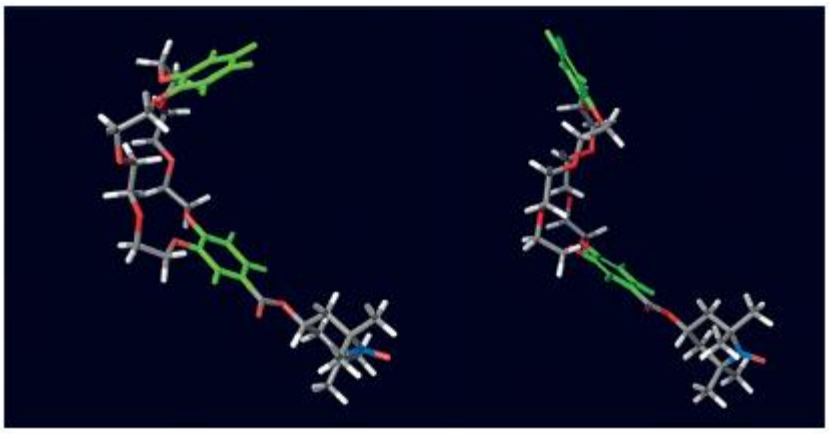

Figure 12. *V-shaped (left) and Z-shaped (right) geometry of spin-labeled macrocycle employed in the SD calculations. Dioxybenzene units are coloured in green for clarity*.

Different results were obtained depending on the relative orientation of the two spin labels for the V-shaped conformation: "close geometry" with the nitroxide units oriented towards the same direction and "far geometry" with the spin labels oriented in opposite directions (Figure 11a).

All possible geometries were calculated considering both the two different macrocyclic conformations (V-shape and Z-shape) and the relative orientation of the two spin labels ("close" and "far" geometries).

The axle and the ring were then translated to have the recognition site (that is, the ammonium or pyridinium nitrogen atoms) located at the symmetry center of the macrocycle. At the end of this procedure, energy minimization of the rotaxane led to the starting geometry for SD simulations. When the macrocycle is on the ammonium station it was obtained a broad distance profile centered at 22.6 Å (Figure 11a). Considering both orientations of the two spin labels, with the "close V-shape geometry", it was obtained a distance distribution, which was not compatible with the experimental data because it was centered at a very short distance (9.2 Å) and its profile was too narrow. On the other hand, with the "far geometry" the distance distribution was centered at a much longer distance

(29.5 Å) than the experimental calculation. On the contrary, when the ring adopted a Z-shaped geometry, a very broad distance profile centered at 22.8Å was obtained independently from the starting relative orientation of the two spin labels. This interesting observation suggested that there was not a distinction between “close” or “far” arrangements for the Z-shape geometry.

In order to prove that the distance distribution was influenced by the macrocycle conformation and not by the flexibility of the axle, we monitored the distance between the nitroxide stopper unit and the ammonium recognition site during the simulations. Such distance profiles resulted to be very similar for all the investigated starting geometries and were centered at 21.2$\pm$0.5 Å. This result indicates that the PELDOR spin-label distance distribution is mainly determined by the ring conformation and by the relative position of the interlocked molecular components.

Comparing the theoretical spin-label distance distributions with that obtained from PELDOR spectroscopy (Figure 11a) it clearly suggested that the macrocycle adopted a Z-shaped geometry when it resided on the ammonium site. This result was conform to the crystallographic structure observed for a similar system.[17b]

The same computational procedure was repeated by positioning the symmetry center of the macrocycle on the pyridinium nitrogen linked to the *p*-Xy portion and calculating all possible geometries and the relative orientation of the two spin labels. An unrealistic short distance profile was obtained (<p(r)> =7.2 Å) when the macrocycle adopted the V-shape as starting geometry, while a suitable profile centered at 24.6 Å was calculated with the far V-shape geometry. When the calculation was started with a Z-shape geometry, the macrocycle rapidly evolved to the far V-shape arrangement, affording the same distance distribution obtained using the far V-shape as the starting geometry. Overall, we have concluded that the V-shape geometry is the mainly adopted form by the macrocyle when it resides on pyridinium station.

However previously studies about the DB24C8/4,4’-bipyridinium inclusion complexes, proved that the orientation of the dioxybenzene units of DB24C8 with respect to the bipyridinium unit is that obtained for the close V-shape conformation in disagreement with our results.[18] In fact spectroscopic and voltammetric measurements[1] showed that this kind of arrangement allowed the occurrence of donor–acceptor interactions between the electron-rich dioxybenzene units and the electron-poor bipyridinium site. The different macrocycle conformation observed in the rotaxane **10**•2PF_6 was due to the presence of the electron-with drawing ester substituent on a dioxybenzene unit which could affect its ability to interact with the bipyridinium site. Such a hypothesis is supported by the fact that the bipyridinium reduction potential in **10**•2PF_6 (-0.50 V vs SCE in ACN) is significantly less negative than that in a similar rotaxane having an unsubstituted DB24C8 ring (-0.59 V).[1b]

2.5 Conclusion

In summary, we have developed an acid–base switchable molecular shuttle based on the rotaxane **1**H•3PF_6, incorporating stable radical units in both the ring and dumbbell components and proved the ring movement by measuring the through-space electron exchange interactions using EPR spectroscopy.[2] A slight structural modification of the rotaxane **1**H•3PF_6 is represented by the rotaxane **10**H•3PF_6. This more rigid system has the necessary requirements to employ PELDOR technique to measure the distance and distance distribution between a pair of spin labels spaced by distances as large as 106 Å by measuring their dipolar coupling. Therefore we have applied for the first time a combined PELDOR/MD study to monitor the structural macrocycle changes promoted by the chemical switching between **10**H•3PF_6 and **10**•2PF_6rotaxanes. In detail the macrocycle goes from a Z-shaped geometry in **10**H•3PF_6 (ring on the ammonium site) to a V-shaped geometry in **10**•2PF_6 (ring on the bipyridinium site).[19] As a result, the distance between the nitroxide labels is not significantly affected by ring shuttling and it remains quite large, suggesting that through-space electron exchange interactions are largely prevented, as shown by continuous-wave EPR spectra.

References

[1] a) M.-V. Martínez-Diaz, N. Spencer, J. F. Stoddart, *Angew. Chem. Int. Ed. Engl*. **1997**, *36*, 1904- 1907; *Angew. Chem*. **1997**, *109*, 1991 –1994; b) P. R. Ashton, R. Ballardini, V. Balzani, I. Baxter, A. Credi, M. C. T. Fyfe, M. T. Gandolfi, M. Gómez-López, M.-V. Martínez-Diaz, A. Piersanti, N.Spencer, J. F. Stoddart, M. Venturi, A. J. P. White, D. J. Williams, *J. Am. Chem. Soc*. **1998**, *120*, 11932 –11942; c) S. Garaudée, S. Silvi, M. Venturi,A. Credi, J. F. Stoddart, *ChemPhysChem* **2005**, *6*, 2145 –2152.

[2] V. Bleve, C. Schäfer, P. Franchi, S. Silvi, E. Mezzina, A. Credi, M. Lucarini, *ChemistryOpen* **2015**, *4*, 18 –21.

[3] C. Casati, P. Franchi, R. Pievo, E. Mezzina, M. Lucarini, *J. Am. Chem. Soc*. **2012**, *134*, 19108 –19117.

[4] S. Silvi, M. Venturi, A. Credi, *J. Mater. Chem*. **2009**, *19*, 2279–2294.

[5] a) T. Yamamoto, H.-R. Tseng, J. F. Stoddart, J. F. V. Balzani, A. Credi, F. Marchioni, M. Venturi, *Coll. Czech. Chem. Commun*. **2003**, *68*, 1488 –1514; b) J. O. Jeppesen, S. A. Vignon, J. F. Stoddart, *Chem. Eur. J*. **2003**, *9*, 4611–4625; c) M. Hmadeh, A. C. Fahrenbach, S. Basu, A. Trabolsi, D. Benitez, H. Li, A.-M. Albrecht-Gary, M. Elhabiri, J. F. Stoddart, *Chem. Eur. J.* **2011**, *17*, 6076–6087; d) J. Baggerman, N. Haraszkiewicz, P. G. Wiering, G. Fioravanti, M. Marcaccio, F. Paolucci, E. R. Kay, D. A. Leigh, A. M. Brouwer, *Chem. Eur. J*. **2013**, *19*, 5566–5577; e) S. S. Andersen, A. I. Share, B. L. Poulsen, M. Korner, T. Duedal, C. R. Benson, S. W. Hansen, J. O. Jeppesen, A. H. Flood, *J. Am. Chem. Soc*. **2014**, *136*, 6373–6384; f) Y. Zhao, R. Zhang, C. Minot, K. Hermann, M. A. Van Hove, *Phys. Chem. Chem. Phys*. **2015**, *17*, 18318–18326.

[6] a) S. Saha, A. H. Flood, J. F. Stoddart, S. Impellizzeri, S. Silvi, M. Venturi, A. Credi, *J. Am. Chem. Soc.* **2007**, *129*, 12159–12171; b) M. Woźny, J. Pawłowska, A. Osior, P. Świder, R. Bilewicz, B. Korybut-Daszkiewicza, *Chem. Sci*. **2014**, *5*, 2836–2842.

[7] See, for example: a) S. Nygaard, K. C.-F. Leung, I. Aprahamian, T. Ikeda, S.Saha, B. W. Laursen, S.-Y. Kim, S. W. Hansen, P. C. Stein, A. H. Flood, J. F.Stoddart, J. O. Jeppesen, *J. Am. Chem. Soc.* **2007**, *129*, 960–970; b) A.Moretto, I. Menegazzo, M. Crisma, E. J. Shotton, H. Nowell, S. Mammi, C.Toniolo, *Angew. Chem. Int. Ed.* **2009**, *48*, 8986–8989; *Angew. Chem.* **2009**, *121*, 9148–9151; c) K. Zhu, V. N. Vukotic, S. J. Loeb, *Angew. Chem. Int. Ed*. **2012**, *51*, 2168–2172; *Angew. Chem.* **2012**, *124*, 2210–2214; d) P. G. Young, K. Hirose, Y. Tobe, *J. Am. Chem. Soc.* **2014**, 136, 7899–7906; e) X. Jiang, B. Rodriguez-Molina, N. Nazarian, M. A. Garcia-Garibay, *J. Am. Chem. Soc*. **2014**, *136*, 8871–8874.

[8] F. Durola, V. Heitz, F. Reviriego, C. Roche, J. P.Sauvage, A. Sour, Y. Trolez, *Acc. Chem. Res.* **2014**, *47*, 633–645.

[9] a) R. Pievo, C. Casati, P. Franchi, E. Mezzina, M. Bennati, M. Lucarini, *ChemPhysChem* **2012**, *13*, 2659–2661; b) C. Casati, P. Franchi, R. Pievo, E. Mezzina, M. Lucarini, *J. Am. Chem. Soc.* **2012**, *134*, 19108–19117; c) G. Jeschke, A. Godt, *ChemPhysChem* **2003**, *4*, 1328–1334.

[10] a) A. D. Milov, A. B. Ponomarev, Y. D. Tsvetkov, *Chem. Phys. Lett*. **1984**, *110*, 67–72; b) G. Jeschke, M. M. Pannier, H. W. Spiess, *In Distance Measurements in Biological Systems by EPR* (Eds.: L. J. Berliner, S. S. Eaton,G. R. Eaton), Kluwer Academic, New York, **2000**; Vol. *19*, 493–512;c) S. S. Eaton, G. R. Eaton, *Specialist Periodical Reports on Electron Spin Resonance* **2004**, *19*, 318–337; d) O. Schiemann, T. F. Prisner, *Q. Rev. Biophys*. **2007**, *40*, 1–53; e) G. Jeschke, *Annu. Rev. Phys. Chem*. **2012**, *63*,419–446; f) A. J. Fielding, M. G. Concilio, G. Heaven, M. A. Hollas, *Molecules* **2014**, *19*, 16998–17025.

[11] S. M. Islam, B. Roux, *J. Phys. Chem. B* **2015**, *119*, 3901–3911.

[12] a) G. L. Closs, M. D. E. Forbes, P. Piotrowiak, *J. Am. Chem. Soc*. **1992**, *114*, 3285–3294; b) V. Barone, A. Bencini, A. Di Matteo, *J. Am. Chem. Soc*. **1997**, *119*, 10831–10837.

[13] The presence of exchange lines in the EPR spectrum of **10**•2PF6 can also depend on the nature of solvent. Actually, in acetonitrile very weak exchange lines were detected at room temperature.

[14] G. Jeschke, V. Chechik, P. Ionita, A. Godt, H. Zimmermann, J. Banham, C. Timmel, D. Hilger, H. Jung, *Appl. Magn. Reson*. **2006**, *30*, 473–498.

[15] The lower limit for reliable PELDOR measurements for broadly distributed distances between nitroxide spin labels is at approximately 1.6 nm. The distance distribution has been extended to lower distances to visualize completely the broad distance distribution for **10**H•3PF_6. See: J. E.Banham, C. M. Baker, S. Ceola, I. J. Day, G. H. Grant, E. J. J. Groenen, C. T.Rodgers, G. Jeschke, C. R. Timmel, *J. Magn. Reson*. **2008**, *191*, 202–218.

[16] P. Franchi, M. Lucarini, E. Mezzina, G. F. Pedulli, *J. Am. Chem. Soc*. **2004**, *126*, 4343–4354.

[17] a) P. R. Ashton, I. Baxter, M. C. T. Fyfe, F. M. Raymo, N. Spencer, J. F. Stoddart, A. J. P. White, D. J. Williams, *J. Am. Chem. Soc*. **1998**, *120*, 2297 –2307; b) S. J. Cantrill, D. A. Fulton, A. M. Heiss, A. R. Pease, J. F. Stoddart, A. J. P. White, D. J. Williams, *Chem. Eur. J.* **2000**, *6*, 2274–2287.

[18] a) F. Huang, PhD Dissertation, Virginia Polytechnic Institute, Blacksburg, Virginia, 2005, Ch. III; b) J. Zhang, F. Huang, N. Li, H. Wang, H. W. Gibson, P. Gantzel, A. L. Rheingold, *J.Org. Chem*. **2007**, *72*, 8935–8938; c) K. Nikitin,H. Miller-Bunz, *New J. Chem*. **2009**, *33*, 2472–2478.

[19] P. Franchi, V. Bleve, E. Mezzina, C. Schäfer, G. Ragazzon, M. Albertini, D. Carbonera, A. Credi, M. Di Valentin, M. Lucarini, *Chem. Eur. J.* **2016**, *22*, 8745 – 8750.

Chapter 3

Bistable [2]rotaxanes based on a novel spin labelled macrocycle

1.1 Novel spin-labelled macrocycle

As illustrated in the previous chapters crown ethers were extensively investigated in host-guest chemistry because of their well-known ability to complex selectively ions and neutral molecules.[1-5] Modified crown ethers containing nitroxide functionality positioned near the cavity had been reported in the past. Detailed studies had highlighted that in particular case the nitroxide oxygen atom can participate directly in the complexation interactions with the host metal ion being located toward the cavity of these molecules.[6] This peculiar skill was deduced by performing EPR spectroscopy and taking into consideration variations in the electron spin resonance (ESR) hyperfine splitting parameter, a_N, upon the complexation process. Actually, the presence of a metal ion within the cavity of these nitroxide-macrocycles is expected to determine an increase of the a_n value in comparison with the uncomplexed nitroxide mainly from changes in the distribution of unpaired spin density upon complexation. On these basis, the employment of such family of macrocycles can extend the use of EPR spectroscopy in the field of host-guest recognition chemistry.

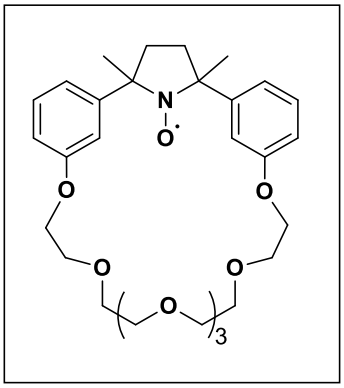

Figure 1. *Structure of the novel spin-labeled crown ether.*

The presence of nitroxide inside the crown ether cavity is an attracting feature because the radical could play a key role in the interaction with suitably chosen recognition sites when this novel spin-labeled macrocycle is employed as wheel in bistable [2]rotaxanes. At the same time EPR spectroscopy is crucial for the characterization of these systems. Moreover, the nitroxidic functionality could be employed to promote the movement of the wheel.

Basing on these appeal considerations, herein I describe the synthesis and paramagnetic properties of a novel spin-labeled crown ether, shown in Figure 1. This macrocycle compared to the spin-labeled crown ether mentioned in Chapter 2, is not functionalized with a nitroxide arm, but the radical is part of the ring structure. However, it is worth noting that it retains an important feature regarding the number of oxygen atoms and consequently the dimension of

the crown ether cavity. These close similarities in terms of dimension and properties has suggested to prepare a derivative containing 7 ethereal oxygen atoms and to evaluate the interaction ability of this macrocycle with the dumbbell containing dialkylammonium (NH_2^+) and 4,4'-bipyridinium (BPY^{2+}) recognition sites in order to obtain a bistable [2]rotaxane composed by a wheel in which the nitroxide group could participate in the interaction with these different stations as well as act as EPR probe.

1.2 Synthesis of the spin labelled macrocycle

As mentioned in the introduction nitroxide spin-labelled crown ethers containing 5 or 7 ethereal oxygen atoms, shown in Figure 2, had been already reported in the literature.[6]

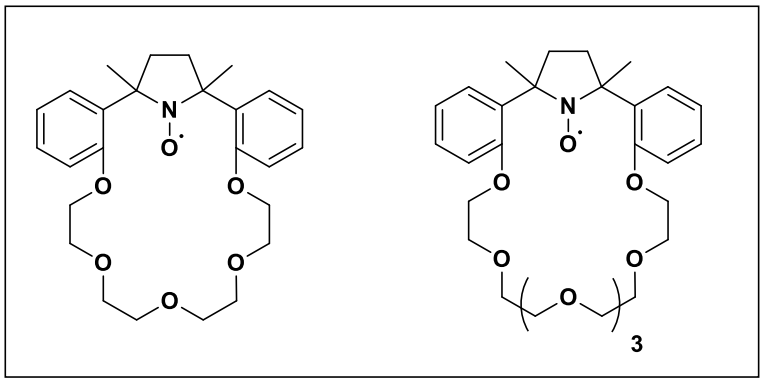

Figure 2. *Structure of spin-labelled crown ethers containing 5 or 7 ethereal oxygen atoms.*

However, the derivative containing 7 ethereal oxygen described here differ from that already reported for the different meta substitution on the two aromatic ring. Numerous attempts was carried out in order to obtain the spin-labeled macrocycle but the unique successful synthetic procedure is outlined in Scheme 1. Oxidation of 2-methyl-1-pyrroline (**1**) with $MeReO_3$/urea•H_2O_2 gave nitrone **2** in 90% yield after column chromatography on silica gel. The nitrone group was then transformed into the corresponding hydroxylamine by reaction with 3-methoxy-C_6H_4MgBr in THF (**3**) which gave compound **4** in 48% yield after purification. The subsequent oxidation by using $Cu(OAc)_2$ under air produced nitrone **5** in 71% yield. Repetition of the two-step sequence, namely the Grignard introduction followed by air oxidation, led to nitrone **6** in 72 % overall yield from **5**. The smooth demethylation to bisphenol **7** was performed by using boron tribromide 1.5 M in diethyl ether. After several abortive attempts to bisalkylate compound **7** with diiodine glycol chain and NaH in DMF, success was achieved by using ditosylate chain **8**, obtained after tosylation of the corresponding dialcohol derivative, and using

THF in place of DMF. A necessary requirement to obtain the attach of the glycol chain and the following cyclization is represented by high dilution conditions which favored the intramolecular substitution avoiding the intermolecular one to give nitrone macrocycle **9** in 30% yield. Reaction of nitrone **9** with MeLi provided the hydroxylamine derivative **10** in quantitative yield as a mixture of *cis* and *trans* isomer, assessed by performing ^{1}H NMR of compound **10**. This hydroxylamine was susceptible to air oxidation and often contained a trace amount of nitroxide **11**, which interfered with the NMR measurement. Hydroxylamine **10** was completely oxidized with air in the presence of Cu^{2+} ion to nitroxide **11**. Further attempts to improve this synthesis are under way in ourlaboratory with the main purpose to increase the overall yield of the synthetic process, clarify the stereochemistry of the addition reaction to the nitrone and consequently achieve a stereoselective synthesis.

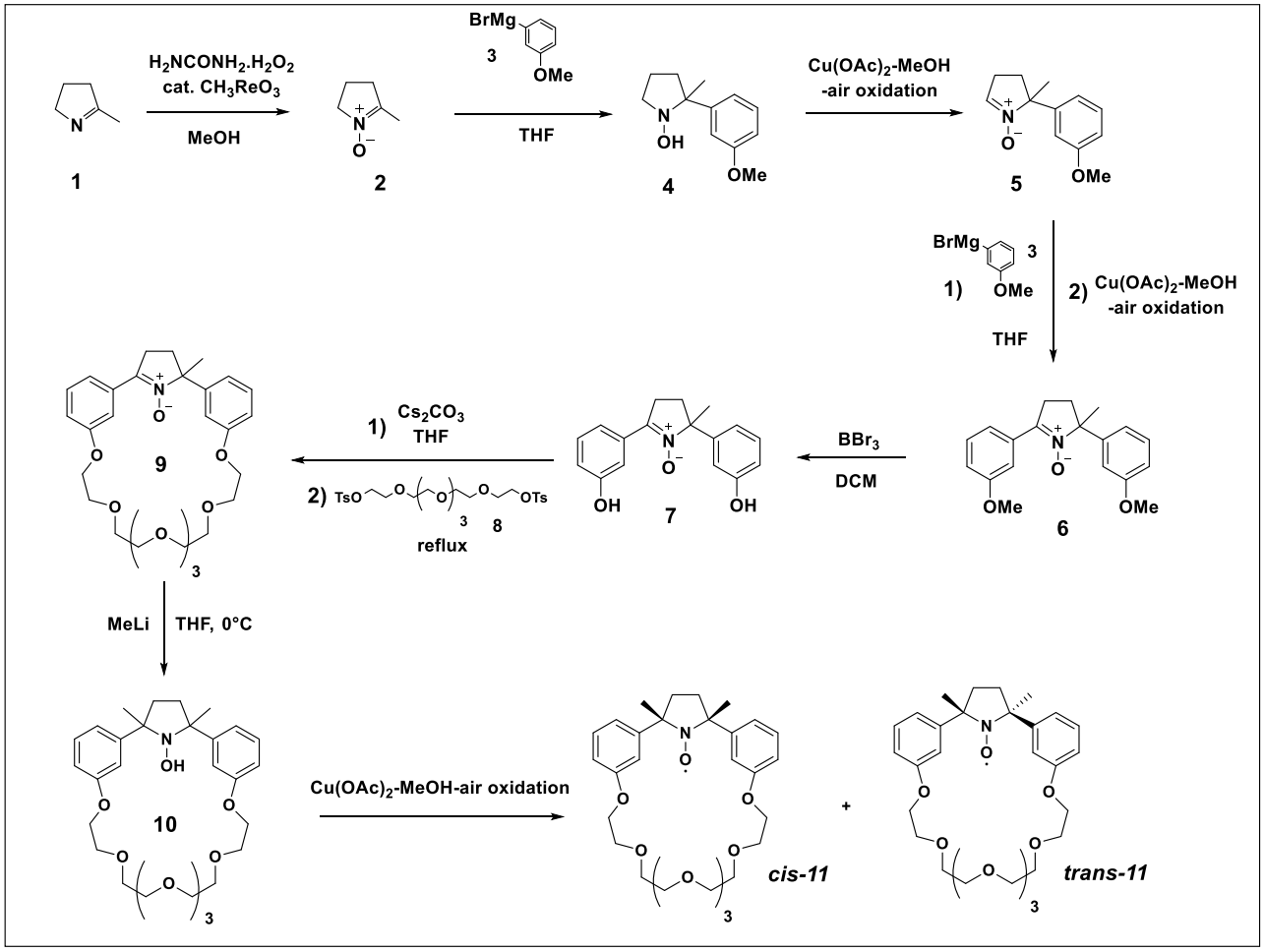

Scheme 1

1.3 EPR characterization of the spin labelled macrocycle

The ESR spectrum of nitroxide **11** recorded in DCM at 298 K (a_N=14.32 G, g=2.0058) is reported in figure 3. As expected, the spectrum is characterized by three lines due to the coupling of the unpaired electron with ^{14}N nucleus.

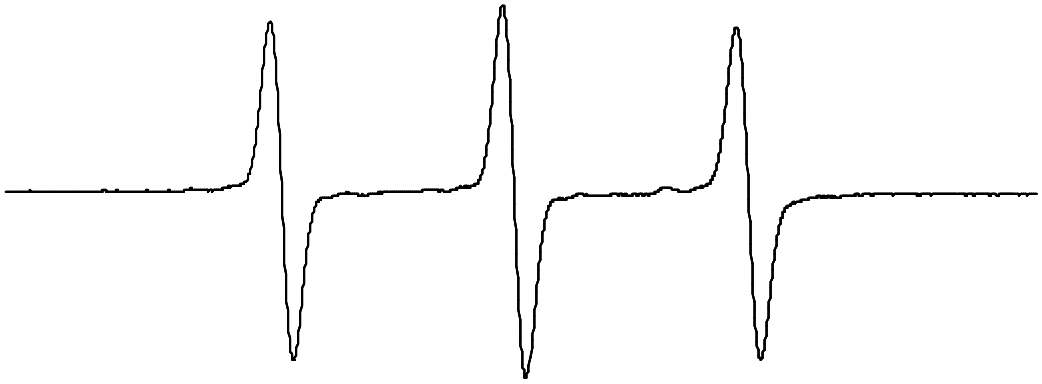

Figure 3. *The EPR spectrum of nitroxide **11** in DCM at 298 K.*

In order to characterize the host properties of derivate **11** by EPR, we have recorded EPR spectra of solutions containing compound **11** with different guest species, which are known to be selectively bound from crown ether derivatives. In the presence of alkaline metal cations like Li^+, Na^+, K^+, or dialkyl ammonium cations the EPR spectra did not show any significant variation in the spin distribution on the nitroxide moiety. However, when the EPR spectrum of **11** is recorded in the presence of dibenzylviologen•PF_6 salt (DBV) an increase of the a_N value is clearly observed. In particular, in acetone at room temperature a_N increases from 14.17 to 14.32 G in the presence of 0.032 M DBV.

We then determined the equilibrium constant, K_{eq}, for the formation of the complex **11**@DBV, by recording EPR spectra of the macrocycle in the presence of increasing concentrations of viologen derivative (EPR titrations). Figure 4 reports the experimental dependence of a_N in acetone solutions at 298 K as a function of DBV concentration.

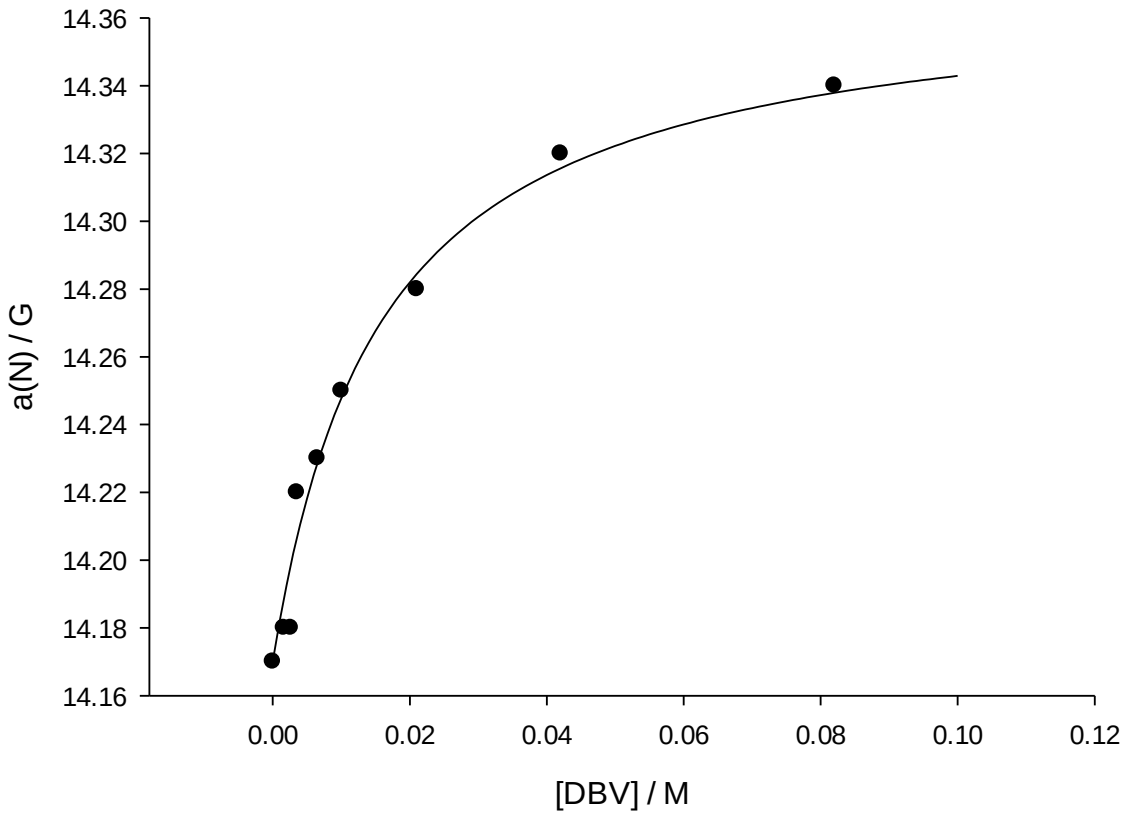

Figure 4. *The trend of a_N value as a function of different concentrations of DBV.*

Because the rate of formation and breaking of the halogen bond is expected to be very large on the time scale of EPR spectroscopy the experimental spectrum represents the concentration-weighted average of the spectra due to the free and complexed species. Therefore, the molar fractions of free and complexed nitroxide (and thus K_{eq}) can be simply estimated from the measurement of the experimental nitrogen coupling (a_{EPR}) by using the following equation:

$$a_{EPR}=a_{11}\,X_{11}+\,a_{11@DBV}X_{11@DBV}$$

Here a_{11} and $a_{11@DBV}$ represent the values of the benzylic splitting for the free and halogen-bonded nitroxides respectively, and X_{11} and $X_{11@DBV}$ are the corresponding molar fractions.
As shown in Figure 4 the changes in coupling constants as a function of viologen salt concentration were well-modeled by the proposed 1:1 binding isotherms using standard curve fitting methods and assuming K_{eq}=75 M^{-1}. In the literature a value for K_{eq}=82 M^{-1} at 298 K in ACN between dibenzo[24]crown-8 and DBV is reported.[7]

1.4 Synthesis and ^{1}H NMR characterization of the rotaxanes R-1 and R-2

Based on these results, we passed to the synthesis of the bistable [2]rotaxanes **R-1** and **R-2** reported in Scheme 2. Both rotaxanes are based on the spin-labeled macrocycle **11** as the wheel interlocked with a dumbbell shape component incorporating the dialkylammonium (NH_2^+) and 4,4'-bipyridinium (BPY^{2+}) units. The only structural difference between two rotaxanes is ascribed to one of the end-cap groups which is represented by 3,5-di-*tert*-butylphenyl (Dtbp) and TEMPO units in rotaxane **R-1** and **R-2** respectively.

The synthesis of both rotaxanes was undertaken by following the Stoddart approach, which involved the *in situ* self-assembly of a pseudorotaxane between the ring **11** and the half-dumbbell intermediate **A-1** followed by the second stopper introduction by means of SN_2-mediated stoppering reaction.[8,9]

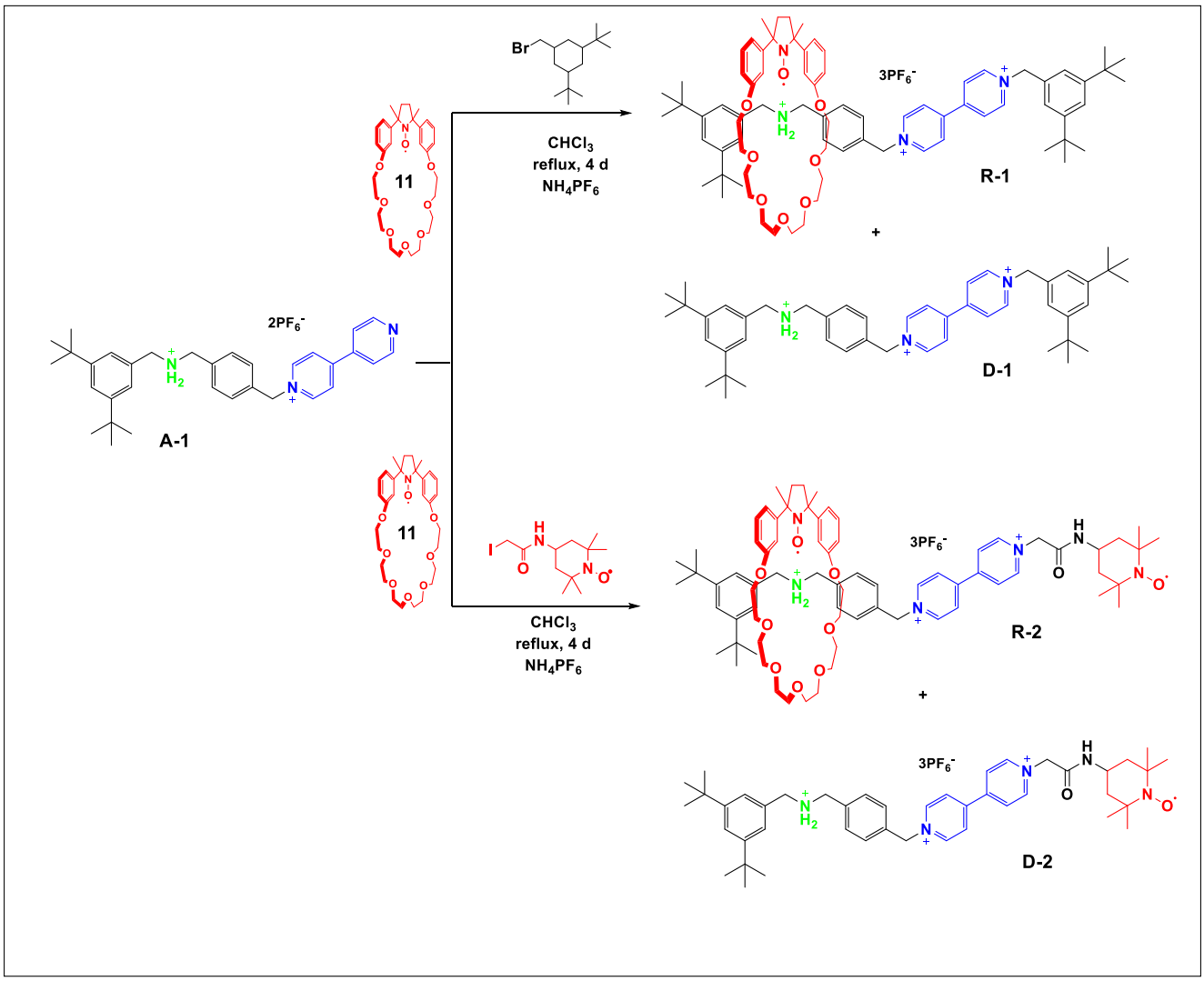

Scheme 2. *Synthesis of the bistable rotaxanes **R-1** and **R-2** and their corresponding dumbbell **D-1** and **D-2**.*

The rotaxane formation was detected by ESI-MS analysis as well as by ^{1}H NMR spectroscopy. As regards ^{1}H NMR studies partial spectra of the dumbbell **D-1** and the rotaxane **D-1** in acetone are reported in Figure 5. The unique evidence of the interlocked structure formation was associated with the broadening of some rotaxane peaks. It is worth noting that although is not possible to reveal the macrocycle signals because of the quenching effect due to the radical on the whole structure, the ^{1}H NMR spectrum shows considerably displaced signals of the guest protons involved in the interlocked assembly respect to the free dumbbell signals. This NMR information together with those achieved by EPR spectroscopy gave a certain evidence of the rotaxane formation. In order to improve the ^{1}H NMR spectral resolution and to obtain a further confirm of the interlocked structure we tried to form the rotaxane using the diamagnetic derivative **10** in place of macrocycle **11** but without success because of the spontaneous air oxidation of the hydroxylamine group into the corresponding nitroxide moiety restoring the paramagnetic derivate **11** and, in turn, its quenching effect.

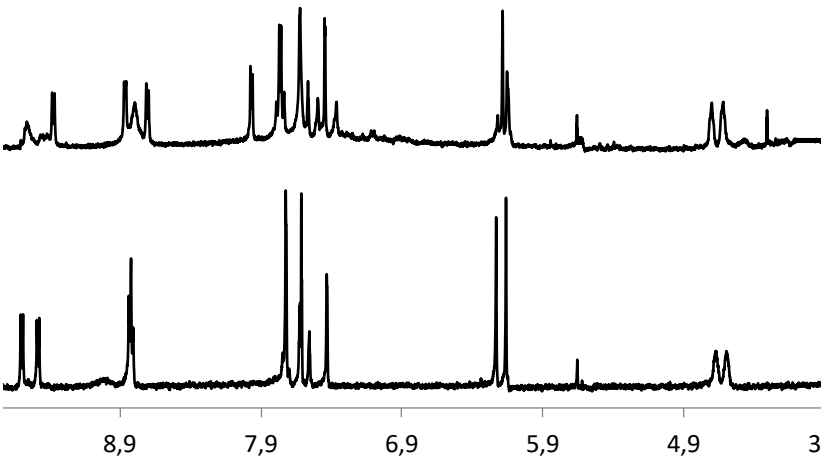

Figure 5. *Partial ^{1}H NMR spectra (400 MHz, $(CD_3)_2CO$, 298 K) of the dumbbell **D-1** (bottom) and the rotaxane **R-1** (up).*

1.5 EPR characterization of the rotaxanes R-1 and R-2

EPR provided clear evidence for the formation of the rotaxane. In Figure 6 is reported the room temperature EPR spectra of rotaxane **R-1** before and after sequential addition of 2 equivalent *i*Pr$_2$EtN. A three-line spectrum (a_N=14,32 G) very similar to that observed for the free macrocycle was observed when the macrocycle is located on the NH_2^+ station. This observation indicates the absence of significant interaction between the nitroxide moiety and the ammonium group, which is expected to interact only with crown ether moiety. Upon addition

of *i*Pr_2EtN, the EPR spectrum showed a noticeable increase in the nitrogen coupling (a_N=14,83 G) similarly to what observed on a mixture of macrocyle **11** and dibenzylviologen.

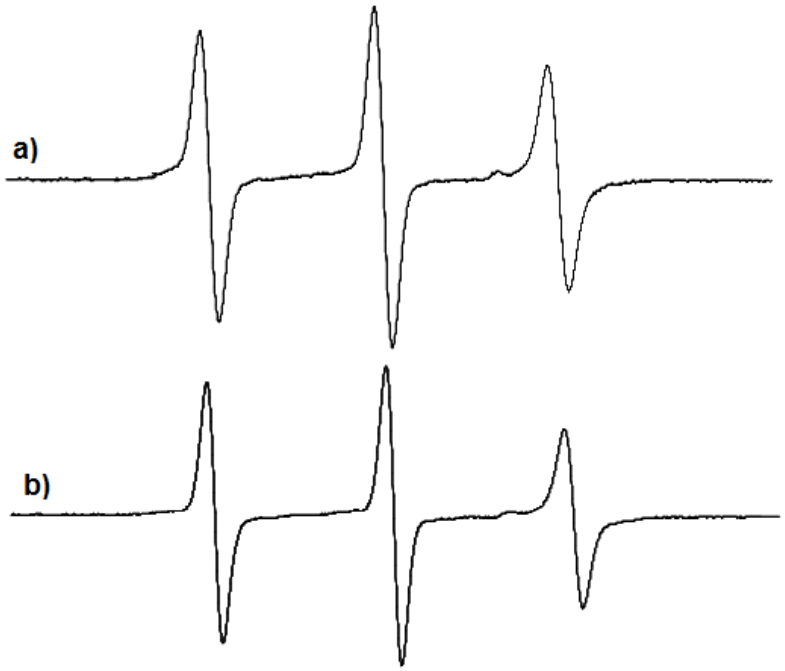

Figure 6. *The EPR spectra of rotaxane **R-1** before (a) and after (b) the addition of iPr₂EtN (0.06 M) in DCM.*

Conversely, the same base addition performed on a 1:1 mixture of the non-interlocked rotaxane components (**11** and the dumbbell) did not cause variations in the EPR signals. According to scheme 3, such a control experiment confirms that the observed nitrogen coupling changes arise from the interaction between the radical unit and the bipyridinium unit, which becomes possible as a result of ring shuttling in the deprotonated rotaxane.

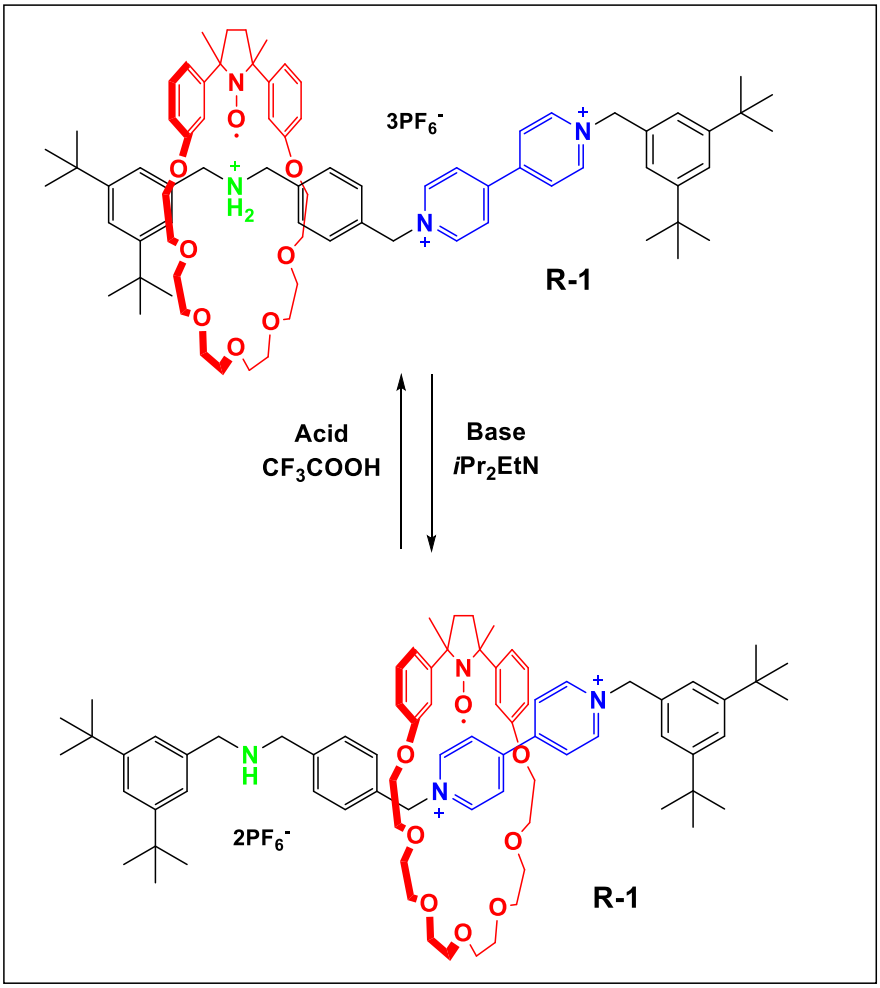

Scheme 3. *Acid-base molecular shuttle.*

The addition of a stoichiometric amount of trifluoracetic acid after the addition of the base caused the quantitative recovery of the initial EPR spectrum because of the replacement of the macrocyclic ring to the ammonium station. The complete base- and acid-induced switching cycle of the EPR pattern was repeated several times without an appreciable loss of signal, highlighting the reversibility of the process.

Acid–base switching procedure was also repeated with rotaxane **R-2**. The superimposition of three-line spectra due to macrocyclic and terminal nitroxide units, typical of isolated nitroxides, was observed when the macrocycle is located on the NH_2^+ station (Figure 7). This observation indicates the absence of significant spin coupling between the two radicals, suggesting that their spatial separation in the starting co-conformations is relatively large. Upon addition of *i*Pr_2EtN, the EPR spectrum showed a change in the nitrogen coupling of the macrocyclic nitroxide unit from 14.26 G to 14.70 G while the nitrogen splitting of the terminal TEMPO unit remains unchanged (a_N=15.70 G). No evidence of exchanging lines was present in the EPR spectrum indicating that the distance between the two nitroxide units is still too high to result

in spin exchange process. The paramagnetic macrocycle denied the possibility of performing the same studies by ^{1}H NMR spectroscopy because of the low spectral resolution.

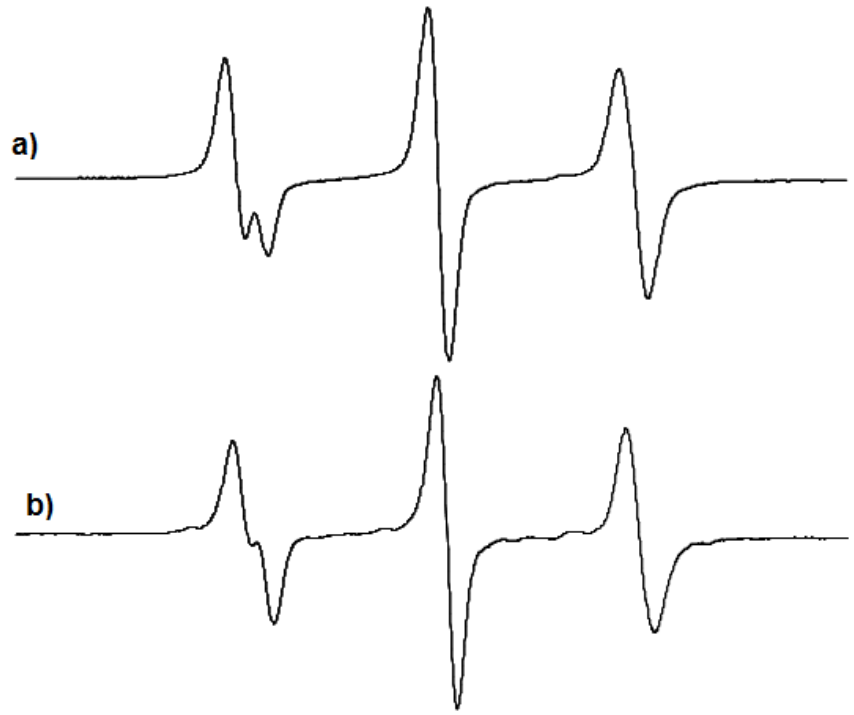

Figure 7. *The EPR spectra of rotaxane **R-2** before (a) and after (b) the addition of iPr_2EtN (0.06 M) in DCM.*

References

[1] C. J. Pedersen, *Journal of the American Chemical Society* **1967**, 7017-7036.

[2] E., Weber, F. Vögtle, *Top. Curr. Chem*. **1981**, *98*, 1.

[3] D. J. Cram, K. N. Trueblood, *Top. Curr.Chem*. **1981**, *98*, 43.

[4] F. De Jong, D. N. Reinhoudt, *Adv. Phys. Org. Chem*. **1981**, *17*, 279.

[5] J. J. Christensen, D. J. Eatough, R. M. Izatt, *Chem. Rev.***1974**, *74*, 351.

[6] J. F. W. Keana, J. Cuomo, L. Lex, S. E. Seyedrezai, *J. Org. Chem*. **1983**, *48*, 2647-2654.

[7] C.J. Bruns, J. F. Stoddart, *The Nature of the Mechanical Bond: From Molecules to Machines,* **2017.**

[8] V. Bleve, C. Schäfer, P. Franchi, S. Silvi, E. Mezzina, A. Credi, M. Lucarini, *ChemistryOpen* **2015**, *4*, 18 –21.

[9] P. Franchi, V. Bleve, E. Mezzina, C. Schäfer, G. Ragazzon, M. Albertini, D. Carbonera, A. Credi, M. Di Valentin, M. Lucarini, *Chem. Eur. J.* **2016**, *22*, 8745 – 8750.

Chapter 4

Spin labelled [2]rotaxanes driven by electrochemical stimulus

1 Historical background of Spin labelled systems

As mentioned in the introduction, the reason for the importance of the "Stoddart-Heath type" bistable [2]rotaxane consisting of cyclobis-(paraquat-*p*-phenylene) ($CBPQT^{4+}$) macrocycle which moves between the tetrathiafulvalene (TTF) station and the 1,5-dioxynaphthalene (DNP) one by oxidation and reduction of the TTF moiety,[1] lies in the redox nature of the switching process, which is usually rapid, precise and can be controlled within solid-state devices as well as on surfaces.[2] Basing on this attractive system, Lucarini et al. reported for the first time the synthesis and characterization of [2]rotaxane possessing $CBPQT^{4+}$ as wheel interlocked with a single station dumbbell containing TTF or DNP as recognition sites and nitroxide spin labels as stoppers at the both ends. The structures of these [2]rotaxanes and their corresponding dumbbells are reported in Scheme 1 and 2 respectively.[3]

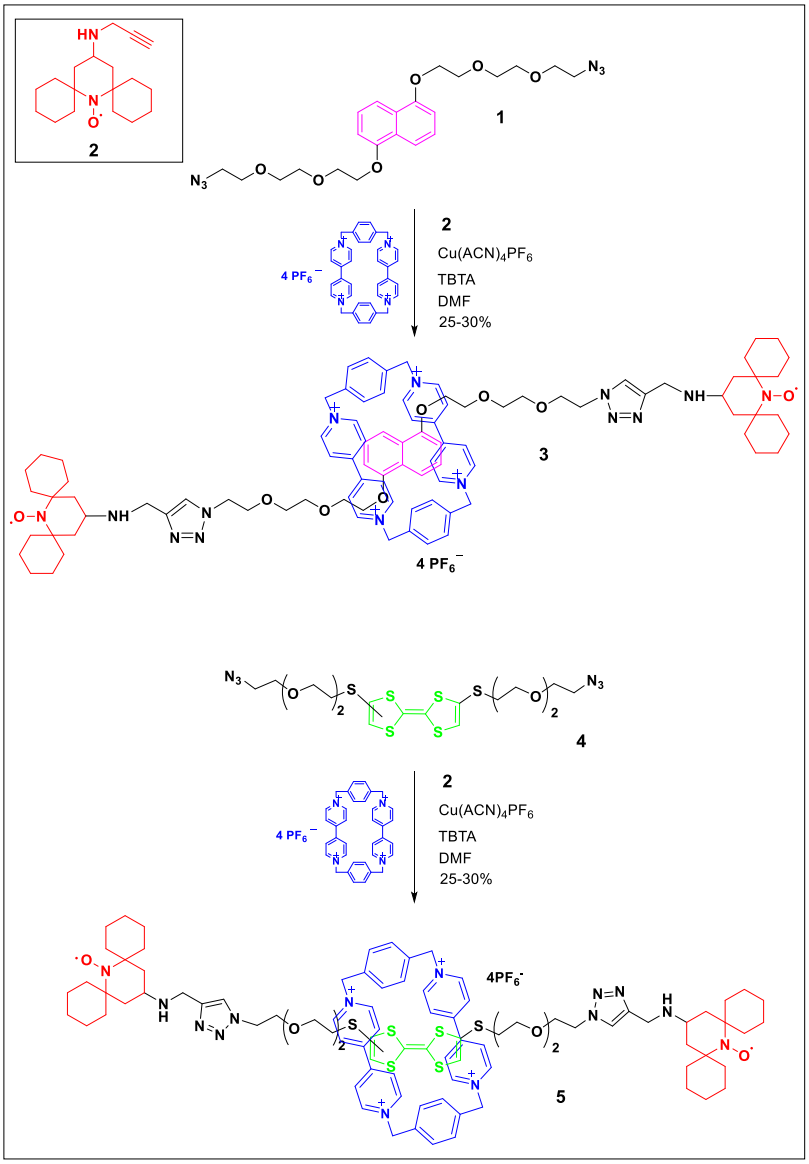

Scheme 1

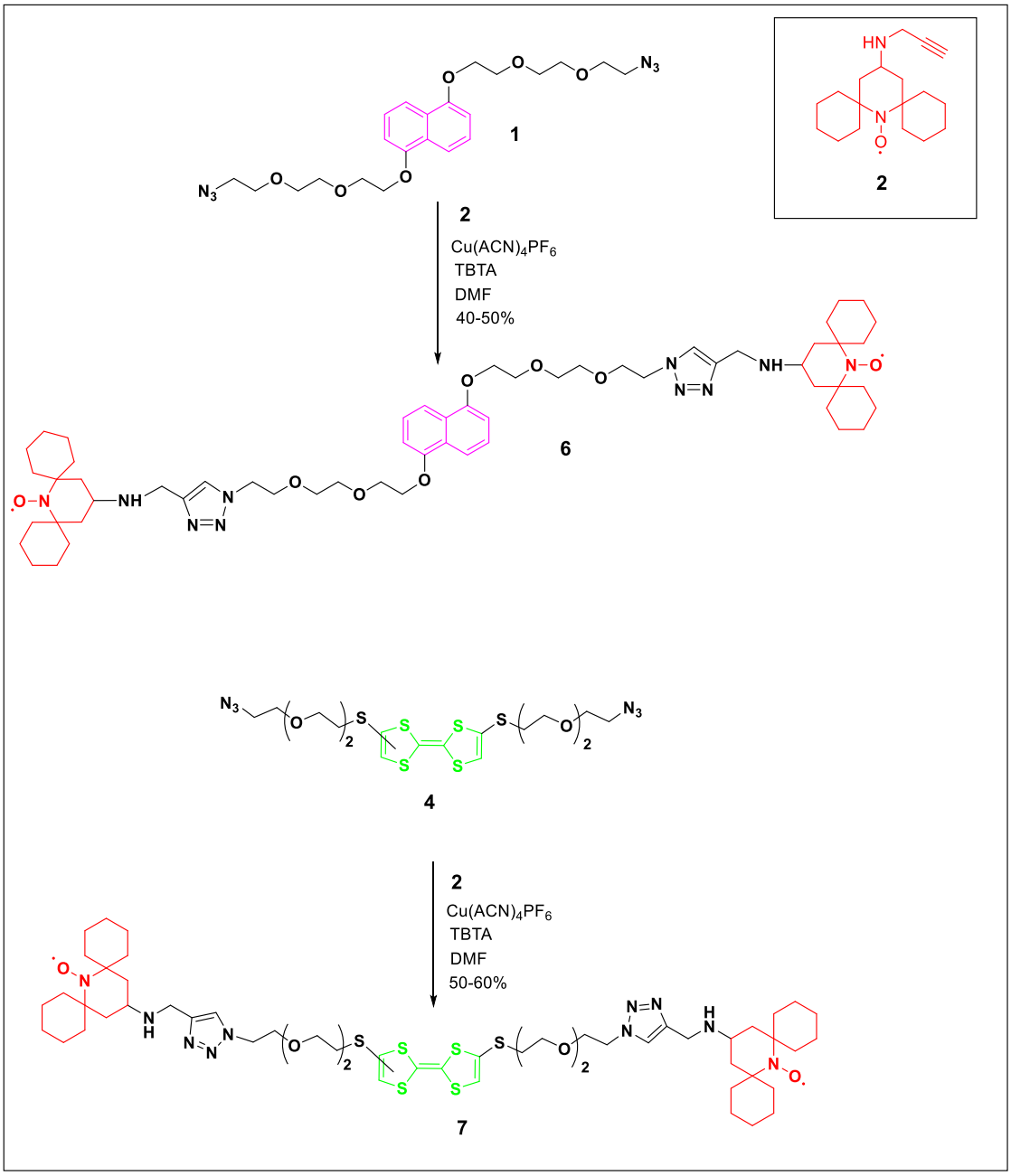

Scheme 2

The [2]rotaxanes were prepared following the synthetic strategy reported by Stoddart and coworkers[4] based on the initial formation of the pseudorotaxane between $CBPQT^{4+}$and DNP or TTF axial derivatives (**1** and **4**, respectively) having at both edges an azide group.

It is worth noting that in the rotaxanes having $CBPQT^{4+}$ as the wheel, the TEMPO (2,2,6,6-tetramethylpiperidine-*N*-oxyl) units, previously used as the end-cap group in cucurbit[6]uril-[5] or α-cyclodextrin[6] based rotaxane, were not large enough to behave as efficient stoppers.[3] For this reason bulkier alkyne nitroxides were prepared bearing spirocyclohexyl substituents at the C2 and C6 positions of the piperidine ring.

The presence of azide moiety on the linear thread and alkyne group on the more hindered nitroxide (**2**) employed as stopper made possible the conversion of the pseudorotaxane into the corresponding rotaxane by using Cu(I)-catalyzed azide-alkyne cycloaddition (CuAAC).[7] The possibility to exploit Huisgen 1,3-dipolar cycloaddition reaction, also known as click reaction, offers some advantages which are mainly represented by the high efficiency, tolerance of sensitive functional groups, and mild reaction conditions.[8]

In addition to the synthesis, unexpected EPR features were found when recording the EPR spectra of the spin-labelled dumbbells and rotaxanes.

Actually, the EPR spectra of the rotaxanes (**3** and **5**, see Scheme 1) and the dumbbells (**6** and **7**, see Scheme 2) in ACN at 338 K are reported in Figure 1.[9] Both dumbbells, regardless of the presence of the TTF or DNP units, showed an EPR spectrum characterized by five lines, which was indicative of the exchange interaction between the paramagnetic moieties.[10]

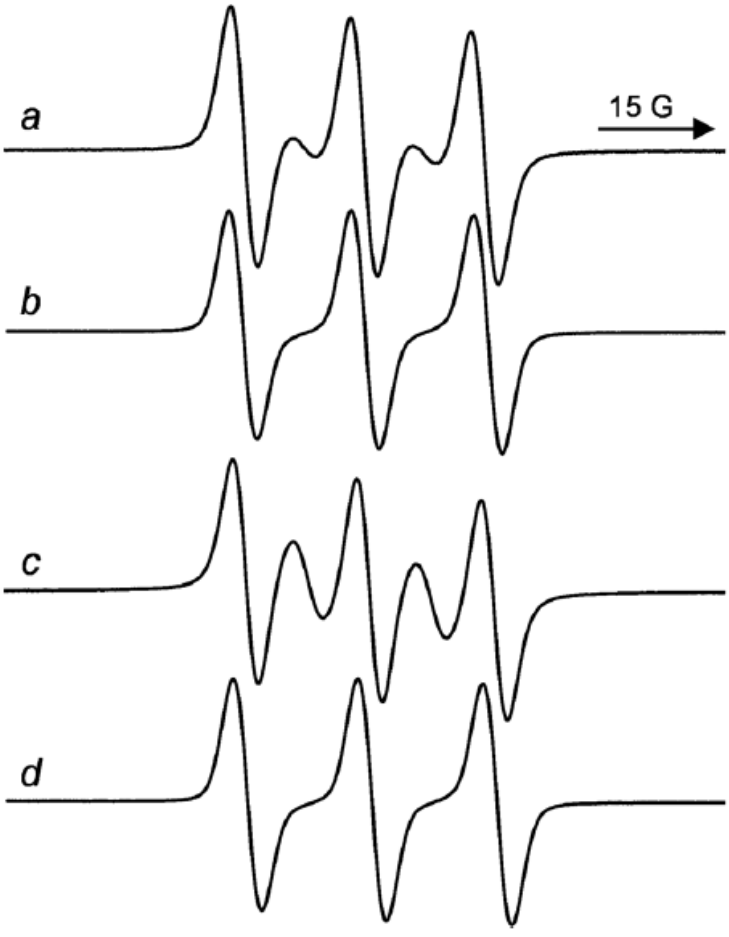

Figure 1. *ESR spectra of the dumbbells **6** (a), **7**(c) and rotaxanes **3** (b),**5** (d) in ACN at 338 K.*

However the intensity of the exchange lines (the second and the fourth lines) of the dumbbell **7** was much higher comparing with the dumbbell **6**. This slight difference was due to the fact

that in the case of dumbbell **7** about 80% of the molecules assumed conformations in which the two nitroxide units were sufficiently close to one another to allow a strong electron exchange ($J>a_N$), while the same interaction was present in ca.40 % of the molecules of dumbbell **6**.[10,11] On the contrary, the EPR spectra of the corresponding rotaxanes **3** and **5** consisted of only three lines, suggesting that the rotaxane formation reduced significantly the probability of exchange coupling between nitroxide units. Thus the spin labelling approach could be a useful and rapid method to differentiate unequivocally the dumbbell from the corresponding [2]rotaxane.

The dumbbell **7** and the rotaxane **5** were the object of a more detailed study owing to the well-known redox properties of the TTF unit.[12] TTF moiety can be oxidized reversibly (at +0.43 V vs. Ag/AgCl in ACN) to the $TTF^{\bullet+}$ radical cation, and then subsequently (at +0.79 V) to the TTF^{2+} dication. The oxidation of TTF station in these systems determined the formation of a heterotriradical derivate, which could be examined in depth by using EPR spectroscopy. In Figure 2 is reported the EPR spectrum of the free dumbbell **7** after TTF oxidation with $Fe(ClO_4)_3$.

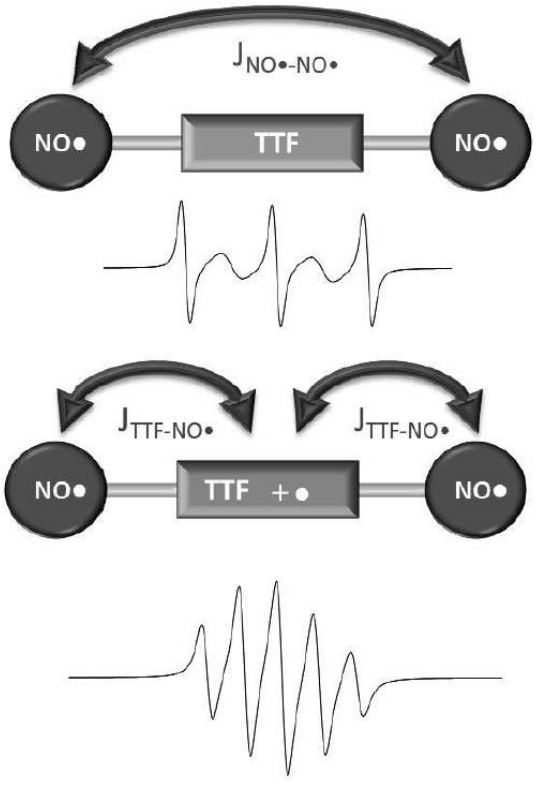

Figure 2. *Representation of the interactions taking place in the hetero-triradical compound.*

The resulting spectrum derived from the contribution of two different spin exchange interactions: the interaction between the nitroxide units, which was responsible for the five line spectrum, and the spin exchange between the nitroxide stoppers with the TTF radical site

(Figure 2). An EPR titration performed by recording the EPR spectra after the addition of increasing amounts of the oxidizing agent showed the appearance of new signals which were related to the triradical compound formation (Figure 3b).

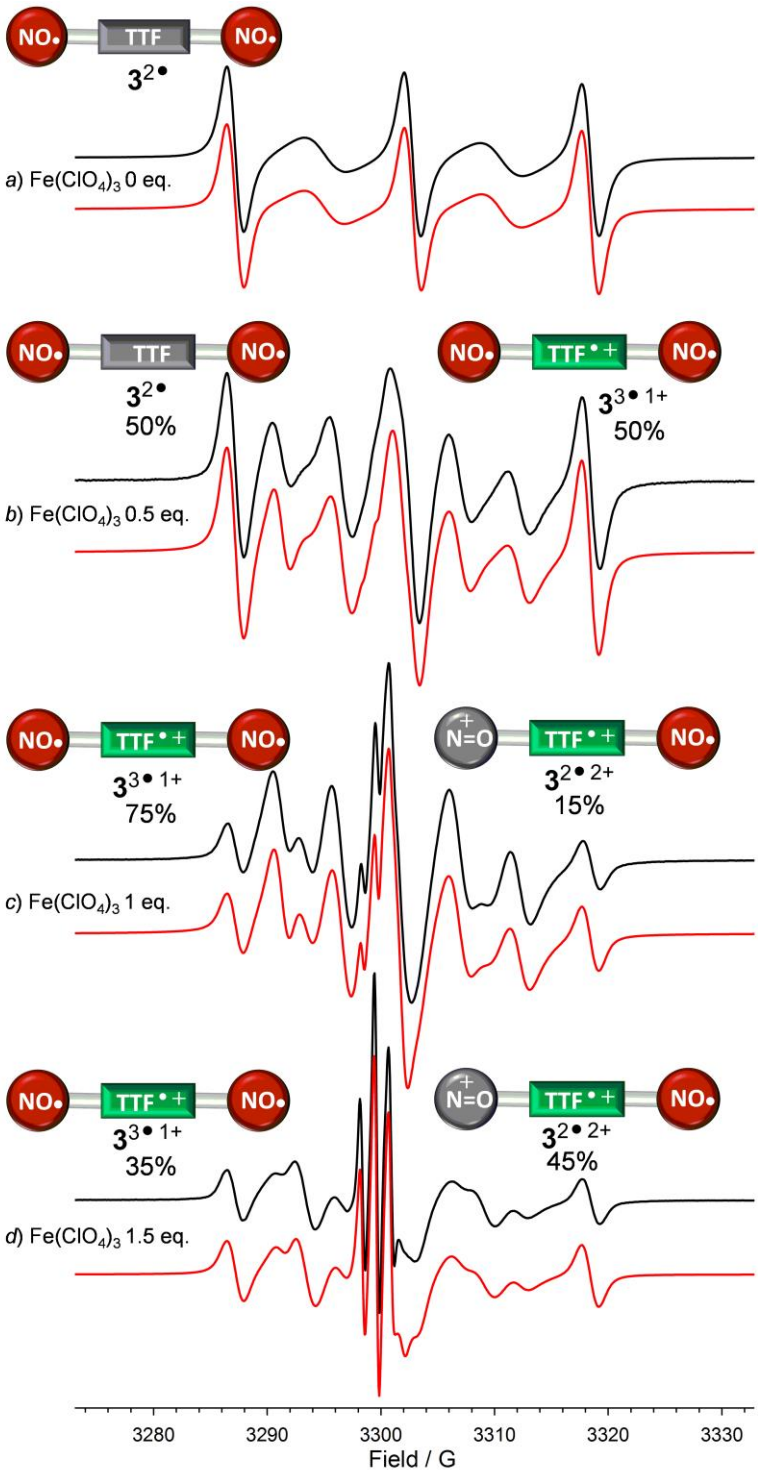

Figure 3. *EPR spectra of* ***7*** *(0.2 mM) recorded in ACN at 298 K in the presence of different amounts of* $Fe(ClO_4)_3$*. Dotted lines represent the corresponding theoretical simulations.*

It is interesting to note that the nitroxide unit, at around 1 equivalent of $Fe(ClO_4)_3$, started to be oxidized to the corresponding diamagnetic oxammonium species originating a different diradical compound whose EPR spectrum was characterized by a new interaction between the TTF and only one nitroxide unit (Figure 3c)[13].

In order to obtain a full characterization of these systems based on TTF recognition site the effect of rotaxanation on the spin exchange was examined as well. In detail, the presence of the $CBPQT^{4+}$ ring had a dramatic influence on the shape of EPR spectrum, which, after the addition of the oxidant, consisted of the superimposed signals of a non exchanging dinitroxide compound (a 1:1:1 triplet with a line separation of a_N=15.40 G) and the TTF radical cation (a 1:2:1 triplet with a line separation of a_{2H}=1.30 G) while no lines due to an interaction between the different radical units were visible (Figure 4b).

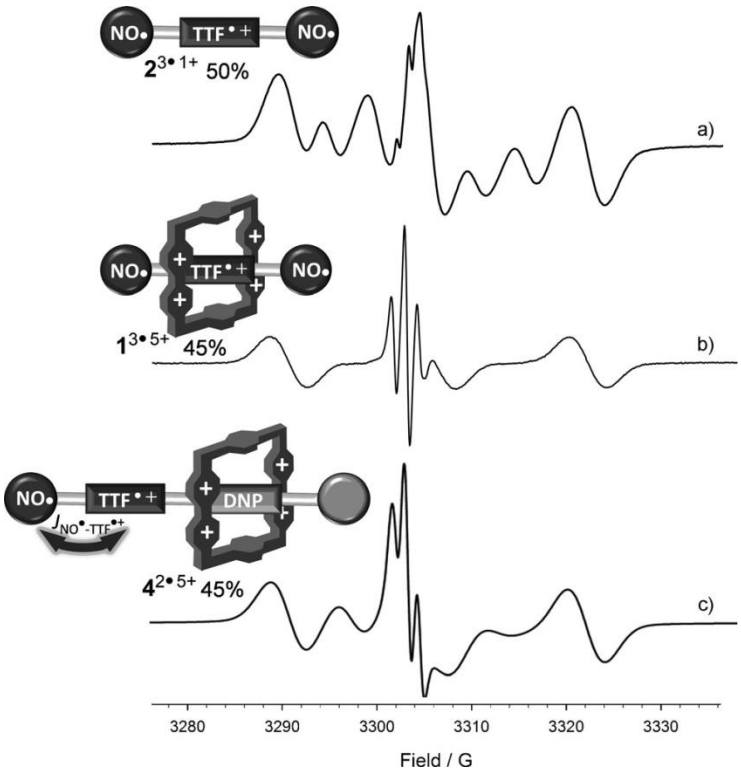

Figure 4. *EPR spectra recorded in ACN at 298 K at a concentration of 0.2 mMol: a) the free thread **7**; b) the [2]rotaxanes **5** in the presence of 0.5 equiv of $Fe(ClO_4)_3$; c) the [2]rotaxane **8** in the presence of 0.5 equiv of $Fe(ClO_4)_3$.*

According to these EPR results, it was possible to deduce that the $CBPQT^{4+}$ ring encircled the TTF unit also after the oxidation process because of the lack of an additional recognition site suitable for the macrocycle. Furthermore the absence of spin exchange was ascribed to a shielding effect of the macrocycle which reduced the exchange interaction between the $TTF^{\bullet+}$ and both nitroxide radicals providing a further evidence of its position.

These interesting observations had been corroborated by carrying out EPR investigations on the bistable spin-labelled [2]rotaxane **8** (Figure 5), which incorporated the TTF and DNP moieties as recognition sites and only one nitroxide spin label as terminal unit.

The $CBPQT^{4+}$ ring preferentially encircled the DNP unit because of the greater affinity of the macrocycle for this station.[14] After the subsequent formation of the $TTF^{\bullet+}$ radical cation a strong spin-exchange interaction between the nitroxidic stopper unit and $TTF^{\bullet+}$ was clearly detectable in the EPR spectrum, suggesting that the macrocycle position was preserved after the TTF oxidation.

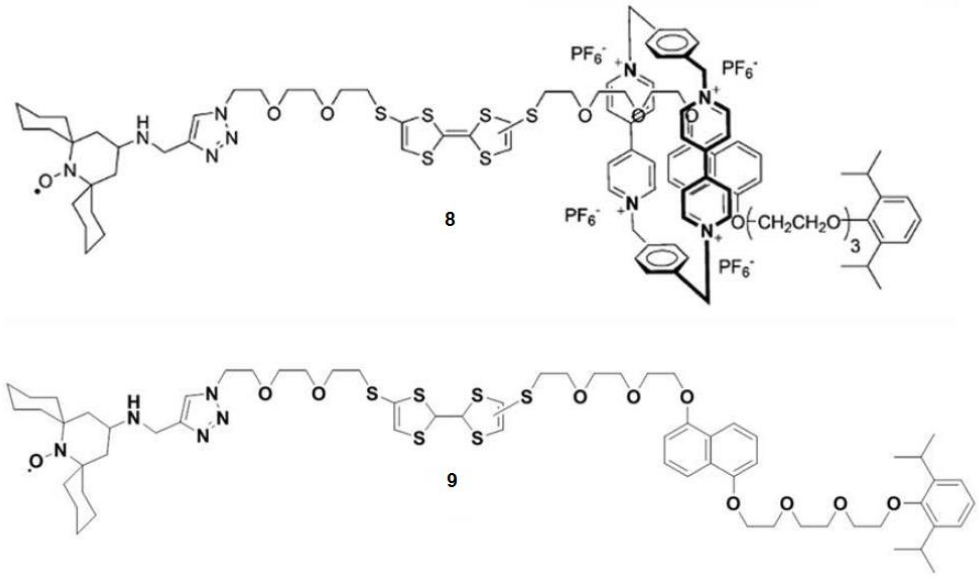

Figure 5. *Structure of the spin labelled [2]rotaxane containing the TTF and DNP stations and of the corresponding spin-labeled dumbbell.*

2 New spin labeled rotaxanes driven by chemical stimulus

2.1 Introduction

Inspired by the possibility to demonstrate the movement of the cycle in a rotaxane assembly by measuring the through-space spin–spin interactions by EPR spectroscopy, my research activity was focused on the design of a series of spin-labeled rotaxanes driven by electrochemical stimuli, containing in the dumbbell either redox active TTF moiety or 1,5-DNP unit, or both and $CBPQT^{4+}$ as macrocycle. In order to examine the magnetic behavior of these systems and extrapolate important information about their structure and operative behavior, the one- and two-station rotaxanes (Figure 6), were labelled both at the wheel and at axle components. It is should be noted that the spin-labels on the ring and axle components are not

identical. In particular the macrocycle is functionalized with the TEMPO moiety, namely 2,2,6,6-tetramethylpiperidine-*1*-oxyl, while the axle possesses at one side the more sterically hindered nitroxide radical containing spirocyclohexyl substituents at 2 and 6 positions of the piperidine-N-oxyl ring, to allow the stoppering of the macrocycle and the formation of the interlocked complex in keeping with previous detailed results.[3]

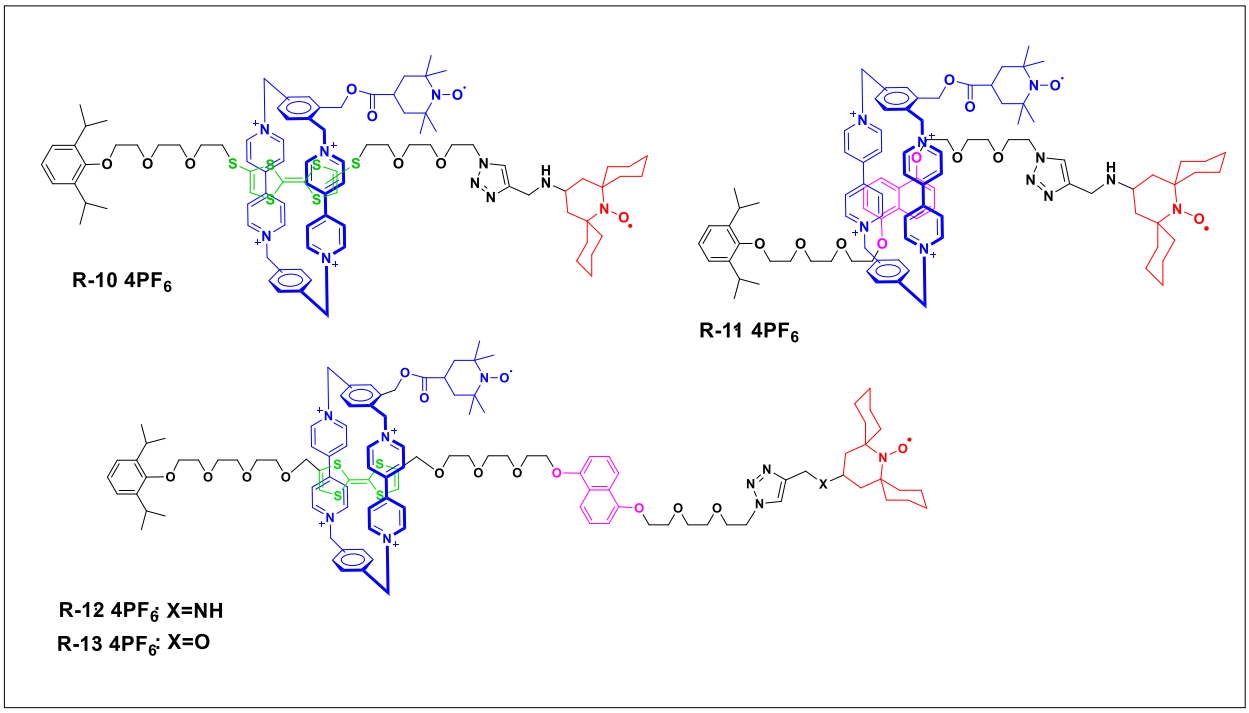

Figure 6. *Structure of the one (**R-10**, **R-11**) and two-station spin-labeled rotaxanes (**R-12**, **R-13**).*

2.2 Synthesis of single station rotaxanes

The starting point toward the synthesis of the two-station rotaxanes **R-12** and **R-13** was the development of single station [2]rotaxanes consisting of a spin-labeled electron accepting ring component **CBPQTNO·4PF$_6$** and electron-donating dumbbell units like bisthiotetrathiafulvalene (STTFS) (**R-10**, Figure 6) or 1,5-dioxynaphthalene (DNP) (**R-11**, Figure 6) respectively, in order to obtain preliminary information about the magnetic proprieties of these new systems investigating the through-space magnetic interactions between the nitroxide units.

In Figure 7 are reported the axial molecules **A-10** and **A-11** representing the half-threads precursors of the single station dumbbells and rotaxanes.

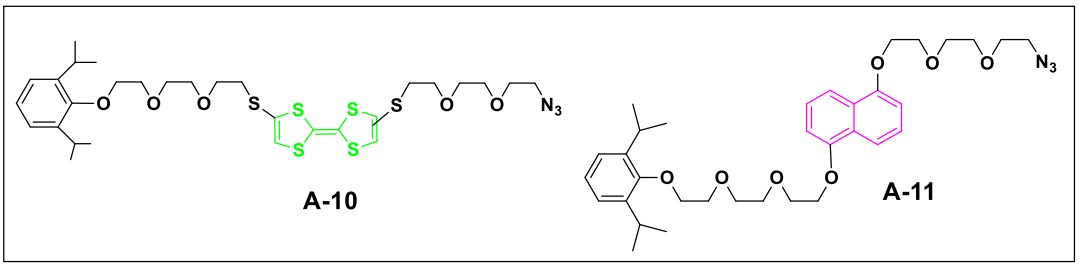

Figure 7. *Structure of the axles containing TTF (left) and DNP (right) recognition sites.*

The synthesis of the axles **A-10** is outlined in Scheme 3 and consisted of the 2,6-diisopropylphenol introduction by alkaline treatment of the STTFS monotosylate **14**, successive tosylation of the hydroxyl moiety (compound **16**) and exchange with NaN_3.

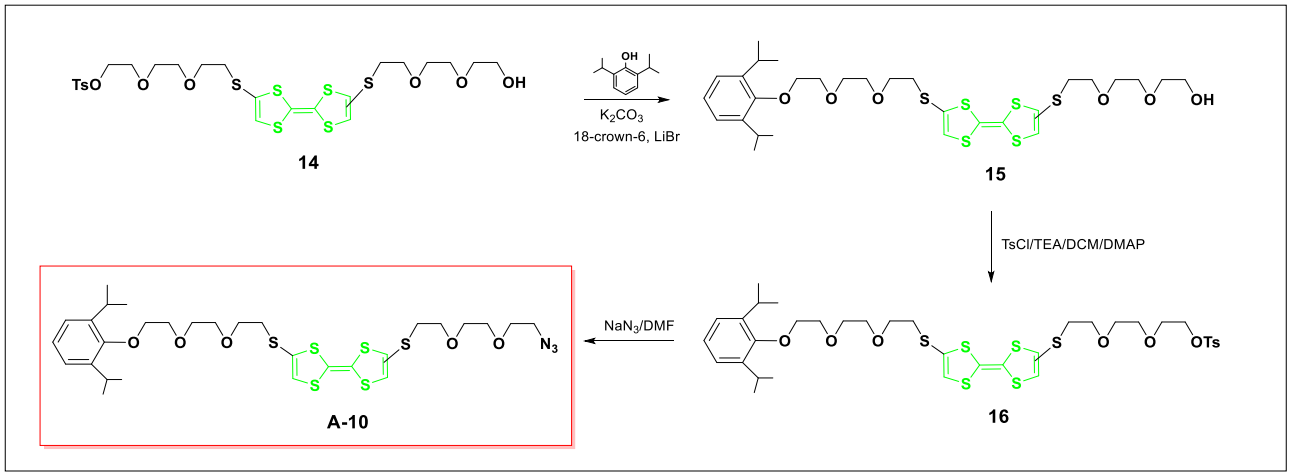

Scheme 3.

The axle **A-11** was obtained followed the well-known synthetic procedure reported in the literature. [15]

The next step was represented by the synthesis of both [2]rotaxanes **R-10** and **R-11**, which was performed following a threading-followed-by-stoppering protocol outlined in Scheme 4.

In detail the rotaxane **R-10** was achieved adding the host **CBPQTNO·4PF$_6$** to a solution of the axle **A-11** and stirring at -10°C for ten minutes in order to obtain the pseudorotaxane derivate which was converted into the corresponding rotaxane after addition of the bulky stopper alkyne spyrocyclic nitroxide **S-2** as the result of Huigsen cycloaddition catalyzed by $[Cu(ACN)_4]PF_6$ in the presence of (benzyltriazolylmethyl) amine (TBTA) as a stabilizer. In addition to the formation of the desired rotaxane obtained in non-optimized 22-26% yield, this synthetic procedure gave a small amount of the corresponding dumbbell **D-10** as byproduct which was particularly useful both to provide evidence of the interlocked structure by means of the ^1H

NMR spectroscopy and to obtain a comparison in terms of paramagnetic proprieties between the rotaxane and dumbbell by using EPR spectroscopy.

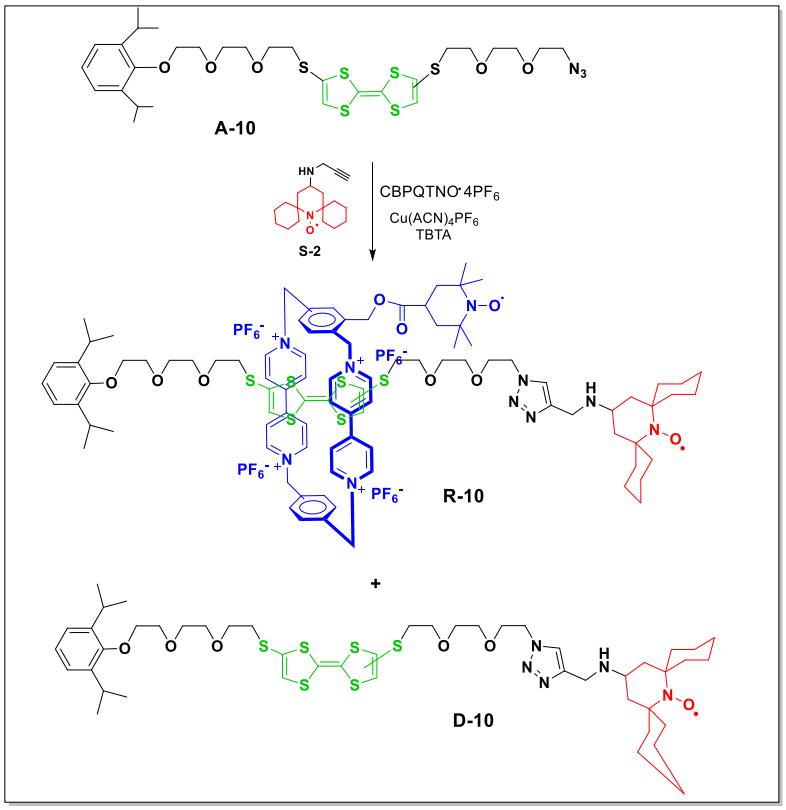

Scheme 4

The above procedure was followed also using the DNP derivative **A-11** in the presence of **CBPQTNO·4PF$_6$**, alkyne functionalized stopper **S-2**, TBTA and Cu(ACN)$_4$PF$_6$ to obtain the rotaxane in non-optimized 22-26% yield. In addition, in this case the rotaxane formation was associated with the achievement of the dumbbell **D-11** (Scheme 5).

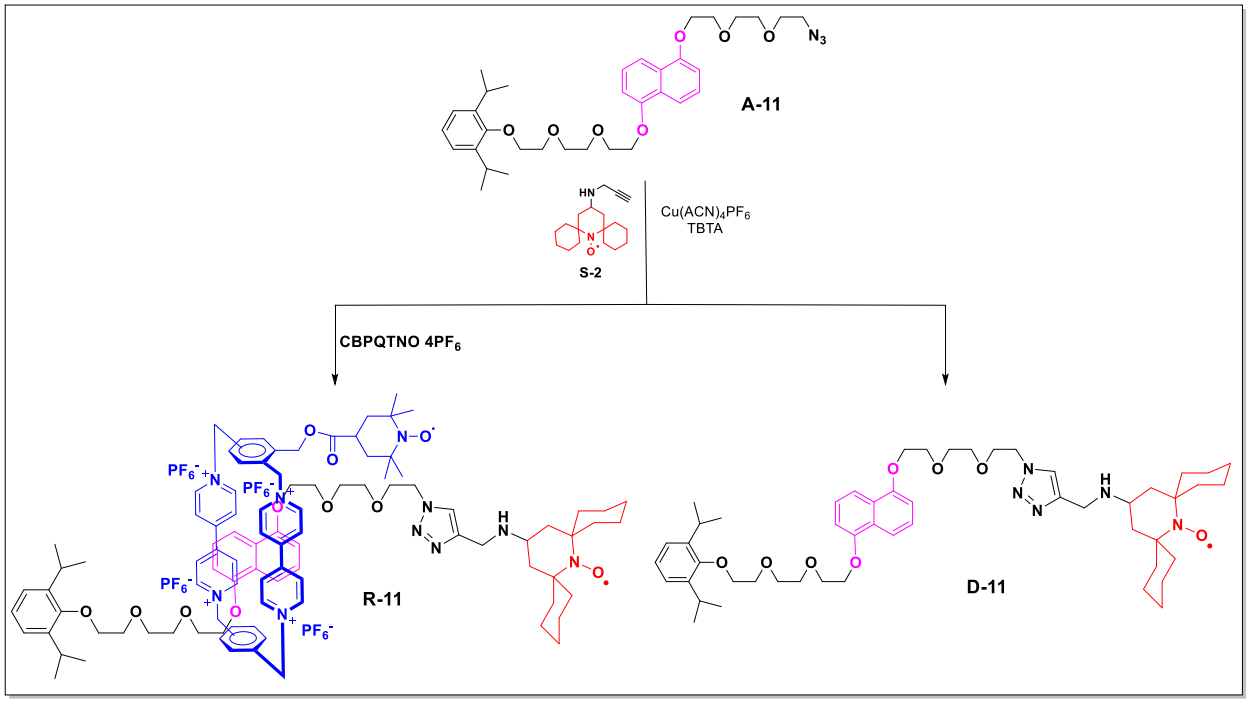

Scheme 5

Both ESI-MS analysis and NMR spectroscopy were used to provide evidence of the formation of the interlocked structures.

2.2.1 ^{1}H NMR characterization of single station rotaxanes

Figure 7 shows partial ^{1}H NMR spectra comparing the [2]rotaxane **R-10**, dumbbell **D-10**, and **CBPQTNO·4PF$_6$** ring (traces a, b, and c respectively). In the ^{1}H NMR spectrum of the rotaxane red dashed lines evidence broadening of the macrocycle signals as a consequence of the decrease of the tumbling rate of the ring in the rotaxane structure, and a deshielding of bipyridinium protons *α*. It should be noted also that the only visible proton signal (labelled with **b**) indicating the presence of the radical pendant in the ring undergoes downfield shift. On the other hand, blue dashed lines show a marked shielding of TTF protons, which is a typical behaviour of the complexation process, indicating that the TTF unit is encircled by CBPQT^{4+}.

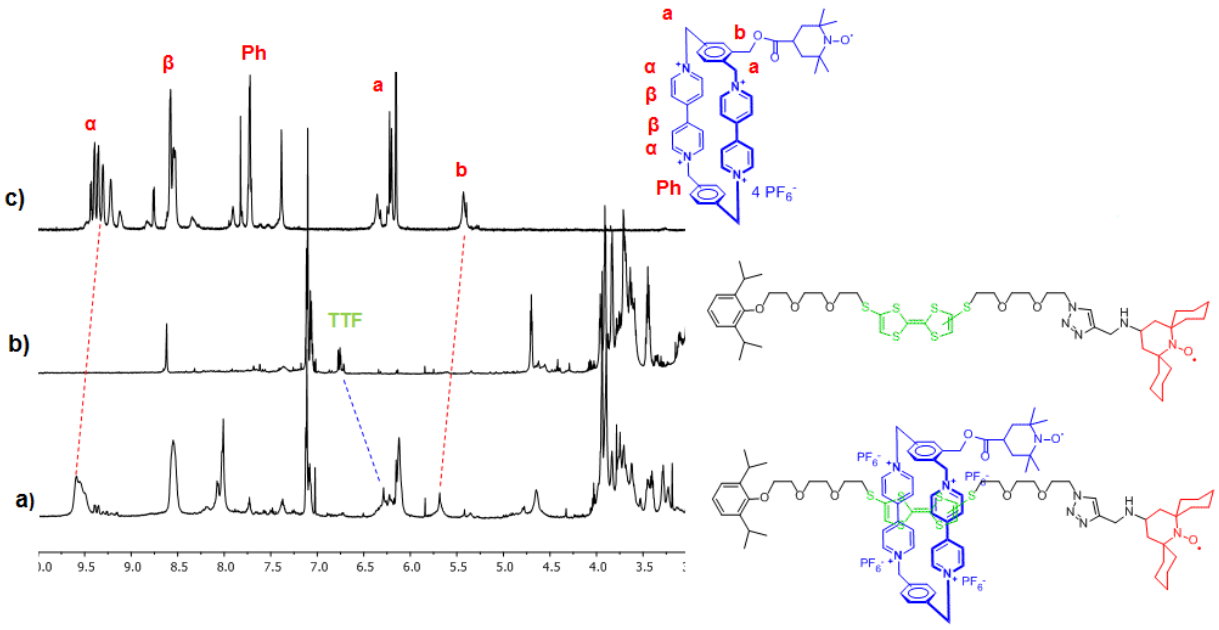

Figure 7. *Partial ^{1}H NMR spectra (600 MHz, CD_3CN, 298 K) of a) rotaxane**R-10**; b) dumbbell **D-10**; c) **CBPQTNO** host.*

The set of these NMR data gave a good indication of the MIM formation and ring position despite the biradical nature of the rotaxane.

Similar arguments also apply to the NMR analysis of the single station rotaxane **R-11**. In Figure 8 the stacked spectra of the paramagnetic host, rotaxane **R-11** and dumbbell **D-11** are reported (traces c, b and a respectively). Similarly, the spectra reveal the substantial broadening and splitting of the signals corresponding to the paramagnetic macrocycle protons, together with the deshielding of the protons **b**, which are diagnostic of the complexation process (red dashed lines). In addition, a significant upfield shift recorded for the peaks corresponding to the DNP protons in the rotaxane provides clear evidence of the macrocycle presence around the electron donor naphthalene station (blue dashed lines).

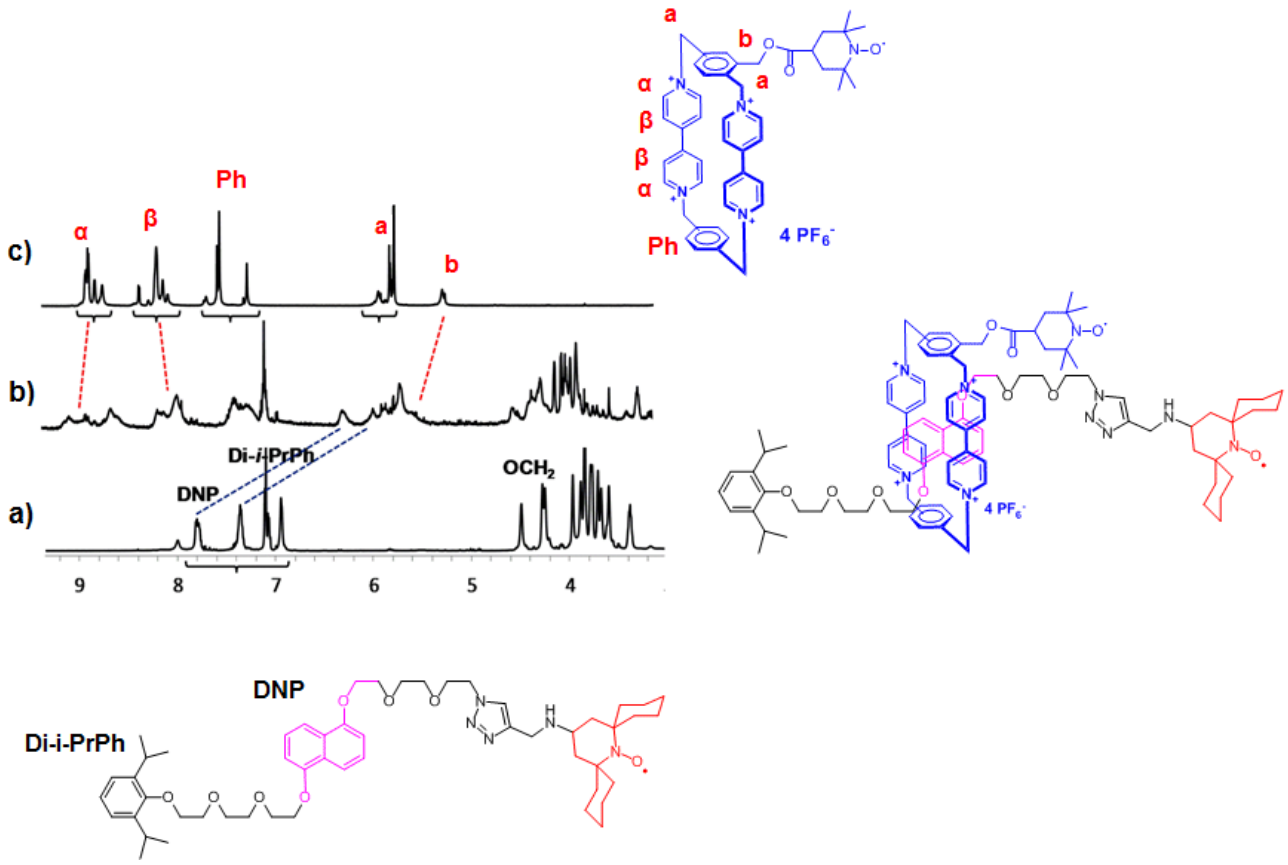

Figure 8. *Partial ^{1}H NMR spectra (600 MHz, CD_3CN, 298 K) of a) dumbbell **D-11**; b) rotaxane **R-11**; c) **CBPQTNO** host.*

2.2.2 ESR characterization of single station rotaxanes

The spin labelling of these systems obtained by introduction of nitroxide radicals allowed, both to detect the rotaxane formation and to clarify their structure and magnetic properties by using EPR technique.

The ESR spectra of the dumbbells containing the DNP unit (a_N = 15.22 G) and TTF station (a_N = 15.26 G) recorded in ACN at 338 K are reported in Figure 9. As expected, the ESR spectra were characterized by only three lines deriving from the presence of a single radical moiety along the dumbbell. Conversely the ESR spectra of the corresponding rotaxanes **R-11** (a_N =15.43 G) and **R-10** (a_N =15.45 G) in ACN at 338 K reported in Figure 10, consisted of five lines due to the exchange interaction between the paramagnetic fragments linked to the macrocycle and dumbbell, as the exchange coupling constant between unpaired electrons, *J*, was greater than the hyperfine splitting, a_N. The ratio of line intensities suggested that the only some conformations of the biradical are characterized by strong exchange between nitroxide units.

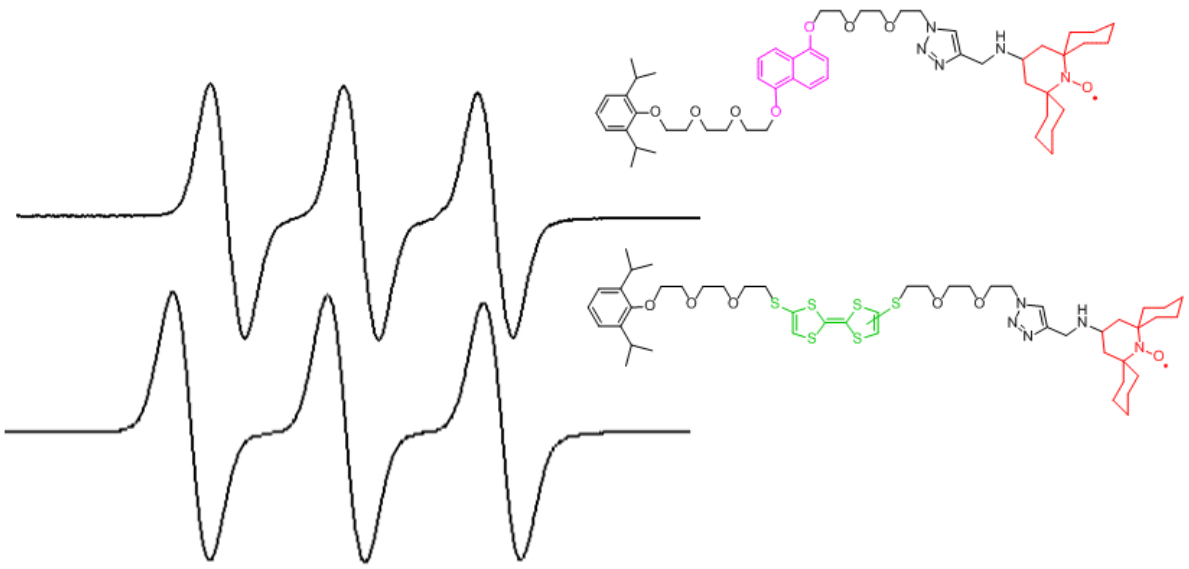

Figure 9. *ESR spectra of dumbbells **D-11** (top) and **D-10** (bottom) in ACN at 338 K.*

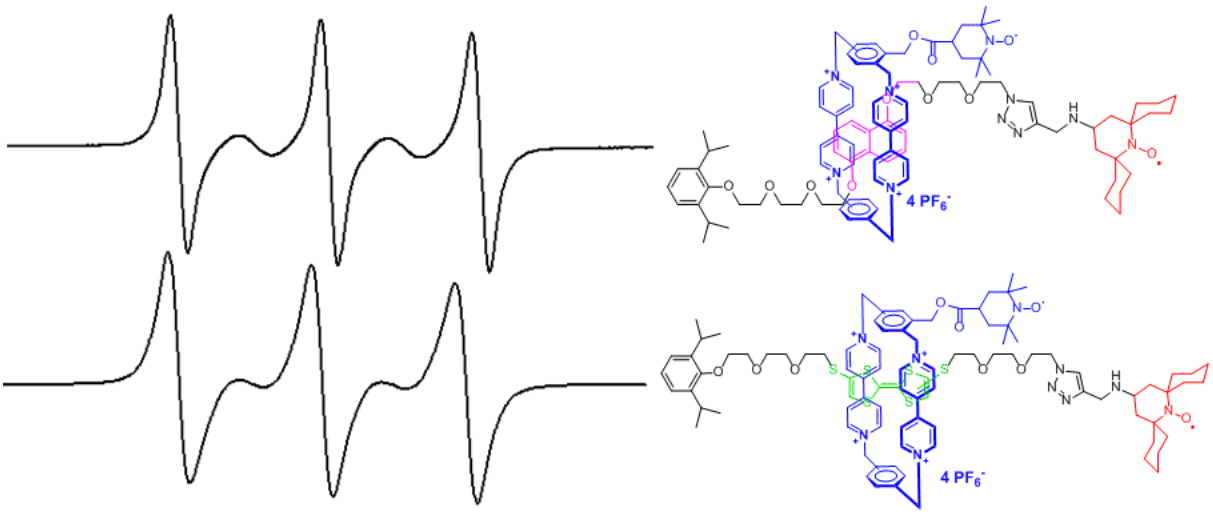

Figure 10. *ESR spectra of rotaxanes **R-11** (top) and **R-10** (bottom) in ACN at 338 K.*

The EPR spectra of the dumbbell and the rotaxane containing the TTF unit were also recorded in the presence of $Fe(ClO_4)_3$ as oxidant. In details, the EPR spectra of the dumbbell **D-10** and the rotaxane **R-10** in MeCN at 338 K after the addition of the oxidizing agent (1.6 mmol) are outlined in figure 11.

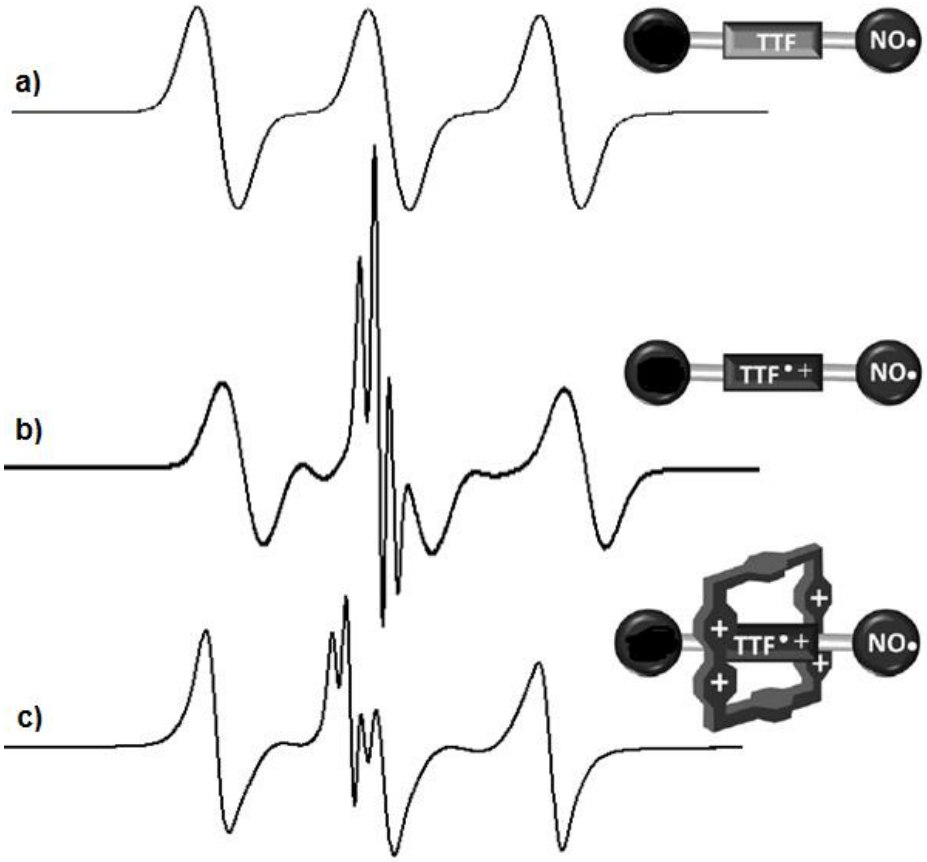

Figure 11. *The EPR spectra of the dumbbells **D-10** before (a) and after (b) the addition of $Fe(ClO_4)_3$, and the rotaxane **R-10** in the presence of the oxidant (c).*

Upon addition of the oxidant, the EPR spectrum of the dumbbell showed a noticeable change from three- to five-lines, retaining the same a_N value (15.26 G) (Figure 11a and b). The appearance of extra lines in the ESR spectrum was due to the exchange interaction between the $TTF^{\bullet+}$ radical cation and nitroxide unit. Having fully characterized the spin labeled dumbbell, we investigated the effect of rotaxanation on the spin exchange, under oxidative condition with the same amount of $Fe(ClO_4)_3$. It was interesting to note that the presence of the spin-labeled $CBPQT^{4+}$ ring changed significantly the shape of the EPR signal. In detail, addition of the oxidant on **R-10** gave rise to an EPR spectrum (figure 11c) which consisted of superimposed signals deriving from TTF radical cation and stopper nitroxide unit and no exchange lines between each other were visible. This behavior suggested a shielding effect of the macrocycle on TTF station preventing the spin coupling, typical of the dumbbell, in the presence of the oxidant. Contrary to all expectations, a very weak exchange interaction between the nitroxide units was instead detected.

2.3 Synthesis of two station rotaxanes

We finally synthesized and characterized the Stoddart–Heath molecular switch consisting of $CBPQT^{4+}$ shuttling between the tetrathiafulvalenestation and the 1,5-dioxynaphthalene one by oxidation and reduction of the TTF moiety. This redox switchable molecular shuttle functionalized with stable radical units in both the ring and dumbbell components is reported in Figure 6.

Previous investigation showed that the presence of higher positive charges on the distal S atoms in STTFS reduced the ability to induce attractive [π…..π] stacking inside the tetracationic cyclophane in comparison with TTF. Basing on this consideration, we replaced the S atoms with CH_2O moiety in order to increase the TTF affinity for the macrocycle and consequently to ensure that the TTF station represents the preferred recognition site for the ring, which in turn, can move from TTF unit toward DNP station by applying of electrochemical stimulus.

2.3.1 Synthetic procedure and ^{1}H NMR characterization

The axle **A-12** (Figure 12) containing both CH_2O-TTF-OCH_2 and DNP as suitable recognition sites for $CBPQT^{4+}$, represents a key intermediate for the rotaxane synthesis. In fact, the presence of azide group at one extremity of the axle component allows the rotaxane formation obtained involving CuAAC click chemistry.

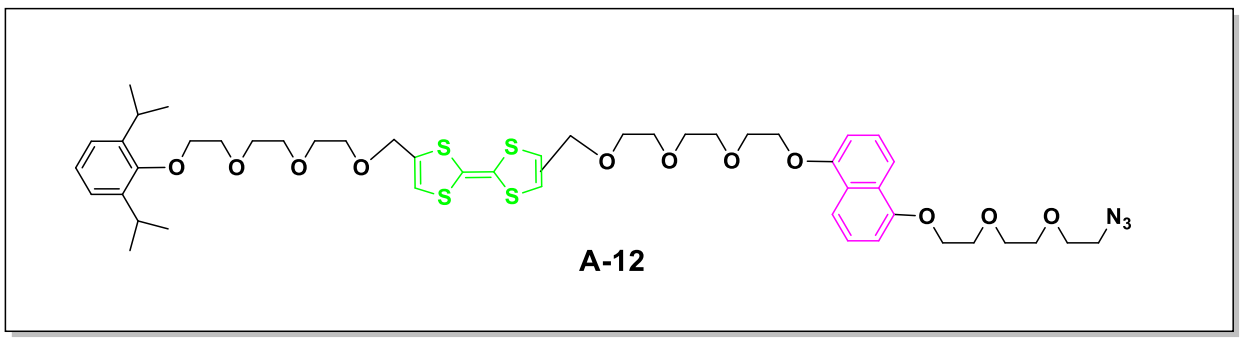

Figure 12. *Structure of the two station axle.*

The synthetic route to provide the two-station azide **A-12** is outlined in Scheme 6. The starting compound **17** was obtained after monotosylation of the corresponding dialcohol. The subsequent introduction of the 2,6-diisopropylphenol as stopper followed by tosylation of the alcohol **18** gave the key intermediate half thread CH_2O-TTF-OCH_2 tosylate **19**. The next step was represented by the reaction between the half thread **19** with the monofunctionalized

naphthol derivative **22** to allow the two stations dumbbell. Compound **22** was obtained after introduction of the tetrahydro-2H-pyranyl (THP) glycol chain to the 1,5-Dihydroxynaphthalene **21**. Selective deprotection of the THP derivative **23**, tosylation of the alcohol **24** and azide exchange of **25** afforded the desired axial thread **A-12**.

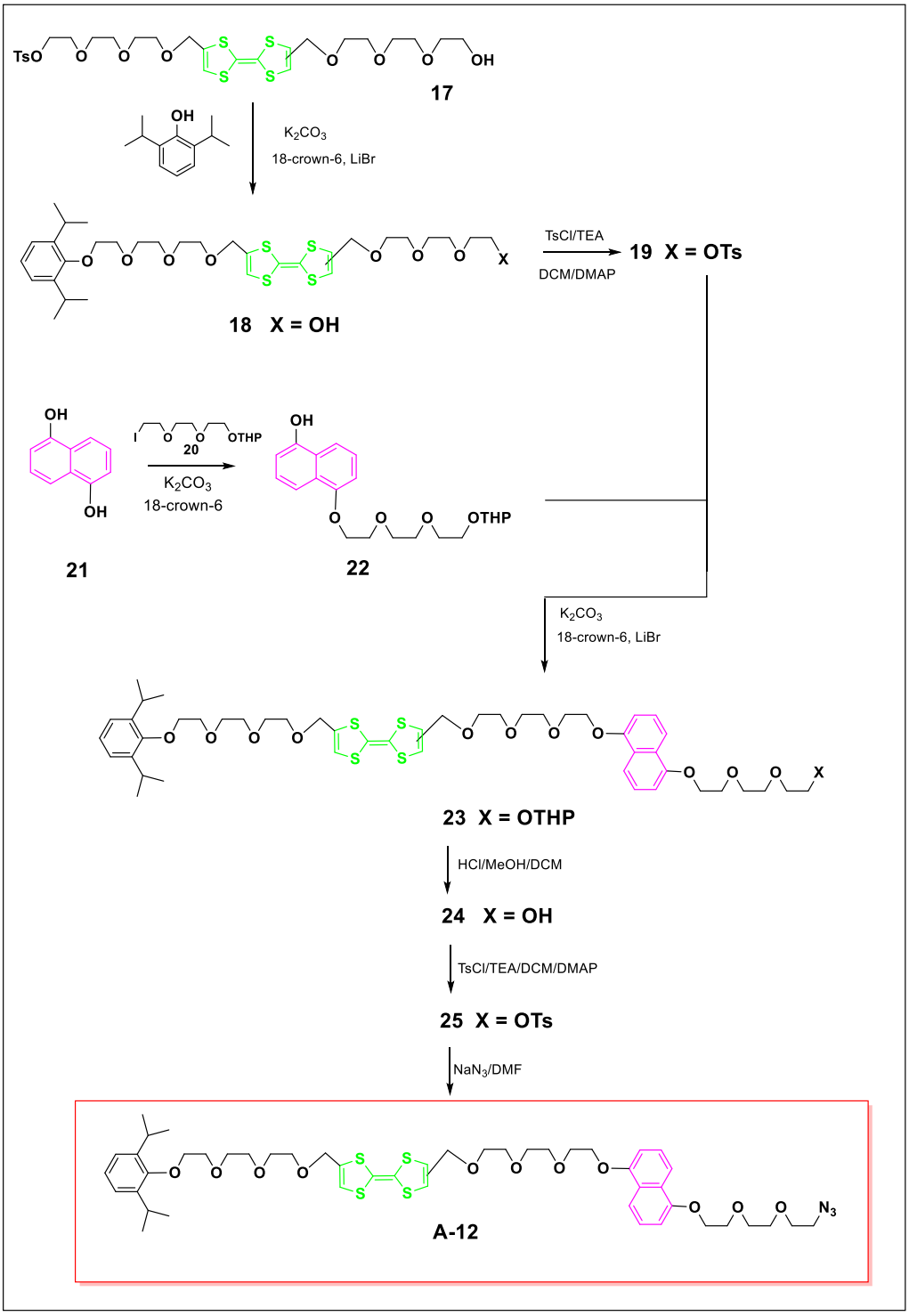

Scheme 6. *The synthetic procedure to obtain the two station thread showing the azide group.*

Once prepared the axle component the synthesis of rotaxanes **R-12** and **R-13** were performed following the threading-followed-by-stoppering protocol outlined in Scheme 7.

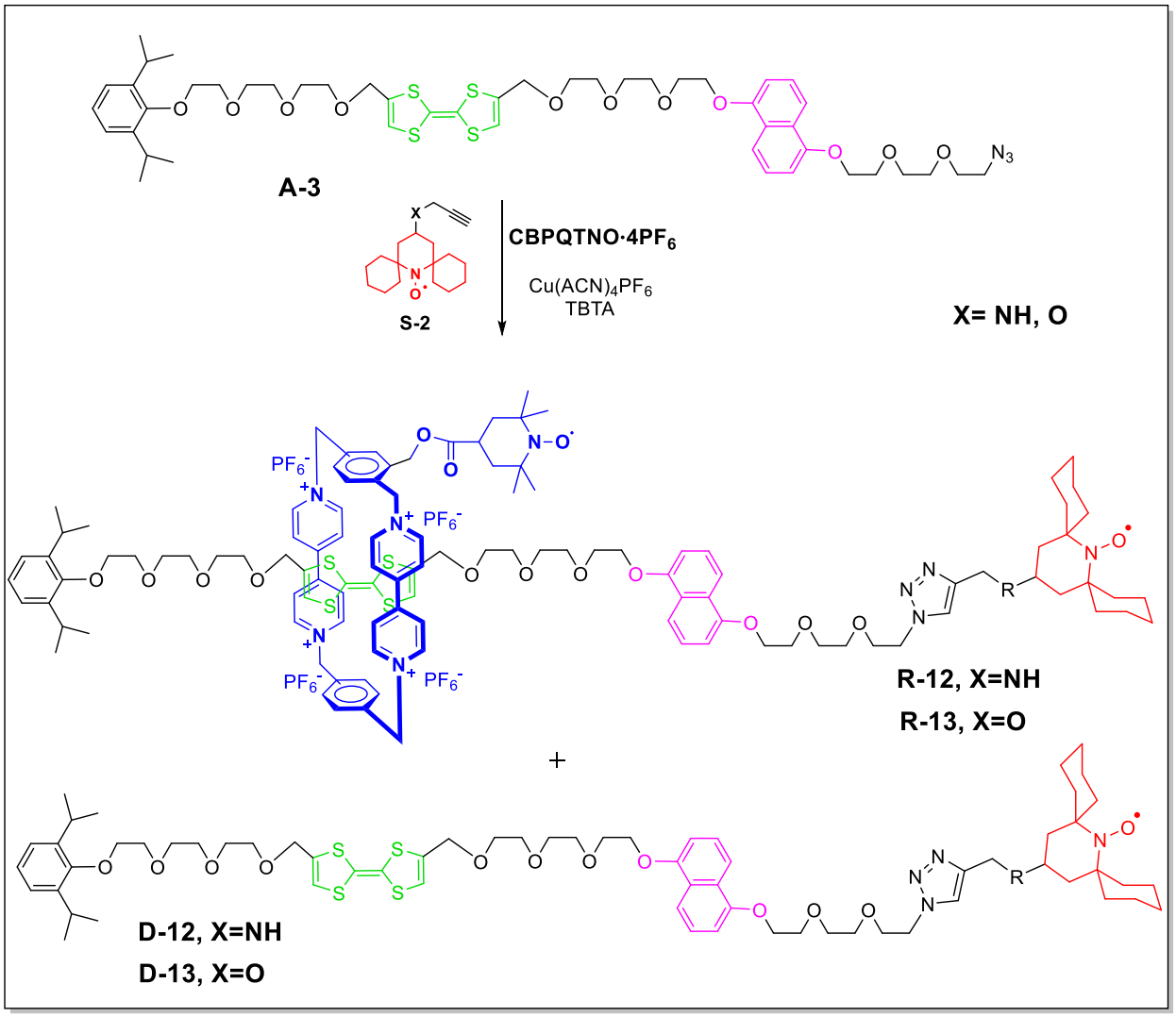

Scheme 7. *Synthesis of the two-station rotaxanes and their dumbbells.*

We applied the experimental procedure described above for the synthesis of the single station rotaxanes, obtaining the desired paramagnetic rotaxanes **R-12** and **R-13** in non-optimized 22% yield. Also in this case, this reaction led to the formation of the corresponding dumbbells as secondary products. The NMR spectra of the dumbbell derivatives helped us to confirm the interlocked structures of **R-12** and **R-13**. The partial spectra of the spin labeled dumbbell **D-12**, spin labeled rotaxane **R-12** and **CBPQTNO** host are reported in Figure 13 (traces a, b, and c respectively).

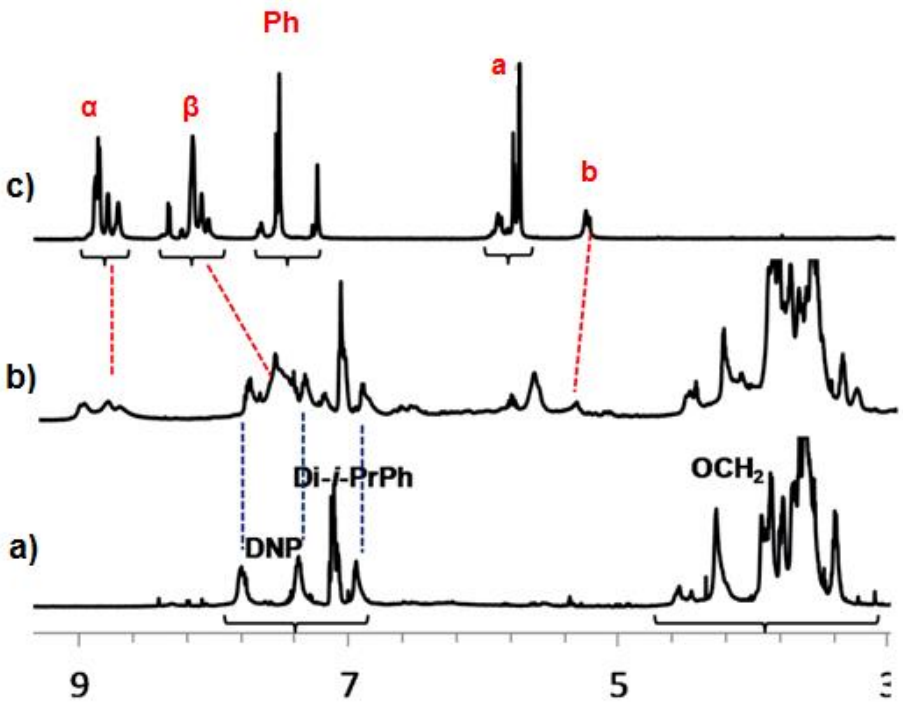

Figure 13. *Partial ^{1}H NMR spectra (600 MHz, CD_3CN, 298 K) of a) dumbbell **D-12**; b) rotaxane **R-12**; c) **CBPQTNO** host.*

Likewise to the single station rotaxanes the interlocked nature of the **R-12** was confirmed by detecting the broadening and splitting of the α,β and **b** macrocyclic proton signals. On the contrary, the signals corresponding to the DNP protons in the rotaxane spectrum did not undergo any change comparing with those of the corresponding dumbbell **D-12** (blue dashed lines). This observation gave evidence that the DNP was not encircled by the macrocycle. Even though the TTF signals were not detected presumably due to a partial air oxidation to the corresponding $TTF^{\bullet+}$ radical cation which caused lost of signal, it reasonable to esteem that the paramagnetic host resides preferentially on this recognizing unit, also in keeping with previous consideration on the DNP protons.

2.3.2 EPR characterization

The most remarkable results regarded the EPR studies performed on the rotaxane **R-12** and the corresponding dumbbell **D-12**. The EPR spectrum of **R-12** in ACN at 338 K (a_N=15.60) outlined in Figure 14, was characterized by the presence of three lines as expected for two non-interacting radicals system. The result, confirmed also by the NMR spectra was due to the

large distance between the TEMPO unit of the macrocycle and the spirocyclohexyl nitroxide stopper.

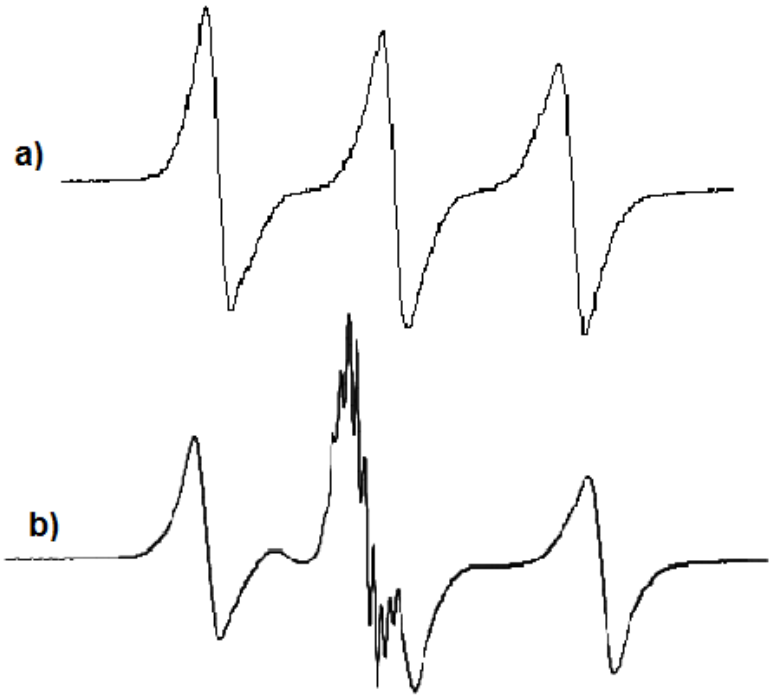

Figure 14. *The EPR spectra of the rotaxane **R-12** in ACN at 338 K before (a) and after (b) the addition of $Fe(ClO_4)_3$.*

After oxidation of the TTF moiety to the corresponding TTF radical cation, the shape of EPR spectrum showed a noticeable change concerning the appearance of new exchange signals. By analyzing in detail the spectrum shape it was possible to stabilize that these extra lines were due to the spin coupling taking place between the TTF radical cation and the nitroxide present on the ring, affording a clear evidence of the macrocycle movement. In contrast, no exchange lines ascribed to the interaction between the two nitroxide units were detected. This unexpected behavior suggest that after the macrocycle displacement the pendant nitroxide is pointing to the opposite direction with respect to the stopper nitroxide, and, thus, cancelling the corresponding spin-spin coupling.

It should be noted that the interaction between TTF radical cation and the nitroxide present on the ring is possible only after the displacement of the ring form the TTF moiety. Actually, this was demonstrated by recording the EPR spectrum of the single station TTF-based rotaxane **R-14** (Figure 15) containing two diamagnetic stoppers at the both ends.

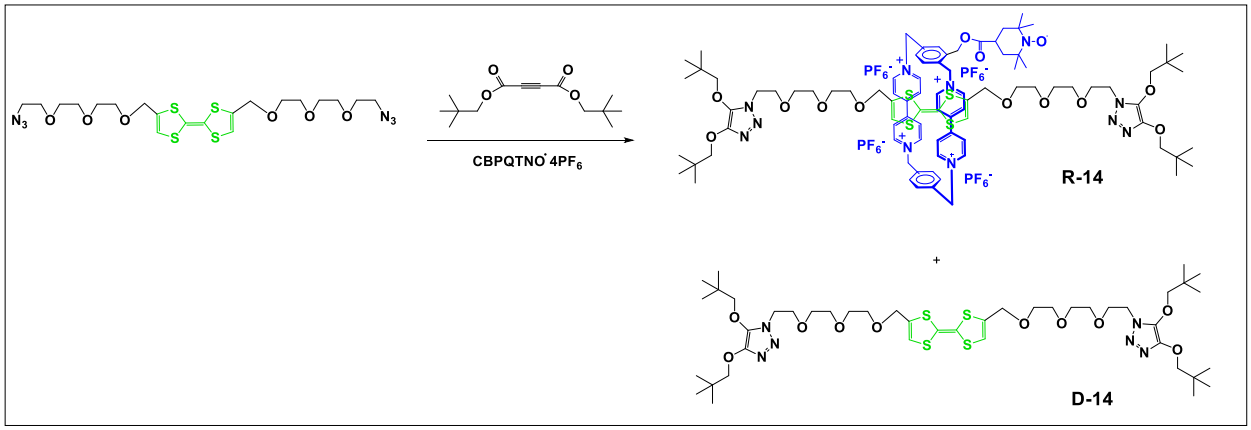

Figure 15. *Structures of the rotaxane **R-14** and the corresponding dumbbell **D-14**.*

This rotaxane was obtained following the synthetic route described above for the previously described rotaxanes. After oxidation of TTF station, the EPR spectrum did not show the appearance of exchange lines, suggesting the absence of through-space spin coupling between TTF radical cation and nitroxide unit (Figure 16). In this case the $CBPQT^{4+}$ ring is forced to remain on the $TTF^{\bullet+}$ radical cation preventing the interaction between the two radical centers due to its shielding effect.

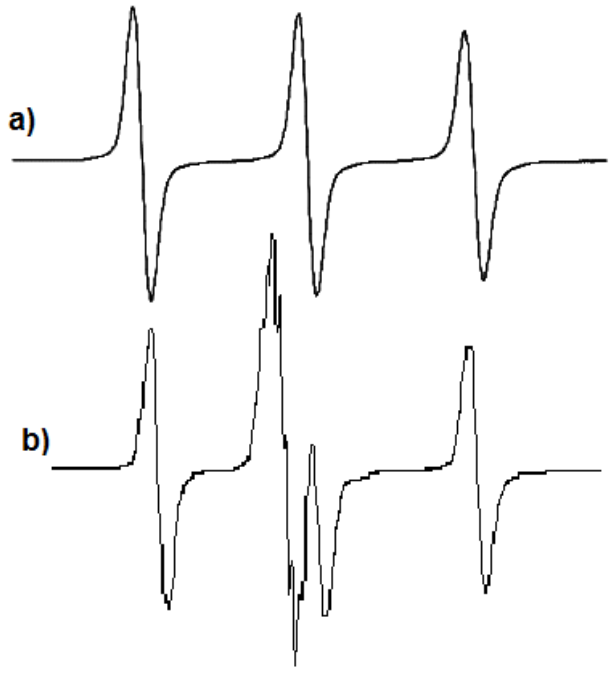

Figure 16. *The EPR spectra of the rotaxane **R-14** in ACN at 338 K before (a) and after (b) the addition of $Fe(ClO_4)_3$.*

Conversely, the possibility to detect this interaction in the rotaxane **R-12** gave a clear evidence of the displacement of the macrocycle, which could move toward the DNP station turning off its shielding effect.

We also recorded the EPR spectrum of the dumbbell **D-12** in ACN at 338 K (Figure 17 a_N=15.35). After the addition of the oxidant agent, the EPR spectrum changed from three to five lines highlighting a strong through-space spin coupling between the different radical species. In this case, it seems reasonable to conclude that the two different radical species are close to each other making possible exchange interaction because of the high flexibility of the glycol chains. Due to the presence of the macrocycle the corresponding rotaxane is expected to be more rigid this preventing the exchange interaction.

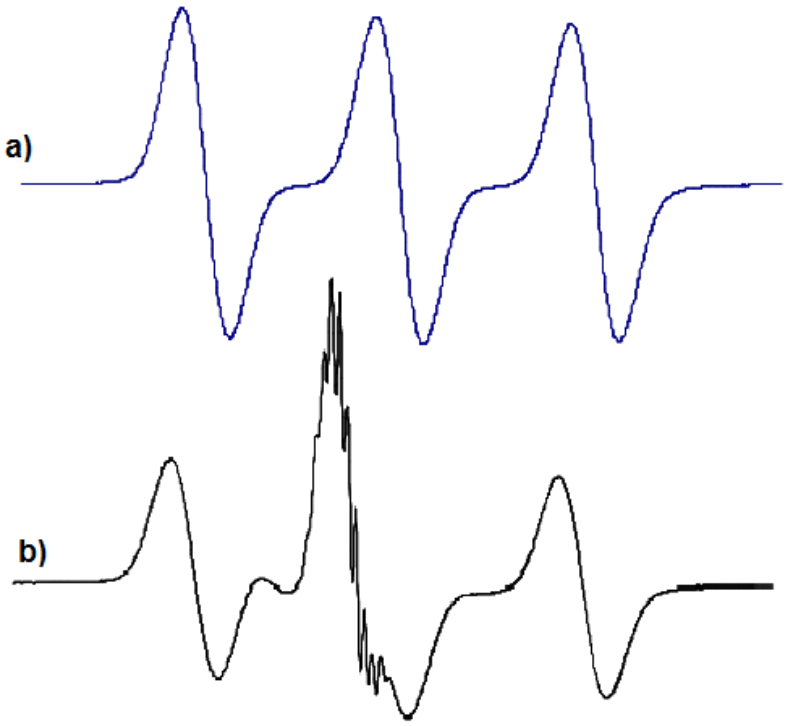

Figure 17. *The EPR spectrum of the dumbbell **D-12** in ACN at 338 K before (a) and after (b) the addition of $Fe(ClO_4)_3$.*

References

[1] R. A. Bissell, E. Cordova, A. E. Kaifer, J. F. Stoddart, *Nature* **1994**, *369*, 133.

[2] A. C. Fahrenbach, C. J. Bruns, D. Cao, J. F. Stoddart, *Acc. Chem. Res* .**2012**, *45*, 1581.

[3] R. Manoni, F. Romano, C. Casati, P. Franchi, E. Mezzina, M. Lucarini, *Org. Chem. Front*. **2014**, *1*, 477–483.

[4] R. W. Dichtel, Š. M. Ognjen, J. M. Spruell, J. R. Heath, J. F. Stoddart, *J. Am. Chem. Soc*. **2006**, *128*, 10388.

[5] R. Pievo, C. Casati, P. Franchi, E. Mezzina, M. Bennati, M. Lucarini, *ChemPhysChem* **2012**, **13**, 2659; E. Mileo, C. Casati, P. Franchi, E. Mezzina, M. Lucarini, *Org. Biomol. Chem.* **2011**, *9*, 2920.

[6] E. Mezzina, M. Fanì, F. Ferroni, P. Franchi, M. Menna, M. Lucarini, *J. Org. Chem.* **2006**, *71*, 3773.

[7] J. Luo, C. Pardin, W. D. Lubell, X. X. Zhu, *Chem. Commun.* **2007**, 2136.

[8] E. Mezzina, R. Manoni, F. Romano, M. Lucarini, *Asian J. Org. Chem*. **2015**, *4*, 296 – 310.

[9] In order to decrease the line width of the exchanging lines, ESR spectra have been recorded at 338 K.

[10] V. N. Parmon, A. I. Kokorin, G. M. Zhidomirov, K. I. Zamarev, *Mol. Phys.* **1975**, *30*, 695.

[11] C. Casati, P. Franchi, R. Pievo, E. Mezzina, M. Lucarini, *J. Am. Chem. Soc*. **2012**, *134*, 19108.

[12] F. Romano, R. Manoni, P. Franchi, E. Mezzina, M. Lucarini, *Chem. Eur. J.* **2015**, *21*, 2775–2779.

[13] M. Kavala, V. Brezová, Ĺ. Švorc, Z. Vihonská, P. Olejníková, J. Moncol, J.Kožíšek, P. Herich, P. Szolcsányi, *Org. Biomol.Chem*. **2014**, *12*, 4491 –4502.

[14] a) C. Wang, D. Cao, A. C. Fahrenbach, L. Fang, M. A. Olson, D. C. Friedman,S. Basu, S. K. Dey, Y. Y. Botros, J. F. Stoddart, *J. Phys. Org. Chem*. **2012**, *25*, 544– 552; b) A. C. Fahrenbach, C. J. Bruns, D. Cao, J. F. Stoddart, *Acc. Chem. Res*. **2012**, *45*, 1581– 1592.

[15] R. S. Stoll, D. C. Friedman, J. F. Stoddart, *Org. Lett.*, **2011**, *13*, 2706–2709.

Chapter 5

Experimental section

General procedures

EPR spectra has been recorded on Bruker-ELEXYS spectrometer by using the following instrument settings: microwave power 0.79 mW, modulation amplitude 0.04 mT, modulation frequency 100 kHz, scan time 180 s, 2K data points.

^{1}H NMR spectra were recorded at 298 K on a Varian Inova spectrometer operating at 600 MHz and 400 MHzusing the solvent peaks as internal standards. Chemical shifts are reported in parts per million (ppm, δ scale). In the ^{1}H NMR of paramagnetic derivatives the presence of nitroxide units interfered with the NMR measurement, quenching the signals of some protons. ESI-MS spectra were recorded with Micromass ZMD spectrometer by using the following instrumental settings: positive ions; desolvation gas (N2) 230 L/h; cone gas (skimmer): 50 L/h; desolvation temperature. 120° C; capillary voltage: 3.2 kV; cone voltage: 40 and 100 V; hexapole extractor: 3 V.

All substances, included the stoppers **S-1, S-2**, **S-3**,**S-4, S-5**and solvents were used without further purification and were commercially available. Dry solvents were bought dry and used directly.

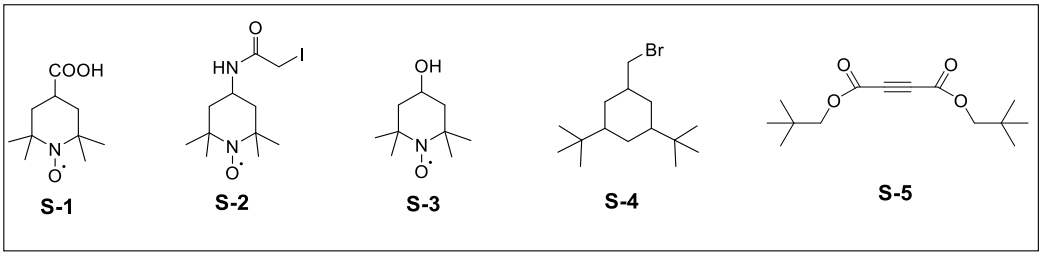

S-1 **S-2** **S-3** **S-4** **S-5**

1 Experimental section of Chapter 2

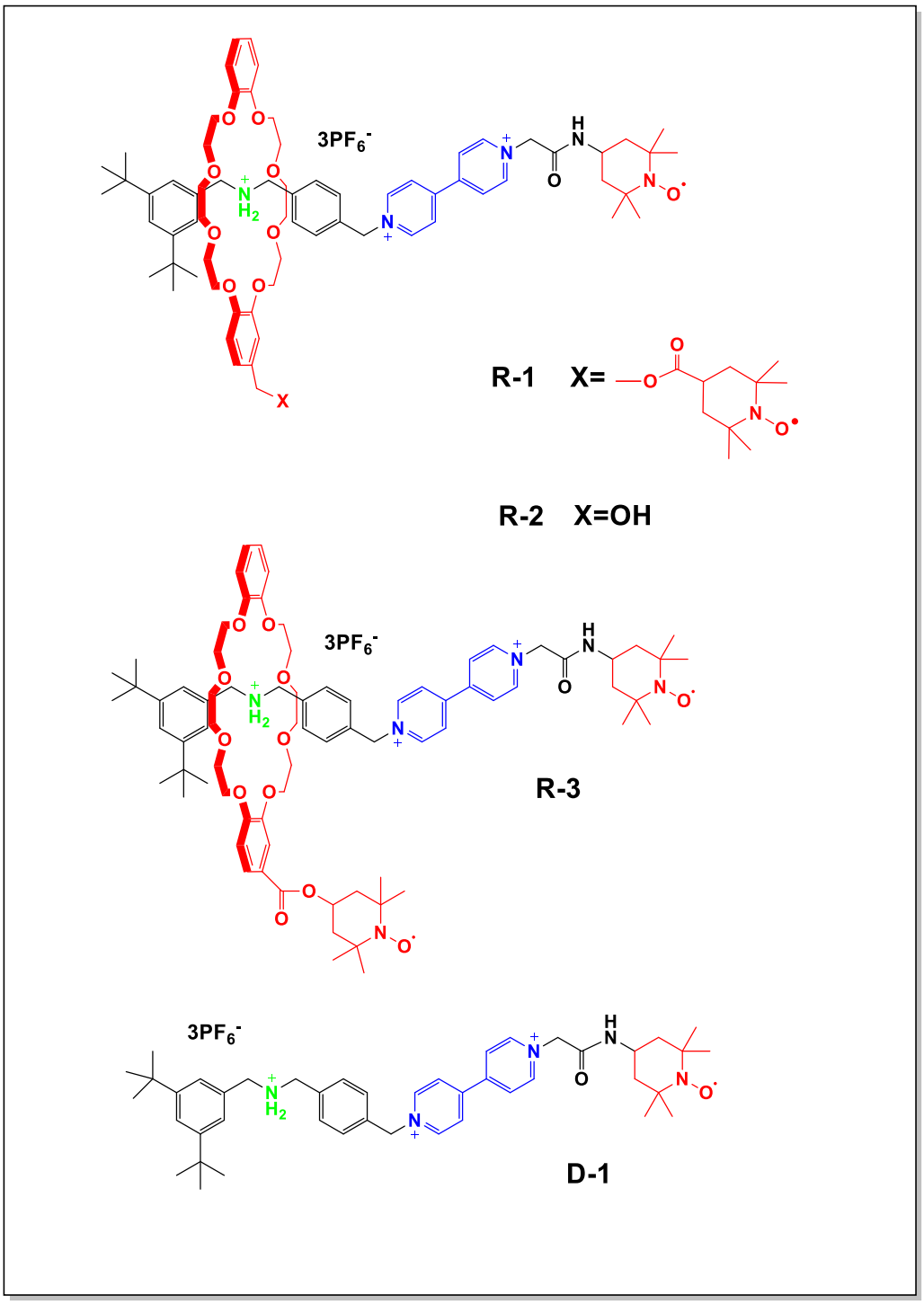

Scheme 1

Compound **A-1** was prepared according to literature.[1]

Compound **1h** was prepared by a modified synthetic protocol based on the procedure reported by Pak *et al.*[2] and Gale *et al.*[3]

1.1 Preparation of the spin labelled rotaxane R-1and dumbbell D-1

- Synthesis of compound **1c**

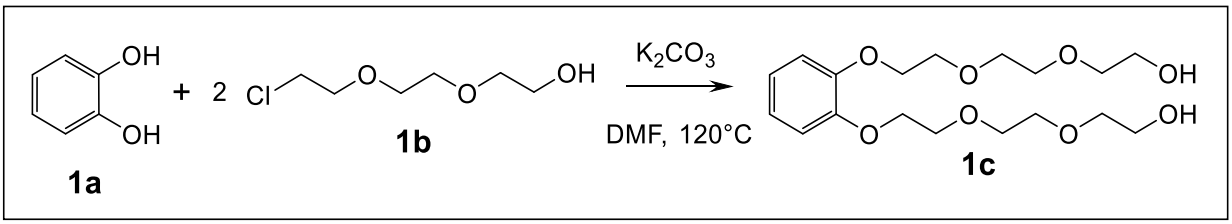

Catechol **1a** (2.80 g, 25.4 mmol) was dissolved in 50 mL dry DMF under nitrogen atmosphere and potassium carbonate (3 equivalents, 10.54 g, 76.2 mmol) was added followed by 2-[2-(2-chloro-ethoxy)-ethoxy]-ethanol **1b** (2.2 equivalents, 9.43 g, 56 mmol). The reaction was heated to 120°C (bath temperature). After 20 h, the suspension was allowed to cool down and the solvent was removed in vacuo. The residue was dissolved in H_2O and TCM, the phases were separated and the water layer was extracted with TCM three more times. The combined organic layers were dried over $MgSO_4$ and the solvent was removed in vacuo. The residue was submitted to column chromatography on silica gel, using EtOAc/MeOH (4:1, v/v) as eluent. Yield: 9.097 g, 24 mmol, 96%.

^{1}H NMR ($CDCl_3$, 400 MHz): δ 3.08 (br, OH, 2 H), 3.57-3.61 (m, CH_2, 4 H), 3.64-3.69 (m, CH_2, 4 H), 3.69-3.75 (m, CH_2, 8 H), 3.84-3.88 (m, CH_2, 4 H), 4.14-4.18 (m, CH_2, 4 H), 6.89 (s, ArH, 4 H).

^{13}C-NMR ($CDCl_3$): δ 61.65, 68.61, 69.70, 70.28, 70.78, 72.61 (CH_2), 114.41 ($C_{Ar}H$), 121.64 ($C_{Ar}H$), 148.68 ($C_{Ar}O$).

- Synthesis of compound **1e**

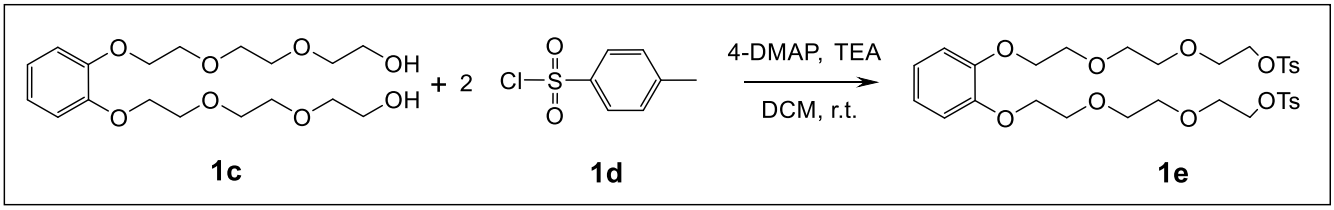

The reagent **1c** (9.51 g, 24.4 mmol) was dissolved in 150 mL DCM under nitrogen atmosphere and TEA (13.5 mL) and 4-(Dimethylamino)-pyridine (38 mg) were added. The solution was cooled down in an ice bath and 4-toluenesulfonyl chloride **1d** (2.2 equivalents, 10.65 g, 55.9 mmol) dissolved in 75 mL DCM was added dropwise at this temperature over 1 h. The ice bath was removed and stirring continued at r.t. over night. Some DCM was removed in vacuo and 100 mL HCl (5 M) were added. The phases were separated and the

organic layer was washed with 2 M HCl, brine, dried over $MgSO_4$ and the solvent was removed in vacuo. The product was isolated by column chromatography on silica gel, starting with pure DCM as solvent and continuing with DCM/EtOAc, 9:1 (v/v). Yield: 12.36 g, 18.1 mmol, 74%.

^{1}H-NMR ($CDCl_3$, 400 MHz): δ 2.40 (s, CH_3, 6 H), 3.56-3.60 (m, CH_2, 4 H), 3.62-3.68 (m, CH_2, 8 H), 3.77-3.81 (m, CH_2, 4 H), 4.09-4.15 (m, CH_2, 8 H), 6.88 (s, ArH, 4 H), 7.30 (d, ^3J=7.9 Hz, ArH, 4 H), 7.76 (d, ^3J=8.4 Hz, ArH, 4 H).

- Synthesis of compound **1g**

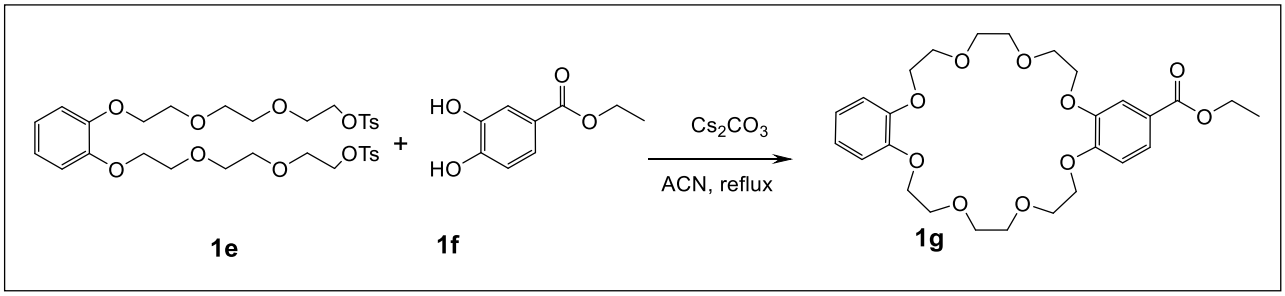

Cs_2CO_3 (25.28 g) was suspended in 630 mL ACN under nitrogen atmosphere and heated to reflux (120 °C bath temperature). A solution of **1e** (10.594 g, 15.5 mmol) and ethyl 3,4-hydroxybenzoate **1f** (2.827 g, 15.5 mmol) in 90 mL ACN was added over 24 h via syringe pump to the boiling suspension. Afterwards, reflux continued for 24 h before the suspension was allowed to cool down. The solvent was removed in vacuo und the residue was dissolved in EtOAc and H_2O. The phases were separated and the water layer was extracted with EtOAc four more times. The combined org. layers were washed with H_2O, dried over $MgSO_4$ and the solvent was removed in vacuo. The product was crystallized from DCM and *n*-hexane. If necessary, the product can be further purified by column chromatography on silica gel with DCM/MeOH, 49:1 (v/v) as eluent. Yield: 7.163 g; 13.76 mmol; 89%.

^{1}H NMR ($CDCl_3$, 400 MHz): δ 1.35 (t, ^3J=7.1 Hz, CH_3, 3 H), 3.80-3.83 (m, CH_2, 8 H), 3.88-3.94 (m, CH_2, 8 H), 4.11-4.15 (m, CH_2, 4 H), 4.15-4.19 (m, CH_2, 4 H), 4.32 (q, ^3J=7.1 Hz, CH_2, 2 H), 6.81-6.89 (m, ArH, 5 H), 7.50 (d, ^4J=2.0 Hz, ArH, 1 H), 7.63 (dd, ^3J=8.4 Hz, ^4J=2.0 Hz, ArH, 1 H).

^{13}C-NMR ($CDCl_3$): δ 14.30 (CH_3), 60.67 (CH_2), 69.20, 69.26, 69.32, 69.41, 69.54, 69.68, 69.84, 71.18, 71.26, 71.36 (CH_2), 111.89 ($C_{Ar}H$), 113.94 ($C_{Ar}H$), 114.25 ($C_{Ar}H$), 121.30 ($C_{Ar}H$), 121.32 ($C_{Ar}H$), 123.12 ($C_{Ar,q}$), 123.72 ($C_{Ar}H$), 148.12 ($C_{Ar}O$), 148.81 ($C_{Ar}O$), 148.82 ($C_{Ar}O$), 152.70 ($C_{Ar}O$), 166.22 (C=O).

- Synthesis of compound **1h**

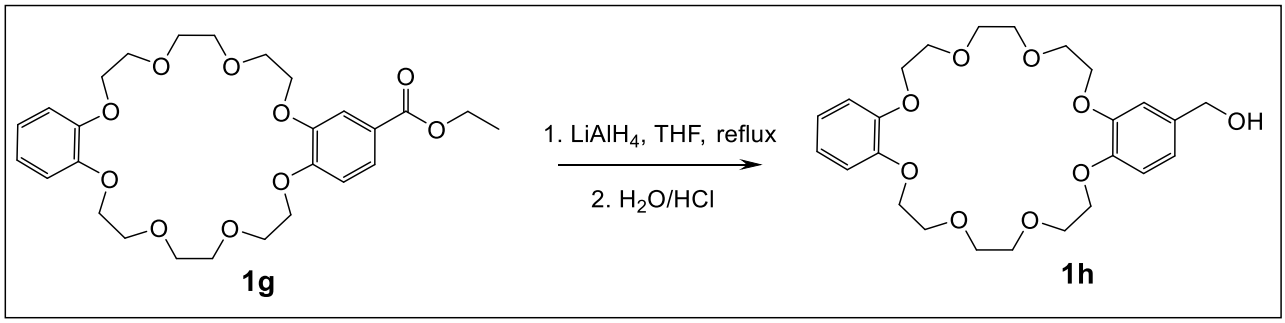

The reagent **1g** (2.07 g, 3.98 mmol) was dissolved in 50 mL dry THF and added dropwise over 1 h to an ice cooled suspension of $LiAlH_4$ (5 equivalents, 755 mg) in 100 mL dry THF under nitrogen atmosphere. After addition, the reaction stirred at r.t. for 1 h und was then heated to reflux for 2 h. Afterwards, the suspension was allowed to cool down and quenched carefully with H_2O and diluted HCl. THF was removed in vacuo and the product was extracted with DCM several times. The combined organic layers were washed with H_2O and brine, dried over $MgSO_4$ and the solvent was removed in vacuo. If necessary, the product can be further purified by column chromatography on silica gel with DCM/MeOH, 19:1 (v/v). Yield: 1.738 g; 3.63 mmol; 91%.

^{1}H NMR ($CDCl_3$, 400 MHz): δ 1.93 (br, OH, 1 H), 3.80 (s, CH_2, 8 H), 3.84-3.90 (m, CH_2, 8 H), 4.08-4.14 (m, CH_2, 8 H), 4.54 (s, CH_2, 2 H), 6.77-6.91 (m, ArH, 7 H).

^{13}C-NMR ($CDCl_3$): δ 65.02 (CH_2OH), 69.32, 69.48, 69.84, 71.19 (CH_2), 112.94 ($C_{Ar}H$), 113.86 ($C_{Ar}H$), 114.06 ($C_{Ar}H$), 119.82 ($C_{Ar}H$), 121.36 ($C_{Ar}H$), 134.25 ($C_{Ar,q}$), 148.31 ($C_{Ar}O$), 148.88 ($C_{Ar}O$), 148.95 ($C_{Ar}O$).

- Synthesis of TEMPO-functionalized DB24C8derivative **1i**[4]

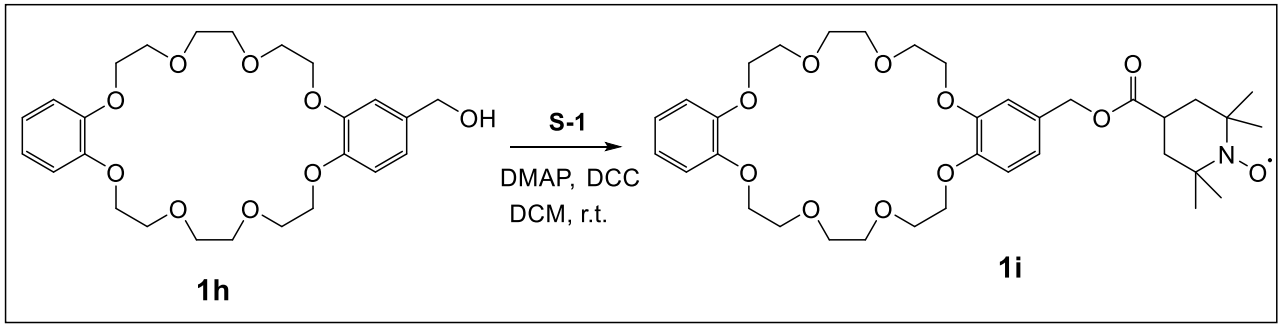

An ice-cooled solution of **1h** (0.15 g, 0.313 mmol), 4-carboxy-TEMPO **S-1** (0.075 g, 0.376 mmol), 1,3-dicyclohexylcarbodiimide (DCC) (0.077 g, 0.376 mmol), and 4-dimethylaminopyridine (DMAP) (0.011 g, 0.094 mmol) in DCC (20 mL) was stirred for 15 min and then for 24 h at r.t. under nitrogen atmosphere. The resulting suspension was filtered, and the filtrate was evaporated and subjected to column chromatography (SiO_2: h

13 cm, i.d. 2 cm, DCM/EtOAc 1:1) to furnish compound **1i** as an orange-brown solid in 70% yield.

^{1}H NMR (600 MHz, CD_3CN): δ 3.68 (s, 8H), 3.80 (s, 8H), 4.05-4.15 (m, 8H), 5.06 (s, 2H), 6.80-7.00 (m, 7H).

ESI-MS: *m/z* 683.1$(M+Na)^+$.

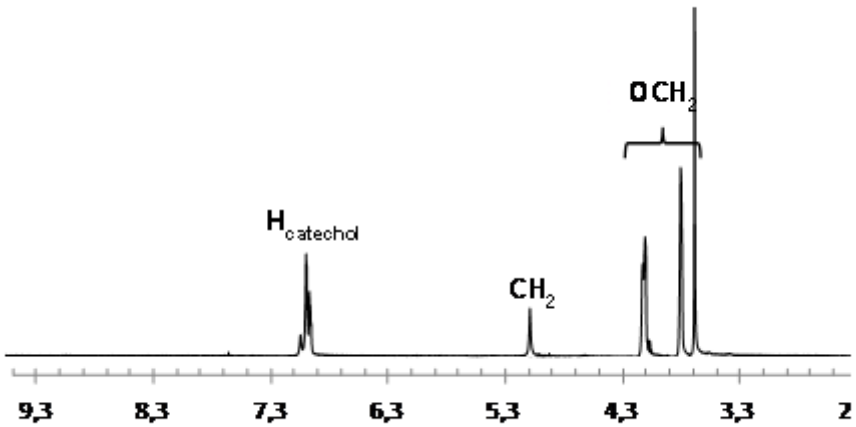

Figure 1. *^{1}H NMR spectrum (600 MHz, CD_3CN, 298 K) of spin labelled ring **1i**.*

The ^{1}H NMR spectrum of *N*-hydroxy amine of **1i** (**1i**-OH) was also recorded after *in situ* reduction of the sample containing the nitroxide**1i** by using phenylhydrazine.

1i-OH: ^{1}H NMR (600 MHz, CD_3CN): δ 1.08 (s, 6H), 1.11 (s, 6H), 1.52 (t, *J* = 12.3 Hz, 2H), 1.77 (d, *J* = 12.3 Hz, 2H), 2.70 (dt, *J* = 12.3 and 3.0 Hz, 1H), 3.68 (s, 8H), 3.78-3.81 (m, 8H), 4.08-4.13 (m, 8H), 4.98 (s, 2H), 6.88-6.95 (m, 7H).

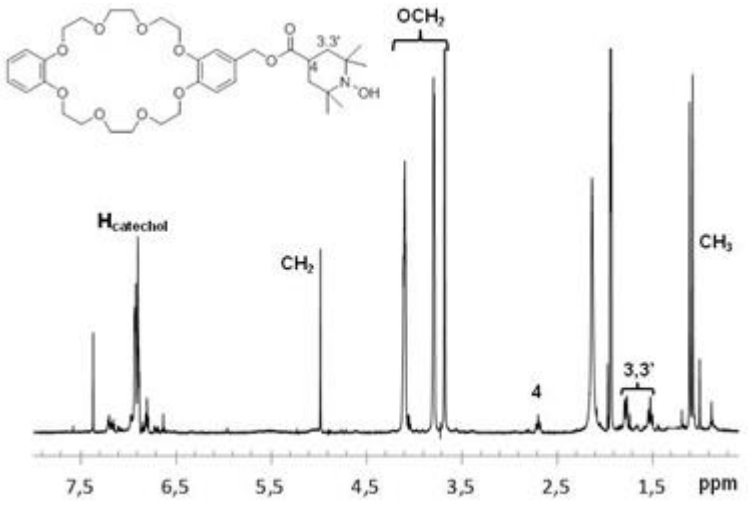

Figure 2. *^{1}H NMR spectrum (600 MHz, CD_3CN, 298 K) of **1i**-OH obtained after in situ reduction of the sample containing the nitroxide **1i** by using phenylhydrazine.*

- Preparation of the spin labelled dumbbell **D-1**[4]

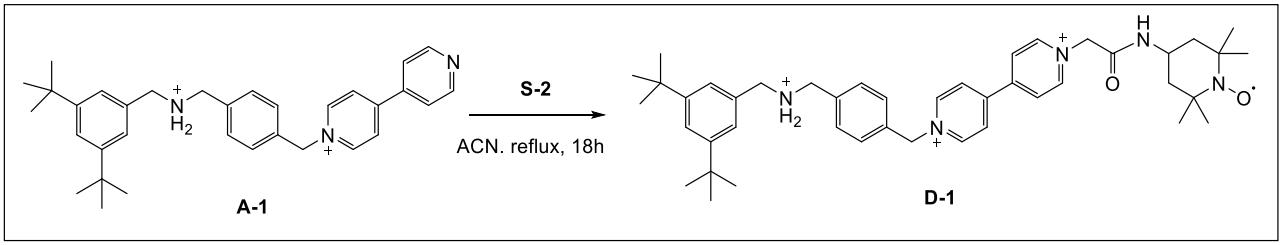

An ACN solution (2 mL) of **A-1** (0.030 g, 0.0389 mmol) and 4-(2-iodoacetamido)-TEMPO (**S-2**, 0.0527 g, 0.156 mmol) was heated under reflux for 18 h under nitrogen atmosphere. After cooling the solution was concentrated in vacuo and the reaction mixture was purified by silica gel column (h 8 cm, i.d. 2 cm, DCM-MeOH 9:1, then MeOH-NH_4Cl 2M-H_2O 7:0.5:2.5). The fractions containing the product were concentrated in vacuo, dissolved in a minimum volume of H_2O, and treated with NH_4PF_6 aqueous solution. The resulting solid was collected by filtration, washed with H_2O to remove the excess of NH_4PF_6, and dried to afford the dumbbell **D-1**as a pink flesh powder (0.022 g, 50% yield).

D-1: ^{1}H NMR (600 MHz, CD_3CN, CF_3COOH): δ 1.30-1.35 (m, 18H), 4.26 (*br* s, 2H), 4.32 (*br* s, 2H), 5.28 (*br* s, 2H), 5.83 (*br* s, 2H), 7.34 (br s, 2H), 7.46-7.68 (m, 5H), 8.35-8.44 (m, 4H), 8.78-8.86 (m, 2H), 8.93-8.99 (m, 2H).

ESI-MS: *m/z* 690.5$(M\text{-}3PF_6)^+$.

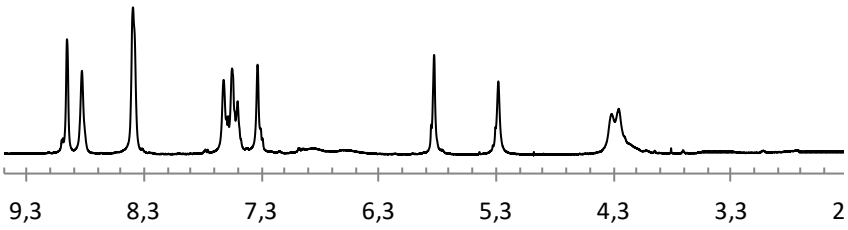

Figure 3. *Partial ^{1}H NMR spectrum (600 MHz, CD_3CN, CF_3COOH, 298 K) of dumbbell **D-1**.*

The ^{1}H NMR spectrum of *N*-hydroxy amine of **D-1** (**D-1**-OH) was also recorded after *in situ* reduction of the sample containing the nitroxide dumbbell **D-1** by using phenylhydrazine.

D-1-OH: ^{1}H NMR (600 MHz, CD_3CN): δ 1.14 (s, 6H), 1.15 (s, 6H), 1.32 (s, 18H), 1.42-1.50 (m, 2H), 1.82 (*br* d, *J* = 9.6 Hz, 2H), 3.64 (s, 2H), 3.69 (s, 2H), 5.27 (s, 2H), 5.81 (s, 2H), 7.38-7.52 (m, 7H), 8.35 (d, *J* = 6.6 Hz, 2H), 8.37 (d, *J* = 6.6 Hz, 2H),8.79 (d, *J* = 6.6 Hz, 2H), 8.95 (d, *J* = 6.6 Hz, 2H).

- Preparation of the spin labelled rotaxane **R-1**[4]

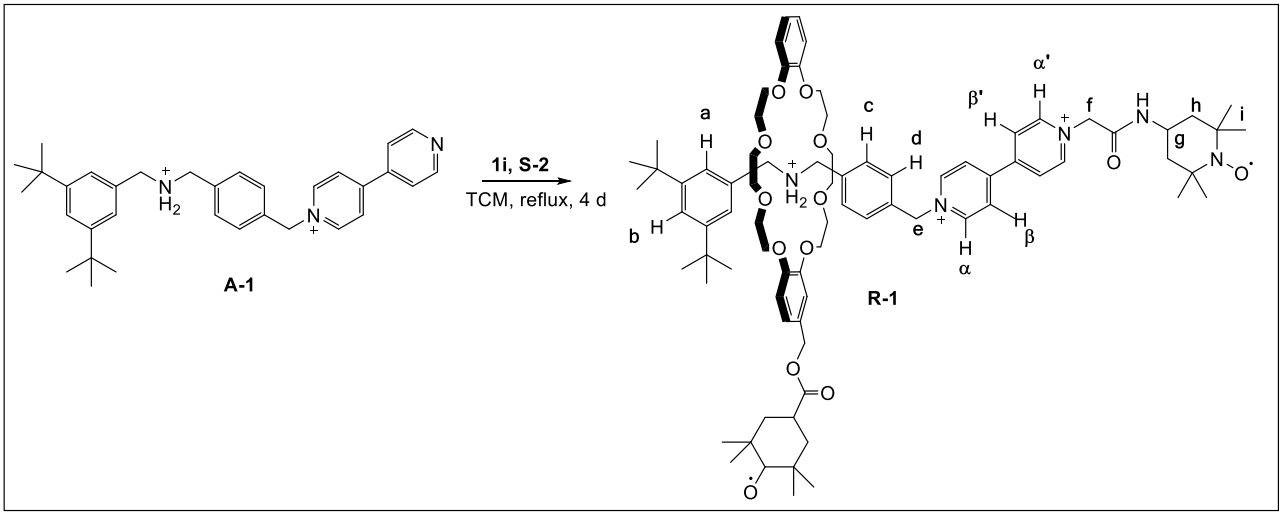

A TCM (1 mL) solution of 4-(2-iodoacetamido)-TEMPO (**S-2**, 0.0725 g, 0.214 mmol) was added to a stirred suspension of compound **A-1** (0.030 g, 0.039 mmol) and **1i** (0.046 g, 0.0972 mmol) in TCM (3 mL) and the mixture was heated under reflux for 4 d under nitrogen atmosphere, until it became a clear solution. After cooling the solution was concentrated in vacuo and the reaction mixture was purified by silica gel column (h 10 cm, i.d. 20 mm, DCM-MeOH 9:1, then MeOH-NH_4Cl 2M-H_2O 7:0.5:2.5). The fractions containing the product were concentrated in vacuo, dissolved in a minimum volume of H_2O, and treated with NH_4PF_6 aqueous solution. The resulting solid was collected by filtration, washed with H_2O to remove the excess of NH_4PF_6, and dried to afford the rotaxane **R-1** as a pink flesh powder (0.021 g, 30% yield).

R-1: ^{1}H NMR (600 MHz, CD_3CN): δ 1.20 (s, 18H), 3.48-3.88 (m, 16H), 3.93-4.16 (m, 8H), 4.68-4.80 (m, 4H), 5.05 (br s, 2H), 5.30 (br s, 2H), 5.49 (s, 2H), 6.69-6.76 (m, 3H), 6.78-6.82 (m, 3H), 6.83-6.90 (m, 1H), 6.94-7.02 (m, 2H), 7.26-7.37 (m, 2H), 7.34 (s, 2H), 7.46 (s, 1H), 7.60-7.72 (m, 2H), 8.41 (br s, 4H), 8.77 (br s, 2H), 8.81-8.90 (m, 2H).

ESI-MS: *m/z* 1810.8$(M+Na)^+$, 1642.9 $(M-PF_6)^+$.

The ^{1}H NMR spectrum of *N*-hydroxy amine of **R-1** (**R-1**-OH) was also recorded after *in situ* reduction of the sample containing **R-1** by using phenylhydrazine.

R-1-OH: ^{1}H NMR (600 MHz, CD_3CN): δ 1.08 (s, 6H), 1.10 (s, 6H), 1.11 (s, 6H), 1.13 (s, 6H), 1.20 (s, 18H), 1.42 (t, *J* = 12.3 Hz, 2H), 1.52 (t, *J* = 13.2 Hz, 2H), 1.75-1.81 (m, 4H), 2.68-2.74 (m, 1H), 3.50-3.86 (m, 16H), 3.93-4.03 (m, 5H), 4.05-4.13 (m, 4H), 4.69-4.80 (m, 4H), 4.97 (s, 2H), 5.29 (s, 2H), 5.48 (s, 2H), 5.62 (br s, 1H), 6.63-6.86 (m, 7H), 6.95 (d, *J* = 7.8 Hz, 2H), 7.28 (d, *J* = 7.8 Hz, 2H), 7.37 (s, 2H), 7.46 (s, 1H), 7.67 (br s, 2H), 8.39 (d, *J* = 6.0 Hz, 2H), 8.41 (d, *J* = 6.6 Hz, 2H), 8.77 (d, *J* = 6.0 Hz, 2H), 8.82 (d, *J* = 6.6 Hz, 2H).

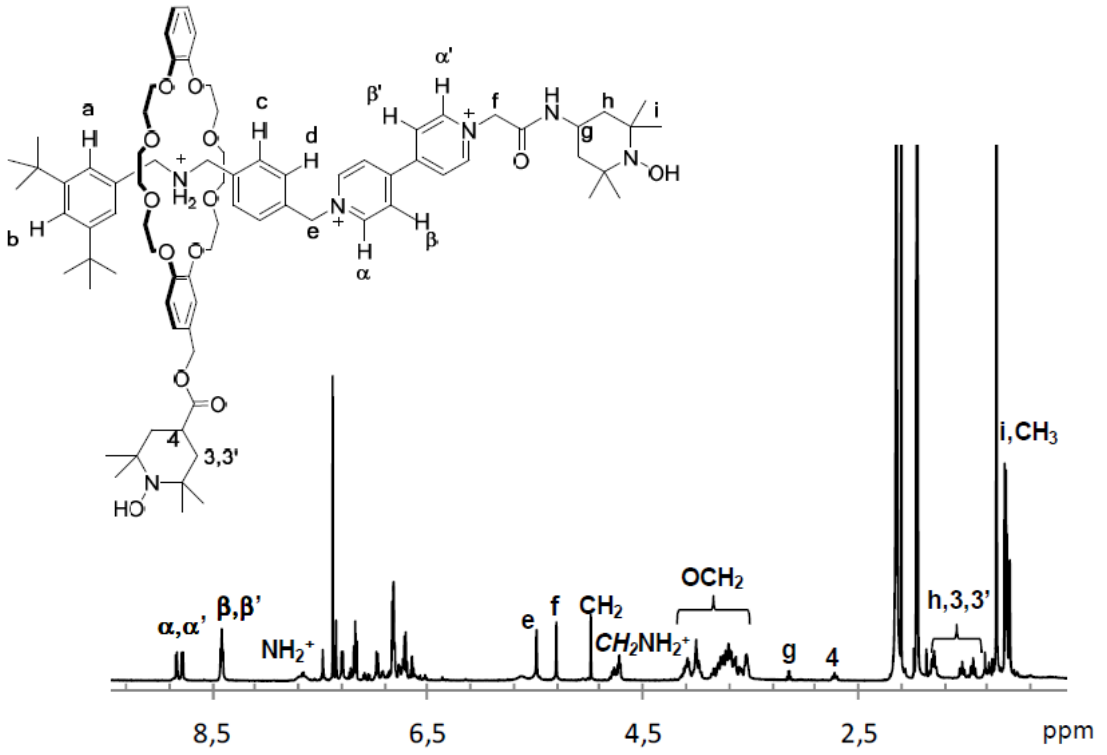

Figure 4. *^{1}H NMR spectrum (600 MHz, CD_3CN, 298 K) of **R-1**-OH obtained after in situ reduction of the sample containing the rotaxane **R-1** by using phenylhydrazine.*

1.2 Preparation of the rotaxane R-2 [4]

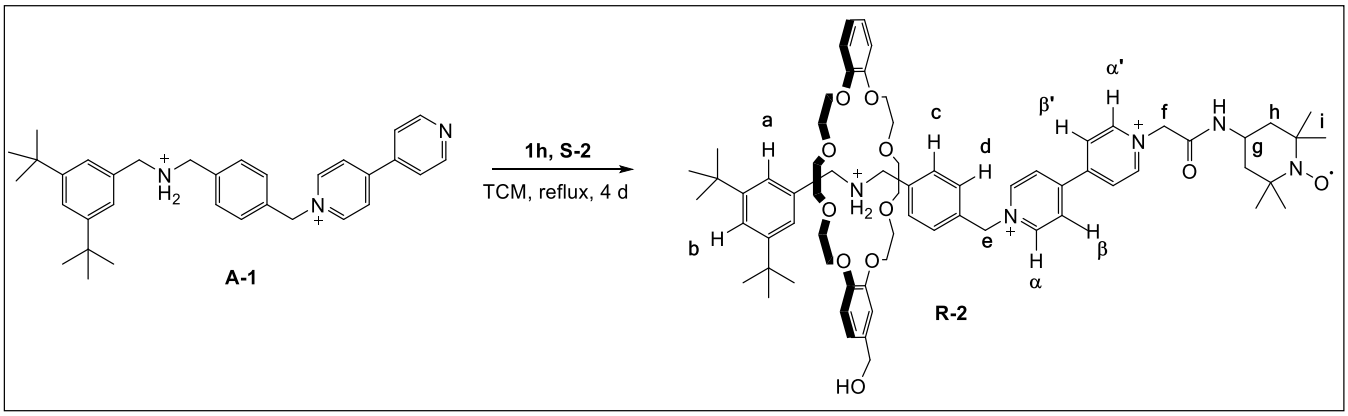

A TCM (1 mL) solution of iodoacetamido-TEMPO (**S-2**, 0.0725 g, 0.214 mmol) was added to a stirred suspension of compound **A-1** (0.030 g, 0.0389 mmol) and **1h** (0.046 g, 0.0972 mmol) in TCM (3 mL) and the mixture was heated under reflux for 4 d under nitrogen atmosphere, until it became a clear solution. After cooling the solution was concentrated in vacuo and the reaction mixture was purified by silica gel column (h 8 cm, i.d. 2 cm, DCM-MeOH 9:1, then MeOH-NH_4Cl 2M-H_2O 7:0.5:2.5). The fractions containing the product were

concentrated in vacuo, dissolved in a minimum volume of H_2O, and treated with NH_4PF_6 aqueous solution. The resulting solid was collected by filtration, washed with water to remove the excess of NH_4PF_6, and dried to afford the **R-2** as a pink flesh powder (0.018 g, 30% yield).

^{1}H NMR (600 MHz, CD_3CN): δ 1.22 (s, 18H), 3.28-3.34 (m, 1H), 3.48-3.60 (m, 4H), 3.64-3.83 (m, 12H), 3.94-3.98 (m, 2H), 3.99-4.10 (m, 7H), 4.45 (*br* s, 2H), 4.70-4.78 (m, 4H), 5.29 (br s, 2H), 5.47 (s, 2H), 6.66 (d, *J* = 7.8 Hz, 1H), 6.73-6.84 (m, 6H), 6.89 (d, *J* = 7.8 Hz, 2H), 7.26 (d, *J* = 7.8 Hz, 2H), 7.37 (s, 2H), 7.49 (s, 1H), 7.67 (br s, 2H), 8.36-8.46 (m, 4H), 8.73-8.77 (m, 2H), 8.85 (br s, 2H).

ESI-MS: *m/z* 1460.8 $(M\text{-}PF_6)^+$, 657.3$(M\text{-}2PF_6)^{2+}$.

The ^{1}H NMR spectrum of the corresponding *N*-hydroxy amine was also recorded after *in situ* reduction of the sample containing the **R-2** by using phenylhydrazine.

R-2-OH: ^{1}H NMR (600 MHz, CD_3CN): δ 1.13 (s, 6H), 1.14 (s, 6H), 1.22 (s, 18H), 1.45 (t, *J* = 12.0 Hz, 2H), 1.81 (d, *J* = 12.0 Hz, 2H), 3.22 (t, *J* = 4.8 Hz, 1H), 3.48-3.60 (m, 4H), 3.65-3.81 (m, 12H), 3.93-3.98 (m, 2H), 4.00-4.10 (m, 6H), 4.45 (s, 2H), 4.71-4.76 (m, 4H), 5.29 (s, 2H), 5.47 (s, 2H), 6.63-6.83 (m, 7H), 6.89 (d, *J* = 7.8 Hz, 2H), 7.26 (d, *J* = 7.8 Hz, 2H), 7.37 (s, 2H), 7.49 (s, 1H), 7.67 (br s, 2H), 8.38-8.44 (m, 4H), 8.74 (d, *J* = 6.6 Hz, 2H), 8.82 (d, *J* = 7.2 Hz, 2H).

1.3 Preparation of the spin labelled rotaxane R-3

- Synthesis of compound **3b**

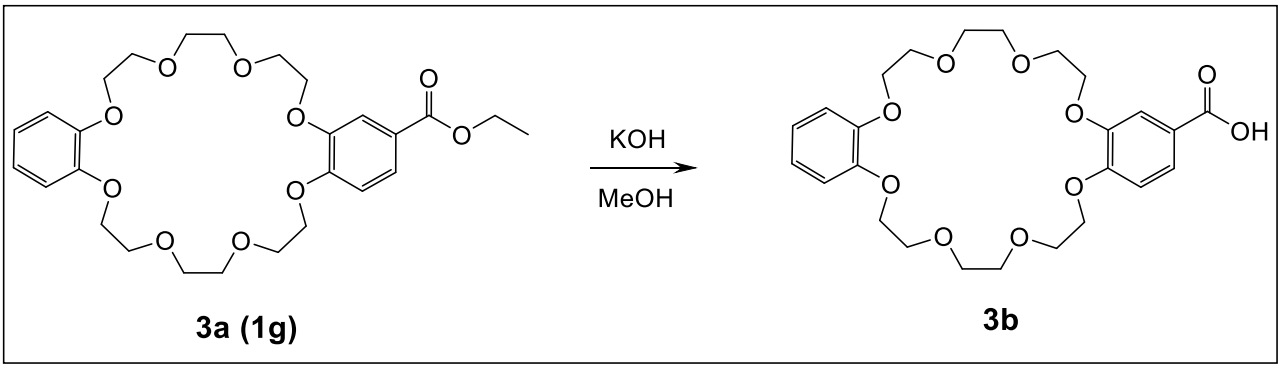

Ester **3a** (0.293 g, 0.56 mmol) was suspended in 5 mL of MeOH in a 25 mL round-bottomed flask and warmed al 35° C under magnetic stirring. KOH was added (0.315 g, 5.6 mmol) and the reaction was stirred overnight until the reaction was complete (controlled by TLC, eluent DCM/EtOAc 1:1).[5] Then the reaction was quenched by addition of 10 mL distilled H_2O and extracted twice by Et_2O to remove the unreacted ester. The aqueous portion was

acidified to pH =2 with 6N HCl and the carboxylic acid **3b** precipitated, filtered off, and dried under vacuum. The crown ether **3b** was obtained in 78% yield (0.216 g, 0.44 mmol).
ESI-MS: *m/z* 491.5 $(M-H)^-$.
^{1}H-NMR (CD_3CN 600 MHz): δ 3.68 (*br* s, 8 H), 3.77-3.84 (m, 8 H), 4.09-4.12 (m, 4 H), 4.15-4.17 (m, 2H), 4.17-4.20 (m, 2H), 6.89-6.92 (m, 2 H), 6.92-6.95 (m, 2H), 6.99 (d, *J*=8.4 Hz, 1H), 7.51 (s, 1H), 7.61 (d, *J*=8.4 Hz, 1H), 9.22 (*br* s, 1H).
^{1}H-NMR (CD_3SOCD_3 600 MHz): δ 3.67 (*br* s, 8 H), 3.74-3.80 (m, 8 H), 4.04-4.07 (m, 4 H), 4.09-4.12 (m, 2H), 4.13-4.16 (m, 2H), 6.85-6.89 (m, 2 H), 6.92-6.95 (m, 2H), 7.03 (d, *J*=8.4 Hz, 1H), 7.43 (s, 1H), 7.54 (d, *J*=8.4 Hz, 1H), 12.6 (*br* s, 1H).

- Synthesis of TEMPO-functionalized DB24C8 derivative **3c**[6]

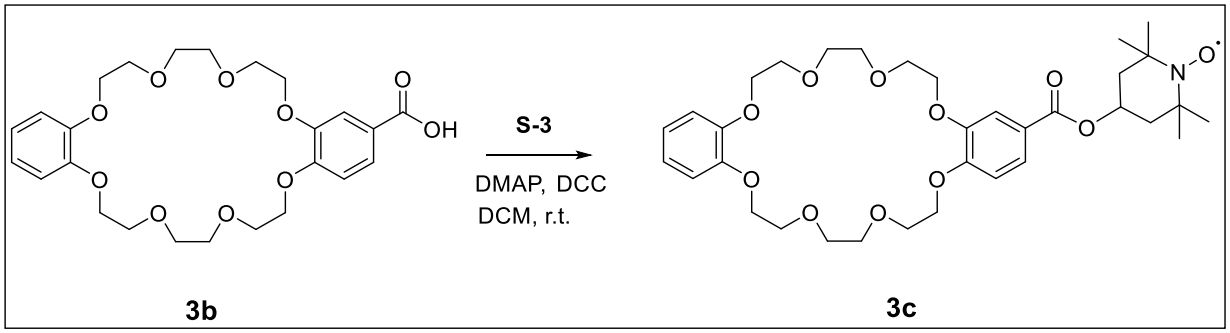

An ice-cooled solution of **3b** (0.216 g, 0.44 mmol), 4-hydroxy-TEMPO (**S-3**, 0.090 g, 0.525 mmol), 1,3-dicyclohexylcarbodiimide (DCC) (0.108 g, 0.525 mmol), and 4-dimethylaminopyridine (DMAP) (0.016 g, 0.131 mmol) in DCM (30 mL) was stirred for 15 min and then for 4 d at r.t. under nitrogen atmosphere. (controlled by TLC, eluent DCM/EtOAc 1:1). The resulting suspension was filtered, and the filtrate was evaporated and subjected to column chromatography (SiO_2: h 13 cm, i.d. 2 cm, dichloromethane/ethyl acetate, 9:1 until 1:1) to furnish compound **3c** as an orange-brown solid in 57% yield (0.161 g, 0.25 mmol).
^{1}H NMR (600 MHz, CD_3CN): δ 3.66-3.72 (m, 8H), 3.78-3.87 (m, 8H), 4.05-4.20 (m, 8H), 6.85-6.95 (m, 4H), 7.01 (*br* s, 1H), 7.50-7.70 (m, 2H).
ESI-MS: *m/z* 647.6 $(M+H)^+$, 669.7$(M+Na)^+$.

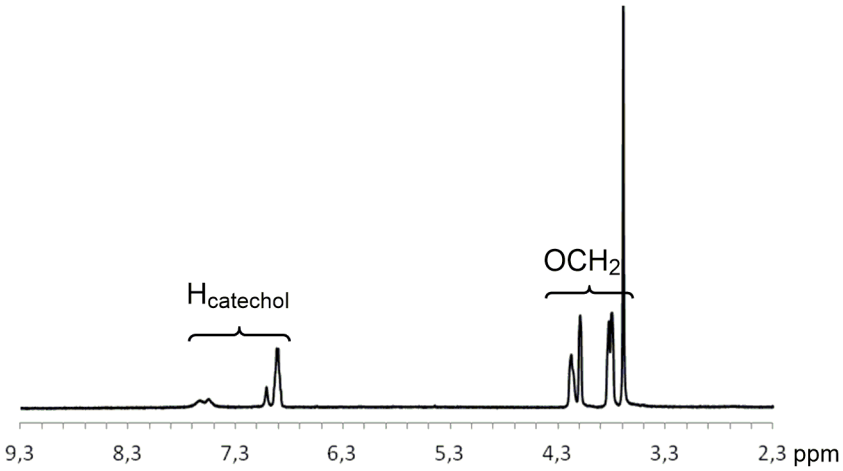

Figure 5. *^{1}H NMR spectrum (600 MHz, CD_3CN, 298 K) of spin labelled ring **3c**.*

The ^{1}H NMR spectrum of *N*-hydroxy amine of **3c** (**3c**-OH) was also recorded after *in situ* reduction of the sample containing the nitroxide **3c** by using phenylhydrazine.

3c-OH: ^{1}H NMR (600 MHz, CD_3CN): δ 1.16 (s, 6H), 1.18 (s, 6H), 1.63 (t, *J* = 12.0 Hz, 2H), 1.99 (dd, *J* = 12.0 and 4.2 Hz, 2H), 3.69 (s, 8H), 3.78-3.84 (m, 8H), 4.08-4.11 (m, 4H), 4.13-4.18 (m, 4H), 5.20 (tt, *J* = 12.0 and 4.2 Hz, 1H), 6.88-6.94 (m, 4H), 6.97 (d, *J* = 8.4 Hz, 1H), 7.50 (d, *J* = 1.8 Hz, 1H), 7.59 (dd, *J* = 8.4 and 4.2 Hz, 1H).

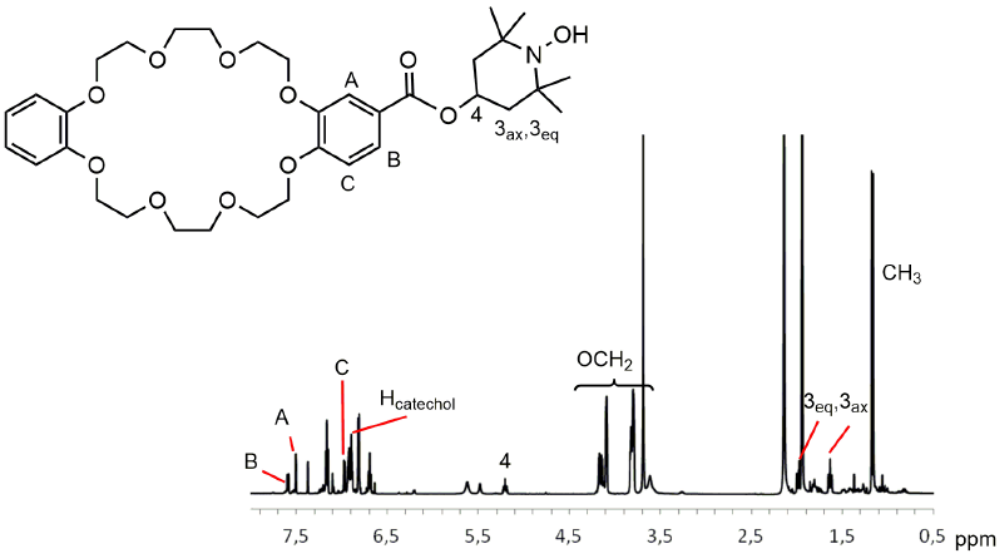

Figure 6. *^{1}H NMR spectrum (600 MHz, CD_3CN, 298 K) of **3c** obtained after in situ reduction of the sample by using phenylhydrazine.*

- Preparation of rotaxane **R-3**[6]

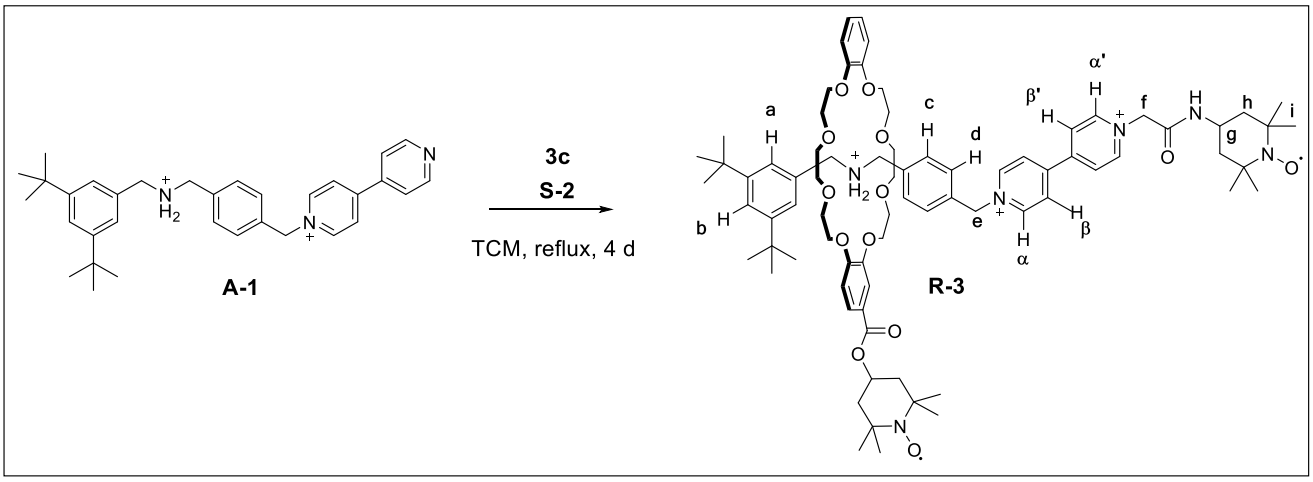

A TCM (1 mL) solution of 4-(2-iodoacetamido)-TEMPO (**S-2**, 0.0725 g, 0.214 mmol) was added to a stirred suspension of compound **A-1** (0.030 g, 0.039 mmol) and **3c** (0.063 g, 0.097 mmol) in TCM (3 mL) and the mixture was heated under reflux for 4 d under nitrogen atmosphere, until it became a clear solution. After cooling the solution was concentrated in vacuo and the reaction mixture was purified by silica gel column (h 10 cm, i.d. 25 mm, DCM-MeOH 9:1, then MeOH-NH_4Cl 2M-H_2O 7:0.5:2.5). The fractions containing the product were concentrated *in vacuo*, dissolved in a minimum volume of H_2O, and treated with NH_4PF_6 aqueous solution. The resulting solid was collected by filtration, washed with water to remove the excess of NH_4PF_6, and dried to afford the rotaxane **R-3** as a beige powder (0.025 g, 36.2% yield).

R-3: ^{1}H NMR (600 MHz, CD_3CN): δ 1.20 (s, 18H), 3.46-4.18 (m, 24H), 4.70-4.80 (m, 4H), 5.29 (*br* s, 2H), 5.47 (s, 2H), 6.64-6.88 (m, 5H), 7.00 (d, *J* = 6.6 Hz, 2H), 7.28-7.35 (m, 4H), 7.44 (s, 1H), 7.60-7.72 (m, 2H), 8.42 (*br* s, 4H), 8.75 (*br* s, 2H), 8.81-8.90 (m, 2H).

^{13}C-NMR (CD_3CN): δ 31.44, 35.38, 52.65, 53.83, 64.94, 68.63, 68.70, 68.96, 69.07, 70.63, 70.67, 70.76, 71.05, 71.17, 71.51, 71.60, 112.57, 112.89, 112.94, 113.45, 121.99, 124.25, 124.50, 127.65, 128.56, 129.70, 131.42, 132.17, 133.59, 134.54, 146.43, 147.72, 147.76, 148.25, 151.36, 152.35, 152.57, 164.08, 165.72.

ESI-MS: *m/z* 1796.0$(M+Na)^+$, 1628.9 $(M-PF_6)^+$, 1482.9 $(M-H-2PF_6)^+$.

The ^{1}H NMR spectrum of *N*-hydroxy amine of **R-3** (**R-3**-OH) was also recorded after *in situ* reduction of the sample containing **R-3** by using phenylhydrazine.

R-3-OH: ^{1}H NMR (600 MHz, CD_3CN): δ 1.11 (s, 6H), 1.13 (s, 6H), 1.15 (s, 3H), 1.16 (s, 3H), 1.17 (s, 6H), 1.20 (s, 18H), 1.41 (t, *J* = 12.3 Hz, 2H), 1.62 (dt, *J* = 12.0 and 6.0 Hz, 2H), 1.80 (d, *J* = 12.3 Hz, 2H), 1.94-1.98 (m, 2H), 3.45-4.15 (m, 25H), 4.71-4.77 (m, 4H), 5.17 (tt, *J* = 11.4 and 4.2 Hz, 2H), 5.29 (s, 2H), 5.45 (s, 2H), 6.76-6.82 (m, 5H), 6.98 (d, *J* = 8.0 Hz, 2H), 7.30-7.32 (m, 4H), 7.35 (*br* s, 1H), 7.44 (s, 1H), 7.46 (dd, *J* = 8.4 and 1.2 Hz, 1H), 7.60-7.72

(*br* s, 2H), 8.41 (d, *J* = 6.6 Hz, 2H), 8.42 (d, *J* = 6.6 Hz, 2H), 8.72 (d, *J* = 6.6 Hz, 2H), 8.82 (d, *J* = 6.6 Hz, 2H).

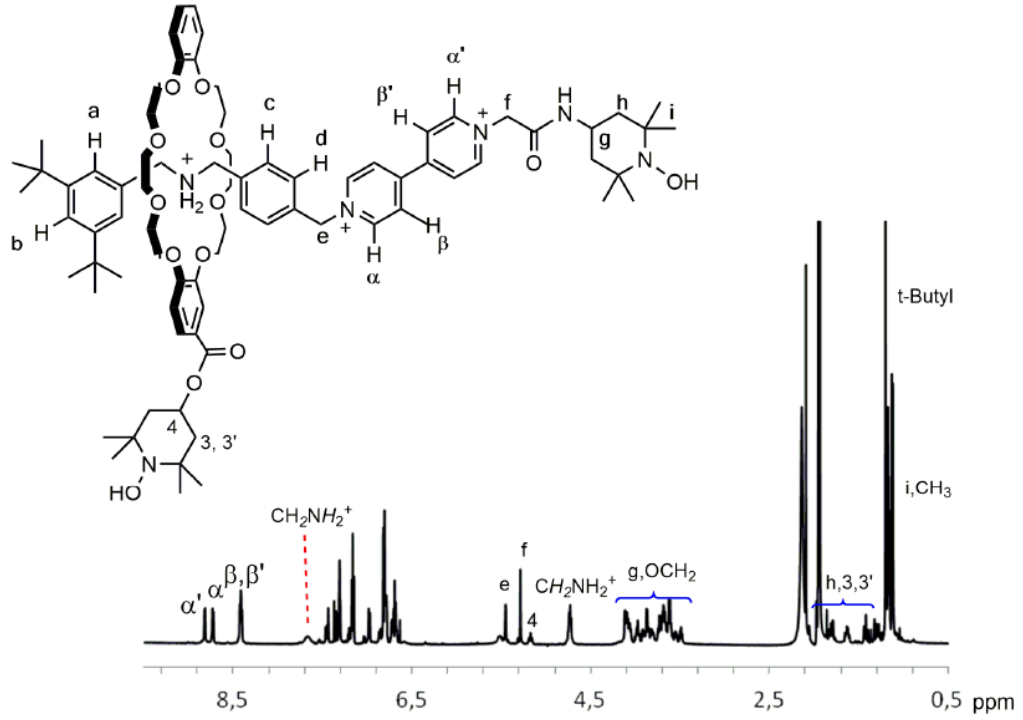

Figure 7. *^{1}H NMR spectrum (600 MHz, CD_3CN, 298 K) of **R-3**-OH after in situ reduction of **R-3** by using phenylhydrazine.*

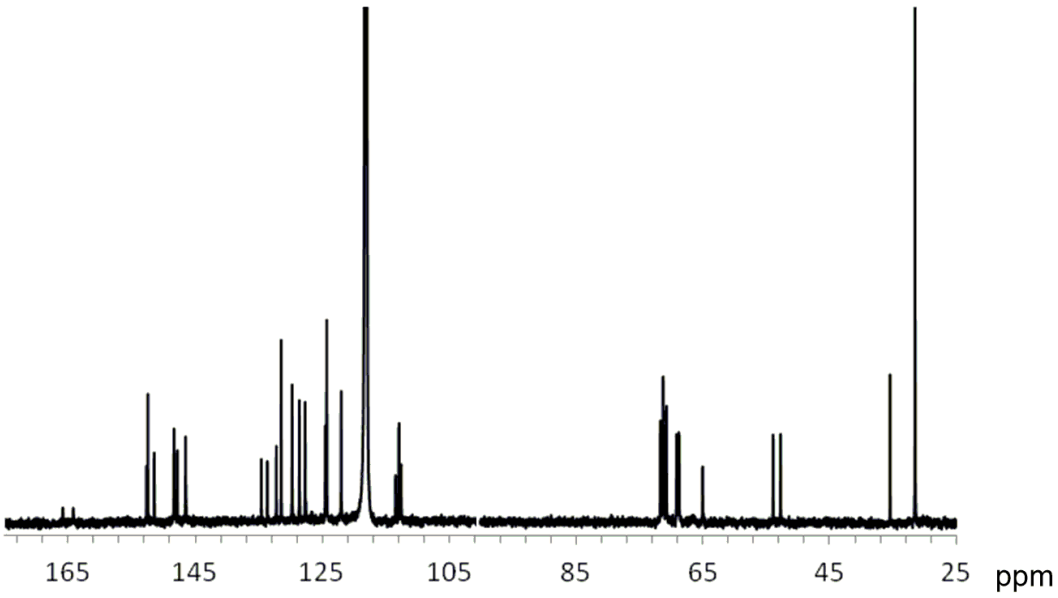

Figure 8. *^{13}C-NMR spectrum (150 MHz, CD_3CN, 298 K) of **R-3**.*

1.4 PULSED EPR spectroscopy[6]

Sample preparation: The bis-labelled samples were dissolved in a mixture of 98% perdeuterated methanol (Sigma Aldrich) and 2% D_2O (Cambridge Isotopes) to reach a final concentration of approximately 80μM. The samples were inserted into a quartz EPR tube (ID = 1.1 mm, OD = 1.6 mm) which were sealed under vacuum after several freeze-thaw cycles.

Pulsed EPR experiments: Pulsed EPR experiments were performed on a Bruker Elexsys E 580 spectrometer equipped with a SuperQ-FT bridge operating at Q-Band (mw frequency 34 GHz). The EN5107D2 probe head was inserted in an Oxford CF935 cryostat and temperature was set to 50K by an Oxford ITC905 temperature controller.

Electron spin-echo experiments were performed using a standard Hahn echo sequence with a nominal length of 40 ns for a π pulse.

A standard four pulse PELDOR sequence was applied to the systems under investigation; the microwave power was adjusted to obtain an observer sequence of 20/40/40 ns and a pump π pulse of 56 ns. τ_1 was set to 200 ns and τ_2 to 2500 ns. The pump pulse was set in correspondence of the maximum of the absorption EPR spectrum of the sample while the frequency offset of the observer sequence was set to -80 MHz. A standard two-step phase cycle was applied for baseline correction while deuterium nuclear modulations were suppressed using a 8 step τ cycle from a starting value of 200 ns and a 16 ns incremental step. PELDOR experiments were performed at a 400 Hz repetition rate for a total time of 4-10 hours of integration of the echo depending on the sample.

PELDOR time traces as obtained from the spectrometer were treated using the *DeerAnalysis2013* routine.[7] Traces were background corrected using an homogeneous background model as implemented in the routine (background dimension = 3); successively a Tikhonov regularization was applied to obtain the distance distribution as presented.

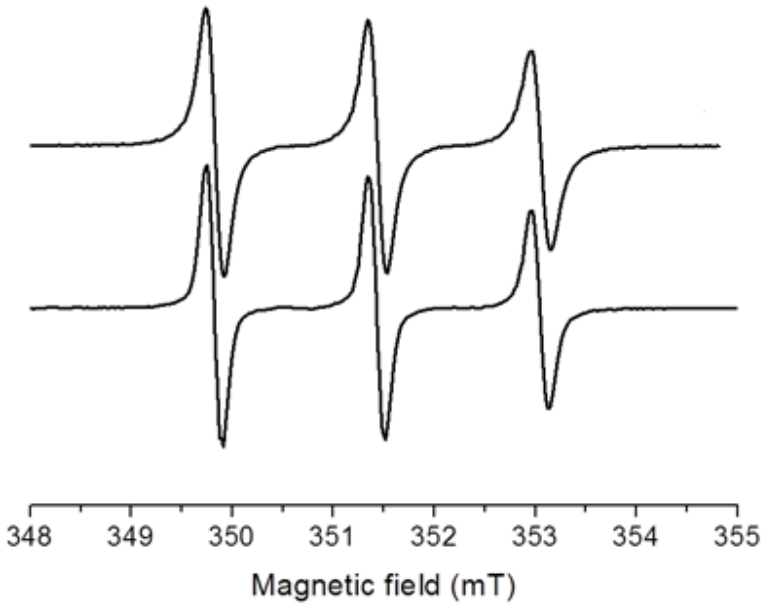

Figure 9. *Room temperature EPR spectra of rotaxane **R-3** (0.15 mm) before (up) and after (bottom) addition of 2 equivalent of DIPEA in MeOH.*

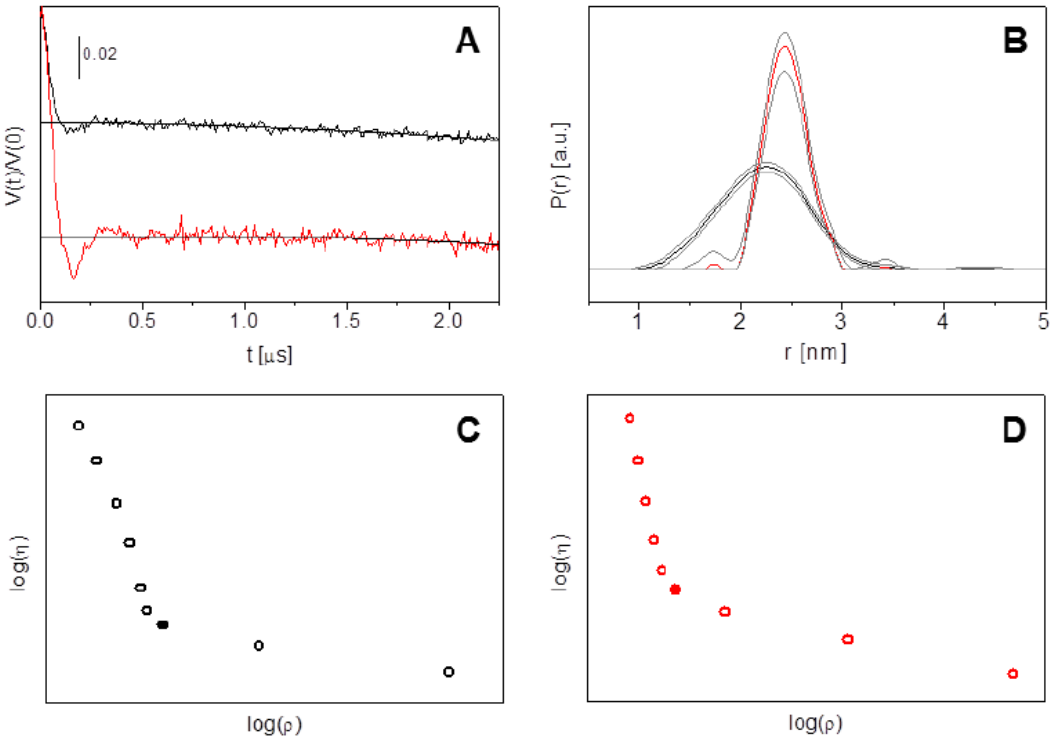

Figure 10. *PELDOR traces before background correction along with intermolecular background fits (A), validated distance distributions and confidence interval (B), L-curves for the Tikhonov regularization analysis (C and D) for **R-3** (black traces and circles) and **R-3** after the addition of the base (red traces and circles). The best fit corresponds to the regularization parameter at the corner of the L-curve (solid circle).*

1.5 Electrochemical measurements[6]

Cyclic voltammetric (CV) experiments were carried out at room temperature in argon-purged acetone (Uvasol) with an Autolab 30 multipurpose instrument interfaced to a PC. The working electrode was a glassy carbon electrode (Amel; 0.07 cm^2); its surface was routinely polished with a 0.3 μm alumina-water slurry on a felt surface. The counter electrode was a Pt wire, separated from the solution by a frit; an Ag wire was employed as a quasireference electrode, and ferrocene (Fc) was present as an internal standard [E1/2(Fc+/Fc) +0.395 vsSCE]. Ferrocene was added from a concentrated acetonitrile solution (typically 0.1 M). The concentration of the compound examined ranged from 3×10^{-4} M to 4×10^{-4} M; tetrabutylammoniumhexafluorophosphate 0.04 M was added as supporting electrolyte. P1-t-Bu was added in the electrochemical cell from a concentrated acetonitrile solution (4 mM). Cyclic voltammograms were obtained at sweep rates varying from 0.05 to 1 Vs^{-1}. Every effort was made throughout the experiments to minimize the resistance of the solution. In any instance, the full electrochemical reversibility of the voltammetric wave of ferrocene was taken as an indicator of the absence of uncompensated resistance effects. The experimental error on the potential values was estimated to be ±5 mV.

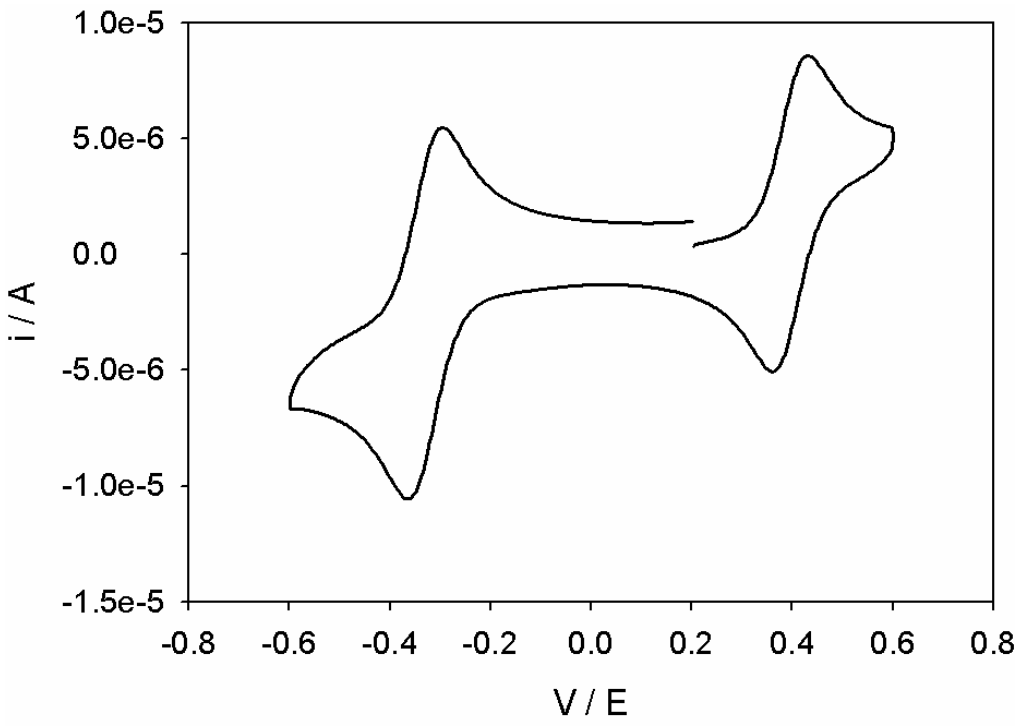

Figure 11. *Cyclic voltammetric pattern of rotaxane **R-3**. Scan rate 200mV/s.*

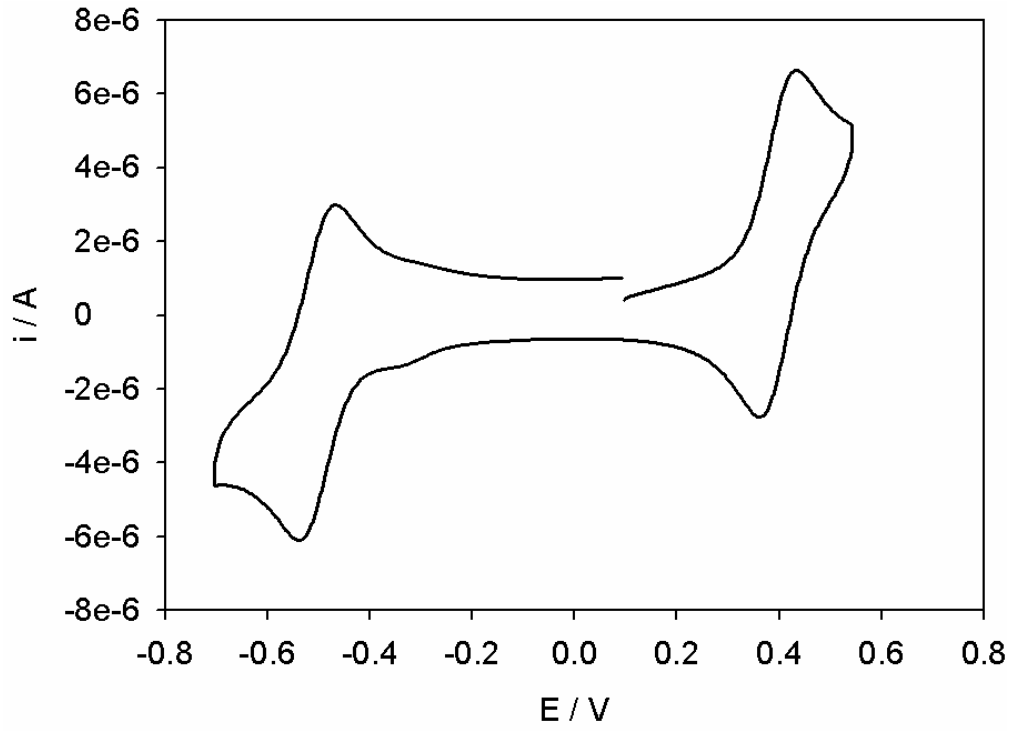

Figure 12. *Cyclic voltammetric pattern of the rotaxane **R-3** upon addition of 1eq.of phosphazene base. Scan rate 200mV/s.*

1.6 Dynamic simulations[6]

Stochastic Dynamic (SD) simulations were carried out with the Macro-Model 7.0 program. The N-O bond was modelled by the C=O bond owing to their similar geometries. Extended non-bonded cut off distances were set to 7 and 12 Å for the van der Waals and electrostatic interactions, respectively. Calculations were performed in *vacuo*. All C-H lengths were held fixed by means of the SHAKE algorithm. The simulations were run at 298 K with time steps of 1.5 fs and an equilibrium time of 2000 ps before each dynamic run. The total simulation time was set to 20000 ps.

2 Experimental section of Chapter 3

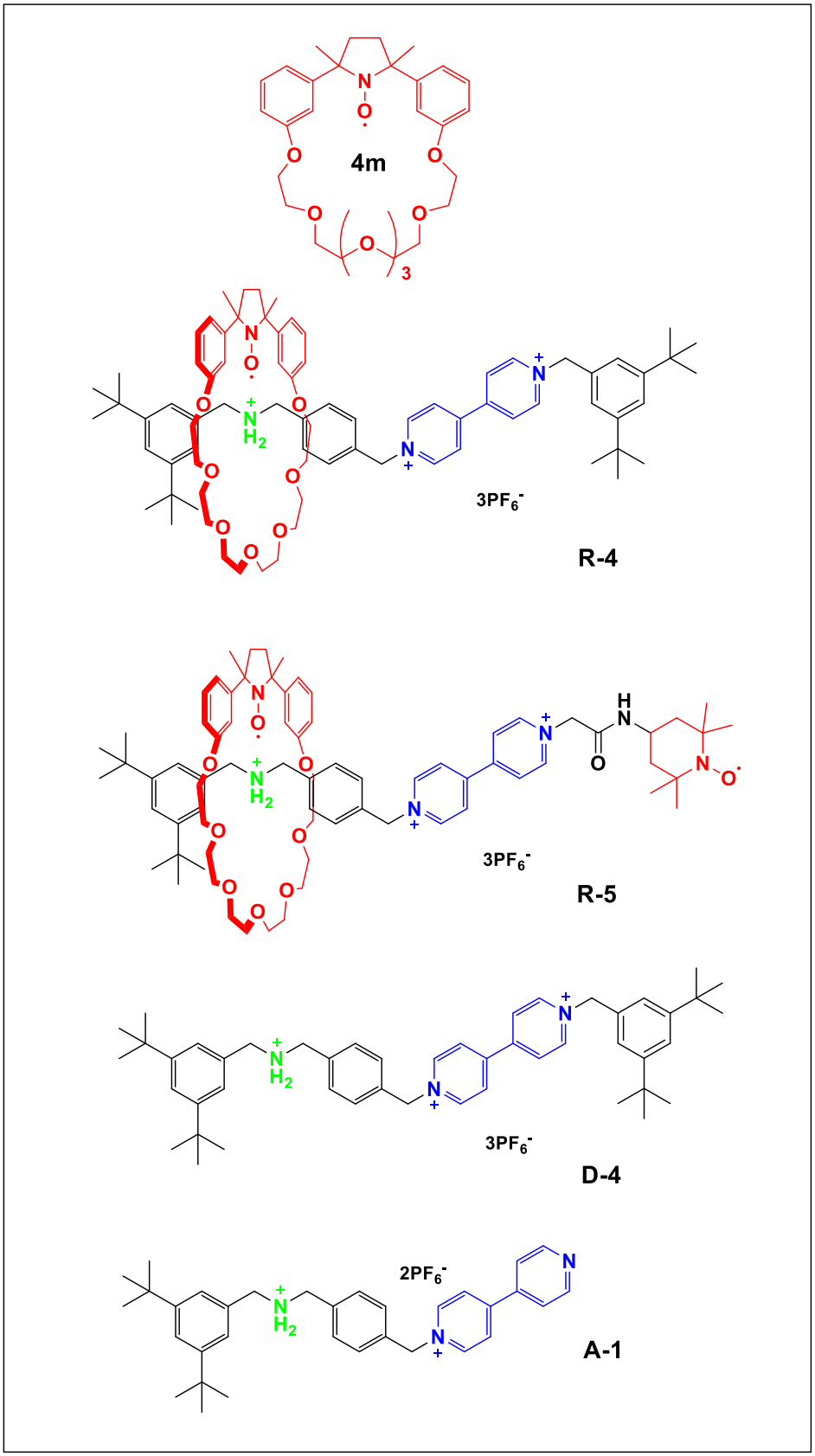

Scheme 2

Compound **A-1**[1] and **D-4**[4] were prepared according to literature.

Compound **4m** was prepared by a modified synthetic protocol based on the procedure reported in literature. [8]

2.1 Preparation of the rotaxane R-4

- Synthesis of **5-methyl-3, 4-Dihydro-2H-pyrrole 1-oxide 4b**

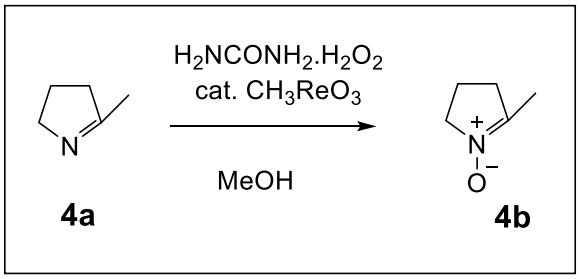

Compound **4b** was prepared following the synthetic procedure reported in literature.[9] To a stirred solution of the imine **4a** (1.5 g, 18 mmol) in MeOH (36 mL), urea hydrogen peroxide (UHP, 5.09 g, 54.13 mmol) and methyltrioxorhenium (MTO, 0.089 g, 0.36 mmol) were added sequentially. The resulting yellow solution was stirred at r.t. until disappearance of the starting material (2 h). After removal of the solvent under reduced pressure, the reaction mixture was added with DCM and the undissolved urea filtered off. Removal of the solvent afforded the crude product which was purified by flash column chromatography on silica gel (SiO_2, h 20 cm, i.d. 40 mm, DCM/MeOH 9:1, Rf=0.4). Fractions containing the product were concentrated in vacuo to give a light yellow oil in 90% yield.

^{1}H NMR (400 MHz, $CDCl_3$): δ 2.01 (s, 3H), 2.07 (m, 2H), 2.72 (m, 2H), 3.98 (m, 2H).

GC-MS: *m/z* 99(100, M), 83 (13, M-OH), 55 (27), 41 (67).

- Synthesis of **2-(3-methoxyphenyl)-2-methylpyrrolidin-1-ol 4d**

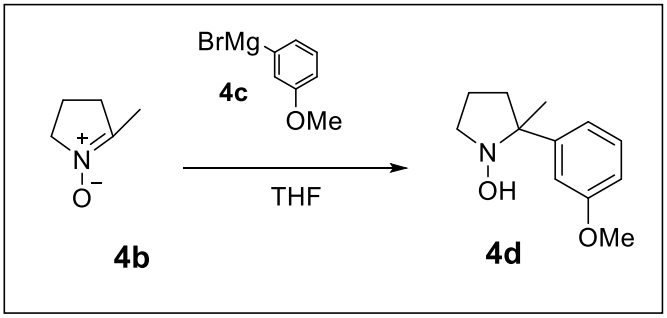

Nitrone **4b** (1 g, 10mmol) dissolved in anhydrous THF (20 mL) was added dropwise at 0 °C over a period of 30 min to a solution of 3-Methoxyphenylmagnesium bromide 1 M in THF **4c** (12 ml). The reaction mixture was stirred for 2 h and after this period was quenched by addition of a saturated solution of NH_4Cl. The aqueous layer was extracted with DCM and then the combined organic extracts were washed with H_2O and brine, dried over $MgSO_4$, filtered, and concentrated under vacuum. The remaining oil was purified by column chromatography eluting with Cy/EtOAc 6:4 (Rf=0.46) to give compound **4d** as an colorless oil in 48 % yield.

^{1}H NMR (400 MHz, $CDCl_3$): δ1.62 (s, 3H), 2.00-2.22 (m, 3H), 2.36-2.48 (m, 1H), 3.33-3.46 (m, 2H), 4.00 (s, 3H), 6.94-6.99 (m, 1H), 7.23-7.29 (m, 2H), 7.41-7.47 (m, 1H).

GC-MS: *m/z* 207 (1, M), 189 (14, M-OH), 176 (100, M-OCH_3), 162, 84.

ESI-MS: *m/z*208.27 $(M+H)^+$.

- Synthesis of**2-(3-methoxyphenyl)-2-methyl-3,4-dihydro-2H-pyrrole 1-oxide 4e**

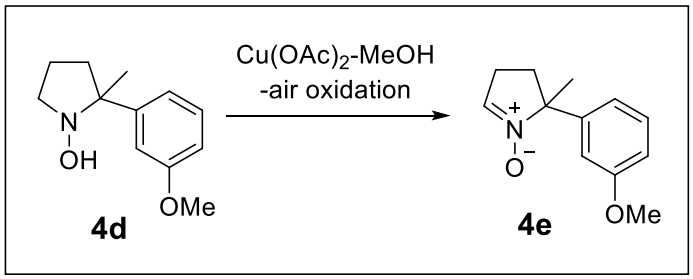

Compound **4d** (0.855 g, 4.12 mmol) was dissolved in MeOH (20 ml) containing concentrated NH_4OH (1.6 ml) and $Cu(OAc)_2$•H_2O (0.029 g, 0.144 mmol) and stirred under air until the pale-yellow solution became dark forest green (2 h). The solution was concentrated and the residue was treated with TCM, the combined organic extracts were washed with satured $NaHCO_3$ solution, brine, dried ($MgSO_4$) and the solvent evaporated. The crude product was chromatographed over silica gel column eluting with EtOAc and then DCM/MeOH 9:1 to obtain compound **4e** as a brown oil in 71 % yield.

^{1}H NMR (400 MHz, $CDCl_3$): δ1.86 (s, 1H), 2.32-2.42 (m, 1H), 2.50-2.74 (m, 3H), 3.81 (s, 3H), 4.10 (*br* s, 1H), 6.83 (dd, *J* = 8.0 and 2.0 Hz, 1H), 6.91-7.00 (m, 2H), 7.28 (t, J=8 Hz, 1H).

ESI-MS: *m/z*206.25 $(M+H)^+$.

- Synthesis of **2,5-bis(3-methoxyphenyl)-2-methyl-3,4-dihydro-2H-pyrrole 1-oxide 4f**

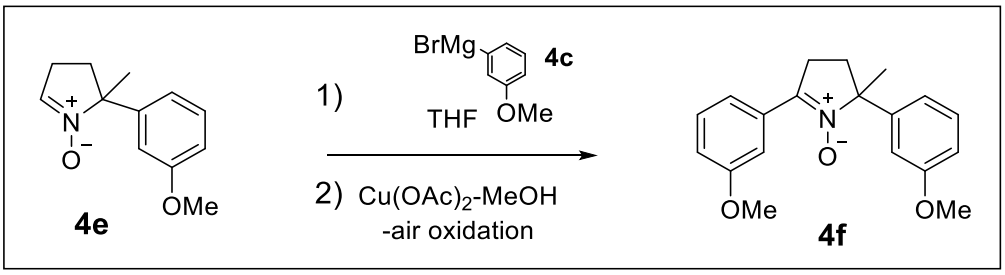

A solution 3-Methoxyphenylmagnesium bromide 1 M in THF(**4c**) (0.64 ml) was treated as above with a solution of nitrone **4e** (0.110, 0.54 mmol) in THF (1 ml) and the usual workup and purification using silica gel column (Cy/EtOAc 6:4, Rf=0.38) followed by the oxidation (see synthesis of compound **4e**) gave **4f** as a turbid oil in 72 % overall yield from **4e**.

^{1}H NMR (400 MHz, $CDCl_3$): δ 1.85 (s, 3H), 2.27-2.37 (m, 1H), 2.46-2.55 (m, 1H), 2.91-3.02 (m, 1H), 3.02-3.13 (m, 1H), 3.76 (s, 1H), 3.85 (s, 1H), 6.78-6.84 (m, 1H), 6.86-6.92 (m, 2H), 6.97- 7.00 (m, 1H), 7.25 (t, *J* = 8.3 Hz, 1H), 7.37 (t, *J* = 8.2 Hz, 1H), 7.74 (d, *J* = 8 Hz,1H), 8.37 (*t, J=2* Hz*,* 1H).

ESI-MS: *m/z*312.438 $(M+H)^+$.

- Synthesis of **2,5-bis(3-hydroxyphenyl)-2-methyl-3,4-dihydro-2H-pyrrole 1-oxide 4g**

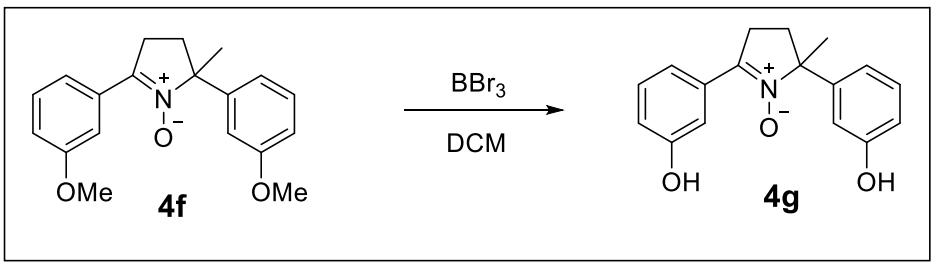

To a stirred solution of **4f** (0.178g, 0.571 mmol) in DCM (6 ml) was added a solution of BBr_3 1M in DCM (1.7 ml). After 5h at 0 °C a mixture of ice and H_2O was added and the resulting mixture was stirred for 30 minutes and then extracted using TCM/*i*PrOH 3:1, dried ($MgSO_4$) and the solvent evaporated. The crude product was purified by using silica gel column (DCM/MeOH 95:5, Rf=0.26) followed by crystallization from TCM-Cy to give **4g** as a white powder in 31 % yield.

^{1}H NMR (400 MHz, $(CD_3)_2SO$): δ 1.73 (s, 3H), 2.23-2.33 (m, 1H), 2.33-2.41 (m, 1H), 2.80-2.91 (m, 1H), 3.01-3.10 (m, 1H), 3.31 (s, 3H), 6.63-6.67 (m, 1H), 6.69 (t, *J*=2 Hz, 1H), 6.73-6.77 (m, 1H), 6.84-6.88 (m, 1H), 7.12 (t, *J*=8, 1H), 7.27 (t, *J*=8, 1H), 7.64-7.67 (m, 1H), 8.11 (t, *J*=1.8, 1H), 9.37 (s, 1H), 9.55 (s, 1H). ESI-MS: *m/z*282.3 $(M-H)^-$.

- Synthesis of macrocycle **4i**

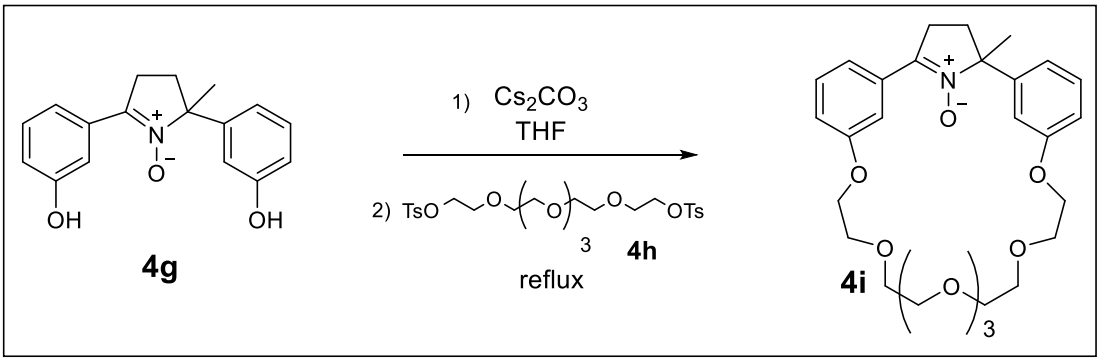

A solution of nitrone **4g** (0.071g, 0.25 mmol) in THF (5 ml) was added to a suspension of Cs_2CO_3 (0.414 g, 1.27 mmol) in THF (13 ml). After 15 minutes the reaction mixture was diluted with THF (50 ml), and a solution of ditosylate **4h** (0.155 g, 0.375 mmol) in THF (50 ml) was added dropwise over 1h while the mixture was refluxed. The resulting mixture was heated at 90 °C for 3h and then 70 °C for 12h. The solvent was evaporated in vacuo, H_2O added and the aqueous layer was extracted with TCM. The extract was washed with H_2O, dried ($MgSO_4$), concentrated and purified by column chromatography eluting with EtOAc to obtain the unreacted products and then with DCM/MeOH 95:5 (Rf=0.27) to give compound **4i** (0.040 g) as colorless oil in 30 % yield.

^{1}H NMR (400 MHz, $(CD_3)_2CO$): δ 1.82 (s, 3H), 2.33-2.47 (m, 1H), 2.55-2.62 (m, 1H), 2.88-2.98 (m, 1H), 3.09-3.18 (m, 1H), 3.47-3.73 (m, 18), 3.83-3.87 (m, 2H), 4.01-4.05 (m, 2H), 4.18-4.22 (m, 2H), 6.83 (ddd, *J*=8, 2.8, 0.8 Hz, 1H), 6.94 (t, *J* =2.2 Hz, 1H), 7.02-7.07 (m, 2H), 7.29 (t, *J*=8 Hz, 1H), 7.37 (t, *J*=8.2 Hz, 1H), 7.64-7.67 (m, 1H), 8.70 (dd, *J*=2.1, 1.6, 1H).

ESI-MS: *m/z*530.445 $(M+H)^+$.

- Synthesis of macrocycle **4l**

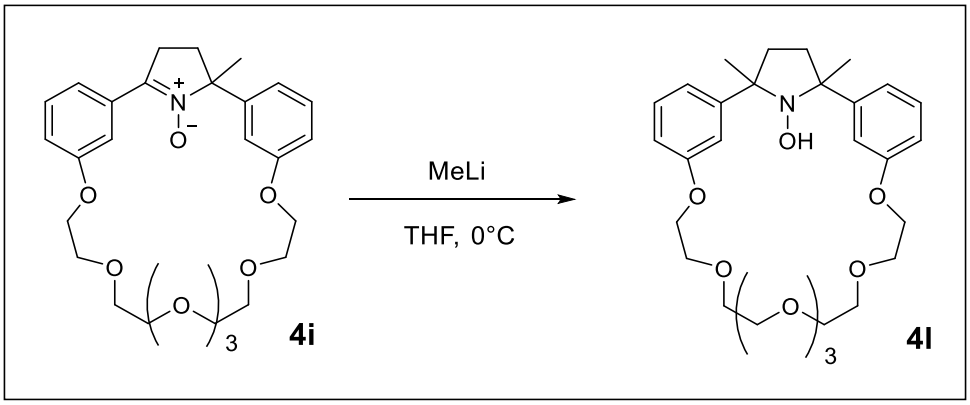

To a stirred solution of nitrone **4i** (0.030 g, 0.056 mmol) in THF (3 ml) at 0 °C was added a solution of MeLi 1.5 M in Et_2O (0.5 ml). After 30 minutes, the reaction was quenched with saturated aqueous NH_4Cl. The aqueous layer was extracted with TCM, dried ($MgSO_4$), concentrated and purified by column chromatography using DCM/MeOH 95:5 to give compound **4l** as light yellow oil in quantitative yield.

^{1}H NMR (400 MHz, $(CD_3)_2CO$): δ 1.63, 1.64 (s, 3H, cis+trans), 1.84-1.98 (m, 2H), 2.04-2.16 (m, 2H), 3.55-3.69 (m, 16H), 3.81-3.88 (m, 4H); 4.12-4.20 (m, 4H), 6.73-6.81 (m, 2H, cis+trans), 6.97, 7.04 (d, *J*=8 Hz, 2H, cis+trans), 7.19, 7.21 (t, *J*=8 Hz, 2H, cis+trans), 7.64, 7.70 (br s, 2H, cis+trans).

ESI-MS: *m/z*546.67 $(M+H)^+$.

- Synthesis of macrocycle **4m**

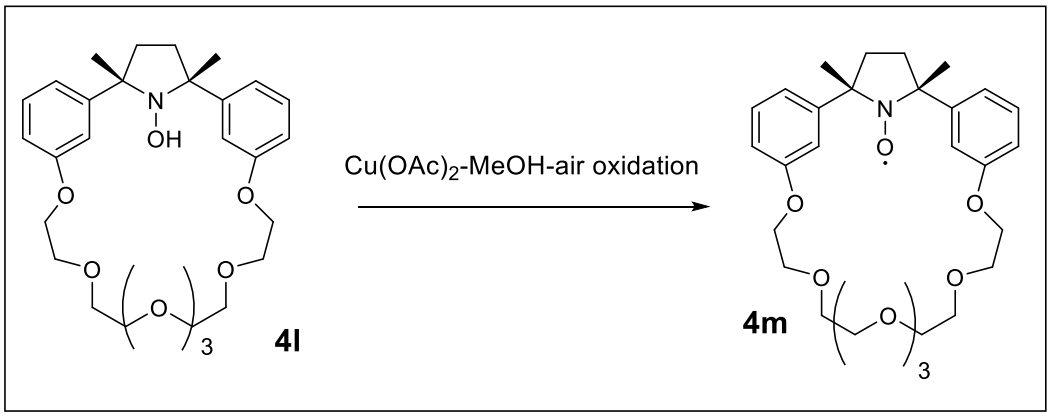

Compound **4l** (0.030 g, 0.055 mmol) was dissolved in MeOH (15ml) containing $Cu(OAc)_2 \bullet H_2O$ and one drop of concentrated NH_4OH and stirred until the pale blue solution became light green (12h). The solution was concentrated and the residue was treated with TCM, the combined organic extracts were washed with satured $NaHCO_3$ solution, brine, dried ($MgSO_4$) and the solvent evaporated. The crude product was chromatographed over silica gel column by using DCM/MeOH 95:5 to obtain compound **4m** (0.029g) as an orange oil in quantitative yield.

ESI-MS: *m/z* 567 $(M+Na)^+$, 545 $(M+H)^+$, 562 $(M+NH_4^+)^+$.

- Synthesis of rotaxane **R-4**

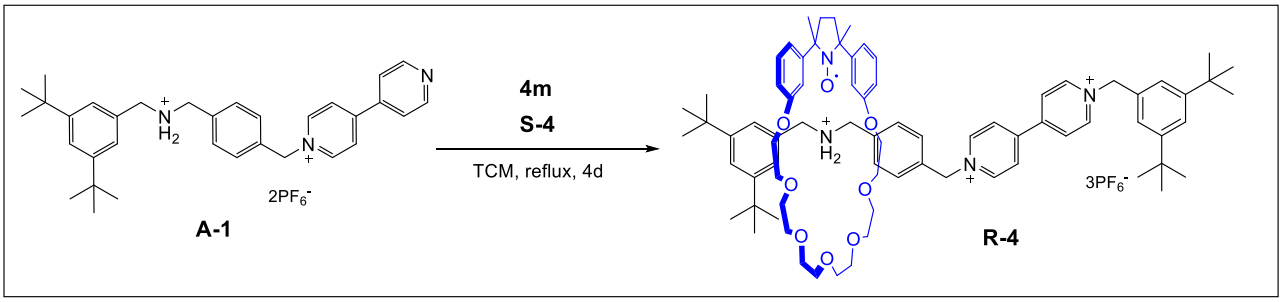

A solution of macrocycle **4m** (0.013 g, 0.024 mmol) in TCM (1 mL) was added to a stirred suspension of compound **A-1** (0.009 g, 0.0117 mmol) in TCM (1 mL) and the mixture was heated under reflux for 30 minutes under nitrogen atmosphere. After this period a solution of 1-(bromomethyl)-3,5-di-tert-butylcyclohexane **S-4** (0.019g, 0.066 mmol) was added and the reaction mixture was stirred under reflux for 4 days. After cooling the solution was concentrated in vacuo and the reaction mixture was purified by silica gel column (h 10 cm, i.d. 25 mm, DCM-MeOH 9:1, then MeOH-NH_4Cl 2M-H_2O 7:0.5:2.5). The fractions containing the product were concentrated in vacuo, dissolved in a minimum volume of H_2O, and treated with NH_4PF_6 aqueous solution. The resulting solid was collected by filtration, washed with H_2O to remove the excess of NH_4PF_6, and dried to afford the rotaxane **R-4** as a beige powder in 20 % yield.

^{1}H NMR (400 MHz, $(CD_3)_2CO$): δ 1.29-1.32 (m, 36H), 4.59-4.64 (m, 2H), 4.67-4.72 (m, 2H), 6.15 (s, 2H), 6.18 (s, 2H), 7.34-7.99 (m, 10H), 8.68-8.90 (m, 4H), 9.35-9.60 (m, 4H).

ESI-MS: *m/z* 1371 $(M\text{-}2PF_6^- + H)^+$.

2.2 Synthesis of rotaxane R-5

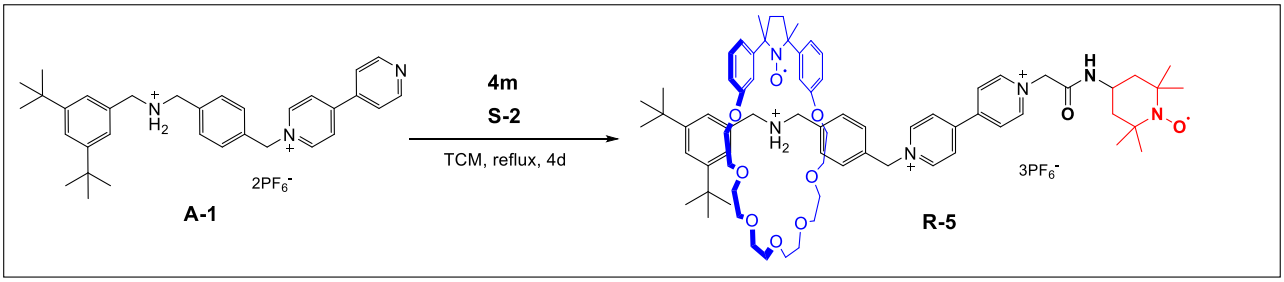

A solution of macrocycle **4m** (0.028 g, 0.051 mmol) in TCM (1.5 mL) was added to a stirred suspension of compound **A-1** (0.016 g, 0.020 mmol) in TCM (1.5 mL) and the mixture was heated under reflux for 30 minutes under nitrogen atmosphere. After this period a solution of 4-(2-iodoacetamido)-TEMPO **S-2** (0.038 g, 0.110 mmol) in TCM (1 mL) was added and the reaction mixture was stirred under reflux for 4 days. After cooling the solution was

concentrated in vacuo and the reaction mixture was purified by silica gel column (h 11 cm, i.d. 2 mm, DCM-MeOH 9:1, then MeOH-NH_4Cl 2M-H_2O 7:0.5:2.5). The fractions containing the product (Rf= 0.7 in MeOH-NH_4Cl 2M-H_2O 7:0.5:2.5) were concentrated in vacuo, dissolved in a minimum volume of H_2O, and treated with NH_4PF_6 aqueous solution. The resulting solid was collected by filtration, washed with water to remove the excess of NH_4PF_6, and dried to afford the rotaxane **R-5** as a beige powder in 30 % yield.

^{1}H NMR (400 MHz, $(CD_3)_2CO$): δ 1.30 (s, 18H), 4.64 (*br* s, 2H), 4.71 (*br* s, 2H), 6.17 (s, 2H), 7.45 (d, *J*=2 Hz, 2H), 7.57 (t, *J*=1.6 Hz, 1H), 7.71-7.80 (m, 4H), 7.95-7.99 (m, 2H), 8.70 (d, *J*=6.8 Hz, 2H), 8.87 (d, *J*=5.6 Hz, 2H), 9.35 (d, *J*=6.8 Hz, 2H).

3 Experimental section of Chapter4

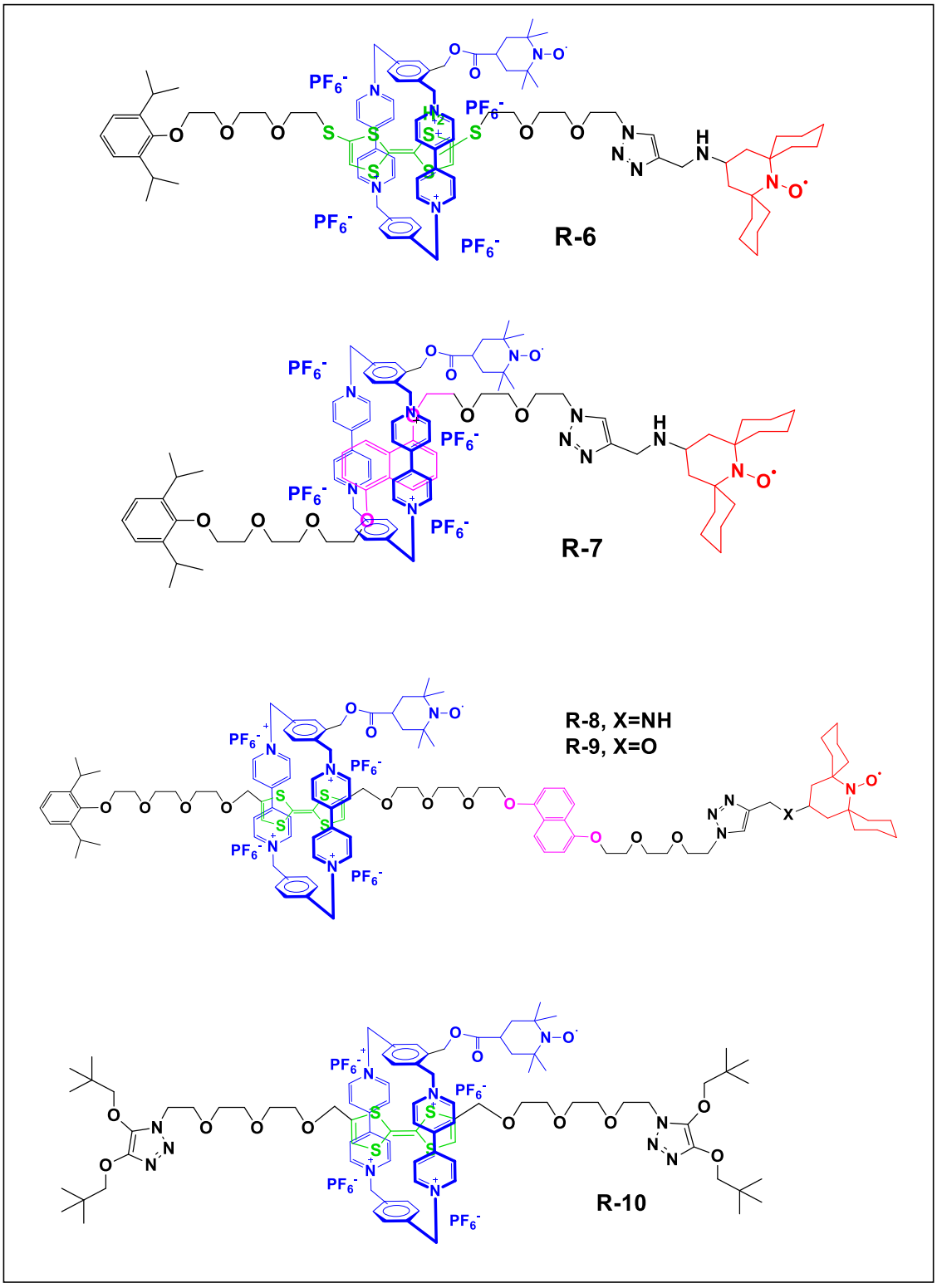

Scheme 3

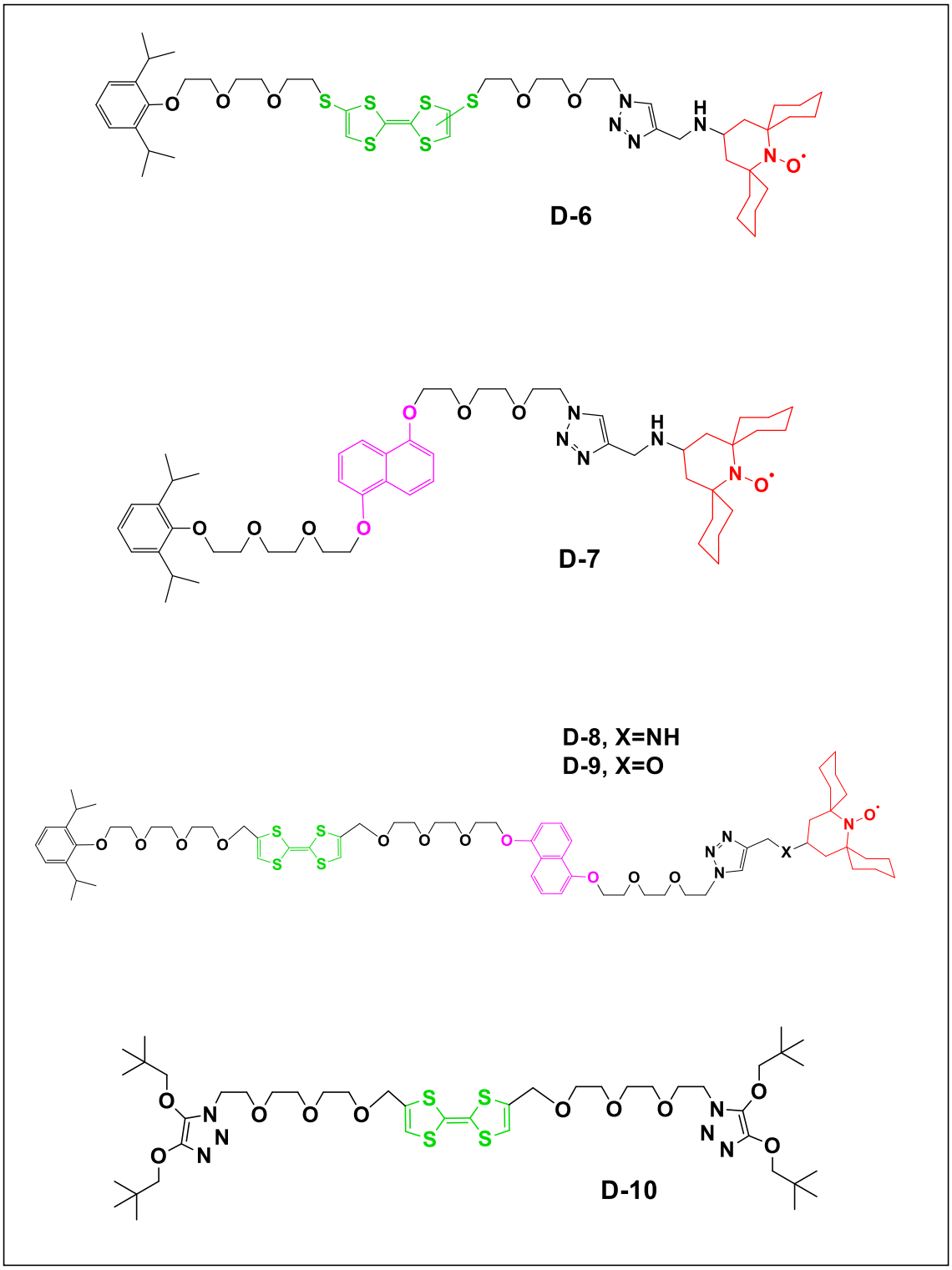

Scheme 4

3.1 Synthesis of rotaxane R-6 and dumbbell D-6

- Synthesis of compound **6b**

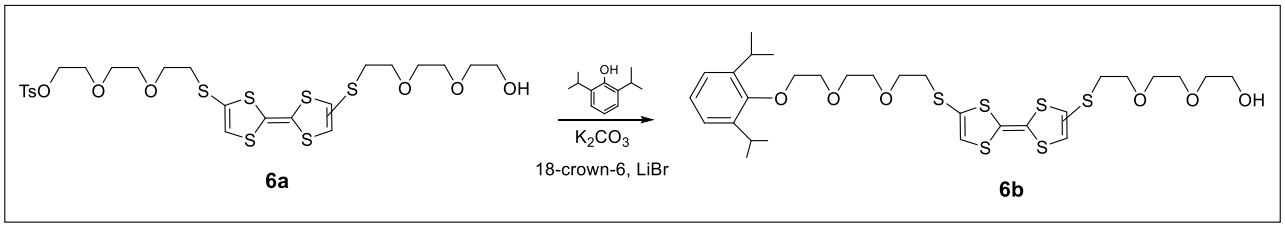

Compound **6b** was prepared following the synthetic procedure reported in ref. [10a]. A solution of compound **6a**[11] (0.04 g, 0.058 mmol), 2,6-diisopropylphenol (0.020 g, 0.116 mmol, 20 μL), K_2CO_3 (0.08 g, 0.58 mmol), 18-crown-6 (0.002 g, catalytic amount), and LiBr (0.0008 g, catalytic amount) in DMF (4.6 mL) was heated under nitrogen atmosphere at 80° C for 48 h. After cooling down to r.t. the reaction mixture was concentrated in vacuo, treated with H_2O, extracted with DCM, dried ($MgSO_4$), and the solvent evaporated. The crude product was chromatographed (SiO_2, Cy/EtOAc 65:35). Fractions containing the product were concentrated in vacuo to give **6b** in 99%.

^{1}H NMR (600 MHz, CD_3CN): δ 1.19 (d, *J* = 7.2 Hz, 12H), 2.68 (t, *J* = 6.0 Hz, 1H), 2.94 (t, *J* = 6.0 Hz, 2H), 2.96 (t, *J* = 6.0 Hz, 2H), 3.39 (septet, *J* = 7.2 Hz, 2H), 3.48 (d, *J* = 4.5 Hz, 2H), 3.55-3.59 (m, 6H), 3.62-3.70 (m, 8H), 3.76-3.79 (m, 2H), 3.85-3.87 (m, 2H), 6.55, 6.56, 6.57 (3 x s, 2H), 7.06-7.13 (m, 3H).

ESI-MS: *m/z* 716.0 $(M+Na)^+$.

- Synthesis of compound **6c**

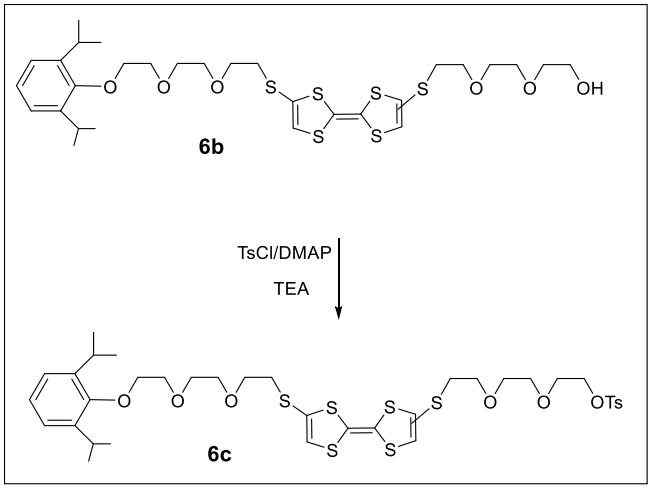

Compound **6c** was prepared following the synthetic procedure reported in ref. [11b]. TsCl (0.024 g, 0.125 mmol) dissolved in anhydrous DCM (1 mL) was added dropwise over a period of 5 min to an ice-cooled solution of **6b** (0.040 g, 0.057 mmol), TEA (0.0127 g, 0.125 mmol, 20 μL) and DMAP (0.008 g, cat.) in anhydrous DCM (2 mL). The reaction mixture was stirred overnight (0°C to rt), whereupon it was washed with satured $NaHCO_3$ solution, brine, dried ($MgSO_4$), and the solvent evaporated. The crude product was chromatographed over silica gel column eluting with Cy/EtOAc 7:3 and then 1:1. The desired product was collected and concentrated to give 0.013 g (27% yield) of **6c**. The yield was not optimized.
^{1}H NMR (600 MHz, CD_3CN): δ 1.18 (d, *J* = 6.6 Hz, 12H), 2.44 (s, 3H), 2.90 (t, *J* = 6.0 Hz, 2H), 2.96 (t, *J* = 6.3 Hz, 2H), 3.39 (septet, *J* = 6.6 Hz, 2H), 3.47 (s, 4H), 3.56-3.69 (m, 10H), 3.76-3.79 (m, 2H), 3.85-3.87 (m, 2H), 4.09-4.12 (m, 2H), 6.51, 6.52, 6.56, 6.57 (4 x s, 2H),7.06-7.13 (m, 3H), 7.43 (d, *J* = 8.0 Hz, 2H), 7.78 (d, *J* = 8.0 Hz, 2H).
ESI-MS: *m/z* 870.5 $(M+Na)^+$.

- Synthesis of axle **A-6**

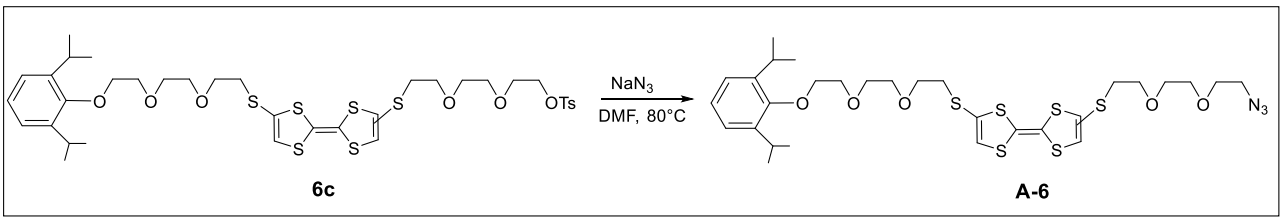

6c **A-6**

Compound **A-6** was prepared following the synthetic procedure reported in ref. [12]. Compound **6c** (0.013 g, 0.015 mmol) and sodium azide (0.005 g, 0.075 mmol) were dissolved in DMF (1 mL) and heated to 80° C for 20 h. After removal of the solvent, in vacuo the crude was partitioned between 10 mL of H_2O and DCM, and the aqueous phase was washed with DCM (3×10 mL). The combined organic extracts were washed with brine, dried ($MgSO_4$), and the solvent evaporated to give 0.011 g (quantitative yield) of **A-6**.
^{1}H NMR (600 MHz, CD_3CN): δ 1.19 (d, *J*=6.6 Hz, 12H), 2.93, 2.94, 2.97, 2.98 (4 x t, *J*=6.3 Hz, 4H), 3.35 (t, *J*=5.1 Hz, 2H), 3.39 (septet, *J*=6.6 Hz, 2H), 3.55-3.59 (m, 4H), 3.61-3.70 (m, 10H), 3.76-3.79 (m, 2H), 3.85-3.87 (m, 2H), 6.53, 6.54, 6.57 (3 x s, 2H), 7.06-7.13 (m, 3H).
ESI-MS: *m/z* 741.5 $(M+Na)^+$.

- Synthesis of rotaxane **R-6** and dumbbell **D-6**.

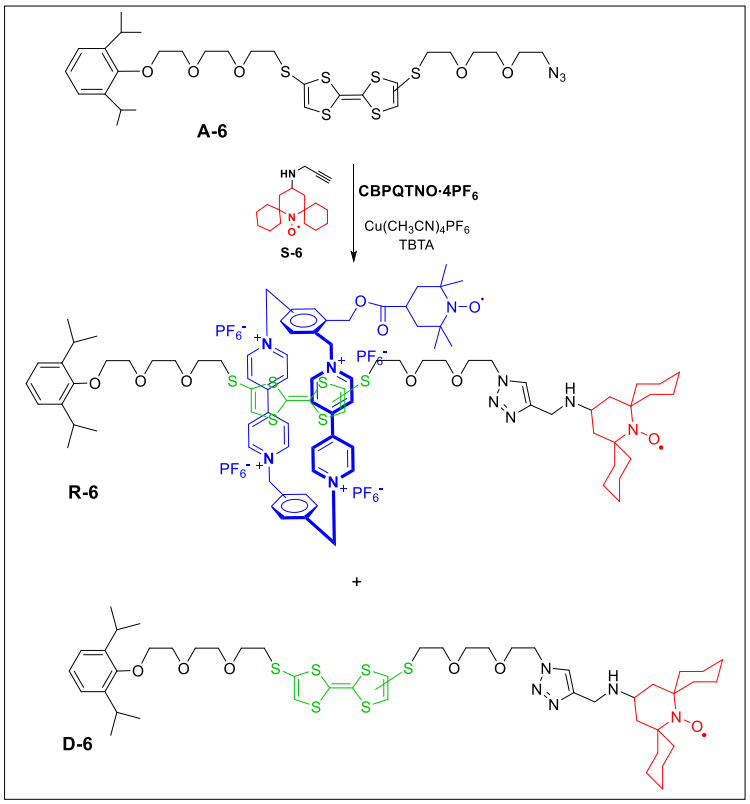

R-6 was prepared following the synthetic procedure reported in ref. [13]. Axle **A-6** (0.014 g, 0.0195 mmol), **CBPQTNO•4PF$_6$**[14] (0.025 g, 0.019 mmol) and stopper **S-6**[13] (0.0056 g, 0.0195mmol) were dissolved in DMF (0.15 mL) at -10 °C under N_2 atmosphere and stirred for 10 min. TBTA (0.001 g, 0.0019 mmol) and $Cu(ACN)_4PF_6$ (0.0007 g, 0.0019 mmol) were added to the solution and the resulting mixture was stirred at r.t. for 48 h, at which time the solvent was evaporated. The crude solid was purified twice by column chromatography (SiO_2: Me_2CO and then 1% w/v NH_4PF_6 solution in Me_2CO, i.d. 15 mm, h 15 cm). The fraction in 1% w/v NH_4PF_6 solution in Me_2CO were collected and concentrated to a minimum volume, and rotaxane **R-6** was precipitated from this solution through the addition of an excess of cold H_2O. The resulting solid was collected by filtration, washed with H_2O to remove the excess of NH_4PF_6, and dried by vacuum pump to afford the desired rotaxane as a green powder (0.010 g, 22% yield). The yield was not optimized.

The fractions in Me_2CO containing the dumbbell **D-6** were collected, concentrated and again purified on silica gel column eluting withMe_2CO:Cy:EtOAc 1:0.5:0.5 to give **D-6** (yield non calculated).

Dumbbell **D-6**: ^{1}H NMR (600 MHz, CD_3COCD_3): δ1.20 (d, *J*=6.6 Hz, 12H), 3.00-3.14 (m, 4H), 3.45 (septet, *J*=6.6 Hz, 2H), 3.56-3.98 (m, 18H), 4.68-4.73 (m, 2H), 6.74-6.78 (m), 7.03-7.14 (m, 3H).

ESI-MS: *m/z* 1006.8 $(M+H)^+$.

Rotaxane **R-6**: ^{1}H NMR (600 MHz, CD_3COCD_3): δ1.18 (d, *J*=6.6 Hz, 12H), 3.20-3.32 (m, 4H),3.40 (septet, *J*=6.6 Hz, 2H), 3.58-4.04 (m, 18H), 4.60-4.70 (m, 2H), 5.68 (*br* s, 2H), 6.07-6.40 (m, 10H), 7.05-7.13 (m, 3H), 7.97-8.20 (m, 9H), 8.47-8.61 (m, 8H), 9.40-9.65 (m, 8H).

ESI-MS: *m/z* 2446.1$(M-PF_6)^+$, 2300.1$(M-2PF_6)^+$.

3.2 Synthesis of dumbbell D-7 and rotaxane R-7

- Synthesis of dumbbell **D-7**

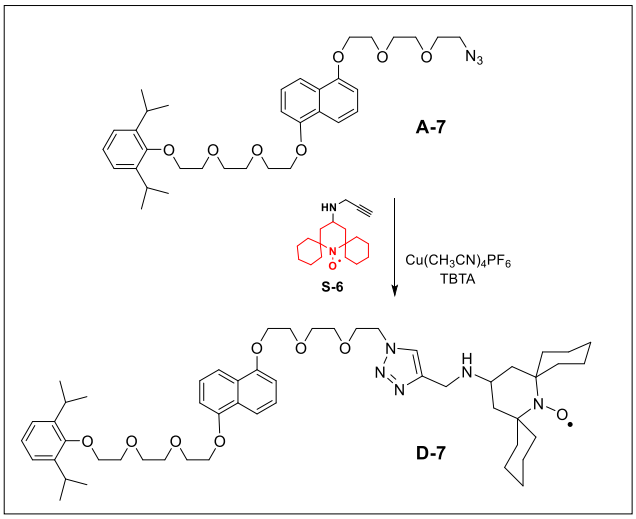

Axle **A-7**[15] (0.0205 g, 0.0336 mmol), and stopper **S-6**[13] (0.0117 g, 0.041 mmol) were dissolved in DMF (0.2 mL) under N_2 atmosphere. TBTA (0.0025 g, 0.0047 mmol) and $Cu(ACN)_4PF_6$ (0.0025 g, 0.0067 mmol) were added to the solution and the resulting mixture was stirred at r.t. for 72 h, at which time the solvent was evaporated. The crude solid was purified by column chromatography (SiO_2, i.d. 15 mm, h 20 cm). The fractions in Me_2CO containing the dumbbell **D-7** were collected and concentrated (0.020 g, 66% yield).

Dumbbell **D-7**: ^{1}H NMR (600 MHz, CD_3CN): δ1.16 (d, *J* = 6.6 Hz, 12H), 3.39 (septet, *J* = 6.6 Hz, 2H), 3.59-4.00 (m, 20H), 4.24-4.31 (m, 4H), 4.48-4.52 (m, 2H), 6.93-6.97 (m, 2H), 7.05-7.13 (m, 3H), 7.33-7.40 (m, 2H), 7.76-7.83 (m, 2H), 8.00 (*br* s, 1H).

ESI-MS: *m/z* 899.5 $(M+H)^+$.

- Synthesis of dumbbell **R-7**

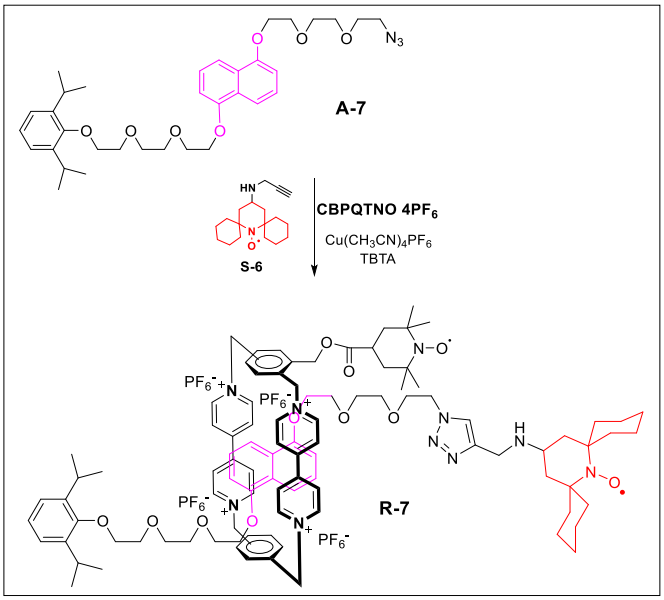

R-7 was prepared following the synthetic procedure reported in ref. [13]. Axle **A-7**[15] (0.020 g, 0.0328mmol), **CBPQTNO•4PF$_6$**[14] (0.040 g, 0.0305 mmol) and stopper **S-6**[13] (0.009 g, 0.031 mmol) were dissolved in DMF (0.15 mL) at -10 °C under N_2 atmosphere. TBTA (0.0022 g, 0.004 mmol) and $Cu(CH_3CN)_4PF_6$ (0.002 g, 0.0054 mmol) were added to the solution and the resulting mixture was stirred at r.t. for 72 h, at which time the solvent was evaporated. The crude solid was purified by column chromatography (SiO_2: Me_2CO and then 1% w/v NH_4PF_6 solution in Me_2CO, i.d. 15 mm, h 17 cm). The fractions in Me_2CO containing the dumbbell **D-7** were collected and concentrated. The fraction in 1% w/v NH_4PF_6 solution in Me_2CO were collected and concentrated to a minimum volume, and rotaxane **R-7** was precipitated from this solution through the addition of an excess of cold H_2O. The resulting solid was collected by filtration, washed with H_2O to remove the excess of NH_4PF_6, and dried by vacuum pump to afford the desired rotaxane as a purple powder (0.019 g, 26% yield). The yield was not optimized.

Rotaxane **R-7**: ^{1}H NMR (600 MHz, CD_3CN): δ1.10 (d, *J* = 6.6 Hz, 12H), 2.40-2.55 (m, 2H), 3.24-3.31 (m, 2H), 3.76-4.58 (m, 26H), 5.50-6.04 (m, 12H), 6.20-6.33 (m, 2H), 7.04-7.12 (m, 3H), 7.15-7.48 (m, 8H), 7.88-8.22 (m, 8H), 8.50-9.17 (m, 8H).

ESI-MS: *m/z* 2212.4 $(M+H)^+$.

3.3 Synthesis of rotaxane R-8 and dumbbell D-8

- Synthesis of compound **8b**

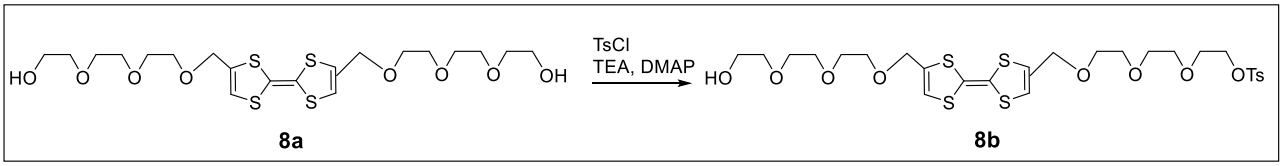

Compound **8b** was prepared following the synthetic procedure reported in ref. [11b]. TsCl (0.034 g, 0.18mmol) dissolved in anhydrous DCM (1.5 mL) was added dropwise over a period of 5 min to an ice-cooled solution of **8a**[16,17] (0.107 g, 0.2mmol), TEA (0.045 g, 0.44mmol, 62 μL) and DMAP (0.008 g, cat.) in anhydrous DCM (1 mL). The reaction mixture was stirred overnight (0°C to r.t.), whereupon it was washed with satured $NaHCO_3$ solution, brine, dried ($MgSO_4$), and the solvent evaporated. The crude product was chromatographed over silica gel column (h 11.5 cm, i.d. 20 mm) eluting with EtOAc. The second band containing the desired product was collected and concentrated to give 0.059 g of compound **8b** (43 % yield).

^{1}H NMR (400 MHz, CD_3CN): δ 2.44 (s, 3H), 2.70 (t, *J*=6.0 Hz, 1H), 3.47-3.58 (m, 20H), 3.58-3.62 (m, 2H), 4.10-4.13 (m, 2H), 4.22-4.33 (m, 4H), 6.39 (*br* s, 2H), 7.41-7.45 (m, 2H), 7.76-7.80 (m, 2H). ESI-MS: *m/z* 705.8 $(M+Na)^+$.

- Synthesis of compound **8c**

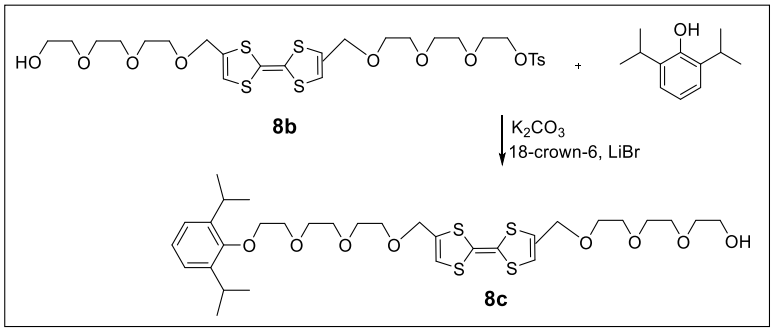

Compound **8c** was prepared following the synthetic procedure reported in ref. [10a]. A solution of compound **8b** (0.06 g, 0.092 mmol), 2,6-diisopropylphenol (0.033 g, 0.183 mmol, 34 μL), K_2CO_3(0.127 g, 0.92 mmol), 18-crown-6 (0.002 g, catalytic amount), and LiBr (0.0008 g, catalytic amount) in DMF (7 mL) was heated under nitrogen atmosphere at 80° C for 48 h. After cooling down to r. t., the reaction mixture was concentrated in vacuo, treated with H_2O, extracted with DCM, dried ($MgSO_4$), and the solvent evaporated. The crude product was chromatographed (SiO_2, h 9 cm, i.d. 25 mm, Cy/EtOAc 35:65 until 20:80). Fractions containing the product were concentrated in vacuo to give **8c** in 71% yield. The yield was not optimized.

^{1}H NMR (400 MHz, CD_3CN): δ 1.19 (d, *J*=7.2 Hz, 12H), 2.70 (t, *J*=6.0 Hz, 1H), 3.39 (septet, *J*=7.2 Hz, 2H), 3.47-3.50 (m, 2H), 3.55-3.68 (m, 18H), 3.76-3.80 (m, 2H), 3.84-3.88 (m, 2H), 4.26 (t, *J*=1.6 Hz, 2H), 4.28 (t, *J*=1.2 Hz, 2H), 6.37, 6.39 (2 x t, *J*=1.2 Hz, 2H), 7.05-7.14 (m, 3H).
ESI-MS: *m/z* 688.1 $(M+H)^+$, 711.2 $(M+Na)^+$, 727.1 $(M+K)^+$.

- Synthesis of compound **8d**

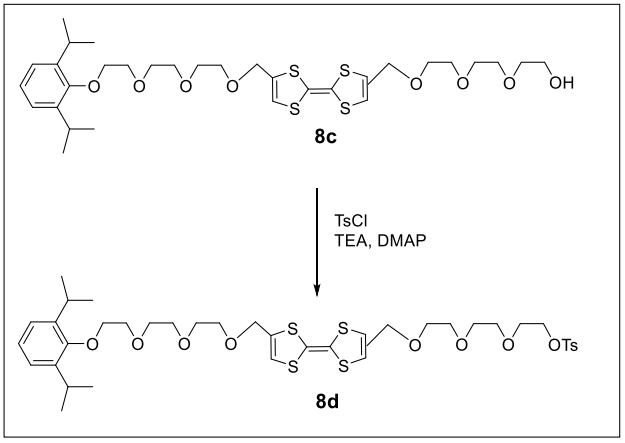

Compound **8d** was prepared following the synthetic procedure reported in ref. [11b]. TsCl (0.053 g, 0.279mmol) dissolved in anhydrous DCM (1.5 mL) was added dropwise over a period of 5 min to an ice-cooled solution of **8c** (0.064 g, 0.093mmol), TEA (0.037 g, 0.37mmol, 52 μL) and DMAP (0.002 g, 0.019 mmol) in anhydrous DCM (1 mL). The reaction mixture was stirred for 24 h (0°C to r.t.), whereupon it was washed with satured $NaHCO_3$ solution, brine, dried ($MgSO_4$), and the solvent evaporated. The crude product was chromatographed over silica gel column eluting with Cy/EtOAc 7:3. The desired product was collected and concentrated to give 0.063 g of compound **8d** (80% yield).
^{1}H NMR (400 MHz, CD_3CN): δ 1.18 (d, *J*=6.8 Hz, 12H), 2.44 (s, 3H), 3.39 (septet, *J*=6.8 Hz, 2H), 3.48 (d, *J*=1.6 Hz, 4H), 3.53 (d, *J*=1.6 Hz, 4H), 3.55-3.68 (m, 10H), 3.76-3.79 (m, 2H), 3.85-3.88 (m, 2H), 4.09-4.12 (m, 2H), 4.25 (t, *J*=1.2 Hz, 2H), 4.28 (d, *J*=1.0 Hz, 2H), 6.35, 6.37, 6.39, 6.42 (4 x t, *J*=1.2 Hz, 2H), 7.05-7.14 (m, 3H), 7.41-7.45 (m, 2H), 7.76-7.80 (m, 2H).
ESI-MS: *m/z* 866.1 $(M+Na)^+$.

- Synthesis of 2-(2-(2-(2-iodoethoxy)ethoxy)ethoxy)tetrahydro-2H-pyran **8e**

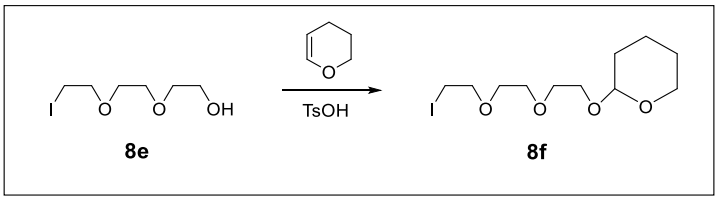

Compound **8f** was prepared following the synthetic procedure reported in ref. [18a, b]. To an ice-cold (0 °C) solution of 2-(2-(2-iodoethoxy) ethoxy) ethan-1-ol[19] **8e** (3 g, 11.53 mmol) and 2,3-dihydro-2*H*-pyran (1.06 g, 1.16 mL, 12.69 mmol) in DCM (150 mL) was added *p*-toluenesulfonic acid monohydrate (0.44 g, 2.31 mmol). The mixture was stirred for 10 min and then warmed gradually to r.t. and stirred overnight. Distilled H_2O was then added to the mixture and the solution extracted with DCM. The combined organic extracts were washed with H_2O and brine, dried over $MgSO_4$, filtered, and concentrated under vacuum. The remaining oil was purified by column chromatographyeluting with Cy/EtOAc 8:2. The desired product was collected and concentrated to give 2 g of compound **8f** (51% yield). The yield was not optimized.

^{1}H NMR (400 MHz, CD_3CN): δ 1.44-1.57 (m, 4H), 1.62-1.71 (m, 1H), 1.72-1.82 (m, 1H), 3.30 (t, *J*=6.4 Hz, 2H), 3.42-3.49 (m, 1H), 3.49-3.54 (m, 1H), 3.57-3.61 (m, 6H), 3.71 (t, *J*=6.4 Hz, 2H), 3.74-3.85 (m, 2H), 4.56-4.60 (m, 1H).

ESI-MS: *m/z* 367.1 $(M+Na)^+$.

- Synthesis of compound **8h**

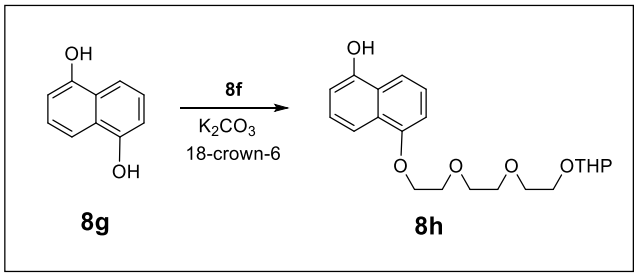

To a stirred suspension of 1,5-dihydroxynaphthalene (**8g**) (0.2 g, 1.25 mmol), K_2CO_3 (0.48 g, 3.5 mmol), and 18-crown-6 (catalytic amount) in anhydrous ACN (30 mL) a solution of compound **8f** (0.43 g, 1.25 mmol) in ACN (8 mL) was added dropwise and the mixture stirred under reflux for 6 h. After cooling down to r.t., the reaction mixture was filtered and the organic filtrate was concentrated. The residue was subjected to column chromatography (SiO_2, h 18 cm, i.d. 20 mm, Cy/EtOAc 1:1). The third spot resulted compound **8h** (0.08 g, 17%). The yield was not optimized.

^{1}H NMR (400 MHz, CD_3CN): δ 1.42-1.53 (m, 4H), 1.58-1.67 (m, 1H), 1.68-1.79 (m, 1H), 3.38-3.45 (m, 1H), 3.46-3.53 (m, 1H), 3.56-3.64 (m, 4H), 3.69-3.82 (m, 4H), 3.91-3.95 (m, 2H), 4.24-4.29 (m, 2H), 4.53-4.56 (m, 1H), 6.90 (d, *J*=7.8 Hz, 1H), 6.92 (d, *J*=8.0 Hz, 1H), 7.30 (t, *J*=8.0 Hz, 1H), 7.36 (t, *J*=7.8 Hz, 1H), 7.45 (s, 1H), 7.72 (d, *J*=8.0 Hz, 1H), 7.74 (d, *J*=7.8 Hz, 1H).
ESI-MS: *m/z* 399.1 $(M+Na)^+$.

- Synthesis of compound **8i**

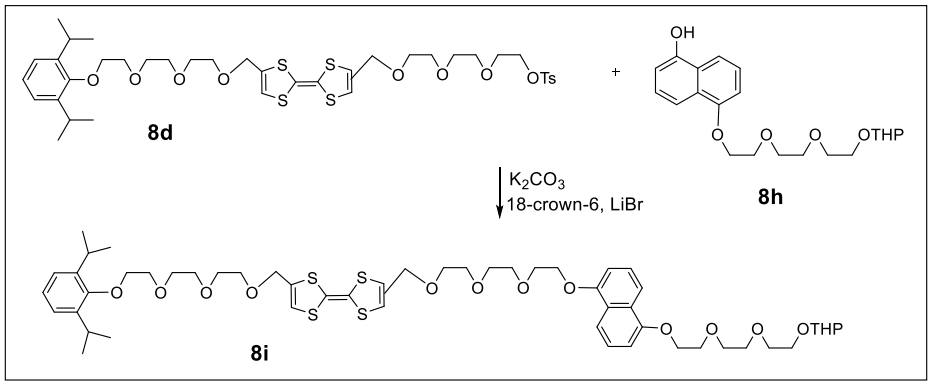

Compound **8i** was prepared following the synthetic procedure reported in ref. [20]. A solution of **8d** (0.015 g, 0.018 mmol), 5-monosubstituted-1-hydroxynaphtalene **8h** (0.007 g, 0.018 mmol), K_2CO_3 (0.01 g, 0.072 mmol), 18-crown-6 (0.001 g, catalytic amount), and LiBr (0.001 g, catalytic amount) in ACN (3 mL) was heated under nitrogen atmosphere at reflux for 48 h. After cooling down to r.t., the reaction mixture was filtered and the solid was washed with ACN (10 mL) and the combined organic filtrate was concentrated in vacuo. The residue was dissolved in DCM (20 mL), washed with brine (2×10 mL), dried ($MgSO_4$), and the solvent evaporated. The crude product was chromatographed (SiO_2, h 10 cm, i.d. 10 mm Cy/EtOAc 1:1) to give 0.018 g of **8i** (quantitative yield) as a yellow-green oil.
^{1}H NMR (400 MHz, CD_3CN): δ1.18 (d, *J*=6.8 Hz, 12H),1.41-1.52 (m, 4H), 1.58-1.67 (m, 1H), 1.68-1.78 (m, 1H), 3.32-3.44 (m, 4H), 3.46-3.80 (m, 28H), 3.83-3.87 (m, 2H), 3.91-3.95 (m, 4H), 4.25-4.29 (m, 4H), 4.53-4.56 (m, 1H), 6.30, 6.32, 6.34, 6.38 (4 x t, *J*=1.2 Hz, 2H), 6.94 (d, *J*=8.0 Hz, 2H), 7.04-7.13 (m, 3H), 7.38 (t, *J*=8.0 Hz, 2H), 7.80 (d, *J*=8.0 Hz, 2H).
ESI-MS: *m/z* 1069.5 $(M+Na)^+$.

- Synthesis of compound **8l**

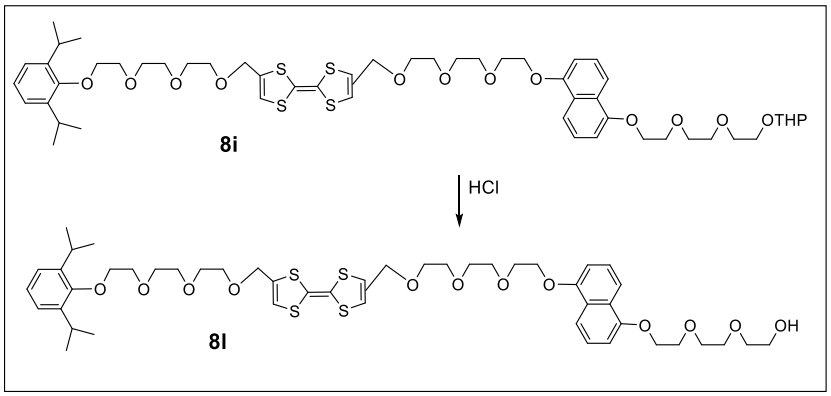

Compound **8l** was prepared following the synthetic procedure reported in ref. [11b, 20]. To a solution of **8i** (0.046 g, 0.043 mmol) in DCM (5 mL) a solution of HCl 12 M (1 mL) was added and the reaction mixture was stirred for 5 h at r.t. A solution of NaOH 1M was then added until neutral pH the reaction mixture was extracted with DCM, the combined organic extracts washed with brine, dried over $MgSO_4$ and concentrated under vacuum. The crude light yellow oil was purified by column chromatographyeluting with Cy/EtOAc 55:45. The desired product was collected and concentrated to give 0.023 g of compound **8l** (55% yield). The yield was not optimized.

^{1}H NMR (400 MHz, CD_3CN): δ1.18 (d, *J*=6.8 Hz, 12H), 3.32-3.44 (m, 4H), 3.46-3.80 (m, 26H), 3.83-3.87 (m, 2H), 3.91-3.95 (m, 4H), 4.25-4.29 (m, 4H), 6.35 (s, 2H), 6.94 (d, *J*=8.0 Hz, 2H), 7.04-7.13 (m, 3H), 7.38 (t, *J*=8.0 Hz, 2H), 7.80 (d, *J*=8.0 Hz, 2H).

ESI-MS: *m/z* 986.3 $(M+Na)^+$.

- Synthesis of compound **8m**

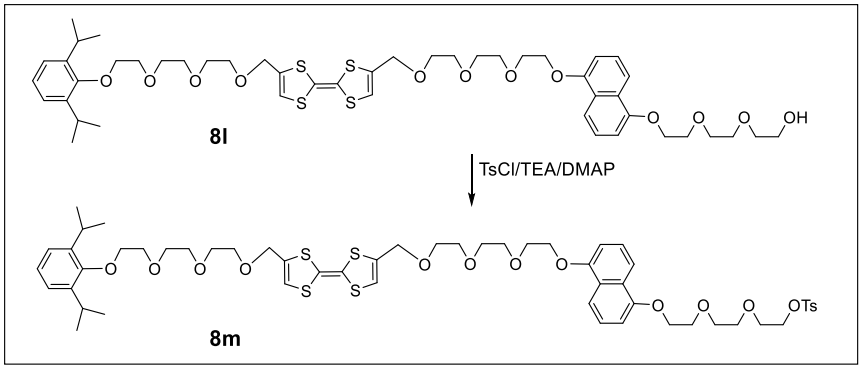

Compound **8m** was prepared following the synthetic procedure reported in ref. [11b]. TsCl (0.014 g, 0.072 mmol) dissolved in anhydrous DCM (1 mL) was added dropwise over a period of 5 min to an ice-cooled solution of **8l** (0.023 g, 0.024 mmol), TEA (0.01 g, 0.095 mmol, 15 μL) and DMAP (0.008 g, cat.) in anhydrous DCM (1 mL). The reaction mixture

was stirred overnight (0°C to r.t.), whereupon it was washed with satured $NaHCO_3$ solution, brine, dried ($MgSO_4$), and the solvent evaporated. The crude product was chromatographed over silica gel column (h 10 cm, i.d. 10 mm) eluting with Cy/EtOAc 1:1. The first band containing the desired product was collected and concentrated to give 0.013 g of compound **8m** (48 % yield). The yield was not optimized.

^{1}H NMR (400 MHz, CD_3CN): δ1.18 (2 x d, *J*=6.8 Hz, 12H), 2.38 (s, 3H), 3.38 (2 x septet *J*=6.8 Hz, 2H), 3.50-3.67 (m, 20H), 3.69-3.73 (m, 2H), 3.74-3.78 (m, 2H), 3.83-3.95 (m, 6H), 4.06-4.09 (m, 4H), 4.20-4.29 (m, 6H), 6.30, 6.31, 6.33, 6.37 (4 x t, *J*=1.2 Hz, 2H) , 6.93 (d, *J*=7.6 Hz, 1H), 6.94 (d, *J*=7.6 Hz, 1H), 7.04-7.13 (m, 3H), 7.34-7.41 (m, 4H), 7.73-7.82 (m, 4H).

ESI-MS: *m/z* 1139.8 $(M+Na)^+$, 1155.8 $(M+K)^+$.

- Synthesis of axle **A-8**

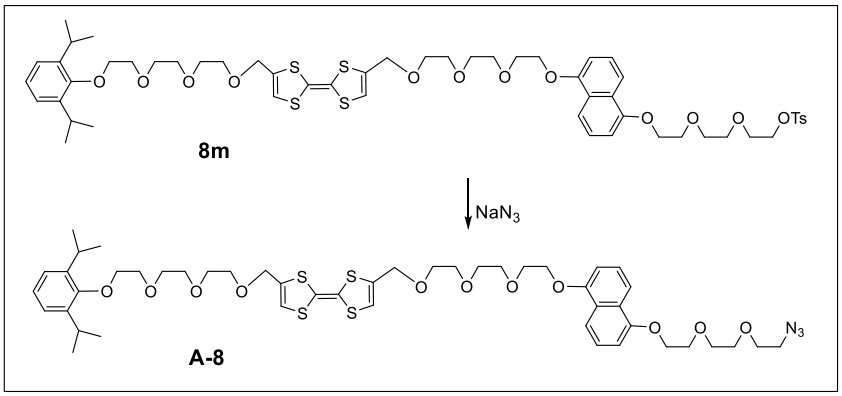

A-8 was prepared following the synthetic procedure reported in ref. [12]. A solution of tosylate **8m** (0.013 g, 0.0116 mmol) and NaN_3 (0.004, 0.058 mmol) in dry DMF (1 mL) was heated at 80 °C for 1 d. After removal of the solvent, the residue was dissolved in DCM (10 mL) and distilled water (10 mL) and extracted with CH_2Cl_2. The combined organic extracts washed with brine and dried over $MgSO_4$ were concentrated under vacuum. The crude product, was purified by column chromatography (SiO_2: Cy/EtOAc 1:1) to give the azide **A-8** in quantitative yield as a yellow oil.

^{1}H NMR (400 MHz, CD_3CN): δ1.18 (d, *J*=6.8 Hz, 12H), 3.32-3.42 (m, 2H), 3.50-3.68 (m, 18H), 3.68-3.74 (m, 4H), 3.74-3.79 (m, 2H), 3.83-3.88 (m, 2H), 3.91-3.95 (m, 4H), 4.22 (s, 2H), 4.24-4.29 (m, 6H), 6.30, 6.32, 6.34, 6.37 (4 x *br* s, 2H) , 6.94 (d, *J*=8.0 Hz, 2H), 7.04-7.13 (m, 3H), 7.38 (d, *J*=8.0 Hz, 2H), 7.80 (d, *J*=8.0 Hz, 2H).

ESI-MS: *m/z* 987.6 $(M+H)^+$, 1010.5 $(M+Na)^+$.

- Synthesis of dumbbell **D-8** and rotaxane **R-8**

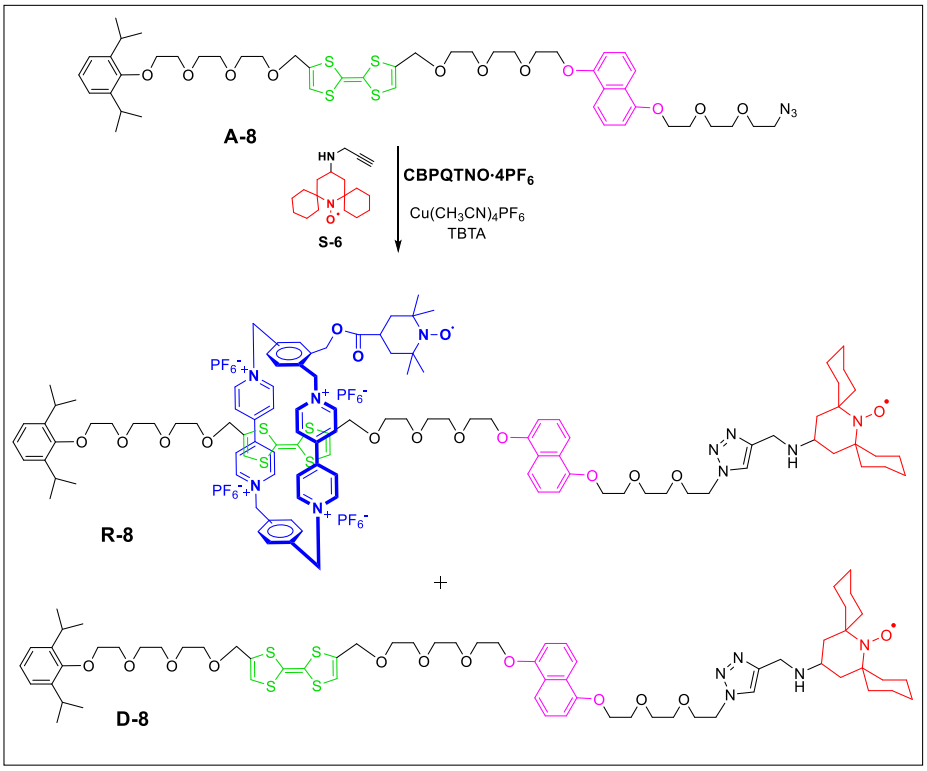

R-8 was prepared following the synthetic procedure reported in ref. [13]. Axle **A-8** (0.0185 g, 0.0187 mmol), **CBPQTNO•4PF$_6$**[14] (0.032 g, 0.024 mmol) and stopper **S-6**[13] (0.0067 g, 0.0234 mmol) were dissolved in DMF (0.15 mL) at -10 °C under N_2 atmosphere, forming a brown solution. TBTA (0.0017 g, 0.0032 mmol) and $Cu(CH_3CN)_4PF_6$ (0.0012 g, 0.0032 mmol) were added to the solution and the resulting mixture was stirred at r.t. for 72 h, at which time the solvent was evaporated. The crude solid was purified by column chromatography (SiO_2: Me_2CO and then 1% w/v NH_4PF_6 solution in Me_2CO, i.d. 10 mm, h 17 cm). The fractions in Me_2CO containing the dumbbell **D-8** were collected and concentrated. The fraction in 1% w/v NH_4PF_6 solution in Me_2CO were collected and concentrated to a minimum volume, and rotaxane **R-8** was precipitated from this solution through the addition of an excess of cold H_2O. The resulting solid was collected by filtration, washed with H_2O to remove the excess of NH_4PF_6, and dried by vacuum pump to afford the desired rotaxane as a green powder in 30% yield.

Dumbbell **D-8**: ^{1}H NMR (600 MHz, CD_3CN): δ1.16-1.20 (m, 12H), 3.35-3.41 (m, 2H), 3.50-3.96 (m, 34H), 4.21-4.30 (m, 4H), 4.42-4.48 (m, 2H), 4.52-4.60 (m, 2H), 6.17-6.30 (*br* m, 2H), 6.82-7.01 (m, 2H), 7.03-7.16 (m, 3H), 7.25-7.46 (m, 2H), 7.69-7.87 (m, 2H), 8.24-8.35 (m, 1H).

ESI-MS: *m/z* 1277.8 $(M+H)^+$.

Rotaxane **R-8**: ^{1}H NMR (600 MHz, CD_3CN): δ1.12-1.19 (m, 12H), 3.35-3.40 (m, 2H), 3.50-3.96 (m, 34H), 4.21-4.29 (m, 6H), 4.44-4.56 (m, 2H), 5.32-5.42 (m, 2H), 5.60-5.91 (m, 10H), 6.84-6.97 (m, 2H), 7.04-7.13 (m, 3H), 7.18-7.83 (m, 12H), 8.64-9.10 (m, 8H).

ESI-MS: *m/z* 2446.1 $(M\text{-}PF_6)^+$, 2300.1 $(M\text{-}2PF_6)^+$.

3.4 Synthesis of rotaxane R-9 and dumbbell D-9

- Synthesis of stopper **S-9**

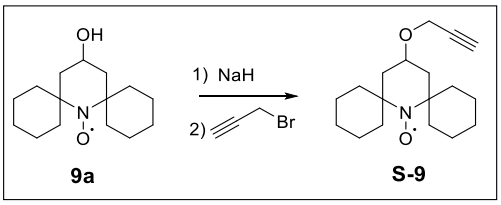

Stopper **S-9** was prepared following the synthetic procedure reported in ref. [21a]. To a solution of **9a**[21b] (0.12 g, 0.48 mmol) and Bu_4NI (0.01 mg, 5 mol%) in THF (4 mL), NaH (0.03 g, 60% dispersion in mineral oil) was added portion-wise at r.t. under inert nitrogen atmosphere. After stirring for 1 h at r.t., the mixture was treated dropwise with an 80 wt % solution of propargyl bromide in toluene (0.3 g, 0.22 mL) and the reaction mixture was heated at reflux overnight, cooled, filtered and concentrated under vacuum. The residue was purified by flash chromatography (SiO_2, i.d. 20 mm, h 12 cm, 100% Cy until Cy/EtOAc 95:5) to give propargyl ether **S-9** as an orange-red crystalline solid (0.104 g, 75%).
GC-MS: *m/z* 290.
The ^{1}H NMR spectrum of *N*-hydroxy amine of stopper **S-9** (**S-9-OH**) was recorded after *in situ* reduction of the sample containing **S-9** by using phenylhydrazine.
S-9-OH: ^{1}H NMR (400 MHz, CD_3CN): δ0.92-1.00 (m, 2H), 1.02-1.12 (m, 2H), 1.22-1.29 (m, 2H), 1.34-1.64 (m, 14H), 1.83-1.91 (m, 2H), 2.46 (dd, *J*=12.0 and 4.0 Hz, 2H), 2.66 (t, *J*= 2.0 Hz, 1H), 3.67 (tt, *J*=12.0 and 4.0 Hz, 1H), 4.17 (d, *J*=2.0 Hz, 2H).

- Synthesis of dumbbell **D-9** and rotaxane **R-9**

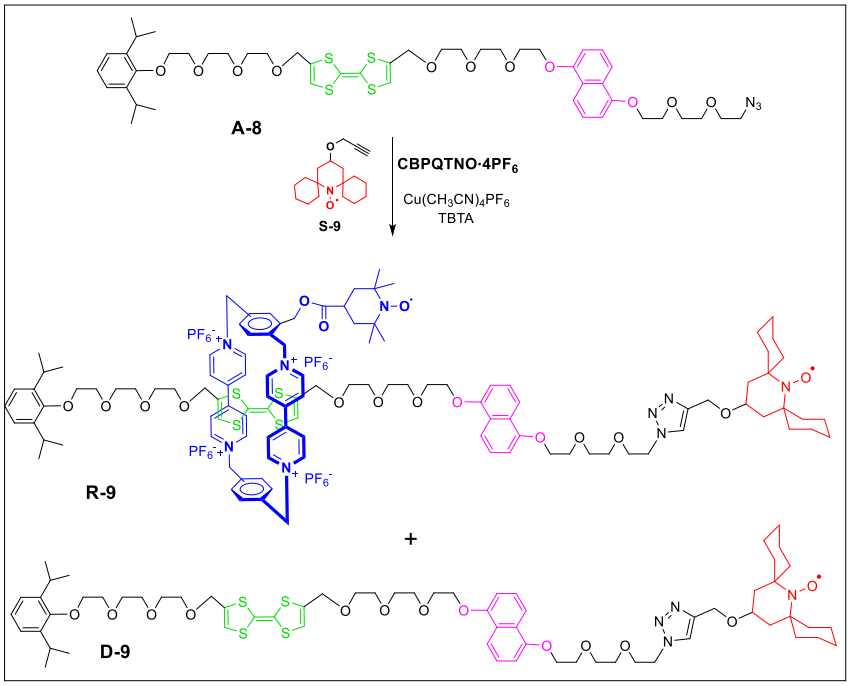

Dumbbell **D-9** and rotaxane **R-9** were prepared following the procedure described for **D-8** and **R-8** using: axle **A-8** (0.0132 g, 0.013mmol), **CBPQTNO•4PF$_6$**[14] (0.0175 g, 0.013 mmol), stopper **S-9**[20] (0.0047 g, 0.0162mmol), TBTA (0.0012 g, 0.0022 mmol) and $Cu(ACN)_4PF_6$ (0.0008 g, 0.0022mmol) in DMF (0.15 mL). The yields were not calculated.

Dumbbell **D-9**: ^{1}H NMR (600 MHz, CD_3CN): δ1.18 (d, *J*=6.6 Hz, 12H), 3.38 (septet, *J*=6.6 Hz, 2H), 3.50-3.72 (m, 20H), 3.75-3.79 (m, 2H), 3.83-3.95 (m, 8H), 4.20-4.50 (m, 12H), 6.22-6.41 (m, 2H), 6.94 (*br* s, 2H), 7.04-7.13 (m, 3H), 7.37 (*br* s, 2H), 7.80 (*br* s, 3H).

ESI-MS: *m/z* 1278.8 $(M+H)^+$.

Rotaxane **R-9**: ^{1}H NMR (600 MHz, CD_3CN): δ1.12-1.19 (m, 12H), 3.35-3.40 (m, 2H), 3.50-3.96 (m, 34H), 4.21-4.29 (m, 6H), 4.44-4.56 (m, 2H), 5.32-5.42 (m, 2H), 5.60-5.91 (m, 10H), 6.84-6.97 (m, 2H), 7.04-7.13 (m, 3H), 7.18-7.83 (m, 12H), 8.64-9.10 (m, 8H).

ESI-MS: *m/z* 2446.1$(M-PF_6)^+$, 2300.1$(M-2PF_6)^+$.

3.5 Synthesis of dumbbell D-10 and rotaxane R-10

- Synthesis of compound **10b**

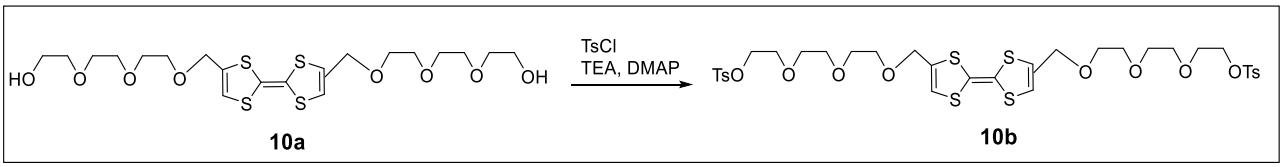

10a **10b**

Compound **10b** was prepared following the synthetic procedure reported in ref. [11b]. TsCl (0.161 g, 0.85 mmol) dissolved in anhydrous DCM (5 mL) was added dropwise over a period of 5 min to an ice-cooled solution of **10a**[16,17] (0.090 g, 0.170 mmol), TEA (0.038 g, 0.375 mmol, 53 μL) and DMAP (0.008 g, cat.) in anhydrous DCM (2 mL). The reaction mixture was stirred overnight (0°C to r.t.), whereupon it was washed with satured $NaHCO_3$ solution, brine, dried ($MgSO_4$), and the solvent evaporated. The crude product was chromatographed over silica gel column (h 10 cm, i.d. 25 mm) eluting with EtOAc. The second band containing the desired product was collected and concentrated to give 0.102 g of compound **10b** (85% yield).

^{1}H NMR (400 MHz, CD_3CN): δ 2.44 (s, 6H), 3.49 (s, 8H), 3.53 (s, 8H), 3.61 (t, *J*=4.4 Hz, 4H), 4.11 (t,*J*=4.4 Hz, 4H), 4.26 (s, 4H), 6.38 (*br* s, 2H), 7.43 (d,*J*=8 Hz, 4H), 7.78 (d,*J*=8 Hz, 4H).

ESI-MS: *m/z* 860.2 $(M+Na)^+$.

- Synthesis of compound **A-10**

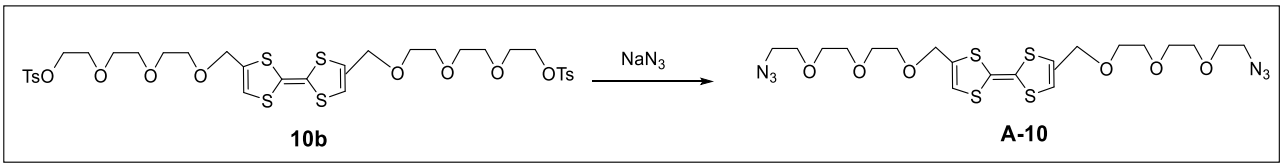

10b **A-10**

A-10 was prepared following the synthetic procedure reported in ref. [12]. A solution of ditosylate **10b** (0.100 g, 0.119 mmol), and NaN_3 (0.077, 1.19 mmol) in dry DMF (10 mL) was heated at 80 °C for 2 d. After removal of the solvent, the residue was dissolved in DCM and distilled H_2O and extracted with DCM. The combined organic extracts washed with brine and dried over $MgSO_4$were concentrated under vacuum to give the azide **A-10** in quantitative yield as a yellow oil (Rf=0.25 in Cy/EtOAc 1/1).

^{1}H NMR (400 MHz, CD_3CN): δ 3.37 (t, *J*=4.8 Hz, 4H), 3.52-3.61 (m, 18H), 3.63 (t, *J*=4.8 Hz, 4H), 4.27 (s, 4H), 6.39 (*br* s, 2H).

ESI-MS: *m/z* 601.1 $(M+Na)^+$.

- Synthesis of dumbbell **D-10** and rotaxane **R-10**

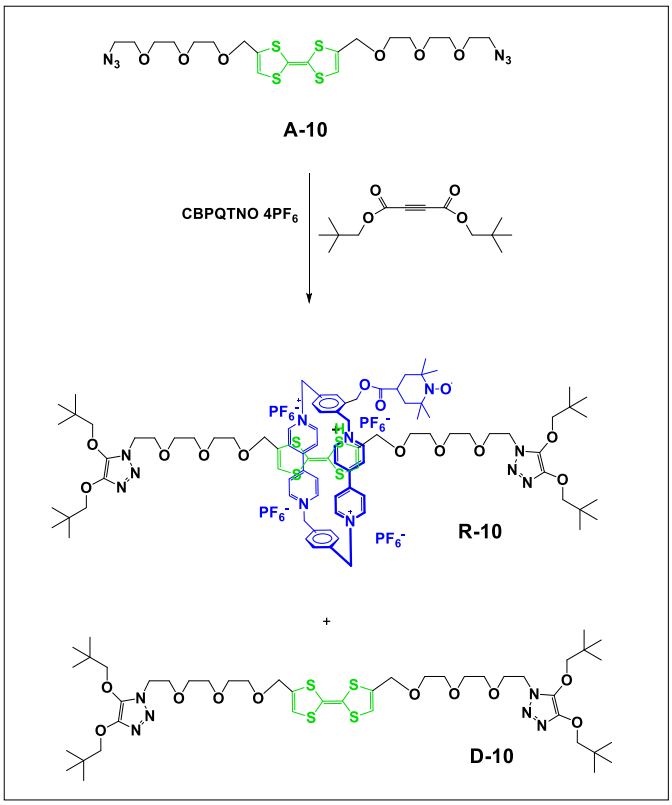

R-10 was prepared following the synthetic procedure reported in ref. [22]. Axle **A-10** (0.015 g, 0.026 mmol), **CBPQTNO•4PF$_6$**[14] (0.034 g, 0.026 mmol) and stopper **S-5** (0.015 g, 0.065 mmol) were dissolved in MeCN (0.13 mL) at 0 °C under N_2 atmosphere and the resulting mixture was stirred at room temperature for 72 h, at which time the solvent was evaporated. The crude solid was purified by column chromatography (SiO_2: Me_2CO and then 1% w/v NH_4PF_6 solution in Me_2CO, i.d. 10 mm, h 17 cm). The fractions in Me_2CO containing the dumbbell **D-10** were collected and concentrated. The fraction in 1% w/v NH_4PF_6 solution in Me_2CO were collected and concentrated to a minimum volume, and rotaxane **D-10** was precipitated from this solution through the addition of an excess of cold H_2O. The resulting solid was collected by filtration, washed with water to remove the excess of NH_4PF_6, and dried by vacuum pump to afford the desired rotaxane as a green powder in 30% yield.

References

[1] P. R. Ashton, R. Ballardini, V. Balzani, I. Baxter, A. Credi, M. C. T. Fyfe, M. T. Gandolfi, M. Gómez-López, M.-V. Martínez-Díaz, A. Piersanti, N. Spencer, J. F. Stoddart, M. Venturi, A. J. P. White, D. J. Williams, *J. Am. Chem. Soc.* **1998**, *120*, 11932–11942.

[2] J. J. Pak, J. L. Mayo, E. Shurdha, *Tetrahedr. Lett.* **2006**, *47*, 233-237.

[3] G. W. Bates, P. A. Gale, M. E. Light, *Chem. Commun.* **2007**, 2121-2123.

[4] V. Bleve, C. Schäfer, P. Franchi, S. Silvi, E. Mezzina, A. Credi, M. Lucarini *ChemistryOpen*, **2015,** *4*, 18–21.

[5] J. M. Khurana, S. Chauhan, G. Bansal, *Monatshefte für Chemie* **2004**, *135*, 83–87.

[6] P. Franchi, V. Bleve, E. Mezzina, C. Schäfer, G. Ragazzon, M. Albertini, D. Carbonera, A. Credi, M. Di Valentin, M. Lucarini, *Chem. Eur. J.* **2016**, *22*, 8745 – 8750.

[7] G. Jeschke, V. Chechik, P. Ionita, A. Godt, H. Zimmermann, J. Banham, C. R. Timmel, D. Hilger, H. Jung, *Appl. Magn. Reson.* **2006**, *30*, 473–498.

[8] J. F. W. Keana, J. Cuomo, L. Lex, S. E. Seyedrezai, *J. Org. Chem*. **1983**, *48*, 2647-2654.

[9] G. Soldaini, F. Cardona, A. Goti, *Org. Lett*. **2007**, *9*, 473-476.

[10] (a) A. Trabolsi, N. Khashab, A. C. Fahrenbach, D. C. Friedman, M. T. Colvin, K. Cotí, D. Benítez, E. Tkatchouk, J.-C. Olsen, M. E. Belowich, R. Carmielli, H. A. Khatib, W. A. Goddard III, M. R. Wasielewski, J. F. Stoddart, *Nature Chemistry* **2010***, 2*, 42–49; (b) C. P. Collier, J. O. Jeppesen, Y. Luo, J. Perkins, E. W. Wong, J. R. Heath, J. F. Stoddart, *J. Am. Chem. Soc.* **2001**, *123,* 12632–12641;

[11] (a) F. Romano, R. Manoni, P. Franchi, E. Mezzina, M. Lucarini, *Chem. Eur. J.***2015**, *21*, 2775-2779; (b) H.-R. Tseng, S. A.Vignon, P. C. Celestre, J. Perkins, J. O. Jeppesen, A. Di Fabio, R. Ballardini, M. T. Gandolfi, M. Venturi, V. Balzani, J. F. Stoddart, *Chem. Eur. J.* **2004**, *10*, 155–172;

[12] T.Avellini, H. Li, A.Coskun, G.Barin, A.Trabolsi, A. N. Basuray, S. K. Dey, A. Credi, S. Silvi, J. F. Stoddart, M. Venturi, *Angew. Chem. Int. Ed.* **2012**, *51*, 1611 –1615.

[13] R. Manoni, F. Romano, C. Casati, P. Franchi, E. Mezzina, M. Lucarini, *Org. Chem. Front.* **2014**, *1*, 477-483.

[14] A. Margotti, C. Casati, M. Lucarini, E. Mezzina, *Tetrahedron Lett.* **2008**, *49*, 4784-4787.

[15] R. S. Stoll, D. C. Friedman, and J. F. Stoddart, *Org. Lett.* **2011**, *13*, 2706–2709.

[16] (a) R. Andreu, J. Garwn, J. Orduna, M. Savwron, J. Cousseau, A. Gorgues, V. Morisson, T. Nozdryn, J. Becher, R. P. Clausen, M. R. Bryce, P. J. Skabara, W. Dehaen, *Tetrahedron Lett.* **1994**, *35*, 9243–9246. (b) L. R. Melby, H. D. Hartzler, W. A. Sheppard, *J. Org. Chem.* **1974**, *39*, 2456-2458. (c) C. U. Pittman, M. Narita, Y. F. Liang,*J. Org. Chem.* **1976**, 41, 2855-2860. (d) S. Saha, E. Johansson, A. H. Flood, H.-R. Tseng, J. I. Zink, J. F. Stoddart, *Chem. Eur. J.* **2005**, *11*, 6846–6858.

[17] J. M. Spruell, W. F. Paxton, J.-C. Olsen, D. Benítez, E. Tkatchouk, C. L. Stern, A. Trabolsi, D. C. Friedman, W. A. Goddard III, J. F. Stoddart, *J. Am. Chem. Soc.* **2009**, *131*, 11571–11580.

[18] (a) S. Arumugam, V. V. Popik, *J. Am. Chem. Soc.* **2011**, *133*, 15730–15736; (b) F. A. Loiseau, K. Kuok (Mimi), Hii Alison M. Hill, *J. Org. Chem.* **2004**, *69*, 639–647.

[19] S. Arumugam, V. V. Popik, *J. Am. Chem. Soc.* **2011**, *133*, 15730–15736.

[20] (a) D. W. Steuerman, H. -R. Tseng, A. J. Peters, A. H. Flood, J. O. Jeppesen, K. A. Nielsen, J. F. Stoddart, J. R. Heath, *Angew. Chem. Int. Ed.* **2004**, *43*, 6486–6491; (b) I. Aprahamian, W. R. Dichtel, T. Ikeda,J. R. Heath, J. F. Stoddart, *Org. Lett.* **2007**, *9*, 1287-1290.

[21] (a) J. Luo, C. Pardin, W. D.Lubell, X. X. Zhu, *Chem. Commun.* **2007**, 2136–2138; (b) J. T. Paletta, M. Pink, B.Foley, S.Rajca, A.Rajca, *Org. Lett.* **2012**, *14*, 5322-5325.

[22] H. Li, Z. Zhu, A. C. Fahrenbach, B. M. Savoie, C. Ke, J. C. Barnes, J. Lei,Y. Zhao, L. M. Lilley, T. J. Marks, M. A. Ratner, J. F. Stoddart, *J. Am. Chem. Soc.* **2013**, *135*, 456 – 467.

Appendix : Cover

V. Bleve, C. Schäfer, P. Franchi, S. Silvi, E. Mezzina, A. Credi, M. Lucarini *ChemistryOpen*, **2015**, *4*, 18–21.

P. Franchi, V. Bleve, E. Mezzina, C. Schäfer, G. Ragazzon, M. Albertini, D. Carbonera, A. Credi, M. Di Valentin, M. Lucarini, *Chem. Eur. J.* **2016**, *22*, 8745 – 8750.